TESIS DE LA UNIVERSIDAD DE ZARAGOZA
2024
13

Lidia Martínez Izquierdo

Captura de CO2 con membranas ultrafinas modificadas con compuestos metalorgánicos porosos

Director/es
Coronas Ceresuela, Joaquín Juan
Téllez Ariso, Carlos

ISSN 2254-7606

Prensas de la Universidad
Universidad Zaragoza

ISSN 2254-7606

Universidad Zaragoza
1542

Tesis Doctoral

CAPTURA DE CO2 CON MEMBRANAS ULTRAFINAS MODIFICADAS CON COMPUESTOS METALORGÁNICOS POROSOS

Autor

Lidia Martínez Izquierdo

Director/es

Coronas Ceresuela, Joaquín Juan
Téllez Ariso, Carlos

UNIVERSIDAD DE ZARAGOZA
Escuela de Doctorado

Programa de Doctorado en Ingeniería Química y del Medio Ambiente

2022

Universidad Zaragoza

1542

ÁREA DE INGENIERÍA QUÍMICA,
DEPARTAMENTO DE INGENIERÍA QUÍMICA Y TECNOLOGÍAS DEL MEDIO AMBIENTE

"Captura de CO_2 con membranas ultrafinas modificadas con compuestos metal-orgánicos porosos"

Memoria para optar al grado de Doctor por la Universidad de Zaragoza presentada por:

Dña. Lidia Martínez Izquierdo

Zaragoza, 2022

Departamento de Ingeniería Química y Tecnologías del Medio Ambiente
Universidad Zaragoza

INMA
INSTITUTO DE NANOCIENCIA Y MATERIALES DE ARAGÓN

D. Joaquín Coronas Ceresuela y D. Carlos Téllez Ariso, ambos catedráticos de Universidad del Departamento de Ingeniería Química y Tecnologías del Medio Ambiente de la Universidad de Zaragoza, y miembros del Instituto de Nanociencia y Materiales de Aragón (INMA, Universidad de Zaragoza -Centro Superior de Investigaciones Científicas),

CERTIFICAN

Que la presente memoria titulada:

"Captura de CO_2 con membranas ultrafinas modificadas con compuestos metal-orgánicos porosos"

Ha sido realizada bajo su dirección por **Dña. Lidia Martínez Izquierdo** en el departamento de Ingeniería Química y Tecnologías del Medio Ambiente de la Universidad de Zaragoza y autorizan su presentación.

Y para que así conste, firman el presente certificado en Zaragoza, a 5 de octubre de 2022.

Fdo. Dr. Joaquín Coronas Ceresuela

Fdo. Dr. Carlos Téllez Ariso

“El 90% del éxito se basa simplemente en insistir”

- ***Woody Allen***

Agradecimientos

En primer lugar, me gustaría agradecer a mis directores de tesis, Joaquín Coronas y Carlos Téllez. Cuando me propusieron realizar la tesis doctoral en su grupo de investigación hace 4 años, el tema que me presentaron me resultó apasionante, iba a poder aportar mi pequeño granito de arena a uno de los retos más difíciles a los que nos enfrentamos actualmente: La descarbonización de la industria. Pensar que por diminuta que fuera dicha contribución, esta podría ayudar a otros a seguir avanzando en esta línea me resultaba, y me sigue resultando, enriquecedor. Sin duda, el desarrollo de esta tesis doctoral no la puedo catalogar como algo fácil, pero lo que sí puedo hacer es afirmar que durante este tiempo he aprendido, me he desarrollado tanto en lo personal como en lo profesional y he conocido a personas interesantes que, como a mí, les apasiona la Ciencia. Por todo ello, gracias.

Agradecer también a todas las personas que han hecho posible de manera directa o indirecta la realización de esta tesis doctoral: personal del Departamento de Ingeniería Química y Tecnologías del Medio Ambiente y del Instituto de Nanociancia y Materiales de Aragón, así como al personal técnico del Laboratorío de Microscopías Avanzadas y del SAI. Además, a Cristina García, que no solo me ha ayudado en parte de mi investigación, sino que también me ha enseñado a enseñar.

A mis compañeros del CREG, a los que siguen y a los que han formado parte de él, en especial a la vieja guardia: Víctor, Javier, Lorena, Adelaida y Carlos. Gracias por las risas, las ideas, el apoyo y la ayuda recibida de todos vosotros durante estos años, habéis hecho que esta experiencia haya sido aún más enriquecedora.

Por supuesto, agradecer a mis amigos, sin duda han conseguido hacer esta tesis más llevadera.

Por último, no puedo olvidarme de mi familia, y en especial de mis padres, mi hermano y Alejandro. Ellos han sido siempre el motor que impulsa mis sueños, quienes estuvieron siempre a mi lado en los días más difíciles. Siempre han sido mis mejores guías. Hoy, cuando concluyo mi doctorado, os dedico a vosotros este logro, como una meta más conquistada. Orgullosa de que estéis a mi lado en este momento tan importante.

A todos vosotros, ¡gracias!

Índice de contenido

Capítulo 1: Contexto, objetivos y estructura de la memoria

1. Contexto, objetivos y estructura de la memoria

La presente tesis doctoral, titulada "Captura de CO_2 con membranas ultrafinas modificadas con compuestos metal-orgánicos porosos", se ha realizado en el grupo CREG ("Catálisis, Separaciones Moleculares e Ingeniería de Reactores") del Departamento de Ingeniería Química y Tecnologías del Medio Ambiente (IQTMA) de la Universidad de Zaragoza (UZ), reconocido como grupo de investigación de referencia por el Gobierno de Aragón. La investigación se ha desarrollado en el Instituto de Nanociencia y Materiales de Aragón (INMA), instituto mixto del Consejo Superior de Investigaciones Científicas (CSIC) y de la UZ.

Desde 2005, el grupo ha investigado en el desarrollo y aplicación de las denominadas membranas híbridas utilizando, en primera instancia, materiales inorgánicos como relleno y, posteriormente, MOF (del inglés "metal-organic frameworks"). Dichas investigaciones han dado como resultado las siguientes tesis doctorales, codirigidas por los Dres. Carlos Téllez y Joaquín Coronas:

- *"Desarrollo de materiales laminares porosos para la preparación de membranas híbridas". Patricia Gorgojo Alonso (2010).*
- *"Membranas híbridas polímero-material nanoestructurado poroso para la separación de mezclas gaseosas". Beatriz Zornoza Encabo (2011).*
- *"Síntesis y aplicación de titanosilicatos y estañosilicatos laminares y deslaminados". César* Rubio Hortells (2012).
- *"Estudio estructural de materiales laminares y su aplicación en membranas mixtas material laminar-polímero". Alejandro Galve Guinea (2013).*
- *"Nanocomposite materials for membrane separations processes". Daniel Sieffert (2013).*
- *"Encapsulación en materiales inorgánicos porosos para aditivar fibras de poliamida". Eduardo Pérez García (2013).*

- *"Nuevas estrategias para sintetizar zeolitas y MOF. Aplicación a la separación de gases con micromembranas".* Marta Navarro Rojas (2013).
- *"Síntesis de materiales nanoestructurados porosos en presencia de cafeína con aplicación a la liberación controlada". Nuria Liédana Pérez (2014).*
- *"Nuevas estrategias de síntesis de MOFs y su aplicación como relleno en membranas poliméricas para separación de gases".* Beatriz Seoane de la Cuesta (2014).
- *"Materiales laminares y porosos para su aplicación al desarrollo sostenible".* Sonia Castarlenas *Sobreviela (2014).*
- *"Desarrollo de materiales nanoestructurados porosos para su aplicación en procesos de separación mediante membranas híbridas de matriz polimérica".* Sara Sorribas R*oca (2015).*
- *"Modelling study of vanadium bases alloys and crystalline porous materials for gas separation membranes".* Jenny Borisova Evtimova (2016).
- *"Innovaciones en sílices mesoporosas, silicatos laminares y MOFs para la transformación de azúcares en ácido láctico y derivados". Beatriz Murillo Esteras (2018).*
- *"Membranas continuas y soportadas de MOF para separación de mezclas gaseosas".* Fernando Cacho Bailo (2017).
- *"Polímeros de coordinación: Transformaciones cristalinas y separación de gases mediante membranas". Adelaida Perea Cachero (2017).*
- *"Synthesis and characterization of polyimide-based mixed matrix membranes for CO_2/CH_4 separation".* Zamidi Ahmad (2018).
- *"Preparation and characterization of mixed matrix membranes for gas separation and pervaporation".* Roberto Castro Muñoz (2018).
- *"Síntesis de materiales metal-orgánicos y encapsulación de moléculas bioactivas".* Rebeca Monteagudo Olivan (2018).

- *"MOF-based polymeric membranes for CO_2 capture".* Javier Sánchez Laínez (2019).
- *"Desarrollo de membranas nanocompuestas de película delgada basadas en materiales metal-orgánicos porosos y grafeno para su aplicación en nanofiltración".* Lorena Paseta Martínez (2019).
- *"Estrategias de síntesis de capas finas de poliamida y MOF-poliamida sobre soportes planos y de fibra hueca para su aplicación en nanofiltración de disolventes orgánicos y agua".* Carlos Echaide Górriz (2020).

La tesis doctoral que aquí se presenta está centrada en la separación de especies gaseosas, en concreto en la separación de CO_2 de las mezclas CO_2/N_2 y CO_2/CH_4, mediante el uso de membranas de película delgada y MOF. Esta tesis continua con parte del trabajo realizado previamente en otra tesis del grupo: "MOF-based polymeric membranes for CO_2 capture" de Javier Sánchez Laínez. La novedad de esta tesis radica en la preparación de capas ultrafinas de polímero (por debajo de 1 µm de espesor) con distintos tipos de MOF, así como la introducción de líquidos iónicos en la matriz polimérica. Además, se han explorado nuevos métodos de preparación de este tipo de membranas, con la intención de obtener espesores de capa selectiva por debajo de 1 µm. Al obtener capas sin defectos y tan finas de material selectivo se pretende aumentar el flujo de gas a través de las membranas, de forma que estas lleguen a ser más atractivas desde el punto de vista comercial.

La realización de esta tesis doctoral ha sido posible gracias a la financiación recibida por parte de las ayudas destinadas a la contratación de personal investigador en formación para el período 2018-2022, cofinanciadas con el Programa Operativo del Fondo Social Europeo (FSE) Aragón 2014-2020 y el Gobierno de Aragón, así como por los siguientes proyectos de investigación, a los cuales se agradece su financiación:

- "Grupo de Investigación en Catálisis, Separaciones Moleculares e Ingeniería de Reactores (CREG)" (T43_20R, T43_17R) financiado por Gobierno de Aragón y Fondo Social Europeo.

- "Advanced MEMBranes and membrane assisted procEsses for pre- and post-combustion CO_2 captuRe (MEMBER)" (European Union's Horizon 2020 research and innovation programme under grant agreement n° 760944).
- Proyecto MAT2016-77290-R financiado por MCIN/AEI/10.13039/ 501100011033 y por FEDER Una manera de hacer Europa (Agencia Estatal de Investigación (AEI)), Ministerio de Ciencia e Innovación (MCIN) y El Fondo Europeo de Desarrollo Regional (FEDER).
- Proyecto PID2019-104009RB-I00 financiado por MCIN/AEI/10.13039/ 501100011033.

Cabe mencionar también que los resultados obtenidos durante la realización de esta tesis doctoral han dado lugar a la publicación de cuatro artículos científicos, los cuales corresponden a los **capítulos 4, 5, 6 y 8**, respectivamente:

- L. Martínez-Izquierdo, A. Perea-Cachero, M. Malankowska, C. Téllez, J. Coronas. "A comparative study between single gas and mixed gas permeation of polyether-block-amide type copolymer membranes", Journal of Environmental Chemical Engineering **2022**, 10, 108324. DOI: 10.1016/j.jece.2022.108324
- L. Martínez-Izquierdo, M. Malankowska, J. Sánchez-Laínez, C. Téllez, J. Coronas. "Poly(ether-block-amide) copolymer membrane for CO_2/N_2 separation: the influence of the casting solution concentration on its morphology, thermal properties and gas separation performance", Royal Society Open Science **2019**, 6, 190866. DOI: 10.1098/rsos.190866
- L. Martínez-Izquierdo, M. Malankowska, C. Téllez, J. Coronas. "Phase inversion method for the preparation of Pebax® 3533 thin film membranes for CO2/N2 separation", Journal of Environmental Chemical Engineering **2021**, 9, 105624. DOI: 10.1016/j.jece.2021.105624
- L. Martínez-Izquierdo, C. Téllez, J. Coronas. "Highly stable Pebax® Renew® thin-film nanocomposite membranes with metal organic framework ZIF-94 and ionic

liquid [Bmim][BF_4] for CO_2 capture", Journal of Materials Chemistry A **2022**, 10, 18822-18833. DOI: 10.1039/d2ta03958c

Asimismo, los resultados del capítulo 7 están en preparación para su publicación:

- L. Martínez-Izquierdo, C. García-Comas, M. Navarro, S. Dai, A. Tissot, C. Serre, C. Téllez, J. Coronas. "Ultra-small functionalized MOF UiO-66/polymer Pebax® 1657 thin film nanocomposite membranes for CO_2 separation".

Finalmente se debe indicar que, aunque no está incluido de forma explícita en esta memoria, la doctoranda ha participado en la redacción y estructuración de una revisión relacionada con membranas de Pebax® para separación de gases, así como en otra investigación relacionada con membranas de matriz mixta. Estos trabajos han sido de apoyo tanto para el desarrollo de esta tesis como para la redacción de la memoria dando lugar a las dos siguientes publicaciones:

- A. Selomon Embaye, L. Martínez-Izquierdo, M. Malankowska, C. Téllez, J. Coronas. "Poly(ether-block-amide) copolymer membranes in CO_2 separation applications", Energy & Fuels **2021**, 35, 17085−17102. DOI: 10.1021/acs.energyfuels.1c01638
- V. Berned-Samatán, L. Martínez-Izquierdo, E. Abás, C. Téllez, J. Coronas. "A facile route for the recovery of the ligand of zeolitic imidazolate framework ZIF-94/SIM-1", Chemical Communications **2022.** DOI: 10.1039/d2cc03661d

1.1 Contexto científico

En los últimos años ha aumentado notablemente la preocupación sobre el cambio climático causado por las emisiones de CO_2, entre otros gases. El Grupo Intergubernamental de Expertos sobre el Cambio Climático (IPCC, del inglés "Intergovernmental Panel on Climate Change") ha predicho un aumento de 1.9 °C en la temperatura media del planeta para el año 2100,[1] lo que hace vital para los seres humanos y el resto de vida en la Tierra reducir las emisiones de CO_2 a la atmósfera. Por tanto, es urgente desarrollar procesos de captura y separación de CO_2 que permitan mitigar este problema y sus consecuencias.[2] Entre las tecnologías de captura existentes se encuentran la pos-combustión, donde el CO_2 se separa del N_2 sobrante del proceso

de combustión, la pre-combustión, donde el CO_2 se elimina del combustible antes del proceso de combustión, para lo cual se gasifica generando una mezcla H_2/CO_2, y la oxicombustión, que emplea oxígeno puro en lugar de aire para quemar un combustible, lo cual reduce el consumo final de combustible.

La separación por membranas supone una alternativa más eficiente, libre de emisiones y fácil de operar en continuo que otras tecnologías existentes, como la absorción, adsorción o destilación criogénica.[3] Por ello, la separación de gases con membranas es una tecnología en expansión donde todavía es necesario el desarrollo de nuevos materiales para lograr separaciones más eficientes y rentables.

Las membranas poliméricas dominan comercialmente la separación de gases, aunque presentan un compromiso entre selectividad y permeabilidad, representado por los llamados límites superiores de Robeson[4] en el caso de mezclas de gran importancia industrial y comercial: aire (O_2/N_2), corrientes que contengan H_2 (H_2/CO_2, H_2/N_2, H_2/CH_4, etc.), corrientes que contienen CO_2 (CO_2/N_2, CO_2/CH_4, etc.) e hidrocarburos ($C_3H_8/C_3/H_6$, etc.). Para mejorar la selectividad de las membranas, entendiéndose esta como la capacidad de separación del gas de interés en una mezcla de gases, pueden fabricarse membranas mixtas (MMM, del inglés "*mixed matrix membranes*"), que suelen combinar las propiedades de materiales inorgánicos o inorgánico-orgánicos porosos o no porosos (mayor estabilidad química, mecánica y térmica; y mejores propiedades texturales y de separación) con las características de los polímeros (bajo coste y procesabilidad).[5]

Entre los materiales inorgánico-orgánicos existentes, los MOF son materiales microporosos cristalinos híbridos (orgánico-inorgánico) formados por iones o clústeres metálicos unidos por enlaces de coordinación con ligandos orgánicos. Aunque había algunos estudios anteriores que podrían considerarse pioneros,[6] fue en 1995 cuando se publicaron los trabajos que determinaron el inicio de lo que podríamos llamar la era de los MOF,[7,8] que hasta hoy han experimentado un gran crecimiento debido a la versatilidad química con la que se sintetizan y a la gran microporosidad permanente que presentan.

Existen membranas de diversos tipos, aunque las que presentan un mejor comportamiento en cuanto a flujo, siendo por tanto más atractivas a nivel industrial y

comercial, son las denominadas membranas de capa fina o TFC, del inglés "*thin film composite*", las cuales se componen de una capa de separación ultrafina en la parte superior de un soporte poroso. Estas capas finas se pueden modificar a su vez con el fin de mejorar las propiedades de separación introduciendo nanopartículas, dando lugar a las denominadas membranas TFN, del inglés "*thin film nanocomposite*".

En cuanto a la elección del material polimérico que conforma la membrana de separación de gases, es importante tener en cuenta el tipo de mezcla que se desea separar, puesto que estos materiales pueden tener más o menos afinidad por un tipo de gas u otro. El óxido de polietileno (PEO), por ejemplo, posee una elevada afinidad por el CO_2 debido a su carácter polar, por lo que el empleo de materiales con este tipo de segmento en su estructura resultará ventajoso a la hora de llevar a cabo separaciones que impliquen este gas. En la actualidad, existen una gran variedad de copolímeros de bloque compuestos por un segmento flexible de óxido de polietileno, o derivados, y otro rígido de poliamida (PA). Estos copolímeros reciben el nombre de poli(éter-bloque-amida), o en inglés, *"poly(ether-block-amide)"* y están disponibles comercialmente bajo la marca registrada PEBAX®. Por otro lado, las condiciones de preparación y operación también jugarán un papel importante en la separación de gases. Dichos parámetros deberán ser estudiados minuciosamente con el fin de obtener membranas óptimas para la separación de CO_2.

1.2 Objetivos

La finalidad de esta tesis doctoral es preparar membranas de capa ultrafina que contengan MOF que permitan la separación del CO_2 en mezclas gaseosas de poscombustión CO_2/N_2 y mezclas CO_2/CH_4 para el enriquecimiento de biogás. Para ello, va a ser necesario sintetizar MOF que sirvan como relleno y cuyo tamaño de poro y composición química permitan la separación de los gases mediante tamizado molecular y/o adsorción, mejorando el rendimiento de las membranas. Para la preparación de las membranas de capa fina se utilizarán diversas técnicas, entre las que se incluyen la inversión de fases, el recubrimiento por inmersión (*"dip-coating"*) o el recubrimiento por rotación (*"spin-coating"*), con el fin de obtener altos flujos, aportando los MOF una mejora de permeación (flujo a través de la membrana) y selectividad con respecto a los

polímeros puros. Para cumplir con dicho objetivo se establecen los siguientes objetivos parciales:

- Seleccionar los materiales poliméricos idóneos para llevar a cabo la separación de CO_2. Entre los materiales a elegir se encuentran cinco códigos de PEBAX®, los cuales difieren en la naturaleza de los segmentos que los componen, así como en la proporción de cada uno de ellos en la matriz polimérica. Se llevará a cabo un estudio completo de las propiedades de estos materiales en términos de permeabilidad, solubilidad y difusión de CO_2 a través de las membranas densas preparadas con estos materiales. Así mismo, se estudiarán sus características físico-químicas y la influencia de la temperatura en las propiedades de separación.

- Estudiar la influencia del método de preparación de dichas membranas en los resultados finales de separación de gases. En concreto, se estudiará la influencia de la concentración de polímero utilizada para preparar la disolución de "*casting*".

- Preparar membranas de capa fina mediante las diversas técnicas previamente indicadas: inversión de fases, "dip-coating" y "spin-coating". Además, a estas membranas se incorporarán MOF (en concreto se estudiarán los siguientes: ZIF-8, ZIF-94, UiO-66, UiO-66-NO_2 y UiO-66-NH_2) en distintos porcentajes con el fin de mejorar las propiedades de separación de CO_2. De igual forma, se explorará la posibilidad de introducir un líquido iónico que actúe como acelerador del transporte de CO_2 a través de las membranas.

- Todos los materiales preparados a lo largo de esta tesis doctoral, tanto membranas como MOF, se caracterizarán mediante diversas técnicas, entre ellas: análisis termogravimétrico (TGA, *"thermogravimetric analysis"*), calorimetría diferencial de barrido (DSC, "*differential scanning calorimetry*"), difracción de rayos X (XRD, "*X-ray diffraction*"), espectroscopia por transformada de Fourier-reflectancia total atenuada (FTIR-ATR, *"Fourier transform infrared - atenuated total reflectance spectroscopy"*), microscopía electrónica de barrido y de transmisión (SEM, "*scanning electron microscopy*" y TEM, "*transmission electron microscopy*"), adsorción/desorción de N_2 y medidas de viscosidad. También se utilizará la técnica de tiempo de retardo ("*time lag*") para obtener la solubilidad y

coeficiente de difusión de los diferentes gases de interés en los polímeros estudiados.

En la Figura 1.1 se muestra un esquema del trabajo realizado en esta tesis doctoral.

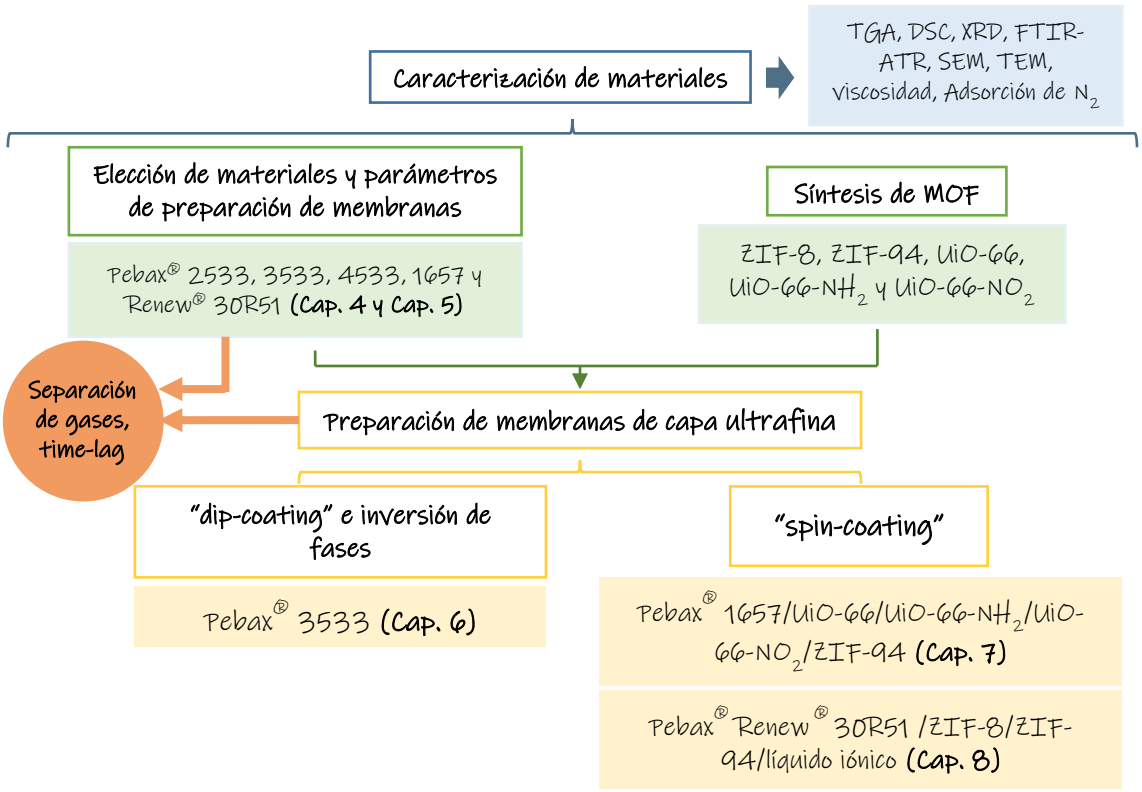

Figura 1.1. Esquema de las tareas desarrolladas en la tesis doctoral.

1.3 Estructura de la memoria

La memoria de esta tesis consta, aparte del presente **capítulo 1** "Contexto, objetivos y estructuración de la memoria", de los descritos brevemente a continuación.

En el **capítulo 2**, se realiza una introducción general sobre los procesos de separación y captura de CO_2 y en concreto de los tipos de membranas disponibles para separación de gases. Así mismo, se introducen los mecanismos de transporte de gas a través de estas membranas, así como las limitaciones que existen a la hora de emplear este tipo de tecnología y las posibles soluciones a las mismas. En el último apartado de este

capítulo, se realiza una revisión de los MOF, introduciendo de forma más específica los empleados en esta tesis doctoral.

En el **capítulo 3**, se describe el procedimiento experimental llevado a cabo para la síntesis de los MOF y la preparación de todas las membranas utilizadas en la tesis. Se describen además las diferentes técnicas empleadas para la caracterización de los MOF y las membranas, así como los sistemas de separación de gases empleados para la determinación de las propiedades de separación de las membranas.

En los **capítulos 4, 5, 6, 7 y 8**, se exponen y discuten los resultados obtenidos con las membranas preparadas. En el **capítulo 4**, se estudian 5 códigos de Pebax® diferentes, los cuales difieren en composición, con el fin de evaluar su comportamiento en separación de gases y seleccionar los más apropiados en función del tipo de aplicación. Se realiza para ello un estudio completo de los parámetros de separación: solubilidad, difusión, permeabilidad y selectividad, y se estudia su comportamiento en función de la temperatura de operación. Por otro lado, en el **capítulo 5**, se elige uno de los códigos estudiados en el capítulo anterior (Pebax® 1657) y se estudia cómo afecta el método de preparación de las membranas densas a las propiedades de separación de gases. En concreto, se estudia el efecto que tiene la concentración de polímero en la disolución polimérica. Así mismo, se lleva a cabo un estudio de tratamiento térmico (*"annealing"*) a alta temperatura (150 °C) durante dos periodos de tiempo diferentes, 3 y 8 días. Los capítulos restantes (6, 7 y 8), se centran en la preparación y caracterización de membranas compuestas de capa fina con y sin MOF. En el **capítulo 6**, se estudia la influencia en las propiedades de separación de gases tanto de la concentración de Pebax® 3533 en su disolución en una mezcla de alcoholes como del número de capas depositadas sobre los soportes asimétricos de polisulfona. Estas membranas se preparan mediante la técnica de inversión de fases, una técnica comúnmente aplicada para la preparación de soportes porosos, pero nunca antes aplicada a la preparación de capas finas. En el **capítulo 7**, se explora la técnica del "spin-coating" para la preparación de membranas de capa fina de Pebax® 1657 con UiO-66 y ZIF-94. En este capítulo, además, se estudia la influencia en las propiedades de separación de CO_2, de la funcionalización del MOF UiO-66 con grupos funcionales amino ($-NH_2$) y nitro ($-NO_2$), así como la importancia del tamaño de dichas partículas en los parámetros de separación.

Se debe indicar que en este capítulo para la preparación y caracterización del MOF UiO-66 se ha contado con la colaboración internacional del grupo de investigación de Christian Serre (Institut Lavoisier, Francia). Por último, en el **capítulo 8**, se emplea esta misma técnica del "*spin-coating*", pero esta vez con un código de Pebax® de origen parcialmente renovable (Pebax® Renew® 30R51) y se introducen MOF de tipo ZIF (ZIF-8 y ZIF-94) junto con un líquido iónico para mejorar las propiedades de separación de manera sinérgica. Además, se realiza una comparación de la estabilidad a largo plazo de las membranas preparadas sin MOF, con líquido iónico y combinando tanto MOF como líquido iónico.

En el **capítulo 9, "resumen y conclusiones"**, se presenta un resumen general y las conclusiones más relevantes de la tesis. Por último, el **capítulo 10** contiene la bibliografía citada a lo largo de esta memoria y el **capítulo 11** un glosario que recopila la nomenclatura y las abreviaturas que aparecen a lo largo del documento.

Capítulo 2: Introducción

2. Introducción

2.1 El CO_2 como contaminante atmosférico

El dióxido de carbono (CO_2) es un gas incoloro e inodoro que se encuentra presente de manera natural en la atmósfera, proveniente tanto de los procesos vitales como de la quema de materias carbonadas como la madera, el carbón o los combustibles fósiles. Aunque este gas no se considera tóxico, ya que el propio ser humano lo genera al respirar, en grandes concentraciones puede llegar a ser perjudicial para la salud. Además, la emisión de grandes cantidades de este gas a la atmósfera está contribuyendo de manera clara al llamado efecto invernadero. El CO_2, por tanto, es considerado uno de los principales gases de efecto invernadero, aunque no es el único, hay otros gases como el metano (CH_4), óxidos de nitrógeno (NO_x) o los clorofluorocarbonos (CFC), entre otros.

Desde la era pre-industrial, la concentración de CO_2 en la atmósfera ha aumentado de manera drástica a una media de 2 ppm/año, desde 280 ppm hasta 412 ppm en 2021.[9,10] Dicho incremento en la concentración de CO_2 atmosférico está provocando así mismo un aumento de la temperatura media terrestre, contribuyendo de esta manera al calentamiento global. Algunos de los efectos derivados del calentamiento global ya son visibles en nuestro planeta: cambios en los patrones climáticos (aumento de las precipitaciones, inundaciones y sequías más frecuentes, tormentas más fuertes, etc.), deshielo de glaciares (lo cual afecta a la vida de las especies que habitan en estos ecosistemas), migración de animales, subida de los mares, etc.

Por todos estos motivos, controlar las emisiones de gases de efecto invernadero a la atmósfera se ha convertido en una prioridad para muchos países, que ya están incorporando en sus políticas medidas para frenar los efectos del calentamiento global. En el año 2015, en París, un total de 196 países acordaron reducir, en la mayor medida posible, sus emisiones de gases de efecto invernadero para limitar el calentamiento global por debajo de 2 °C, preferiblemente a 1.5 °C, en comparación a los niveles preindustriales. Para alcanzar dicho objetivo, cada vez se está impulsando más el uso de energías más limpias y no contaminantes, provenientes de fuentes renovables, así como el desarrollo de tecnologías de captura y secuestro de CO_2. Con estas medidas, se busca

alcanzar otro de los acuerdos establecidos en la 26ª Conferencia de las Naciones Unidas sobre el Cambio Climático (COP26) de Glasgow 2021; que las emisiones de CO_2 netas sean prácticamente nulas en el año 2050.[11]

2.2 Tecnologías de captura y secuestro de CO_2

A pesar de que la transición desde el uso de fuentes de energía no renovables hacia alternativas más limpias sería lo ideal para prevenir las emisiones de CO_2, actualmente no existe una tecnología lo suficientemente desarrollada como para hacer de este objetivo una realidad a corto-medio plazo. Por ello, es necesario desarrollar tecnologías capaces de separar y capturar el CO_2 generado durante los diversos procesos industriales, para evitar su emisión a la atmósfera y conseguir así que las emisiones netas lleguen a ser nulas.

Las tecnologías de captura y secuestro de CO_2 (CCUS, del inglés *"carbon capture, utilisation and storage"*) son un conjunto de tecnologías dedicadas a capturar el CO_2 emitido en diversos procesos industriales y transportarlo para posteriormente almacenarlo y secuestrarlo, o emplearlo como materia prima en otros procesos (Figura 2.1).

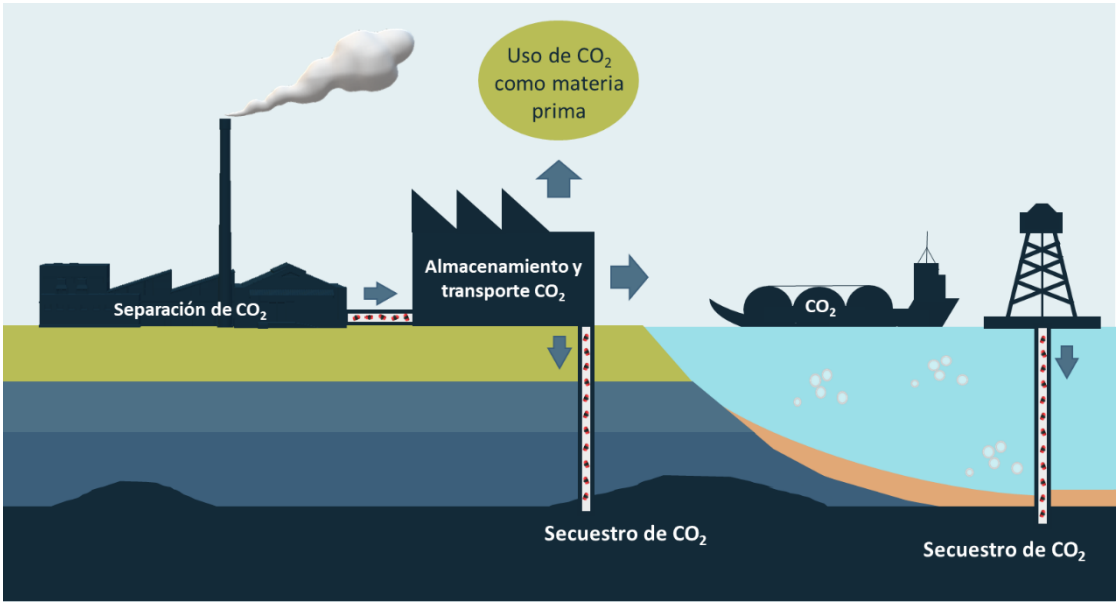

Figure 2.1. Esquema del funcionamiento de las tecnologías de captura y secuestro de CO_2.

Dependiendo de la naturaleza de dichas emisiones, las tecnologías de captura de CO_2 se dividen en tres opciones (Figura 2.2):

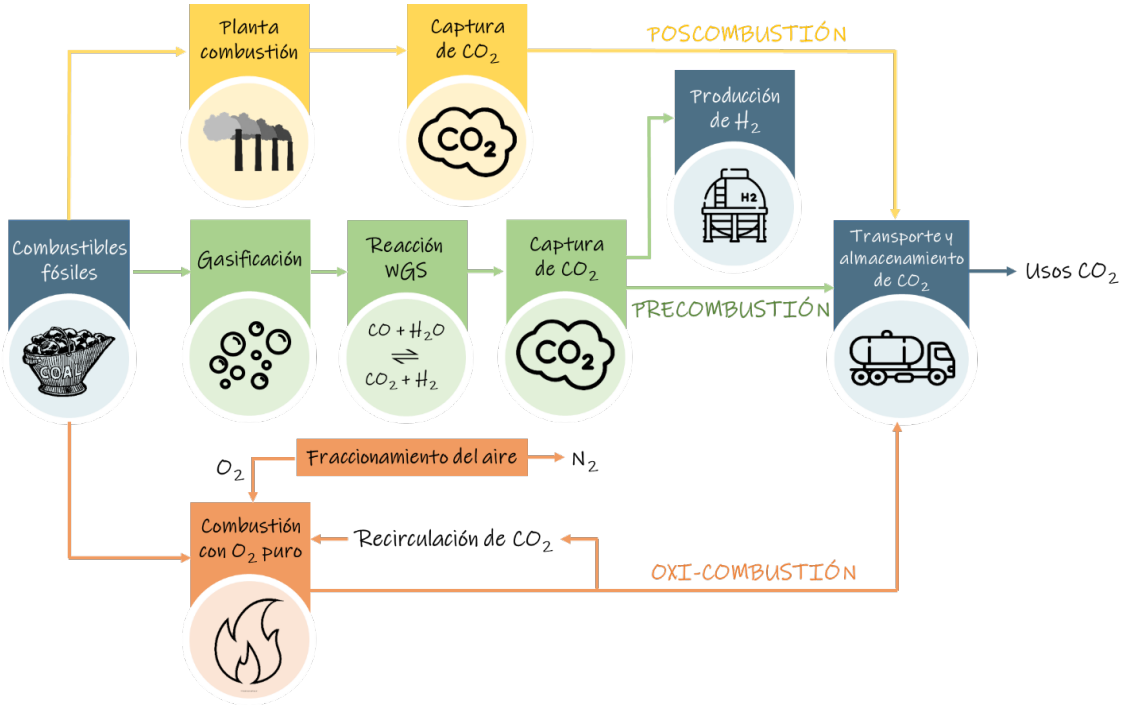

Figure 2.2. Representación esquemática de las tecnologías de captura de CO_2 existentes.

- **<u>Precombustión:</u>** esta tecnología consiste en eliminar el CO_2 del combustible antes del proceso de combustión. Para ello, el combustible se gasifica en una primera etapa, convirtiéndose en gas de síntesis ($CO + H_2$). Posteriormente, el monóxido de carbono se oxida para dar CO_2 mediante la reacción de desplazamiento del gas de agua (abreviada comúnmente como WGSR, proveniente del inglés "*water-gas shift reaction*"), obteniéndose una mezcla H_2/CO_2.[12] Esta mezcla es la que en última instancia deberá separarse para eliminar el CO_2 del H_2, pudiéndose emplear este último como combustible.

- **<u>Oxicombustión:</u>** esta tecnología se caracteriza porque emplea oxígeno puro en lugar de aire para quemar un combustible. Al emplear oxígeno en lugar de aire se reduce el consumo final de combustible, puesto que el N_2 que lleva el aire no se calienta, y son posibles unas mayores temperaturas de llama. Por este motivo, es necesario enfriar los gases de entrada para no dañar los materiales. Dicho enfriamiento se logra recirculando parte de los gases de salida de la combustión,

mayoritariamente CO_2. Además, debido al alto poder oxidante del oxígeno en comparación con el aire, dicha recirculación permite así mismo diluir la concentración de oxígeno que entra en la caldera. Aunque esta tecnología no implica en ningún momento la separación de CO_2, está englobada dentro de las tecnologías CCS puesto que la recirculación de parte del CO_2 saliente disminuye la cantidad emitida a la atmosfera. El inconveniente a tener en cuenta en este tipo de tecnología es la necesidad de obtener oxígeno puro mediante su separación del aire para lo que se utiliza principalmente la destilación criogénica, aunque otras tecnologías con menor consumo de energía como la adsorción y el uso de membranas están siendo más utilizadas a nivel comercial.

- **Poscombustión:** de las tres, es la tecnología menos complicada y, por tanto, más viable industrial y comercialmente, puesto que se basa en incorporar una etapa de separación posterior a la combustión, es decir, básicamente consiste en separar una mezcla CO_2/N_2. Por lo general, el CO_2 sale del proceso de combustión diluido mayormente en N_2, en una concentración de 10-15 % en volumen.[13] El hecho de que se encuentre tan diluido en la corriente gaseosa hace que su separación sea complicada. Actualmente existen diferentes métodos para la separación de CO_2, aunque los más comunes son: absorción (usando un líquido absorbente, generalmente aminas), adsorción (usando sólidos que tengan afinidad por el CO_2) y separación con membranas.[14] Cabe decir aquí que existen corrientes de CO_2 más concentradas (hasta del 30 %), que provendrían de las industrias de producción de acero y cemento, que podrían tratarse por estas mismas técnicas de poscombustión.

En la actualidad, el método más extendido a nivel industrial para la separación de CO_2, dado su desarrollo tecnológico, es la absorción. Sin embargo, esta tecnología no es la ideal, puesto que lleva implícitos muchos inconvenientes derivados especialmente del tipo de compuestos empleados para absorber CO_2. Dichos absorbentes son generalmente aminas, las cuales, además de ser tóxicas, deben regenerarse una vez que han absorbido el CO_2, lo que conlleva un alto gasto energético. Además, tienden a degradarse con el tiempo y la temperatura, se pierde parte debido a la evaporación y son corrosivas.[15,16]

Por su parte, en el método de adsorción, las moléculas de CO_2 se separan de la mezcla gaseosa, o bien formando enlaces químicos con el sólido adsorbente (quimisorción), o adhiriéndose superficialmente al mismo mediante interacciones débiles (fisisorción). Una vez adsorbido el CO_2 al sólido, se regenera dicho material alterando la temperatura y/o presión, consiguiendo desprender el CO_2 adsorbido.[17] El CO_2 que se desorbe puede ser transportado y almacenado en una etapa posterior. Con esta tecnología se pueden conseguir grandes rendimientos de separación de CO_2, sin embargo, conlleva un considerable gasto energético, a lo que se suma la degradación de los materiales adsorbentes con el tiempo.

En este contexto, la tecnología de membranas se posiciona como una alternativa prometedora, debido a su bajo coste, eficiencia energética, baja huella de carbono y fácil escalado.[18]

2.3 Tecnología de membranas

Una membrana se define como una barrera semipermeable que favorece el transporte preferencial de uno o más componentes de una cierta mezcla mediante la acción de una fuerza impulsora (gradiente de presión, de temperatura, de concentración o de potencial eléctrico). Esto permite separar los componentes de la mezcla. De esta manera, el flujo que pasa a través de la membrana se denomina permeado, mientras que el que no lo hace es el retenido (Figura 2.3).

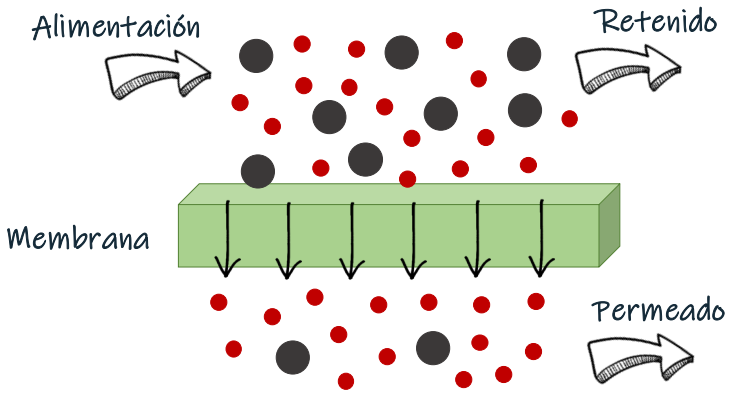

Figure 2.3. Esquema de la separación de dos componentes mediante tecnología de membranas.

Este tipo de tecnología se empleó por primera vez para la separación de sustancias gaseosas en el año 1980, atrayendo una especial atención en el mundo de la investigación e industria debido a sus potenciales ventajas respecto a las demás tecnologías disponibles.[19] Como se ha comentado anteriormente, las membranas permiten reducir no solo la energía necesaria en el proceso de separación, sino también todos los costes de operación derivados de la gestión de los líquidos o sólidos empleados en otro tipo de tecnologías.[20]

Además de separación de gases, la tecnología de membranas también está siendo ampliamente desarrollada en otros procesos de separación como son la micro, ultra y nanofiltración,[21–24] ósmosis inversa,[25,26] pervaporación,[27–29] destilación, destilación osmótica,[30] diálisis[31] o electrodiálisis.[32]

Para que una membrana sea viable industrialmente, debe ser eficiente. Se habla de membrana eficiente cuando tanto la permeabilidad relacionada con el flujo de gas a través de la membrana, como la selectividad, o preferencia de paso de una especie respecto de otra, son elevadas y esta actividad se mantiene, en principio, estable en el tiempo. Conseguir una membrana eficiente depende, entre otros factores, del tipo de membrana y de la naturaleza de los materiales de los que están compuestas.

2.3.1 Tipos de membranas

Existen diversos tipos de membranas que pueden ser clasificadas en función de diversos parámetros como, entre otros, su naturaleza, y su estructura macroscópica o microscópica. La Figura 2.4 esquematiza una clasificación de los tipos de membranas disponibles en función de los parámetros mencionados.

Atendiendo a su naturaleza, las membranas se pueden clasificar en naturales o sintéticas. Dentro de las membranas sintéticas se encuentran a su vez tres tipos de membranas: inorgánicas, poliméricas o mixtas, siendo estas últimas una combinación de las dos anteriores.

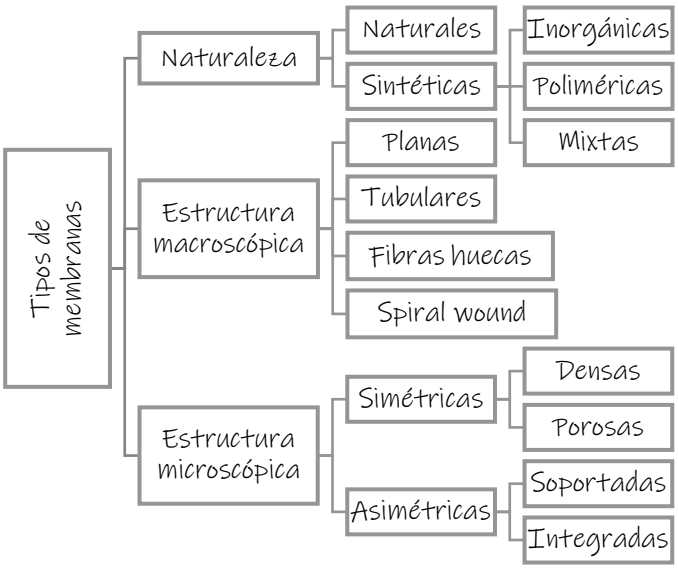

Figure 2.4. Clasificación de los tipos de membranas existentes atendiendo a su naturaleza y estructura macroscópica y microscópica.

Si se tiene en cuenta su estructura macroscópica, se pueden clasificar las membranas en planas, tubulares, de fibra hueca o "*spiral wound*". La diferencia entre las membranas tubulares y las de fibra hueca radica en el diámetro interno, siendo menor en las fibras huecas (inferior a 0.1 μm). Este tipo de membranas, además, suelen emplearse en módulos con varios capilares dispuestos longitudinalmente, lo que hace que sean las más interesantes a nivel industrial, puesto que con ellas se consiguen las mayores áreas por unidad de volumen, es decir, una mayor intensificación del proceso, lo que supone una mayor capacidad de separación. Por su parte, en las membranas de tipo "*spiral wound*" o membranas enrolladas en espiral, la membrana se envuelve alrededor de un núcleo central en forma de espiral.

Por último, se pueden clasificar las membranas en función de su estructura microscópica. De esta forma se pueden encontrar membranas simétricas, pudiendo ser a su vez densas o porosas, o membranas asimétricas, donde se encuentran las membranas soportadas o integradas. Las membranas densas se caracterizan porque son homogéneas, es decir, su estructura no varía a lo largo del espesor de la membrana y, además, todo este espesor es selectivo para la separación. En cambio, se habla de membranas asimétricas cuando estas son heterogéneas en porosidad y estructura, es decir, la selectividad la aporta únicamente la capa superficial habitualmente más densa, mientras que el resto de la membrana posee una estructura altamente porosa que

aporta resistencia mecánica, pero poca resistencia difusional, y no selectividad. En este caso, se definen las membranas soportadas cuando éstas se forman en dos pasos, y además la capa selectiva que se "soporta" es densa y con un espesor muy fino (idealmente, por debajo de 1 µm), mientras que las membranas integradas se forman en un solo paso usualmente mediante el método de inversión de fases.[33] Las membranas soportadas pueden ser compuestas si el material de la capa selectiva es de diferente naturaleza química que el del soporte.

En la Figura 2.5 se muestra de forma más detallada cómo sería la sección transversal de una membrana en función de su estructura microscópica.

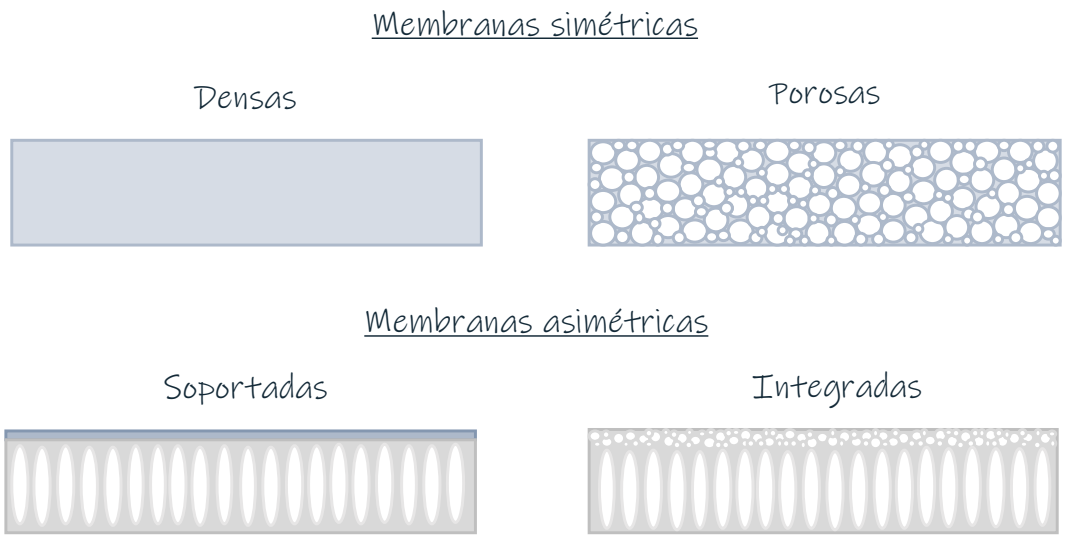

Figure 2.5. Representación esquemática de los tipos de membranas en función de su estructura microscópica.

De todas las conformaciones mencionadas, las membranas densas, aunque suelen ser altamente selectivas, conllevan muy bajos flujos a través de la membrana, puesto que las sustancias a separar tienen que vencer grandes espesores, lo que las hace poco competitivas a nivel industrial.[34] Para afrontar este problema, las membranas asimétricas y/o compuestas ofrecen la posibilidad de obtener igualmente altas selectividades, con la ventaja de tener, así mismo, altos flujos.[35] Es por ello que en la actualidad estas membranas son las que más se utilizan a nivel comercial y están siendo investigadas con especial atención.[36–38]

2.4 Membranas para separación de gases

La elección del material que conforma una membrana para separación de gases es clave en este tipo de aplicaciones. Dicha elección depende, sobretodo, de la mezcla de gases que se pretende separar, ya que, en función de las propiedades físicas y/o químicas del material, este va a presentar más o menos afinidad por una molécula de gas u otra.

Por tanto, se puede indicar que las propiedades de una membrana para separación de gases dependen de:[39]

- El material, puesto que de éste dependen tanto la permeabilidad como los factores de separación (selectividad).
- La estructura microscópica de la membrana donde el espesor selectivo juega un papel fundamental en el flujo.
- La estructura macroscópica de la membrana, que afectará sobre todo a la permeabilidad de la misma.

Por lo general, una membrana para separación de gases debería tener una capa selectiva lo más fina posible, con espesores por debajo de 1 µm, para conseguir altos flujos de gas a través de ella (permeación), así como alta selectividad por el gas que se pretende separar sin olvidar alta resistencia mecánica.[35] Las membranas de capa fina TFC son capaces de proporcionar todas estas características. Generalmente, éstas están compuestas por las siguientes capas (Figura 2.6):

- **Soporte poroso**. Este soporte es generalmente asimétrico y altamente poroso. Por lo general no tiene selectividad por ningún gas y es altamente permeable. Su función es aportar resistencia mecánica a la membrana.

- ***"Gutter layer"***. Se trata de una capa intermedia entre el soporte y la capa selectiva. Generalmente se emplea para evitar la penetración de la capa selectiva en el soporte poroso, lo cual haría que disminuyese drásticamente la permeación, y sería más probable que se formasen defectos en esta última capa. Además, esta capa intermedia ayuda también a reducir la tortuosidad, lo que ayuda a conducir las moléculas de gas hacia los poros del soporte.[40] Como

materiales para esta capa se eligen aquellos que sean, así mismo, altamente permeables.

- **Capa selectiva**. Esta capa estará compuesta del material que se haya elegido para llevar a cabo la separación, es decir, del material selectivo. Además, lo ideal será que el espesor de esta capa se encuentre entre 0,1 y 1,0 µm, para que el flujo a través de ella sea el mayor posible, siempre que no se generen defectos.

- **Capa protectora**. Esta capa es opcional y por lo general se emplea para proteger la capa selectiva en su manejo y reparar los micro-defectos que se hayan podido generar en la capa selectiva. Al igual que la "gutter layer" esta capa debe estar hecha de un material altamente permeable, que no ofrezca ninguna resistencia extra en la separación. Generalmente se suele emplear el mismo material para ambas capas.

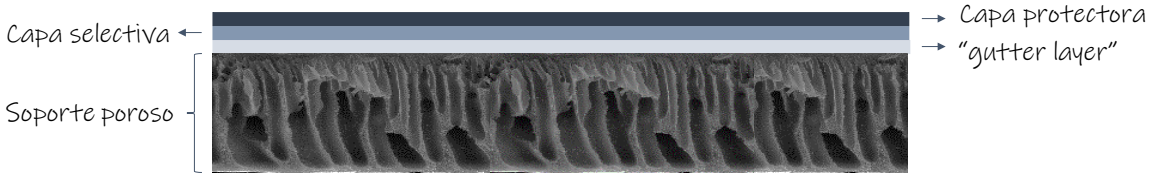

Figure 2.6. Estructura de capas de las membranas de capa fina.

Como se ha mencionado anteriormente, en función del tipo de separación que se quiera llevar a cabo, la elección del tipo de material resulta esencial, puesto que estos materiales pueden tener más o menos afinidad por un tipo de gas u otro. Por ejemplo, en el caso de la separación de mezclas gaseosas de CO_2 con otros gases no polares (N_2, CH_4, $H_{2...}$), la introducción de grupos polares con afinidad por el CO_2 hace que la selectividad de la membrana aumente significativamente.[41]

El óxido de polietileno (PEO) es un buen ejemplo de polímero con alta afinidad por el CO_2. Sin embargo, este material posee una serie de limitaciones que no se pueden pasar por alto, entre ellas, su alta sensibilidad al agua, su baja permeabilidad (debido a la alta cristalinidad de este material) y su baja temperatura de fusión.[42] Para evitar dichas limitaciones, una de las opciones es el entrecruzamiento del PEO, lo que disminuiría la cristalinidad, puesto que se reduciría la movilidad de las cadenas

poliméricas, evitando así su reorganización. Como resultado de la disminución de la cristalinidad y del aumento de la distancia entre cadenas poliméricas, se conseguiría un aumento de la permeabilidad y una disminución de la selectividad.[43,44] Además, se reduciría la sensibilidad de este material al agua y aumentaría su resistencia mecánica. Sin embargo, a pesar de todas estas ventajas, la humedad seguiría teniendo un efecto que no habría que pasar por alto.[45]

Con el fin de conseguir altos flujos, a la vez que alta selectividad y resistencia a la humedad, la copolimerización del PEO con otro tipo de polímeros es una de las técnicas que mejores resultados está arrojando. En la actualidad, existe una gran variedad de copolímeros de bloque compuestos por un segmento flexible de óxido de polietileno, o derivados, y otro rígido de poliamida (PA). Este tipo de copolímeros reciben el nombre de Poli(éter-bloque-amida), o en inglés *"poly(ether-block-amide)" (PEBA)*, y están disponibles comercialmente bajo la marca registrada PEBAX®.

Existen multitud de códigos de PEBAX® disponibles en el mercado, diferenciándose en el tipo de segmentos (PEO y PA) que conforman su estructura, así como en el porcentaje de cada uno de ellos en la matriz polimérica. La Tabla 2.1 muestra algunos ejemplos de códigos de PEBAX® que se pueden encontrar comercialmente, junto con el tipo de segmento y el porcentaje en peso de cada uno de ellos.

El hecho de poseer diferente tipo y proporción de segmento hace que las características de estos copolímeros difieran de unos a otros. Por ejemplo, una mayor concentración de segmento flexible hará que la permeabilidad del CO_2 aumente, debido a las interacciones que se establecen entre este segmento y la molécula de CO_2, que aumenta la solubilidad de este gas en la matriz polimérica. Por otro lado, la longitud de cadena también juega un papel importante, puesto que, por lo general, una mayor longitud de cadena se traduce en un peor empaquetamiento de las cadenas poliméricas, es decir, en una menor cristalinidad. Como ya se ha mencionado, menor cristalinidad, a su vez, se traduce en mayor permeabilidad de CO_2 y menor selectividad. Esto es lo que ocurre con los códigos compuestos de PA12, por ejemplo.

Tabla 2.1. Códigos de PEBAX® que se han utilizado en esta tesis doctoral junto con los segmentos flexible y rígido de los que están compuestos y el porcentaje en peso de segmento flexible. PTMO se refiere a óxido de politetrametileno, PA a poliamida y PEO a óxido de polietileno. El porcentaje en peso (wt%) de segmento flexible se calculó experimentalmente en esta tesis doctoral (capítulo 4).

Código	Segmento flexible	Segmento rígido	wt% (segmento flexible)
1657	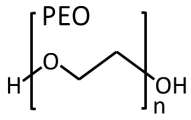	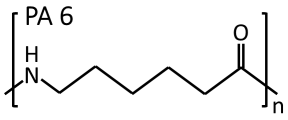	59
2533	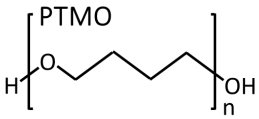	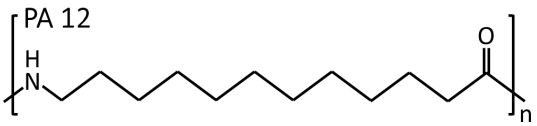	84
3533	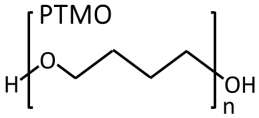	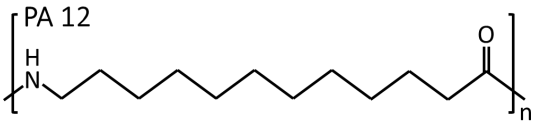	77
4533	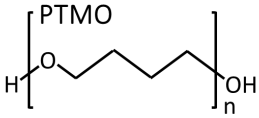	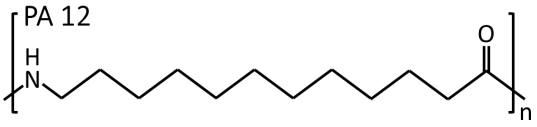	55
Renew® 30R51	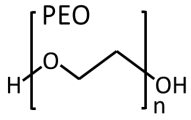	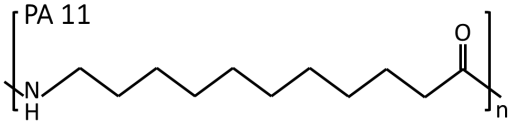	81

Además de estas características, otras como la resistencia mecánica o la capacidad de absorción de agua, etc. también varían de unos códigos a otros. Todas estas características, efectividad de separación de gases, así como resistencia mecánica o la absorción de agua, son factores que deben tenerse en cuenta a la hora de seleccionar un código para la aplicación final a la que estará destinado.

2.4.1 Mecanismos de transporte de gas

El mecanismo por el cual un gas se transporta a través de una membrana depende fundamentalmente de la estructura de esta, es decir, de si se trata de una membrana porosa o densa. En el caso de las membranas porosas, se establecen cinco tipos de mecanismo diferentes: difusión Knudsen, tamizado molecular, flujo viscoso tipo Hagen-Poiseuille, difusión superficial y condensación capilar. Que se dé uno u otro dependerá básicamente del tamaño de poro que tenga la membrana. En membranas densas, el tipo de transporte más aceptado es el de disolución-difusión. A continuación, se explica más detalladamente cada tipo de mecanismo. Así mismo, en la Figura 2.7 se muestra esquemáticamente cada uno de ellos.

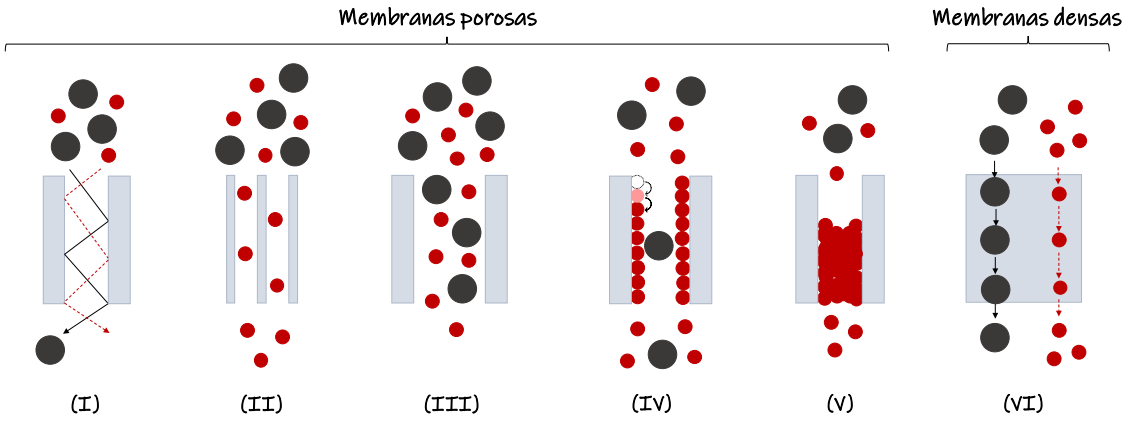

Figure 2.7. Representación esquemática de los tipos de mecanismos de transporte que se pueden dar en una membrana. (I) Difusión Knudsen, (II) tamizado molecular, (III) flujo viscoso tipo Hagen-Poiseuille, (IV) difusión superficial, (V) condensación capilar y (VI).

- **Difusión Knudsen.** La difusión Knudsen se considera un mecanismo de transporte selectivo, puesto que los flujos de difusión son inversamente proporcionales a las raíces cuadradas de las masas moleculares de las sustancias que se quieren separar. De esta manera, la velocidad de las moléculas disminuye a medida que aumenta su masa molecular.[46] Por lo general, este tipo de mecanismo ocurre en membranas mesoporosas que de acuerdo a la clasificación de la IUPAC tienen tamaños de poro comprendidos entre 2 y 50 nm. Este mecanismo que seguramente deja ya de ser influyente cuando se acerca al valor

de 50 nm puede combinarse con otros mecanismos aquí comentados como condensación capilar, difusión superficial o tamizado molecular.

- **Tamizado molecular.** El mecanismo de separación por tamizado molecular se basa en la exclusión por tamaño y forma de las moléculas. Dicho en otras palabras, solo las moléculas con diámetros cinéticos lo suficientemente pequeños pueden atravesar la membrana.[47] Este tipo de mecanismo predomina en membranas con microporos, es decir, tamaños de poro según la clasificación de la IUPAC inferiores a 2 nm, siendo posible encontrarlo también en membranas de mayor tamaño a 2 nm.

- **Flujo viscoso tipo Hagen-Poiseuille.** En este tipo de mecanismo solo existe la separación que da la difusión ordinaria si no hay diferencia de presión. Se da cuando los poros de la membrana son lo suficientemente grandes como para que no se dé la separación por difusión Knudsen. Por lo general, este tipo de mecanismo se asocia a defectos en la membrana.

- **Difusión superficial.** Este tipo de mecanismo implica el movimiento de las moléculas de gas en la superficie de los poros de materiales sólidos, "saltando" entre sitios de adsorción adyacentes de dicha superficie. Este mecanismo puede proporcionar altas selectividades en membranas micro y mesoporosas, ya que la adsorción preferencial y la elevada presión relativa de uno de los componentes de la mezcla a separar, respectivamente, juegan un papel fundamental.

- **Condensación capilar**. Este mecanismo ocurre cuando los poros de la membrana son lo suficientemente pequeños (< 3 nm) como para que las moléculas de gas condensen en la superficie del poro creando múltiples capas moleculares del mismo hasta que la cavidad se llena por completo.[48] Una característica importante de este tipo de transporte es que se produce cuando la presión de vapor es inferior a la de saturación del gas, a diferencia de la condensación propiamente dicha.

- **<u>Modelo de disolución-difusión.</u>** Este mecanismo se da en membranas densas sin defectos. El modelo de disolución-difusión fue propuesto por primera vez en 1965 por Lonsdale y cols.[49,50] para explicar el transporte a través de membranas de ósmosis inversa. Posteriormente, fue adaptado para explicar el mecanismo de transporte de moléculas gaseosas a través de membranas poliméricas densas. El modelo consta básicamente de tres etapas. En un primer instante (etapa 1), las moléculas de gas que entran en contacto con la membrana por el lado de la alimentación (donde la fuerza impulsora es mayor), se solubilizan en la superficie de esta. Posteriormente (etapa 2), estas moléculas de gas solubilizadas difunden atravesando el espesor de la membrana para, por último (etapa 3), desorberse en el lado del permeado.[51]

2.4.1.1 Modelo de disolución-difusión

En el modelo de disolución-difusión en gases, la fuerza impulsora es habitualmente el gradiente de concentración y el flujo a través de una membrana densa se puede explicar mediante la Ley de Fick (ecuación 2.1).

$$J_i = -D_{i,m} \frac{dc_{i,m}}{dx} \qquad \text{(eq. 2.1)}$$

donde J_i es el flujo del compuesto i en mol m^{-2} s^{-1}, $D_{i,m}$ es el coeficiente de difusión de i en la membrana en m^2 s^{-1}, $c_{i,m}$ es la concentración de i en la membrana en mol m^{-3} y x, la posición en la dirección del flujo en m.

Al integrar la ecuación 2.1, tomando como límites ambos lados de la membrana (alimentación y permeado), se obtiene la siguiente expresión (ecuación 2.2):

$$J_i = D_{i,m} \frac{\Delta c_{i,m}}{l} \qquad \text{(eq. 2.2)}$$

donde $\Delta c_{i,m}$ es la diferencia de concentración del componente i solubilizado entre el retenido y el permeado, y l, el espesor de la misma.

La concentración del componente i solubilizado , a su vez, se expresar como el producto de la solubilidad de dicho compuesto i en la membrana ($S_{i,m}$) y su presión parcial (p_i), mediante la Ley de Henry (ecuación 2.3).

$$c_{i,m} = S_{i,m} \cdot p_i \qquad \text{(eq. 2.3)}$$

Por tanto, combinando las ecuaciones 2.2 y 2.3 y suponiendo la solubilidad del compuesto i constante a lo largo de la membrana, se obtiene la siguiente expresión (ecuación 2.4):

$$J_i = D_{i,m} \cdot S_{i,m} \frac{\Delta p_i}{l} \qquad \text{(eq. 2.4)}$$

donde Δp_i es la variación de presión parcial entre ambos lados de la membrana.

Por otro lado, el flujo de gas a través de la membrana es directamente proporcional a la permeabilidad de la misma (P_i), y se puede expresar de la siguiente manera (ecuación 2.5):

$$J_i = P_i \frac{\Delta p_i}{l} \qquad \text{(eq. 2.5)}$$

Sustituyendo esta expresión en la ecuación 2.4, y simplificando términos, podemos relacionar la permeabilidad de un gas a través de una membrana con su solubilidad y difusión a través de la misma, siendo en este caso directamente proporcional al producto de los mismos, como sigue (ecuación 2.6):

$$P_i = S_{i,m} \cdot D_{i,m} \qquad \text{(eq. 2.6)}$$

Esta expresión es la que define de manera general el mecanismo de transporte de un compuesto i en fase gas mediante el modelo de disolución-difusión. Estos tres parámetros, permeabilidad, solubilidad y difusión, son propiedades intrínsecas del material que conforma la membrana. La solubilidad indica la cantidad del compuesto i que puede solubilizarse en la membrana, mientras que la difusión se refiere a la velocidad con la que dicho compuesto se mueve a través de ella, y la permeabilidad está relacionada con el flujo de gas que es capaz de atravesar la membrana. En separación de gases, la unidad de permeabilidad más empleada es el Barrer (1 Barrer = 1×10^{-10} cm^3(STP) cm cm^{-2} s^{-1} $cmHg^{-1}$), siendo un parámetro clave para definir el desempeño de una membrana para separación de gases. Sin embargo en membranas de capa fina resulta muy difícil calcularlo, puesto que el espesor de la membrana no se puede medir con exactitud y lo que es más determinante, en estas membranas se reduce el espesor (la permeabilidad es independiente de este) con el fin de maximizar el flujo y, por tanto, la comparación entre membranas se debe hacer con el parámetro denominado

permeación (Q_i), que no es más que el cociente entre la permeabilidad y el espesor de la membrana (ecuación 2.7).

$$Q_i = \frac{P_i}{l} \qquad \text{(eq. 2.7)}$$

Este parámetro refleja la resistencia a la transferencia de materia a través de la membrana, y suele expresarse en unidades de GPU (del inglés "*gas permeation unit*", unidad de permeación de gas), siendo 1 GPU = 1 × 10^{-6} cm^3(STP) cm^{-2} s^{-1} $cmHg^{-1}$. Cuando se tiene una membrana de 1 µm de espesor, un Barrer de permeabilidad equivale a 1 GPU de permeación.

Además de la permeabilidad y la permeación, otro parámetro que refleja el rendimiento de una membrana es la selectividad. La selectividad (α_{ij}), indica la capacidad de la membrana de separar una mezcla de dos compuestos (i,j) y se puede calcular como el cociente de permeabilidades o permeaciones de cada compuesto, de la siguiente manera (ecuación 2.8):

$$\alpha_{ij} = \frac{P_i}{P_j} = \frac{Q_i}{Q_j} = \frac{S_{i,m} \cdot D_{i,m}}{S_{j,m} \cdot D_{j,m}} \qquad \text{(eq. 2.8)}$$

siendo P_i, Q_i, $S_{i,m}$ y $D_{i,m}$, la permeabilidad, permeación, solubilidad y difusión del gas más permeable, respectivamente, y P_j y Q_j, $S_{j,m}$ y $D_{j,m}$, las del menos permeable. Al tratarse de un cociente, este parámetro es adimensional. Se puede observar en la ecuación 2.8 como la selectividad sería un producto de selectividades de solubilidad (cociente de solubilidades) y difusión (cociente de difusiones).

2.4.1.2 Modelo de resistencias en serie

En el caso de membranas compuestas, como la de la Figura 2.8, donde la membrana está formada por varias capas de diferentes polímeros, así como diferentes estructuras, las moléculas de gas deben atravesar cada una de las capas de las que está compuesta dicha membrana. Cada una de estas capas ofrece una resistencia a la transferencia de materia. Para explicar el transporte a través de estos sistemas surge el modelo de resistencias en serie.

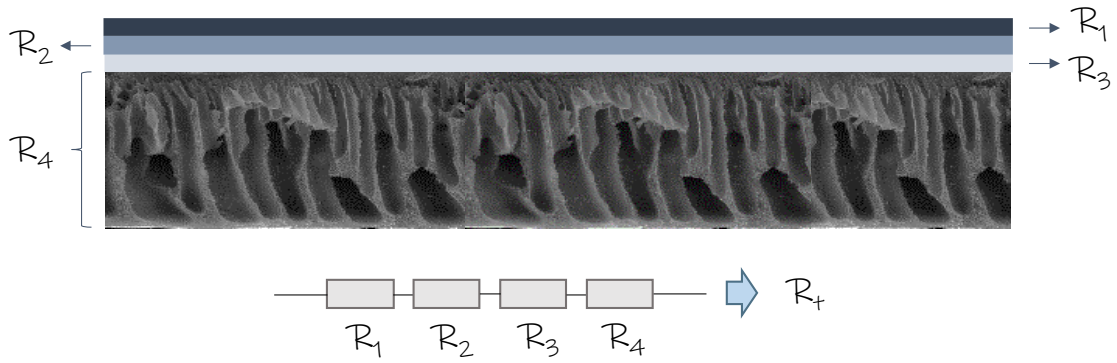

Figure 2.8. Ejemplo de aplicación del modelo de resistencias en serie en una membrana compuesta por un total de 4 capas.

Este modelo fue propuesto por Henis y Tripodi en 1980,[52] y considera que la resistencia al flujo de gas es análoga, en sentido matemático, a la resistencia eléctrica en un circuito eléctrico. Dicha resistencia (R) al flujo viene representada por la ecuación 2.9:

$$R = \frac{l}{P_i \cdot A} \qquad \text{(eq. 2.9)}$$

donde l es el espesor del material, P_i es la permeabilidad del material para el gas i, y A el área superficial de permeación del material.

De acuerdo a este modelo, en una membrana compuesta de varias capas, cada una de ellas ofrecerá una resistencia al flujo, de manera análoga a lo que ocurre en un circuito eléctrico (Figura 2.9). Por tanto, la Resistencia total (R_t) puede expresarse como la suma de cada una de dichas resistencias, de la siguiente manera (ecuación 2.10):

$$R_t = R_1 + R_2 + \cdots + R_i \qquad \text{(eq. 2.10)}$$

Es por ello que, para evitar que las resistencias ofrecidas por las capas adicionales a la capa selectiva sean altas y restrinjan el paso de los gases a través de la membrana, los materiales que conforman dichas capas deben elegirse minuciosamente. Se elegirán siempre materiales con elevada permeabilidad, para que la resistencia ofrecida por esas capas pueda considerarse despreciable en comparación con la ofrecida por la capa selectiva.

2.4.1.3 Parámetros que afectan al transporte de gas a través de una membrana

Ciertos factores afectan al transporte de gas a través de una membrana, entre ellos, el tamaño y forma de las moléculas de gas que se pretenden separar, así como su condensabilidad, además de otros parámetros operacionales como la temperatura o presión de trabajo y las propiedades del material del que está compuesta la membrana. Mientras que con los dos primeros no se puede hacer nada, los últimos pueden modificarse para lograr mayores rendimientos de separación. A continuación, se detalla cómo afecta cada uno de estos parámetros al transporte de gas a través de una membrana.

- **Tamaño y forma de las moléculas de gas.** Por lo general, el flujo será mayor para aquellos gases con menores tamaños moleculares, ya que son estos los que más rápido difunden a través de la membrana. Además del tamaño, la forma de las moléculas de gas a separar también es un factor importante, puesto que la difusión de estas también se ve afectada por ella. Por ejemplo, en el caso de tener dos moléculas de gas con la misma masa molecular, difundirá más rápido aquella que tenga una dimensión limitante menor. En la Tabla 2.2 se recogen los diámetros cinéticos de algunos gases de interés.

Tabla 2.2. Diámetros cinéticos de algunos gases de interés

Gas	H_2	CO_2	O_2	N_2	CH_4
Diámetro cinético (nm)	0,289	0,330	0,346	0,364	0,380

- **Condensabilidad de los gases.** A diferencia del tamaño y forma molecular, la condensabilidad de los gases afecta a la solubilidad de estos en el material. Este parámetro está relacionado con la temperatura crítica (T_c). Algunos valores de T_c están recogidos en la Tabla 2.3.

Tabla 2.3. Valores de temperatura crítica de algunos gases de interés.

Gas	H_2	CO_2	O_2	N_2	CH_4
Temperatura crítica (T_c) (K)	33	304	155	126	191

Generalmente, la solubilidad de un gas aumenta a medida que lo hace su condensabilidad. Por este motivo, en mezclas CO_2/N_2 o CO_2/CH_4, el flujo de CO_2 a través de la membrana no sólo se ve favorecido por su menor tamaño molecular respecto de la otra molécula gaseosa, sino que también está favorecido por su mayor solubilidad. En el caso de separaciones de mezclas H_2/CO_2, sin embargo, existe cierta competencia entre qué parámetro gobierna la separación (solubilidad o difusión), puesto que, a pesar de que el H_2 tiene un menor tamaño molecular, por lo que difundiría más rápido que el CO_2 a través de la membrana, la condensabilidad de este gas es muy inferior a la del CO_2, lo que significa que la solubilidad de este último es superior a la del H_2. Para solventar este problema, la separación de este tipo de mezclas se suele realizar a temperaturas elevadas donde predominan los efectos difusionales.

- **Temperatura de operación.** La temperatura de operación afecta tanto a la difusión como a la solubilidad de los gases. Por tanto, el producto final de la permeabilidad también se verá afectado por los cambios en la temperatura a la cual se lleve a cabo la separación. La relación entre permeabilidad y temperatura de operación se puede dar por la ecuación de Arrhenius de la siguiente manera (ecuación 2.11):[53]

$$P_i = P_{0i} \cdot \exp\left(\frac{-E_{p,i}}{R \cdot T}\right) \qquad \text{(eq. 2.11)}$$

donde P_i es la permeabilidad del gas i en Barrer, P_{0i} el factor pre-exponencial del gas i en Barrer, $E_{p,i}$ es la energía de activación aparente de la permeación de i en J mol^{-1}, R es la constante de los gases ideales, 8,314 J mol^{-1} K^{-1}, y T la temperatura de operación en K.

Si tenemos en cuenta la ecuación 2.6, la permeabilidad es el resultado del producto de la solubilidad y la difusión, y es sabido que la difusión se ve favorecida al aumentar la temperatura de operación puesto que aumenta la difusividad de las moléculas y el movimiento de las cadenas poliméricas lo que por tanto implicaría energías de activación positivas, mientras que la solubilidad disminuye con el aumento de temperatura al tratarse de un proceso exotérmico con calores de adsorción negativos. A pesar de que ambos coeficientes

evolucionan de forma opuesta, habitualmente el término de difusión predomina sobre el de solubilidad, traduciéndose finalmente en un aumento de la permeabilidad con la temperatura. En gases condensables como el CO_2, la energía de activación es menor que en gases no condensables, ya que en la $E_{p,i}$ influye en el calor de adsorción que como se ha indicado es negativo, por lo que la selectividad respecto del CO_2 disminuirá con el aumento de temperatura.

- **Presión.** La presión de trabajo y en concreto la presión parcial del compuesto a permear puede influir en los parámetros de solubilidad y difusión de los gases, y, por ende, en la permeabilidad. Además, en el caso de gases muy solubles como el CO_2. se puede producir el fenómeno denominado plastificación, si la presión de CO_2 es lo suficientemente elevada, y que se ha visto que puede evitarse gracias al uso de ciertos rellenos como los MOF.[54] En general con la presión, se observa una disminución en la permeabilidad al gas con el aumento de la presión de alimentación debido a la compresión del polímero. Esto ocurre hasta que se produce la plastificación. En la presión de plastificación, la concentración de CO_2 es lo suficientemente alta como para "hinchar" el polímero, por lo que aumenta el volumen libre, así como la movilidad de las cadenas poliméricas que forman la membrana aumentando con ello los coeficientes de difusión del gas. Debido a este efecto, la permeabilidad de todos los gases (no solo del CO_2) aumenta irreversiblemente, dando lugar además a una disminución de la selectividad de los gases condensables respecto de los no condensables.[55,56]

- **Propiedades del material.** Referido al volumen libre entre cadenas de polímero, así como a la movilidad de las mismas. Como norma general, al aumentar tanto el volumen libre (FFV, del inglés "*free fractional volume*") como la movilidad de las cadenas poliméricas, el coeficiente de difusión aumenta, provocando también un aumento de la permeabilidad de gas. La introducción de grupos voluminosos, el entrecruzamiento de las cadenas poliméricas, o la síntesis de copolímeros de bloque (ver apartado 2.4), por ejemplo, pueden ayudar a modificar estas propiedades, pudiendo conseguir de esta forma materiales adaptados a la aplicación final.

2.4.2 Limitaciones de las membranas para separación de gases

Las membranas poliméricas presentan algunas limitaciones en su eficiencia en la separación de gases. Por lo general, las membranas que son muy permeables, son poco selectivas, de igual forma que las membranas con elevada selectividad suelen ser poco permeables. Está limitación hace que las membranas poliméricas se encuentren lejos de ser comercialmente atractivas, puesto que para ello lo ideal sería encontrar una membrana que fuese igualmente altamente permeable y selectiva. La relación entre permeabilidad y selectividad fue establecida en 1991 por Robeson,[57] el cual definió el "límite superior de Robeson". Este límite se estableció a partir de más de 300 referencias donde se habían reportado datos de permeabilidad y selectividad de membranas poliméricas. En 2008, Robeson volvió a revisar dicho límite, incorporando nuevas referencias, así como otras mezclas de interés como CO_2/N_2.[4] Recientemente, en 2019, Comesaña-Gándara y cols.[58] redefinieron los límites de Robeson para las mezclas CO_2/N_2 y CO_2/CH_4. Para ello, emplearon una serie de polímeros ultra-permeables con micro-porosidad intrínseca basados en benzotripticeno.

Este límite superior se representa en un gráfico en escala logarítmica, donde en el eje de abscisas aparece la permeabilidad del gas más permeable (P_i), y en el eje de ordenadas, el factor de separación o selectividad (α_{ij}). De esta manera, la ecuación que representa dicho límite es una expresión del tipo $P_i = k\alpha_{ij}^n$, donde k es el factor preexponencial. Además, la pendiente de esta ecuación, una vez linealizada (n), puede considerarse en algunos casos relacionada con la diferencia entre los diámetros moleculares de los gases que se representan.

En la Figura 2.9, se representa un ejemplo de este tipo de diagrama, para la mezcla CO_2/N_2. En este gráfico, los puntos rojos corresponden a los datos de separación de las referencias bibliográficas empleadas por Robeson. Teniendo en cuenta este límite, el desafío es conseguir una membrana capaz de sobrepasarlo, llegando a obtener de esta manera una membrana comercialmente atractiva.

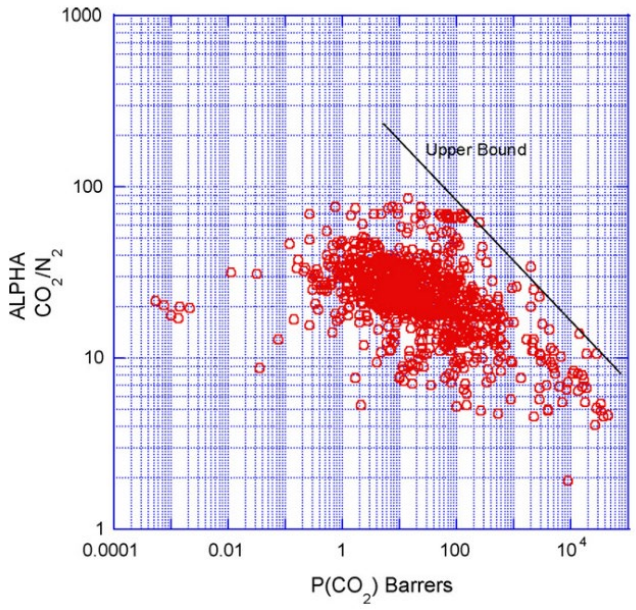

Figure 2.9. Límite superior de Robeson (2008) para la mezcla CO2/N2 (imagen reproducida del artículo "The upper bound revisited. L. M. Robeson, J. Membr. Sci 2008 320, 390-400", copyright 2008, con permiso de Elsevier).[4]

Además de la modificación del material polimérico en sí mismo, la incorporación de materiales de relleno en la matriz polimérica es una de las estrategias que más atención está atrayendo en el mundo de la investigación, ya que es una manera sencilla de modificar el transporte de gas, pudiendo además seleccionar las propiedades de dichos materiales de relleno en función de los requerimientos finales. Las membranas que incorporan materiales de relleno en su estructura reciben el nombre de **membranas de matriz mixta (MMM)** (Figura 2.10). Además, cabe mencionar que estos materiales de relleno también se pueden emplear para limitar el envejecimiento físico que sufren algunas membranas poliméricas constituidas por ciertos polímeros vítreos (como, por ejemplo, poly(trimetilsililpropino) (PTMSP) o polímeros con microporosidad intrínseca (PIM)) y que se traduce en una reducción de la permeabilidad con el tiempo.[59]

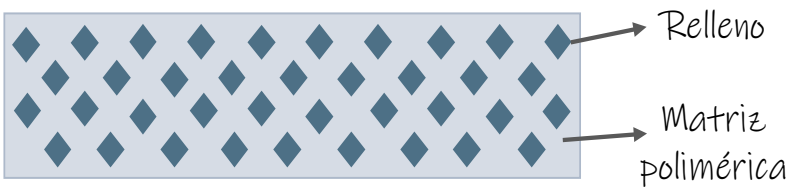

Figure 2.10. Esquema de una membrana de matriz mixta (MMM).

Existen multitud de materiales que pueden emplearse como relleno en este tipo de membranas, pudiendo ser de origen inorgánico, orgánico o incluso, una combinación de ambos, además de los materiales derivados del carbono. Entre los materiales inorgánicos más empleados encontramos las zeolitas,[60,61] entre los materiales orgánicos, otros polímeros o los llamados COF ("*covalent organic framework*")[62,63] y entre los derivados del carbono, el grafeno o los nanotubos de carbono.[64,65]

Los materiales inorgánicos que inicialmente fueron los más utilizados, a pesar de arrojar propiedades de separación de gases mejoradas, tienden a generar problemas a medida que se incrementa la carga de los mismos en la matriz polimérica. Esto es debido a la incompatibilidad de estos materiales con el polímero, siendo este un material orgánico. La falta de compatibilidad puede dar como resultados una mala dispersión de las partículas en la matriz polimérica, que puede conllevar a la generación de agregados y defectos en el interior de la membrana. Como se ha visto en el apartado 2.4.1, dichos defectos cambian el tipo de flujo a través de la membrana, volviéndose no selectiva.

Como alternativa a estos materiales inorgánicos, han surgido en los últimos años los denominados compuestos metal-orgánicos porosos (MOF). Estos compuestos, además de tener unas propiedades muy interesantes para la separación de gases, poseen una matriz híbrida, es decir, combinan partes inorgánicas y orgánicas en su estructura, lo que aumenta su compatibilidad con el material polimérico con respecto a los materiales inorgánicos como las zeolitas. En la siguiente sección se describen de manera más detallada estos compuestos.

2.5 Compuestos metal-orgánicos porosos (MOF)

Los compuestos metal-orgánicos porosos (MOF), también denominados polímeros de coordinación porosos (PCPs, del inglés "*porous coordination polymers*"), son materiales cristalinos constituidos por un ion o clúster metálico unido mediante enlaces de coordinación a ligandos orgánicos, formando de esta manera redes uni-, bi- y tri-dimensionales[66] (Figura 2.11).

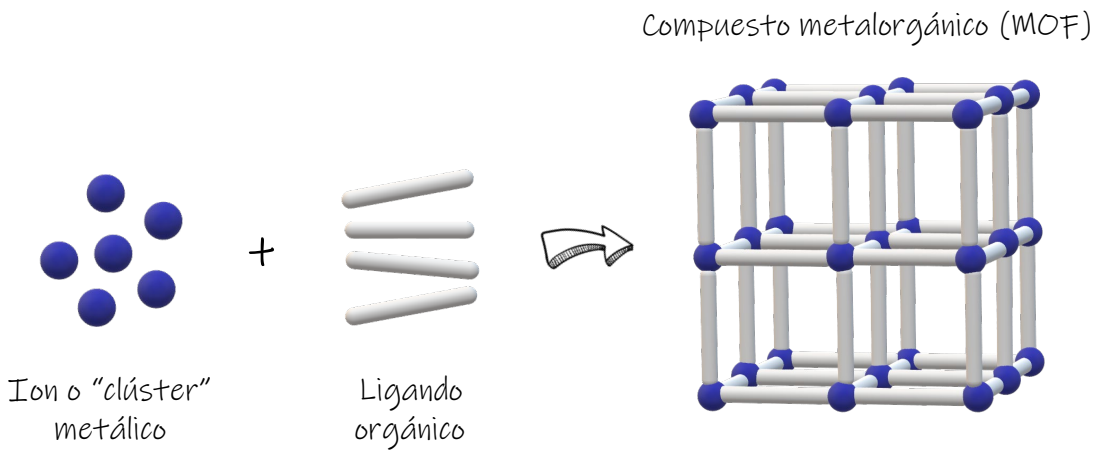

Figure 2.11. Representación esquemática de la formación de una red tri-dimensional cristalina mediante la reacción de un ion o "clúster" metálico y un ligando orgánico.

Aunque los primeros trabajos que aparecieron en la literatura referidos a polímeros de coordinación son anteriores a 1990, no fue hasta mediados de esta década cuando empezaron a aparecer los primeros estudios relacionados con el diseño y la construcción de este tipo de materiales,[67] que de forma generalizada mostraban porosidad permanente. Desde entonces, estos compuestos han ido emergiendo como materiales adsorbentes en multitud de aplicaciones, desde la separación y almacenamiento de gases, pasando por la nanofiltración,[68,69] la catálisis,[70,71] la adsorción propiamente dicha[72,73] o la encapsulación,[74,75] entre otras.

El hecho de que estos materiales hayan recibido tanta atención en los últimos años se debe, principalmente, a sus propiedades. Entre las más destacables se encuentran su elevada porosidad (con más de un 90% de volumen libre en algunos casos) y área superficial, siendo los materiales con las mayores áreas superficiales reportadas hasta la fecha, algunos de ellos llegando a aportar un área superficial interna por encima de los 6000 m^2g^{-1}.[76] Así mismo, la posibilidad de modificar el tamaño de poro o la química de

estos compuestos variando el tipo de clúster metálico o ligando orgánico, así como las condiciones de reacción,[77] los hace ser unos materiales muy versátiles. Por otro lado, hay que destacar también su elevada compatibilidad con los materiales poliméricos que suelen conformar las membranas para separación de gases. Esta gran compatibilidad se debe a la buena interacción que existe entre la parte orgánica de la red cristalina y el polímero orgánico.

A pesar de estas ventajas, es importante señalar alguna de las desventajas que presentan estos materiales con respecto a otros compuestos porosos de origen inorgánico. Entre estas desventajas se encuentra su menor estabilidad térmica, llegando a degradarse a temperaturas entre los 250 y 500 °C, debido a la presencia de parte orgánica en su estructura. Por otro lado, cabe destacar también la necesidad de llevar a cabo un proceso de activación durante la preparación de los MOF, dado que, al tener porosidades tan elevadas, parte del disolvente con el cual se ha llevado a cabo la reacción (en el caso de que se haya sintetizado en disolución) puede quedar ocluido en dichos poros. De igual forma, durante el proceso de síntesis, para aumentar el rendimiento de la reacción, se suele trabajar con exceso de ligando orgánico, por lo que además del proceso de activación, se debe llevar a cabo otro previo de lavado, para eliminar dicho ligando sin reaccionar del medio.

En la bibliografía, existen multitud de compuestos metal-orgánicos porosos, los cuales difieren en su forma, tamaño, estructura, área superficial o cristalinidad, entre otras propiedades. El primer denominado MOF fue reportado en 1995 por Yaghi y su grupo de investigación.[7] Este MOF estaba basado en un clúster metálico de cobalto y 1,3,5-bencenotricarboxilato como ligando orgánico. Dentro de la familia de los MOF, cabe destacar el HKUST-1 ("The Hong Kong University of Science and Technology")[78] siendo de los primeros MOF sintetizados, la familia de los MOF denominados MIL ("Materiaux de l'Institut Lavoisier")[79] algunos de ellos con el denominado fenómeno de respiración (cambios en la estructura con moléculas huésped), los ZIF ("*zeolitic imidazolate framework*") y los UiO ("University of Oslo").[80] A estas dos últimas familias pertenecen los MOF empleados en la presente tesis doctoral para su aplicación en membranas para separación de gases por lo que se detallan a continuación.

2.5.1 ZIF

Los ZIF consisten en clústeres metálicos de zinc o cobalto coordinados tetraédricamente con ligandos orgánicos tipo imidazolato (Im).[81] Reciben su nombre debido a la similitud que existe entre la topología de estos materiales y la de las zeolitas. En los ZIF dos iones metálicos están enlazados con un imidazolato en un ángulo de enlace de aproximadamente 145°, análogo al ángulo del enlace Si-O-Si de las zeolitas (Figura 2.12). Al igual que los MOF, estos materiales también poseen todas las ventajas anteriormente citadas.

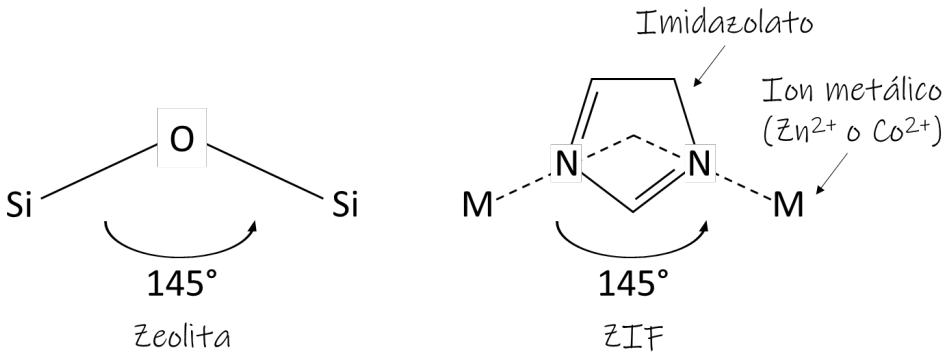

Figure 2.12. Comparación del ángulo de enlace de de las zeolitas y los ZIF.

A continuación, se van a explicar más detalladamente el ZIF-8 y ZIF-94.

2.5.1.1 ZIF-8

El ZIF-8 es el ZIF más ampliamente estudiado para membranas de separación de gases. Está compuesto por el ion metálico de zinc (Zn^{2+}) y el ligando orgánico 2-metilimidazol (2mIm) (Figura 2.13). Con una masa molar de 229.50 g mol^{-1}, cristaliza formando una estructura **sod** (ver en la Figura 2.13) y tiene un diámetro de la cavidad de 1.16 nm con una apertura de poro de 0.34 nm.[82]

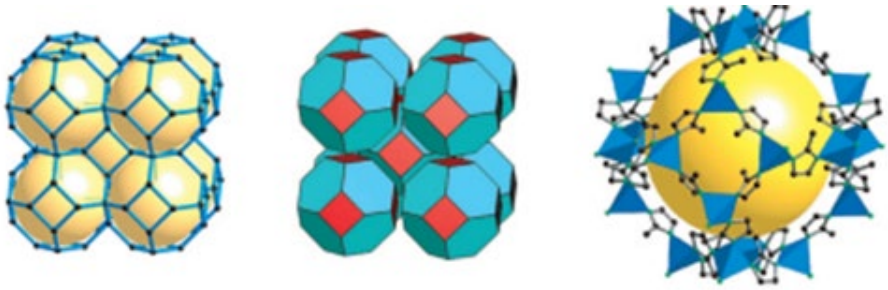

*Figure 2.13. Estructura del ZIF-8. Las imágenes de la izquierda y el medio representan la estructura **sod** típica del ZIF-8. En la derecha, en azul, se muestran los clústeres tetraédricos ZnN_4, los átomos de C se representan en negro, los de N en verde indicando la esfera amarilla el espacio de la cavidad. Los átomos de H se han omitido por claridad. (Reproducida con permiso de "Exceptional chemical and termal stability of zeolitic imidazolate frameworks. Kyo Sung Park et al. PNAS **2006**, 103, 10186-10191" Copyright (2006) National Academy of Sciences, U. S. A.).*[83]

Este ZIF, además, posee una elevada resistencia térmica (450-550 °C) y química, siendo estable en agua hirviendo y otros disolventes orgánicos como el metanol, benceno, o incluso en disolución acuosa de hidróxido de sodio.[83]

2.5.1.2 ZIF-94

Este ZIF también conocido como SIM-1 ("*Substituted Imidazolate Material-1*") (Figura 2.14), al igual que el ZIF 8, está compuesto de iones metálicos de zinc (Zn^{2+}) coordinados con ligandos 4-metil-5-imidazolcarboxialdehido (4m5Imca) en una estructura tipo **sod,** con una masa molecular de 283.38 g mol^{-1}, un diámetro de la cavidad de 0.96 nm y una apertura de poro de 0.26 nm.[84]

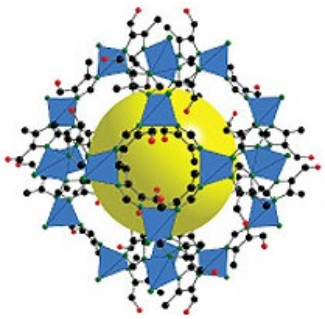

Figure 2.14. Estructura del ZIF 94. En azul se muestran los clústeres tetraédricos ZnN_4, los átomos de C se representan en negro, los de N en verde y los de O en rojo, indicando la esfera amarilla el espacio de la cavidad. Los átomos de H se han omitido por claridad. (Reproducida con permiso de "A combined Experimental-Computational Investigation of Carbon Dioxide Capture in a Series of Isoreticular Zeolitic Imidazolate Frameworks. W. Morris et al., J. Am. Chem. Soc. 2010, 132, 32, 11006-11008" Copyright (2010) American Chemical Society).[85]

Las ventajas de este ZIF con respecto al ZIF-8 son su carácter hidrófilo[69] y su mayor capacidad de adsorción de CO_2, llegando a ser esta tres veces mayor para el ZIF-94 que para el ZIF-8 (2.4-2.9 mmol g^{-1} para el ZIF-94 vs. 0.7 mmol g^{-1} para el ZIF-8, medidas ambas a 1 bar y 25 °C).[86] En cuanto a estabilidad térmica, este ZIF empieza a degradarse a 350 °C.

2.5.2 UiO-66, UiO-66-NH_2 y UiO-66-NO_2

El UiO-66 (Figura 2.15) es un MOF isorreticular basado en circonio (Zr), en el que el ligando orgánico es tereftalato (BDC, 1,4-bencendicarboxilato). Este material fue reportado por primera vez por Cavka y cols. en 2008.[80] La estructura de este MOF posee ventanas triangulares de 0.6 nm que conectan dos tipos de cavidades: octaédricas de 1.1 nm y tetraédricas de 0.8 nm.

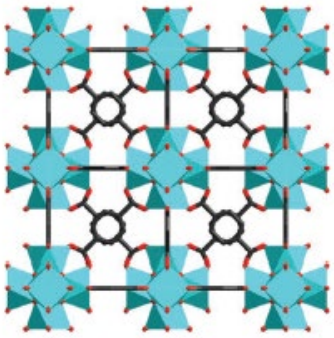

Figure 2.15. Estructura del UiO-66. En rojo se representan los átomos de O, en negro los de C y en azul los clústeres de Zr. Los átomos de H se han omitido por claridad. (Reproducida con permiso de "Stable Metal-Organic Frameworks: Design, Synthesis, and Applications. S. Yuan et al. Adv. Mater. 2018, 30, 1704303" Copyright (2018) WILEY-VCH Verlag GmbH & Co).[87]

La coordinación isorreticular de los átomos de circonio hace que la estructura posea una elevada estabilidad, tanto térmica, llegando hasta 500 °C, como química, siendo estable tanto en agua hirviendo como en disolventes orgánicos. Además, al igual que el ZIF-94 posee una alta capacidad de adsorción de CO_2 de 2.3 mmol g^{-1} a 1 bar y 25 °C.

En esta tesis, se ha estudiado, además, la influencia de la funcionalización de este MOF con grupos amino (-NH_2) y nitro (-NO_2), entre otros. Como se ha observado en estudios anteriores,[62,88] la introducción de dichos grupos funcionales mejora la compatibilidad de este MOF con el polímero que conforma la membrana, así como las propiedades de adsorción. Esto se debe en gran medida a la creación de enlaces de hidrógeno entre los grupos funcionales del MOF y la matriz polimérica.[89]

Capítulo 3: “Experimental methodology”

3. Experimental methodology

3.1 Synthesis of MOF

3.1.1 Synthesis of ZIF-8

ZIF-8 was synthesized for the preparation of TFN membranes in **chapter 8**. Furthermore, ZIF-8 crystals were used to obtain ZIF-94 by a solvent assisted ligand exchange reaction (SALE), as explained in the following section (3.1.2), and use it as filler in the TFN membranes of **chapter 7** and **chapter 8**.

ZIF-8 nanoparticles (20 nm) were synthesized according to a previously reported method (Figure 3.1)[12] with some variations. Typically, 1.467 g of $Zn(NO_3)_2 \cdot 6H_2O$ (4.93 mmol) (98%, Sigma Aldrich) and 3.245 g of 2-methylimidazole (2-mIm) (39.52 mmol) (99.0% Sigma Aldrich) were first dissolved in 150 mL of methanol (MeOH) (≥ 99.9%, Análisis Vinicos, Spain), respectively. Once dissolved, the ligand solution (2-mIm) was poured into the metal solution under stirring. The resulting solution was further stirred for 30 min at room temperature (RT), followed by centrifugation (Beckman Coulter Allegra X-30) at 9,000 rpm for 10 min and several washing steps with MeOH. The final product was then dried and activated at 40 °C overnight.

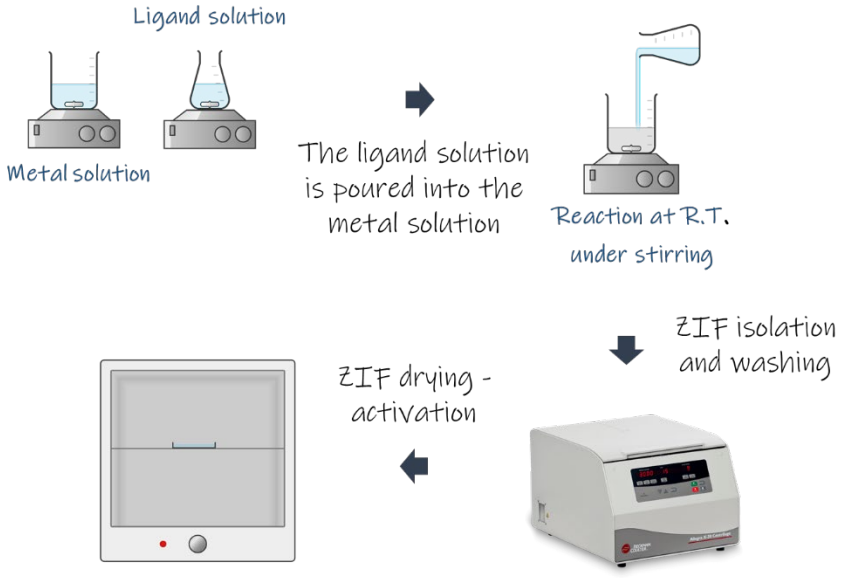

Figure 3.1. ZIF-8 synthesis scheme.

3.1.2 Synthesis of ZIF-94: original route (OR) and solvent assisted ligand exchange (SALE)

ZIF-94 (SALE) was used as filler in the TFN membranes of **chapter 7** and **chapter 8**. ZIF-94 (OR) was used for comparison in the characterization section of **chapter 8**.

In order to compare and confirm the successful ligand exchange in the synthesis of ZIF-94 from ZIF-8 nanoparticles, ZIF-94 powder was firstly synthesized according to a previous two-step procedure (Figure 3.2).[90] Initially, the metal solution was prepared by dissolving zinc acetate dihydrate (7.2 mmol) (≥ 98.0%, Sigma Aldrich) and NaOH (14.4 mmol) (≥ 98.0%, Sigma Aldrich) in 6 mL of MeOH. The ligand solution was prepared by dissolving the stoichiometric amount of 4-methyl-5-imidazole-carboxyaldehyde (14.4 mmol) (99.0%, Acros Chemicals) in 15 mL of tetrahydrofuran (THF) (≥ 99.9%, Sigma Aldrich). Once the metal and ligand solutions were prepared, the MeOH solution was poured into the THF solution under vigorous stirring. Reaction was carried out at RT for 16 h. Afterwards, ZIF-94 powder was collected by centrifugation at 9,000 rpm for 10 min and washed several times with fresh MeOH under the same conditions. Finally, ZIF-94 crystals were activated by refluxing with 50 mL MeOH/g ZIF-94 for 1.5 h and collected by centrifugation at 9,000 rpm. The resulting product was dried overnight at RT and named ZIF-94 (OR).

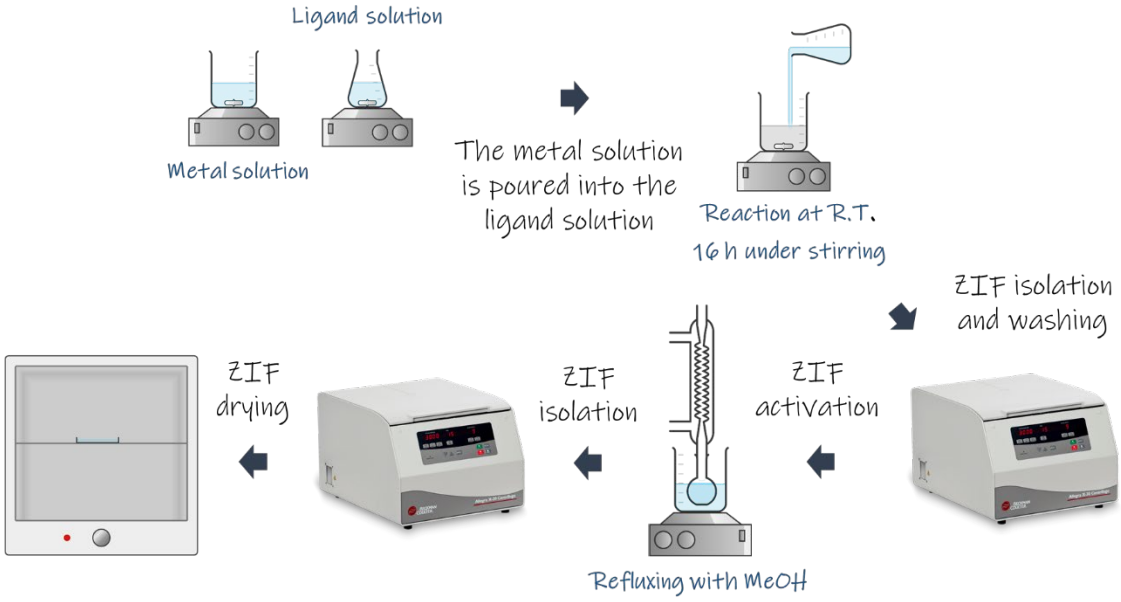

Figure 3.2. ZIF-94 (OR) synthesis route scheme.

The SALE reaction was carried out according to a previously reported method by Marti and Balkus[77] (Figure 3.3). Briefly, 0.323 g of 4-methyl-5-carboxyaldehyde (2.94 mmol) were first dissolved in 20 mL of 1-butanol (1-butOH) (99.5%, Scharlab, Spain). Then, 100 mg of nano ZIF-8 were suspended in the precursor solution and stirred at RT for 24 h. The resulting product was collected by centrifugation at 9,000 rpm for 10 min and washed several times with fresh 1-butOH under the same conditions. The final crystals were dried and activated at 40 °C overnight. The ZIF-94 particles obtained this way were named ZIF-94 (SALE).

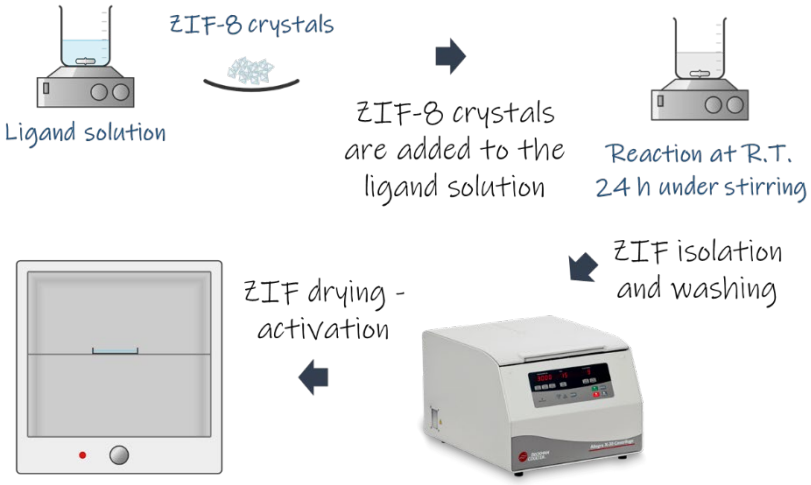

Figure 3.3. Scheme of ZIF-94 (SALE) synthesis route

3.1.3 Synthesis of UiO-66, UiO-66-NO_2 and UiO-66-NH_2

Ultra-small (4-6 nm) UiO-66, UiO-66-NO_2 and UiO-66-NH_2 particles have been incorporated as fillers in the TFN membranes prepared in **chapter 7**. For comparison, larger particle size (150 nm) UiO-66-NH_2 was also prepared.

Synthesis of Zr_6 oxoclusters

Zirconium tetrachloride ($ZrCl_4$, 98.0% Acros Chemicals) (2 g, 8.4 mmol) was added into a mixture of 3 mL of glacial acetic acid and 5 mL of isopropanol under stirring at 500 rpm and heated at 120 °C for 60 min. The product was collected either through suction filtration or centrifugation at 10,000 rpm. The collected white solid was subsequently washed with acetone twice and dried under vacuum at room temperature (RT).

Synthesis of ultra-small UiO-66-NH_2

Zr_6 oxoclusters (0.3 g) were dispersed in acetic acid (2 mL) under stirring at 600 rpm. H_2O (5 mL) was subsequently added, and the reaction mixture was stirred until it became completely colorless. 0.32 L ethanol was introduced into the solution followed by the immediate addition of 2-aminobenzene-1,4-dicarboxylic acid (BDC-NH_2, Acros Chemicals) (220 mg, 1.2 mmol), and the reaction was stirred for 2 h at RT. The resulting solution was evaporated by rotary evaporation at RT until approximately 50 mL volume was left. The colloidal suspension was centrifuged at 14,500 rpm for 45 min and then washed twice with the mixture of 30 mL acetone and 30 mL ethanol (14,500 rpm, 1.5 h). The collected solid was dried in a vacuum for 3 h for characterizations and applications.

Synthesis of ultra-small UiO-66-NO_2

Zr_6 oxoclusters (0.3 g) were dispersed in acetic acid (2 mL) under stirring at 600 rpm. H_2O (5 mL) was subsequently added and the reaction mixture was stirred until it became completely colorless. 80 mL ethanol was introduced into the solution followed by the immediate addition of 2-nitrobenzene-1,4-dicarboxylic acid (250 mg, 1.2 mmol), and the reaction was stirred for 2 h at RT. The solution was centrifuged at 14,500 rpm for 45 min and then washed twice with the mixture of 30 mL acetone and 30 mL ethanol (14,500 rpm, 1.5 h). The collected solid was dried in a vacuum for 3 h for characterizations and applications.

Synthesis of 150 nm UiO-66-NH_2

The synthesis protocol followed the reported paper:[91] 2 mmol (677 mg) of zirconyl chloride octahydrate ($ZrOCl_2 \cdot 8H_2O$, Alfa Aesar) was weighted in a glass vial, 7 mL of formic acid and 16 mL of distilled water were stepwise introduced in the reactor, following by 1 min of stirring at 600 rpm. 2 mmol (352 mg) of 2-aminoterephthalic acid (BDC-NH_2) and 20 mL ethanol were 3 subsequently added to the solution. The solution became very cloudy solution after 12 h, indicating the formation of UiO-66-NH_2. The product was collected by centrifugation (14,500 rpm), washed with ethanol and acetone and finally dried under vacuum.

3.2 Membrane preparation

3.2.1 Preparation of dense membranes

The Pebax® codes used were kindly provided by Arkema (France). All membranes of **chapter 4** were prepared by the casting-solution method (Figure 3.4). Pebax® 1657 was dissolved in a mixture of absolute ethanol (EtOH) (Gilca, Spain) and deionized water (Gilca, Spain) (70/30 (v/v)) and Pebax® 2533 in EtOH.[92,93] Both were dissolved under reflux for 2 h. Pebax® 3533, 4533 and Renew®, were dissolved in a mixture of 1-propanol (1-prOH) (HPLC, Labbox, Spain) and 1-butOH (3/1 (v/v)) under reflux for 3 h. Once dissolved and cooled down to RT, all casting solutions (3 wt%) were poured onto glass Petri dishes and left to evaporate in a solvent saturated atmosphere for 48 h. Membranes prepared in this way (40-50 µm thick) were peeled off from the Petri dish and tested for gas permeation.

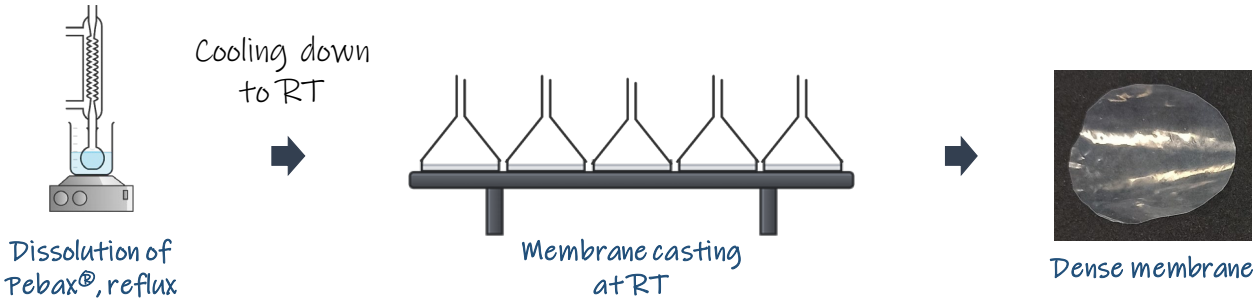

Figure 3.4. Dense membrane preparation procedure by casting-solution.

In **chapter 5**, Pebax® 1657 dense membranes were prepared under the same conditions but using different casting solution concentrations (1, 3 and 5 wt%). In this case, the same amount of polymer (0.2 g) was used to prepare the three casting solutions. The amount of polymer was fixed to obtain membranes of above the same thickness (40 µm) to be easily compared. Afterwards, membranes were treated at 50 °C in a vacuum oven for 6 h to evaporate the residual solvent retained in the films. For clarity, the synthesized membranes were abbreviated as PEBA1, PEBA3, and PEBA5, corresponding to the numbers of the concentration of PEBA in the mixture of solvents. PEBA3 membranes were introduced in an oven at 150 °C during different periods of time (3 and 8 days) in order to check their thermal annealing. These last membranes were abbreviated as PEBA3_3d and PEBA3_8d for the periods of 3 and 8 days, respectively.

For comparison, in **chapter 6**, Pebax® 3533 dense membranes were prepared following the same procedure than those prepared in **chapter 4**.

3.2.2 TFC and TFN membranes preparation

3.2.2.1 Preparation of polysulfone (PSF) asymmetric supports

PSF (Udel® P-3500 LCD, Solvay Advanced Polymers) was used as asymmetric support in all TFC and TFN membranes prepared in this thesis (**chapters 6-8**). The same procedure was followed in each configuration, however, different amount of PSF was used for the preparation of the dope solution. The TFC membranes prepared in **chapter 6** were prepared with a PSF support made with a 20 wt% dope solution, whereas the TFN membranes of **chapter 7** and **chapter 8** were made with a 15 wt% dope solution.

All PSF supports were prepared by casting followed by phase inversion[94] (Figure 3.5). First, PSF pellets (15 or 20 wt%) were dissolved in N-methyl-2-pyrrolidone (NMP) (99.0%. Panreac, Spain) at RT under stirring overnight. After complete degasification, the PSF solution was cast onto a Teflon plate using an Elcometer 4340 Automatic Film Applicator at a thickness of 250 µm and with a casting speed of 0.05 m s^{-1}. After casting, the phase inversion was carried out by immersing the supports in a water bath at room temperature for 1 h, transferred to a deionized (DI) water bath overnight, rinsed with isopropanol (HPLC, Panreac, Spain) and dried at 40 °C overnight.

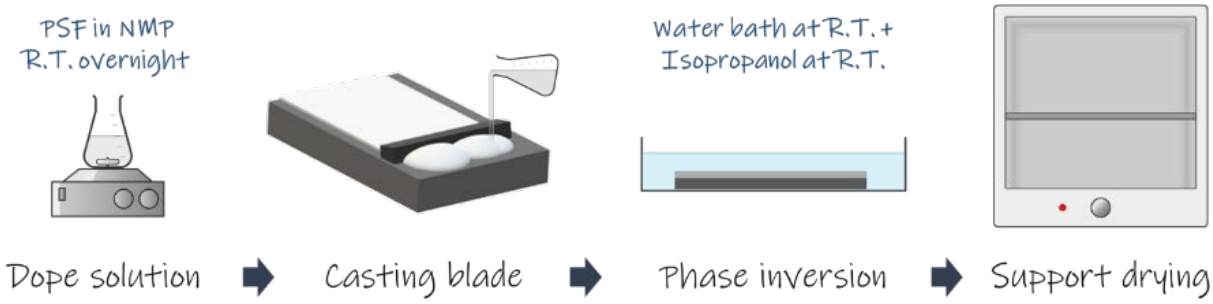

Figure 3.5. Preparation of PSF asymmetric supports

3.2.2.2 Preparation of Pebax® 3533 supported membranes by phase inversion and dip-coating

To prepare the Pebax® 3533 thin film composite (TFC) supported membranes used in **chapter 6** by phase inversion, the first step was to obtain the polymer solution by

dissolving Pebax® 3533 in the mixture of 1-propanol:1-butanol (3:1 v/v) at different concentrations (0.25, 0.5, 1.0 and 1.5 wt.%). These solutions were obtained following the steps previously explained for dense membranes (section 3.2.1). With these solutions, supported membranes were prepared applying different number of layers on top of PSF supports by phase inversion following the steps in Figure 3.6. Firstly, PSF support was horizontally fixed with the aid of a vacuum pump. Pebax® 3533 casting solution, in the form of a liquid, was applied just to the selective side of the support. In the second step, the Pebax® solution, previously poured into a Petri dish, was put in contact with the support by lifting the platform where the casting solution was located and maintained in contact for approximately 2-3 s. Immediately after this short time, the platform was lowered again and the Petri dish containing the Pebax® solution was replaced by another one with DI water (phase inversion) (third step). In the fourth and fifth steps, the same procedure was carried out, but this time with the DI water bath, where the phase inversion of Pebax® took place. After 2-3 min in contact with water, the membrane was gently dried for ca. 1 min with compressed air (sixth step). Once the excess of water was removed, the membrane was ready to repeat the cycle, as many times as necessary depending on the desired number of layers and membrane total thickness. The total time required to complete each cycle was scarcely 4-5 min. Finally, membranes were dried in an oven at 40 °C for 48 h before gas permeation tests. Membranes obtained by this method were abbreviated as Xwt%_Y, where X is the concentration of Pebax® in the casting solution, and Y the number of layers.

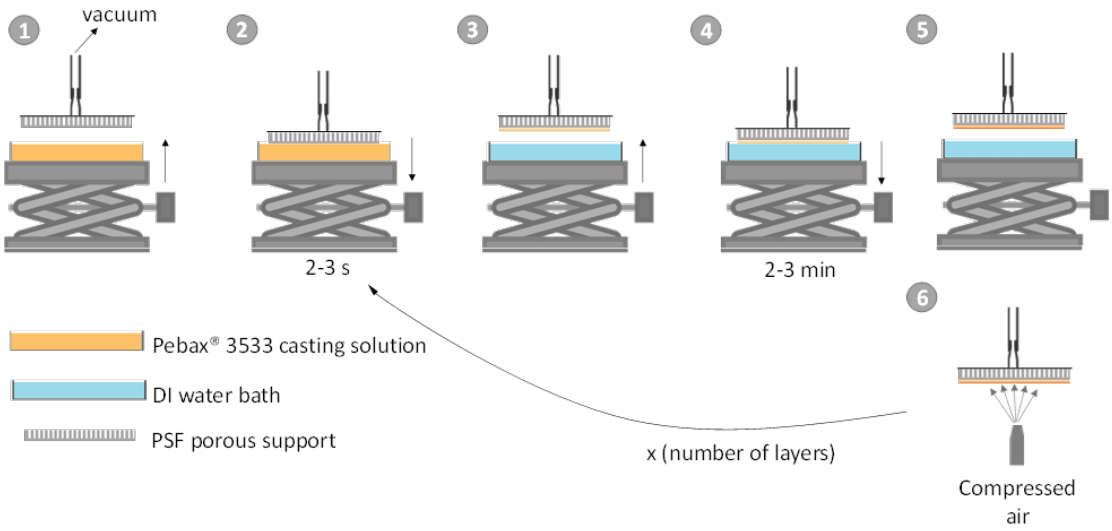

Figure 3.6. Layer-by-layer method by phase inversion. Including drying time (ca. 1 min). The total time is 4-5. min.

The best conditions found with the supported membranes prepared by phase inversion were applied to obtain the conventional ones by dip-coating.[95] Briefly, a casting solution with a Pebax® concentration of 0.5 wt% was obtained as explained before. PSF supports were horizontally fixed with the aid of a vacuum pump. Once fixed, the Pebax® 3533 solution was dip-coated for 30 seconds. Membranes were then placed in an oven at 40 °C to allow solvent evaporation for 1 h, before the deposition of the remaining layers. This procedure was repeated three more times to obtain a membrane with a total of 4 layers. Finally, membranes were dried in an oven at 40 °C for 48 h before characterization. Membranes prepared this way were called 0.5wt%_4_dip-coating.

3.2.2.3 Preparation of Pebax® 1657 and Pebax® Renew® TFC and TFN membranes by spin-coating

The TFC and TFN membranes studied in **chapter 7** and **chapter 8** were prepared using the spin-coating method schematically represented in Figure 3.7.

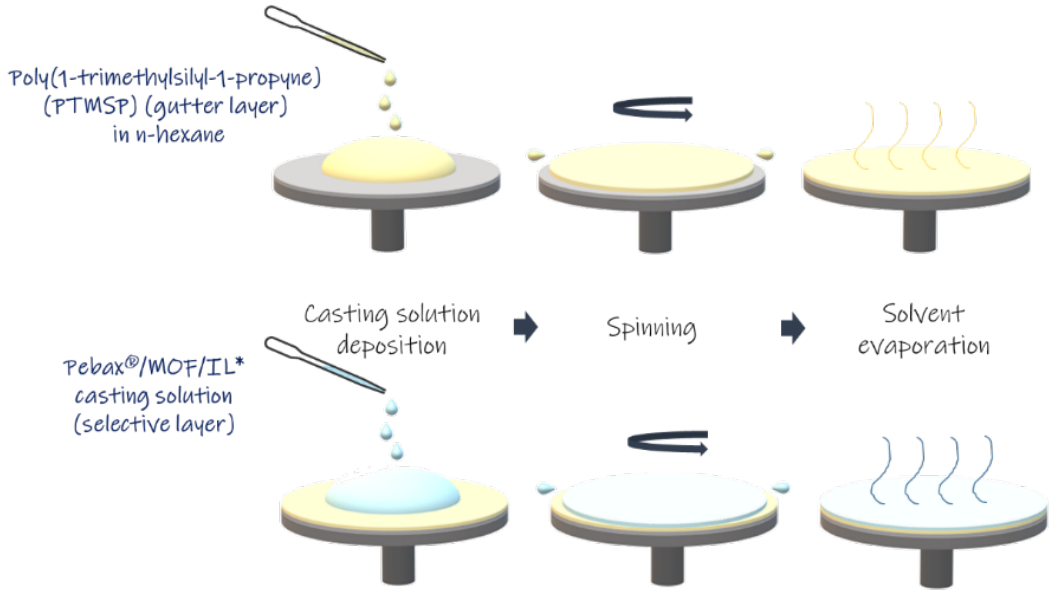

Figure 3.7. Spin-coating method: from the coating of the PTMSP gutter layer to that of the Pebax®/MOF/IL in one step. *IL was only incorporated in chapter 8.*

To avoid pore penetration of the selective layer and support geometric constraints, a gutter layer of poly[1-(trimethylsilyl)prop-1-yne] (PTMSP) (Fluorochem, United Kingdom), a highly permeable and glassy polymer, was spin-coated (Laurell Technologies Corporation, model WS-650MZ-23NPP/A1/AR1) onto the PSF support. The PTMSP solution was prepared by dissolving the polymer in n-hexane in a concentration of 2 wt%. After that, 0.7 ml of the PTMSP solution were spin-coated on top of the PSF support at 2,500 for 20 s. Supports with the gutter layer were introduced in an oven at 40 °C for 2 h for complete solvent evaporation.

Finally, the selective layer of Pebax® 1657 or Pebax® Renew® was spin-coated onto the PTMSP/PSF supports under the same conditions as the PTMSP layer. For this purpose, the Pebax® 1657 solution was prepared by dissolving under reflux 0.25 g of the Pebax® in 4.75 g of an EtOH/H_2O (70/30 v/v) mixture at 90 °C for 2 h and the Pebax® Renew® casting solution was prepared by dissolving under reflux 0.2 g of the polymer in 9.8 g of a 1-prOH/1-butOH (3/1 v/v) mixture at 80 °C for 2 h. To avoid gelation, the Pebax® Renew® polymer solution was immersed in a water bath at 45 °C before spinning. Once dissolved and cooled down to room temperature, 0.6 mL of the Pebax® solution was poured onto the PTMSP/PSF support and spun to obtain the Pebax®1657/PTMSP/PSF and Pebax® Renew®/PTMSP/PSF TFC membranes.

In the case of Pebax®/UiO-66/ZIF-94 TFN membranes, the polymer was dissolved in 2/3 of the total solvent under the same conditions while different amounts of UiO-66, UiO-66-NO_2 and UiO-66-NH_2 suspensions and 10 wt% of ZIF-94 (if used it) were mixed with the remaining solvent (1/3 of the total) using an ultrasonic bath (Ultrasons H-D, Selecta®). Once the polymer was dissolved, the UiO-66 suspensions were added to the Pebax® solution and stirred for 1 h before spinning. This procedure is schematically portrayed in Figure 3.8. Finally, membranes were placed in an oven at 40 °C for 18 h after spinning to remove any residual solvent.

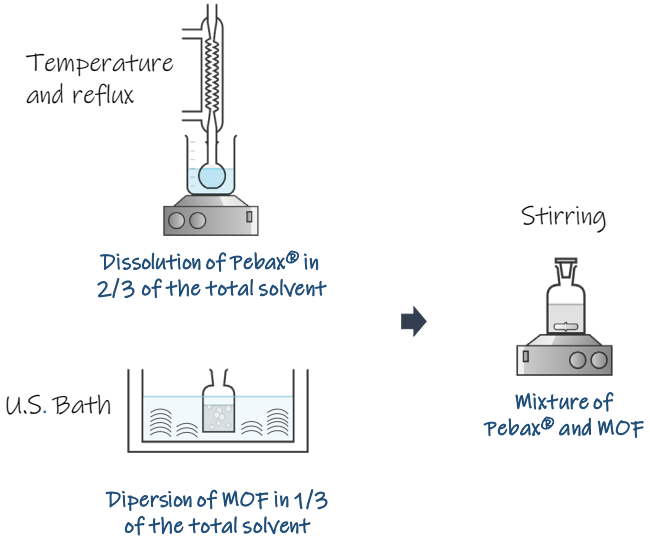

Figure 3.8. Preparation of Pebax/MOF casting solution.

Similarly, Pebax®Renew®(IL)/PTMSP/PSF membranes were prepared by adding the ionic liquid (IL) 1-butyl-3-methylimidazolium tetrafluoroborate [Bmim][BF_4] (Fisher Scientific, Spain) (from 5 to 20 wt%, respect to the polymer) to the Pebax® solution once cooled down. Solutions of Pebax® with the IL were stirred at 45 °C for 1 h before spinning. The TFC membranes prepared this way were abbreviated as TFC_PEBA(XIL), where X is the IL concentration. After testing the TFC_PEBA(XIL) membranes in the gas separation setup, the optimal condition (10 wt% of IL, see **chapter 8**) was selected to prepare the TFN membranes with the nanocrystals of ZIF-8 and ZIF-94 prepared by the SALE reaction. In this case, the polymer was dissolved in 2/3 of the total solvent under the same conditions while different amounts of ZIF-8 and ZIF-94 particles (from 10 to 20 wt%, respect to the polymer) were suspended in the remaining solvent (1/3 of the total) using an ultrasonic bath. Once the polymer was dissolved and cooled down to 40-45 °C,

the IL was added to the solution and stirred for 5 min before incorporating the ZIF suspension. Casting suspensions with the IL and ZIFs were stirred for 1 h at 45 °C before spinning. The membranes prepared this way were named as TFN_PEBA(10IL)_ZIF8(Y) and TFN_PEBA(10IL)_ZIF94(Y), where Y is the wt% concentration of ZIF-8 and ZIF-94. All the membranes were placed in an oven at 40 °C for 18 h after spinning to remove any residual solvent.

3.3 Materials characterization

3.3.1 Scanning electron microscopy (SEM)

SEM images of MOF powders (**chapters 7 and 8**) and membranes (**chapters 4, 5, 6, 7 and 8**) were obtained using an Inspect F50 model scanning electron microscope (FEI), operated at 10 kV. This instrument was also used for measuring (at 5-6 different positions along the membrane) the thickness of the selective skin layer (**chapters 6, 7 and 8**). Cross-sections of membranes were prepared by freeze-fracturing after immersion in liquid N_2 and subsequently mounted on a stub with carbon tape and coated with Pd (14 nm).

3.3.2 Transmission electron microscopy (TEM)

TEM imaging of the cross section of the membrane TFN_UNO2(5)_Z94(10) prepared in **chapter 7** was performed using a Tecnai T20 (ThermoFisher Scientific, formerly FEI) operated at an accelerating voltage of 200 kV in order to find out in detail each layer thickness, structure and arrangement. For this purpose, the membrane was embedded in epoxy resin EMBed 812, at 60 °C for 48 h. After epoxy polymerization, the sample was ultrathin-sectioned using the ultramicrotome Leica EM UC7 to slices of 70 nm in thickness and they were directly deposited over a carbon film on 200 mesh copper grid. Chemical information from these sections was acquired by means of X-ray spectrometry (EDS) using a probe aberration corrected Titan Low-Base transmission electron microscope (Thermo-Fisher Scientific) at a working voltage of 300 kV, in scanning transmission electron microscopy (STEM) mode. The microscope was fitted with a silicon drift detector (SDD) Oxford energy dispersive X-ray spectrometer.

3.3.3 Thermal analyses: Thermogravimetric analysis (TGA) and differential scanning calorimetry (DSC)

TGA and differential thermogravimetry (DTG) were carried out using a Mettler Toledo TGA/STDA 851e. In **chapters 4, 5 and 6**, small pieces of membranes (~ 3 mg) placed in 70 µL alumina pans were heated under an air flow (40 cm^3 (STP) min^{-1}) from 35 to 700 °C at a heating rate of 10 °C min^{-1}. Besides, in **chapter 5**, TGA analyses were also carried out at 5, 15 and 20 °C min^{-1}. In **chapters 7 and 8**, small amounts of ZIF powder (~ 3 mg) placed in 70 µL alumina pans were heated under an airflow (40 cm^3 (STP) min^{-1}) from 35 to 700 °C at a heating rate of 10 °C min^{-1}.

To calculate the crystallinity of membranes in **chapter 5**, differential DSC analyses were performed on a Mettler Toledo DSC822e. Samples (~2 mg) placed in 70 µL aluminum pans were heated in 40 cm^3(STP) min^{-1} of nitrogen flow from 25 to 250 °C at a heating rate of 10 °C min^{-1}.

3.3.4 Fourier transform infrared-attenuated total reflectance spectroscopy (FTIR-ATR)

Membranes (**chapters 4, 6 and 8**) and ZIF (**chapter 8**) were also characterized by FTIR-ATR, which was performed with a Bruker Vertex 70 FTIR spectrometer equipped with a DTGS detector and a Golden Gate diamond ATR accessory. The spectra were recorded by averaging 40 scans in the wavenumber range of 4000-600 cm^{-1} at a resolution of 4 cm^{-1}.

3.3.5 X-ray diffraction (XRD)

Membranes (**chapters 4, 5 and 7**) and MOFs (**chapters 7 and 8**) crystallinity was also analyzed by XRD using a Panalytical Empyrean equipment with CuKα radiation (λ = 0.154 nm), over the range of 5° to 40° at a scan rate of 0.03° s^{-1}.

3.3.6 N_2 adsorption analysis

The N_2 adsorption isotherms of the ZIFs used in **chapters 7 and 8** were measured using a Micromeritics Tristar 3000 at -196 °C Prior to the isotherm measurement, the samples were degassed for 8 h under vacuum at 200 °C, using a heating rate of 10 °C

min^{-1}. The specific surface area (SSA) of the porous materials was calculated by the Brunauer-Emmett-Teller (BET) method.

3.3.7 Viscosity tests

The viscosity of the Pebax® 1657 casting solutions used to prepare the membranes in **chapter 5** and the Pebax® 3533 casting solutions employed in **chapter 6** were measured with a SMART L Fungilab Rotational viscometer. Casting solutions (∼15 mL) placed in a APM/B adapter were subjected to different rotational speeds (from 50 to 200 rpm) at 20 °C.

3.4 Gas separation tests

3.4.1 Mixed gas separation

Membranes (**chapters 4-8**) were cut and placed in a module consisting of two stainless steel pieces and a 316LSS macro-porous disk support (Mott Co.) with a 20 μm nominal pore size. Membranes, 2.12 cm^2 in area, were gripped inside with Viton O-rings. To control the temperature of the experiment (in the 25-50 °C range), which has an effect on gas separation, the permeation module was placed in a UNE 200 Memmert oven. In this thesis, the gas separation measurements were carried out by feeding the post-combustion gaseous mixture CO_2/N_2 (15/85 cm^3(STP) min^{-1}) and the mixture CO_2/CH_4 (50/50 cm^3(STP) min^{-1}) to the feed side at an operating pressure of 3 bar to favor CO_2 permeation. Gas flows of the mixtures were controlled by mass-flow controllers (Alicat Scientific, MC-100CCM-D). The permeate side of the membrane was swept with a 4.5 cm^3(STP) min^{-1} of He, at atmospheric pressure (∼ 1 bar) (Alicat Scientific, MC-5CCM-D). The stage cut (θ), defined as the ratio of permeate to feed flow rate is ∼2%. Concentrations of CO_2, N_2 and CH_4 in the outgoing streams (permeate side) were analyzed online by an Agilent 3000A micro-gas chromatograph or an Agilent 990 Micro GC and data were collected in a computer. Permeabilities (dense membranes) of CO_2, N_2 and CH_4 were calculated in Barrer (10^{-10} cm^3(STP) $cm \cdot cm^{-2} \cdot s^{-1} cmHg^{-1}$) and permeances (TFC and TFN membranes) in GPU (gas permeance unit, 10^{-6} cm^3(STP) $cm^{-2} \cdot s^{-1} cmHg^{-1}$), once the steady state of the exit stream was reached. The CO_2/N_2 and CO_2/CH_4 separation selectivities were calculated as the ratio of the corresponding

permeabilities or permeances. A scheme of the mixed gas separation setup is depicted in Figure 3.9. The retentate is released to the vent.

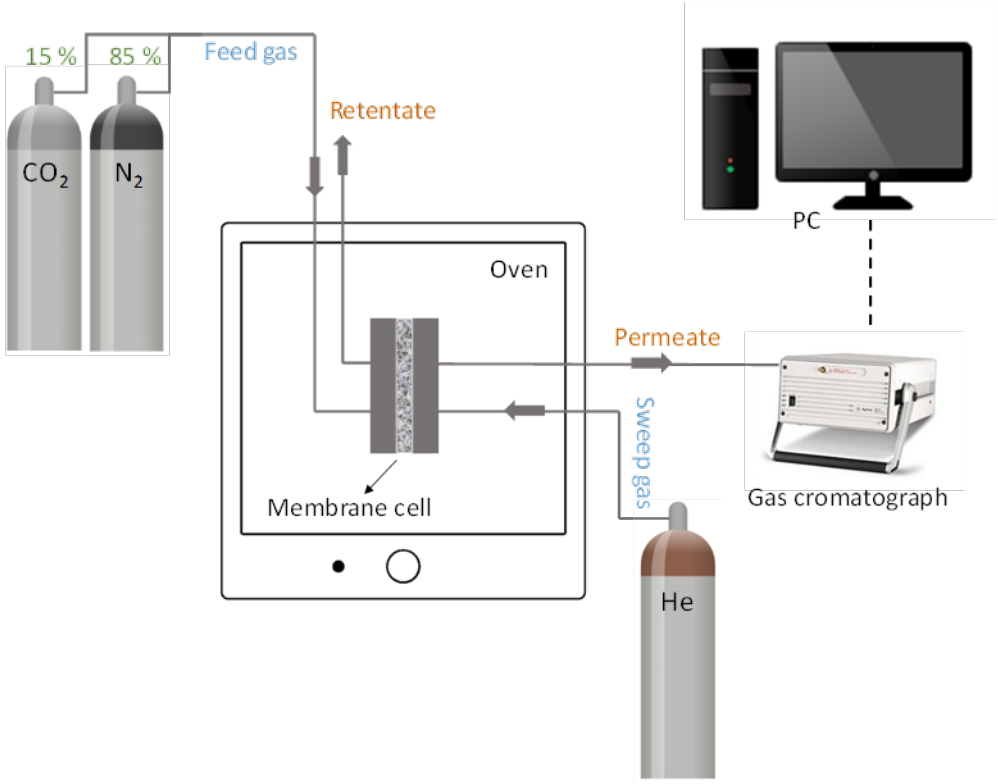

Figure 3.9. Mixed gas separation setup for CO_2/N_2 separation. For the CO_2/CH_4 separation, the same system is used, changing N_2 for CH_4 and with 50/50 ratio in such a case.

3.4.2 Single gas separation – time lag method

Time lag experiments were carried out at different temperatures using a constant volume/pressure instrument (Figure 3.10) built by our group. In the time-lag method, dense membranes are placed in a stainless steel membrane cell with two separated compartments (feed and permeate side). The downstream reservoir (permeate side) consists of 3/8" stainless steel tubing to minimize resistance. Two membrane cells are available with different diameters: 3.2 and 4.5 cm. Circular membranes were inserted in the stainless steel module similar to the one described in section 3.4.1. The system can be fed by 6 distinct gases: Ar, CH_4, CO_2, H_2, He and N_2. The inlet pressure of the feed gases can reach a value of up to 6 bar. The feed or upstream pressure is measured by a Wika A-10 pressure transducer (PT1, absolute pressure range of 0-10 bar). The

downstream pressure is measured by a Pfeiffer TPR 271 Pirani gauge (PT2, pressure range of $5 \cdot 10^{-4}$-10^{3} mbar). The resolution of both pressure transducers is 1% of reading. The inlet tubing to the membrane module, the membrane module, and the downstream compartment are placed in an oven (Memmert UN55) to control the temperature. To ensure that the feed gas is at the desired temperature, a loop made of stainless steel tubing was mounted inside the oven before the membrane cell. Evacuation is performed by a rotary vacuum pump (Pfeifer Pascal 2010-C1) (vacuum level down to $5 \cdot 10^{-4}$ mbar).

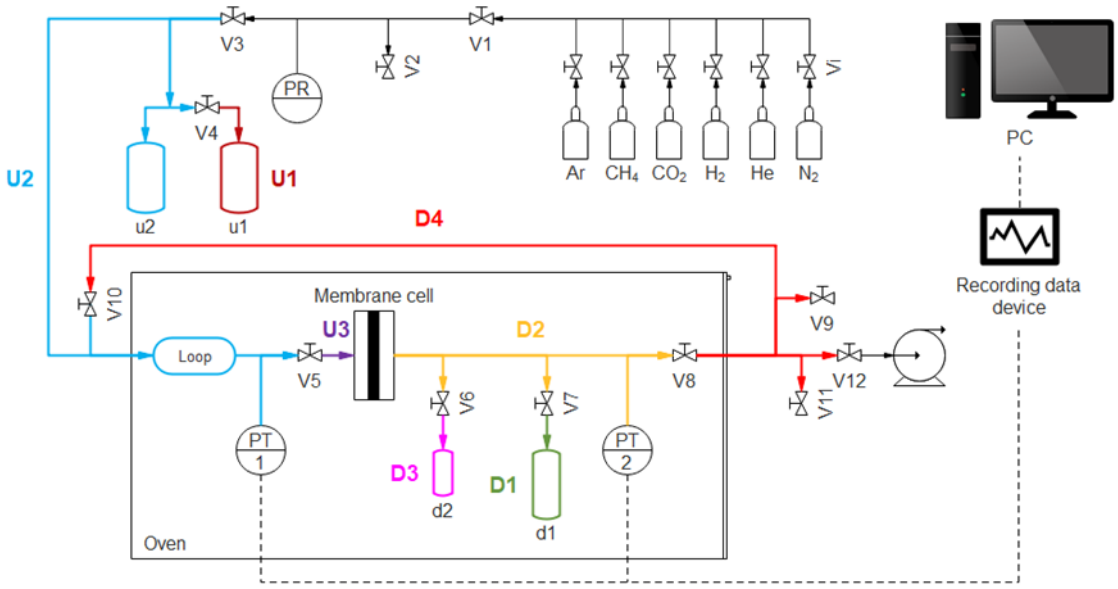

Figure 3.10. Time lag setup. Vi: valves; PR: pressure regulator; Ui: upstream volumes; Di: downstream volumes; PT: pressure transducer.

Circular membranes with an effective area of 5.7 cm^2 (3.2 cm in diameter) were used. All the measurements were performed at 25, 35, and 50 °C with a feed pressure of 3 bar. The order of gases was first N_2 and second CO_2 to avoid possible effects of CO_2 on the measurement of N_2 whose condensability is lower (Tabla 2.3). The leak rate was determined for each membrane after the first measurement. The maximum leak rate was two orders of magnitude lower than the lowest permeation flux. Before every experiment, the membranes were evacuated (10^{-3} mbar) at both sides for at least 10 times the time lag (θ) to remove any gas traces from the membrane surface and from the rig. The experiments started when the membranes were exposed to the feed gas. The downstream pressure (p_d) was recorded during all the test. Experiments were performed for 10 times the time lag at least. To fulfil the boundary conditions of the

time lag method and obtain an effective stationary state of flux, the downstream pressure should be much lower than the upstream pressure, so that the maximum downstream pressure was fixed at 0.1% of the upstream pressure.[96] Once this value was reached, the experiment was finished. Permeability (P_i) was calculated using the slope of the p_d-t curve in the stationary region. The diffusion coefficient (D_i) was estimated through the time lag value and the solubility coefficient (S_i) was obtained from P_i and D_i.[97,98]

Briefly, the time lag experiment consists of the following. After the complete evacuation of the membrane, it is exposed to the gas of interest (N_2 and CO_2 in this study). Once the gas is in contact with the feed side (upstream side) of the membrane, it is dissolved and starts diffusing through the membrane until it reaches the permeate side (downstream side), where it is desorbed. A typical curve of a time lag experiment represents the permeate pressure as a function of time and it is usually divided into three different regions, as shown in Figure 3.11.[99]

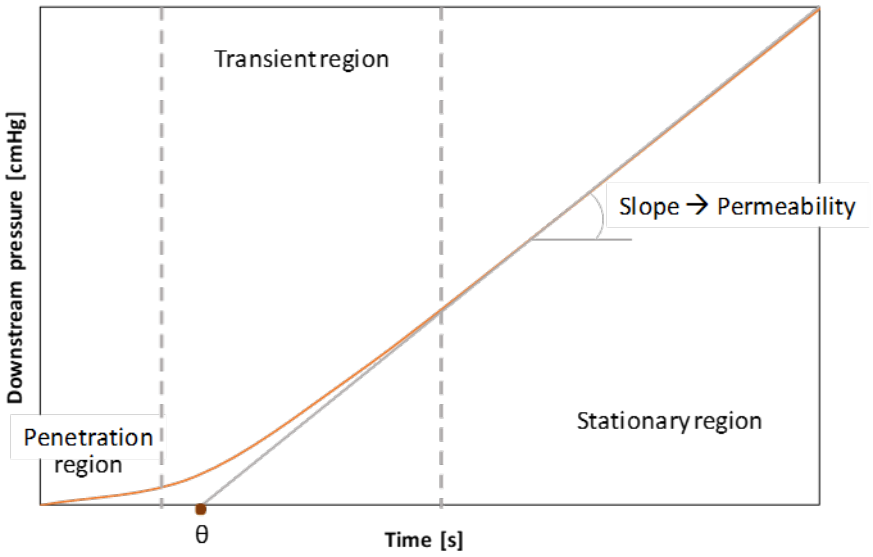

Figure 3.11. Time-lag typical curve.

In the first region, corresponding to the penetration of the gas molecules into the membrane, the gas pressure in the permeate side remains practically invariable. The second region, also called the transient region, corresponds to the absorption-desorption of the initial gas molecules. In this phase, the pressure in the permeate side increases gradually until it reaches a stationary state, where the flux through the

membrane is constant (stationary region). It is in the two initial phases where the diffusion (D_i) coefficient is determined whereas the permeability (P_i) of the gases can be calculated in the stationary phase. Usually, gas diffusion through a dense membrane follows Fick's law.[100] In consequence, the diffusion coefficient can be calculated with equation 3.1. In this equation, l is the membrane thickness in cm and θ is the time lag in s. The time lag can be estimated as the intersection of the tangent to the steady-state curve and the horizontal axis (as represented in Figure 3.11).

$$D_i\ [cm^2 s^{-1}] = \frac{l^2}{6\theta} \qquad \text{(eq. 3.1)}$$

The solubility coefficient (S_i) is calculated as the ratio between permeability and diffusivity as follows (equation 3.2):

$$S_i\ [cm^3(STP)cm^{-3}cmHg^{-1}] = \frac{Pi}{Di} \qquad \text{(eq. 3.2)}$$

As mentioned before, the permeability is determined in the stationary phase and depends on the slope of the time-lag curve in this region. It calculates with the following equation (equation 3.3):

$$Pi\ [Barrer] = \frac{V_d \cdot l \cdot T_0}{A_{ef} \cdot T \cdot p_{u,0} \cdot p_0} \cdot \left[\left(\frac{dp_d}{dt}\right)_{ss} - \left(\frac{dp_d}{dt}\right)_{leak}\right] \cdot 10^{10} \qquad \text{(eq. 3.3)}$$

where V_d is the downstream volume in cm^3, T_0 is the STP temperature (273.15 K), A_{ef} the effective membrane area in cm^2 (in this case, 5.73 cm^2), T the test temperature in K, $p_{u,0}$ the upstream pressure at time 0 in cmHg, p_0 the STP pressure (76 cmHg), p_d the downstream pressure in cmHg and t, the time elapsed in s.

In equation 3.3, $(dp_d/dt)_{ss}$ is determined as the slope of the time lag curve at the steady-state and $(dp_d/dt)_{leak}$ was estimated for each membrane, as explained before.

Capítulo 4: "A comparative study between single gas and mixed gas permeation of polyether-block-amide type copolymer membranes"

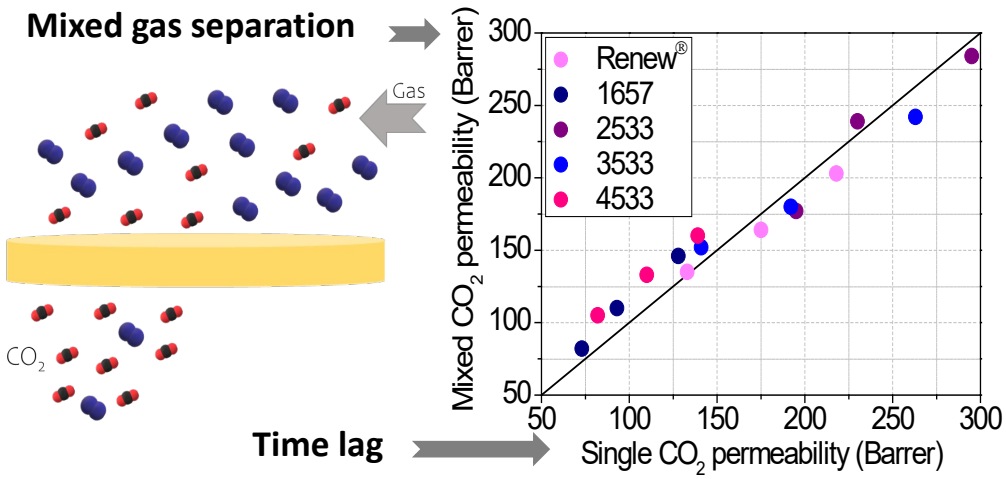

Adapted from "L. Martínez-Izquierdo, A. Perea-Cachero, M. Malankowska, C. Téllez, J. Coronas. A comparative study between single gas and mixed gas permeation of polyether-block-amide type copolymer membranes. Journal of Environmental Chemical Engineering 10 (2022) 108324. DOI: 10.1016/j.jece.2022.108324", with permission from Elsevier.

4. A comparative study between single gas and mixed gas permeation of polyether-block-amide type copolymer membranes

4.1 Introduction

The processes applied to obtain the majority of the current energy forms (electricity, fuel or gas) result in CO_2 emissions to the atmosphere. CO_2 holds a major share in causing global warming and its impact can now be seen on the world panorama affecting not only the climate but also the economy simultaneously having important social implications. The treatment of post-combustion flue streams as well as exhausts from cement and stainless steel factories, focused on separating CO_2 from N_2, is one of the possible remediation approaches for decreasing the CO_2 concentration in the corresponding outlet streams,[13,101] particularly efficient when carried out with membrane technology.[102] This CO_2/N_2 separation, properly carried out at industrial scale thanks to the energetic and economic advantages of the membrane technology, would allow the decrease of the CO_2 concentration in the atmosphere alleviating the current climatic situation.

Membranes can provide an eco-friendly and low energy consumption alternative to traditional separation techniques.[103,104] They are characterized by low requirement of weight and space, process flexibility and simplicity, good mechanical complexity and low cost of implementation and operation, to name a few. Even though membrane separation is a very attractive technology, it shows some limitations, especially for the gas separation application. The inherent trade-off between permeability and selectivity reported by Robeson in 1991 and 2008 remains the biggest challenge in developing polymeric membranes. Polymers with high permeability usually exhibit low selectivity and vice versa.[4,57] One approach to overcome such limitation is to combine the flexibility of polymers such as polyethylene oxide (PEO) with the mechanical stability of hard or crystalline polymers like polyamide (PA), polyimides (PI) and polystyrene (PS). Among the many polymers studied, polyether-block-amide (PEBA) copolymers are considered some of the most promising materials.[18,61,105–108] PEBA copolymers, commercialized

under the trademark of Pebax®, are a series of novel thermoplastic elastomers comprised of rigid polyamide blocks (PA) and flexible polyether (PE) segments which are glassy and rubbery at room temperature, respectively.[109]

In the membrane gas separation process, gas molecules are transported through due to the partial pressure difference between the feed and permeate sides. In a nonporous membrane, gas mixtures are fractionated in virtue of the differences in solubility and diffusivity of the mixture components through the polymer. Such transport is described by the solution-diffusion mechanism, which dominates the gas separation application.[110] Based on the solution-diffusion mechanism, the permeability of gases in polymeric membranes depends on their gas sorption and diffusion intrinsic properties. On the one hand, diffusion is a kinetic phenomenon related to the velocity of the gaseous permeant that passes through the membrane under a concentration gradient. On the other hand, sorption is a thermodynamic phenomenon where the usually reversible interactions between the membrane material and the gaseous permeants determine the sorption interaction.

In this work, we aim at studying how the segment nature and the proportion of each of them (PE/PA) within five different Pebax® codes affect the solubility, diffusivity and permeability parameters and hence the CO_2/N_2 gas separation performance of the membranes. Moreover, the intention of this study is also to compare two well established methods for the gas separation performance estimation from single and mixed gas permeation experiments. Single gas permeation measurements allow estimating the solution and diffusion parameters, whereas mixed gas permeation constitute a more realistic approach to the evaluation of the separation ability of the membrane. Further investigation was carried out by measuring the gas separation performance at different operational temperatures to calculate the apparent activation energy of permeation. Membranes have also been characterized in terms of thermal stability and crystallinity by thermogravimetric and X-ray diffraction analyses, respectively. Some other works have reported the preparation and CO_2 separation performance of Pebax® type copolymers;[111–114] however, as far as we are concerned, such a complete study has never been reported in the open literature before, and it is our belief that it could be useful to select the appropriate polymer for gas separation

applications concerning the CO_2/N_2 post-combustion mixture. In addition, the results gathered here will allow to gain insight into the use of single gas permeability measurements as a means to predict the gas separation performance of a certain membrane material.

4.2 Results

4.2.1 Membrane characterization

Five different Pebax® codes were analyzed (Table 4.1). All codes in the form of pellets were kindly provided by Arkema, France. As seen in Table 4.1, three of the five codes (2533, 3533, and 4533) are constituted by the same segments, which are present in different proportions, whereas Pebax® 1657 and a new code based on renewable sources (Pebax® Renew® 30R51) are comprised by the same soft phase but a different hard segment. The chemical structures of the hard and soft segments constituting these copolymers, as well as the molecular weight of their repeated unit are depicted in Figure 4.1. These codes also have different mechanical and water absorption properties, which could be decisive when selecting a polymer for its application in gas separation. In the case of Pebax® 4533, the proportion of flexible segment within the polymer is still unknown from the supplier. However, the greater tensile modulus value suggests that this code is constituted by a greater proportion of hard segment than its analogues (2533 and 3533), probably comparable to that of Pebax® 1657. Similarly, the Renew® code would have a higher percentage of soft phase than Pebax® 1657. This is in agreement with the results obtained by elemental analysis, measuring the content of C, N and H (Table 4.1).

Dense polymeric membranes made of these Pebax® codes (Table 4.1) have been prepared by the casting-solution method. As aforementioned, dense membranes usually follow the solution-diffusion mechanism of permeation,[51] which assumes that gas species are separated due to their distinct solubility and diffusivity through the membrane.[115] The non-porous character of the prepared membranes has been confirmed by cross-sectional SEM images shown in Figure 4.2.

Table 4.1. Properties of the Pebax® type copolymers studied in this work. The theoretical content of flexible segment was given by the supplier, while the measured content of flexible segment was obtained in this work from elemental analysis.

Pebax® code	Rigid segment of polyamide (PA)	Flexible segment of polyether (PE)	Theoretical flexible segment (wt.%)	Measured flexible segment (wt.%)	Ref.
1657	PA6	PEO	60	59	116,117
2533	PA12	PTMO	80	84	118,119
3533	PA12	PTMO	70	77	120
4533	PA12	PTMO	-	55	
Renew® 30R51	PA11	PEO	-	81	

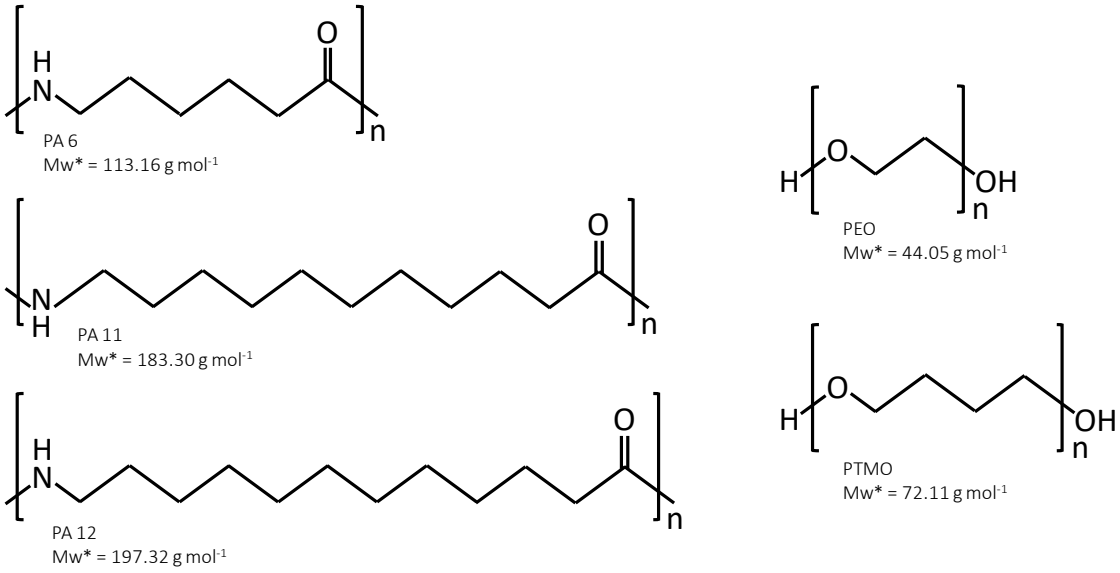

Figure 4.1. Chemical structures and their molecular weights of the hard and soft segments of the Pebax® copolymers studied in this work.

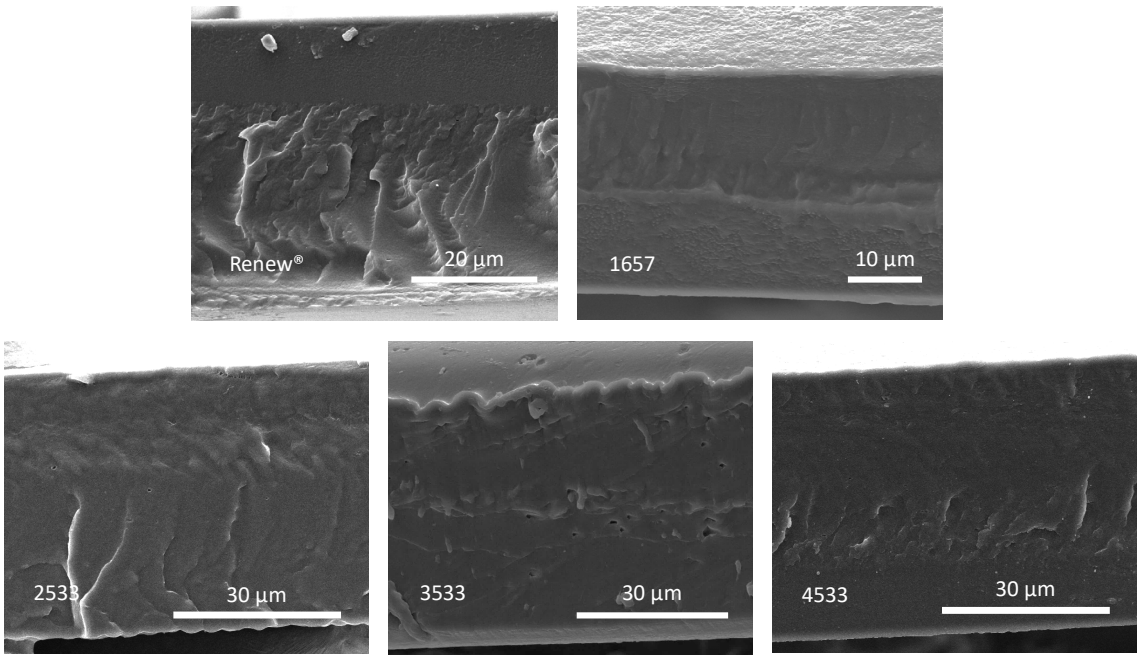

Figure 4.2. Cross-section images taken by SEM of the five membranes prepared by casting-solution. The Pebax® code is indicated inside the images.

Further characterization was carried out by testing the thermal stability of the membranes. TGA and DTG analyses are represented in Figure 4.3a and b, respectively. As shown in these figures, even if all the membranes start degrading at above 300 °C, a slight difference in the thermal stability can be observed for the codes which are constituted by the same segments (Pebax® 2533, 3533, and 4533). Such differences deal with the ratio between the rigid segment of polyamide and the flexible segment. The greater proportion of the hard block (PA) in Pebax® 4533 code provokes a higher resistance to temperature, whereas the major proportion of flexible PTMO in Pebax® 2533 code increases the polymer chain mobility and therefore accelerates the thermal degradation of the polymer. In any event, PEBA type membranes generally work at low temperature, the highest operating temperature reported being in the 65-70 °C range.[111] The differences in the nature of the segments, as well as the proportions of each one within the copolymer, can also be observed in Figure 4.3c, corresponding to the XRD patterns of the membranes. The codes constituted by PA12 and PTMO (2533, 3533, and 4533) show three characteristic peaks at 5.7°, 11.1°, and 22.3° consistent with

both, the PA12 and PTMO segments.[94] The differences in the peak intensities found for these codes are due to the proportion of each segment within the polymer.

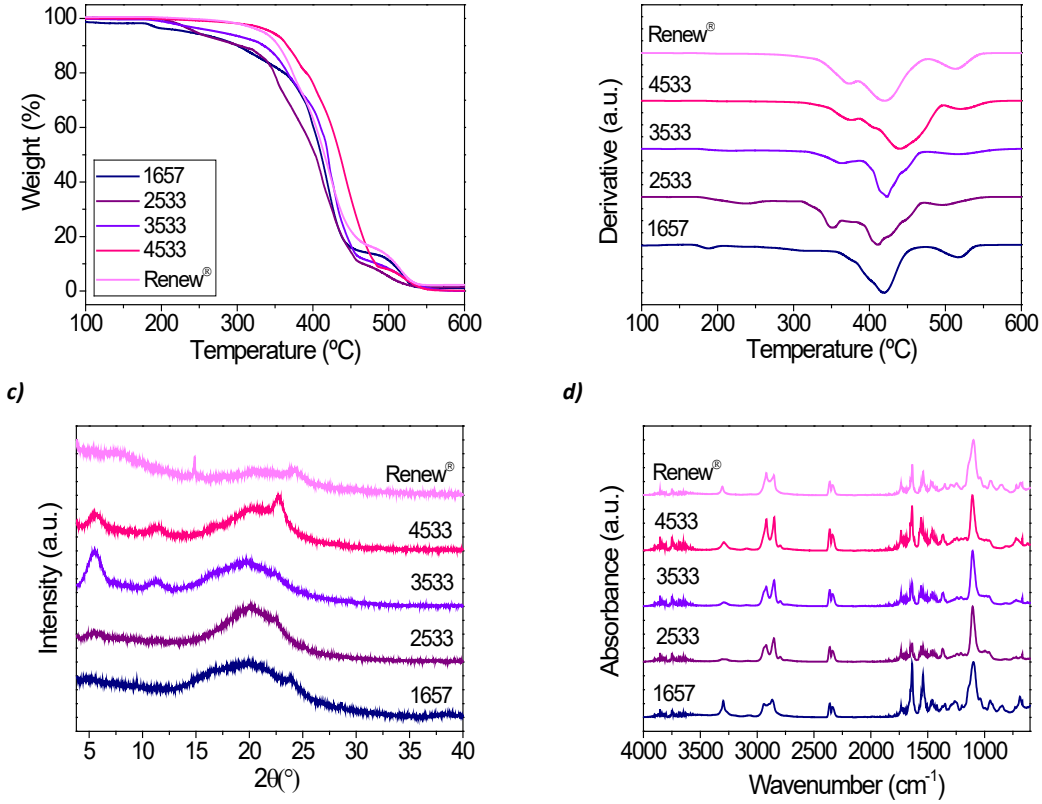

Figure 4.3. Thermal properties: TGA (a), DTG (b) and XRD patterns (c) and ATR-FTIR spectra of the membranes (d).

A property of Pebax® type copolymers is their semicrystalline nature,[121] which is related to both the amorphous PTMO and the crystalline PA12 segments. As shown in Figure 4.3c, the increment in the hard segment (PA12) proportion is associated with an increase in the intensity of the crystalline peaks. Although all peaks can be appreciated in the three XRD patterns (2533, 3533 and 4533 codes), in that corresponding to the 3533 code the 5.7° and 11.1° intensities are higher than in the 2533 code, while in the XRD pattern corresponding to the 4533 code the three peaks, including that at 22.3° associated to the hard PA,[20] appear to be intense. This suggests that the crystallinity increases as the PA12/PTMO ratio increases, which could be a crucial parameter affecting the gas separation performance of the membranes. The XRD pattern corresponding to Pebax® 1657 shows two characteristic peaks at 20.0° and 23.8° 2θ values, also corresponding to the soft and hard phases of the copolymer, the PEO and the PA6, respectively.[20,122,123] In the case of the renewable source code (Pebax® Renew®

30R51), three weak and broader peaks at ca. 7.6°, 20.4° and 24.2° 2θ values appear in the XRD pattern, the two first related to the PEO and the last to the PA11 segments.[124]

The FTIR-ATR spectra of the Pebax® membranes are shown in Figure 4.3d. In this figure, different bands associated with both the polyamide and the polyether segments can be appreciated. In spite of the different nature of each segment, it can be seen that the bands appear at the same wavenumber values. Regarding the hard segments (PA6, PA11 and PA12), the band at 1640 cm^{-1} corresponds to the vibrations of the H-N-C=O group,[125] and the band at 3298 cm^{-1} to the –N-H- linkages.[20] Vibrations corresponding to the soft segments (PEO and PTMO) are visible in the bands at 2925 and 1100 cm^{-1}, assigned to the stretching and bending vibrations of the aliphatic C-H group and the stretching vibration of the C-O-C ether group, respectively, in accordance with the literature.[36,126]

4.2.2 Single and mixture gas permeation at room temperature

A comparison was accomplished between the two well established methods for the estimation of the gas separation performance of membranes, single gas permeation using the time lag method and mixture separation assisted by a gas chromatograph. Single gas permeation experiments, carried out using a constant volume/pressure instrument, are regarded as an ideal separation test, whereas mixed gas separation considering a binary mixture in a specific proportion is closer to a real situation. However, the single gas permeation measurements allow the characterization of the membranes in terms of solubility, diffusivity and permeability parameters. This can be of interest to perform some mathematical modelling or to understand the effect of the membrane composition and operation conditions on the separation parameters of solubility and diffusivity. Conversely, the mixed gas separation only gives information about the permeability and selectivity of the membranes when they are exposed to a mixture of gases which, however, undoubtedly has a practical interest as already commented. As seen in Figure 4.4 and collected in Tables S4.1 and S4.2, there are remarkable differences in the gas separation performance of the five different membrane polymers. As expected, these differences are mainly related to the nature of the segments as well as

their proportion in the corresponding copolymer. Pebax® block copolymers have recently emerged as potentially interesting materials since it is possible to combine the properties of two different polymers into one obtaining a customized polymeric material, what is of particular interest in the membrane field. In fact, the final copolymer made of hard and soft phases would provide a relatively high CO_2 permselectivity in CO_2/non-polar gas separations (for example in CO_2/N_2 separations, among others[111]). The polyether segment has a strong affinity to CO_2 due to the dipole-quadrupole interactions between this molecule and the polyether chains, whereas the polyamide block mainly provides mechanical stability.[127] Also in Pebax®, the rigid segment of the polyamide is much less permeable than the soft polyether.[123] Therefore, it is expected that the higher the proportion of the soft segment, the higher the CO_2 solubility and permeability values.

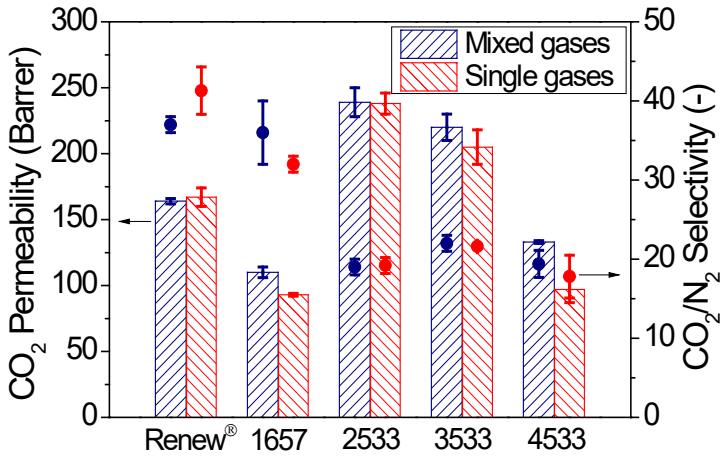

Figure 4.4. Gas separation performance of Pebax® type copolymer membranes measured with mixed and single gases at 3 bar feed pressure and 35 °C.

The renewable source (Renew®) and Pebax® 1657 codes are both composed of the same soft phase (PEO) but with a different hard segment (PA11 and PA6, respectively). As seen in Figure 4.4, the permeability of CO_2 is higher in the Renew® code than in the 1657 code, no matter the method used for the estimation of this parameter: 164 ± 2 and 167 ± 7 Barrer vs. 110 ± 4 and 93 ± 1 Barrer for the Renew® and the 1657 codes, respectively, corresponding the first value to mixed gas and the second to single gas permeation. This phenomenon can be related to the different proportions of the

polyether in the copolymer, favoring Pebax® Renew® (81 wt.% PEO, see Table 4.1) over Pebax® 1657 (59 wt.% PEO). It is also worth mentioning that the nature of the polyamide phase (longer PA11 for the Renew®, shorter PA6 for the 1657) can be involved in the higher or lower permeation of gases. Polyamides are named based on their chain length and usually the higher the chain length, the worse the chain packing efficiency, which means a higher free volume and thus a superior gas diffusion.[128] The diffusion and solubility parameters measured by the time lag method are plotted in Figure 4.5a and b, respectively, and collected in Table S4.3. As expected, the Renew® code has a greater diffusivity value ($12.9 \cdot 10^{-7}$ cm^{-2} s^{-1}) than the 1657 code ($7.3 \cdot 10^{-7}$ cm^{-2} s^{-1}) due to the PA chain length. Furthermore, the CO_2 solubility is also slightly higher in the renewable source code ($131 \cdot 10^{-4}$ cm^3(STP) cm^{-3} $cmHg^{-1}$) than in the 1657 code ($127 \cdot 10^{-4}$ cm^3(STP) cm^{-3} $cmHg^{-1}$) due to the higher PE/PA ratio (4.3 vs 1.4, respectively). As already explained, the permeability parameter depends on both the solubility and diffusivity values, being directly proportional to them (i.e. $P_i = D_i \cdot S_i$). Hence, the higher the diffusivity and solubility, the higher the permeability. As shown in Table S4.4, the CO_2/N_2 ideal selectivity is somehow greater in the case of the Renew® code membranes (ca. 37-51 at 25-50 °C) than for the Pebax® 1657 membranes (ca. 26-37) what can be justified by the higher PE/PA ratio for the former polymer.

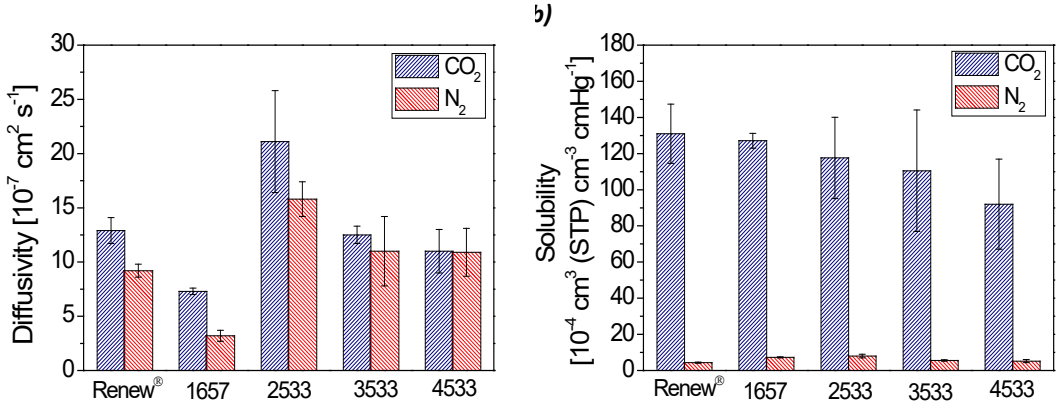

Figure 4.5. Diffusivity (a) and solubility (b) parameters measured by the time lag method at 35 °C.

The same behavior is shown for the codes made of PA12 and PTMO. First, in general, it is worth mentioning that copolymers with PEO (monomer with molecular weight of 44.05 $g \cdot mol^{-1}$) are less permeable and have smaller diffusivities than those with PTMO

(monomer with molecular weight of 72.11 $g \cdot mol^{-1}$), what is explained due to the fact that the smaller PEO with a higher mobility than larger, cyclic PTMO would pack more densely with PA segments. In this case, for the 2533, 3533 and 4533 series, the permeability increases as the percentage of PTMO increases (from 84 to 55 wt.%, see Table 4.1). This is related to both higher solubility and diffusivity values, which produced the best performance of code 2533. In fact, the highest CO_2 solubility for code 2533 is due to the greatest PTMO/PA12 ratio (5.3), which means stronger interactions of the PTMO block with the CO_2 molecule. Moreover, the highest proportion of PTMO in Pebax® 2533 (84 wt.%) code than in the 3533 (77 wt.%) and 4533 (55 wt.%) codes would hinder the chain rearrangement worsening the packing efficiency of the PA segments, which would be translated into an increase in the free volume, and thus in the CO_2 diffusivity in addition to the soft nature of the PTMO that favors diffusion as compared to the rigid PA12. Besides, the diffusivity of N_2 is also accelerated due to the chain packing, which limits the CO_2/N_2 selectivity of Pebax® 2533 to values below 20, this code being the one with the lowest selectivity (19 ± 1 for both, mixed and single gases at 35 °C).

From Figure 4.5a and b it is also possible to deduce which mechanism, solution or diffusion, is prevailing in each membrane and which would be the main responsible for the final separation performance. Such information can be analyzed from the diffusivity and solubility selectivities. As seen in these figures and in Table S4.3, for all codes the predominating mechanism is based on the high solubility of CO_2 in the polymer. This is an expected behavior since the soft phase of the Pebax® type copolymers has a strong affinity towards CO_2, as aforementioned. It is Pebax® Renew® which holds the greatest solubility selectivity value (30.5 ± 5.6), whereas the rest of the codes have similar solubility selectivity values, ranging from 14.7 ± 1.1 (2533) to 19.4 ± 4.6 (3533). Despite the similar solubility selectivity value of Pebax® 1657 (17.5 ± 0.1) and the codes composed of PA12 and PTMO, the diffusion of CO_2 through Pebax® 1657 is more favored in comparison to the N_2 diffusion. This difference is what gives Pebax® 1657 higher CO_2/N_2 ideal/separation selectivity values (32.0/37.0) as compared to Pebax® 2533 (19.0/19.1), 3533 (22.0/21.5) and 4533 (18.0/20.9), as shown in Figure 4.4 and Tables S4.4 and S4.5 at the same temperature of 35 °C.

4.2.3 Gas permeation as a function of temperature

Further characterization was carried out by measuring the gas separation performance of the membranes at different operational temperatures (25, 35 and 50 °C). The maximum temperature of 50 °C was chosen since hysteresis effects as a function of temperature have been found in the CO_2 permeability with similar types of membrane copolymers when the temperature reached 70 °C.[114] This can be related to some non-reversible phase separation favored by the polyether segregation from its blend with the amorphous copolymer having in mind that melting points of PEO and PTMO are ca. 14 and 53 °C, respectively.[129] In any event, an increase in temperature leads to a higher chain mobility and a decrease of solubility, which means higher permeability of permeants and thus lower CO_2/N_2 selectivity (Figure 4.6a-d). As seen in Figure 4.6a and c, the relationship between permeability and temperature is usually linear and follows the Arrhenius equation, as already explained in section 2.4.1.3 (equation 2.11).[53]

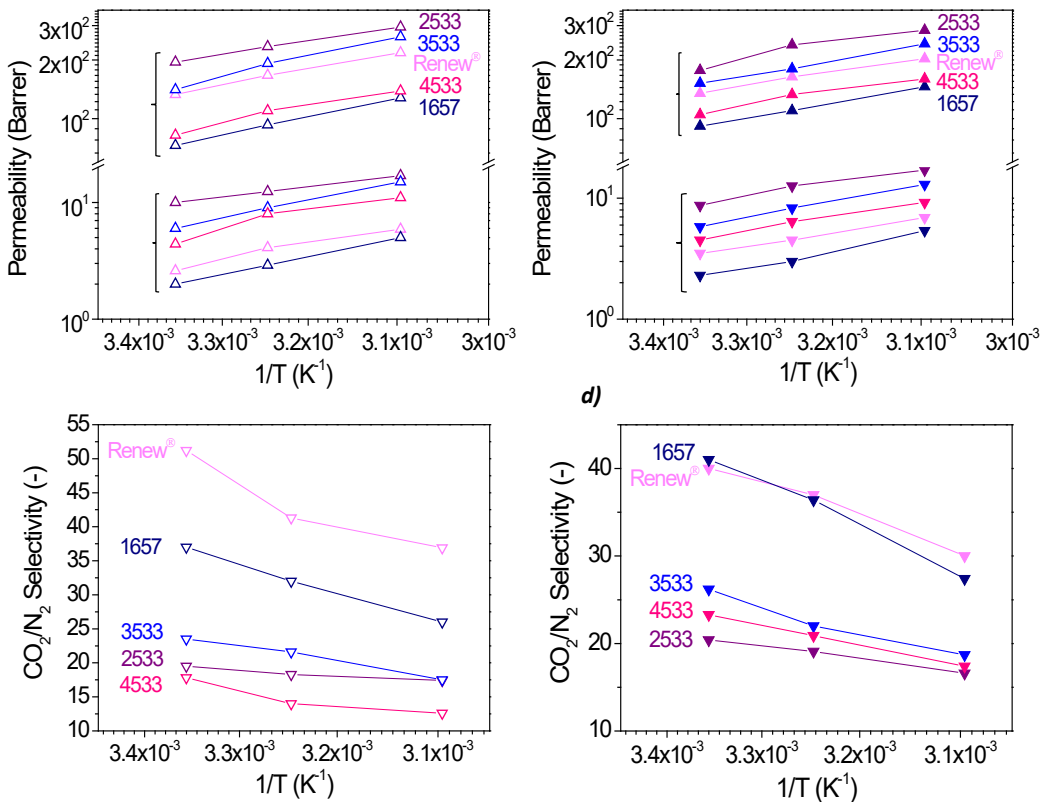

Figure 4.6. Gas permeation of membranes measured at different temperatures: (a) and (b) correspond to single gas permeation (time lag), (c) and (d) correspond to the mixed gas separation.

Therefore, with the data obtained at different temperatures (Tables S4.4 and S4.5) and plotting the gas permeability vs. the inverse of the temperature, it was possible to obtain the apparent activation energy of permeation from the slope of the linear regression, as follows (equation 4.1):

$$\ln P = \ln P_0 - E_p \cdot \frac{1}{R \cdot T} \qquad \text{(eq. 4.1)}$$

Based on this equation, higher E_p values indicate more activation with temperature. In this sense the E_p parameters were calculated from mixed and single gas permeations results. The values obtained for CO_2 and N_2 are collected in Table 4.2 and compared with data obtained from the literature. As shown in this table, the E_p values ranged from 13.3 to 19.8 kJ mol^{-1} for CO_2 and from 26.0 to 29.3 kJ mol^{-1} for N_2 when obtained from single gas permeability measurements, and from 13.0 to 15.0 kJ mol^{-1} for CO_2 and from 21.8 to 27.6 kJ mol^{-1} for N_2 in the case of mixed gas separation. These values are also in agreement with the data found in the literature for Pebax® type copolymers.[53,114,130,131] It is worth mentioning that, in general, the E_p values measured by single gas permeation are higher than those measured by mixed gas separation. Higher activation energy corresponds to a higher slope in the Arrhenius equation. This means that the variation of temperature causes larger changes in the permeability of the membranes measured by single gas permeation. This could be explained by taking into account the presence of nitrogen in the mixed gas separation, hindering the permeation of CO_2 and thus decreasing its activation with temperature. Furthermore, this effect can be due to the competitive sorption of CO_2 and N_2 molecules. Finally, activation energies are greater for N_2 than for CO_2 in line with the fact that with increasing temperature the most soluble CO_2 reduces its concentration in the membrane facilitating the N_2 transport.

Table 4.2. Apparent activation energies of permeation. Comparison between mixed and single gas permeation.

Pebax® code	Single gas, E_p (kJ mol^{-1})		Mixed gases, E_p (kJ mol^{-1})		Ref.
	CO_2	N_2	CO_2	N_2	
1657	13.3	30.4			[114]
1657			14.9	28.0	Chapter 5
1657	18.6	32.0			[130]
1657	14.6	33.6			[123]
2533	16.7	27.2			[130]
2533	18.2	31.0			[131]
2533	18.5-18.6	33.2-34.6			[132]
1074	13.4	30.3			[53]
3533			14.2	29.6	Chapter 6
Renew®	15.6	26.0	13.0	21.8	This chapter
1657	18.0	29.3	15.0	27.6	This chapter
2533	13.3	27.7	14.8	25.6	This chapter
3533	19.8	29.3	15.0	22.2	This chapter
4533	16.7	28.6	13.3	22.7	This chapter

To conclude this part, the permeability and selectivity data obtained with both methods have been plotted together with the Robeson upper bound[4] and they are depicted in Figure 4.7. With this figure it is possible to compare all the codes in terms of their efficiency for CO_2/N_2 gas separation performance. A good membrane for gas separation will be that surpassing the Robeson limit. Therefore, the polymer closer to that limit can be consider to be the best for the separation of the gases studied. In this case, Pebax® Renew® can be considered the code with the best performance in gas separation, whereas Pebax® 4533 would be the one with the worst separation performance, no matter the method used for its determination. It is also worth mentioning that the data sets of permeability and selectivity obtained in this work are in agreement with the values found in the literature for some of these codes.[114,131,132]

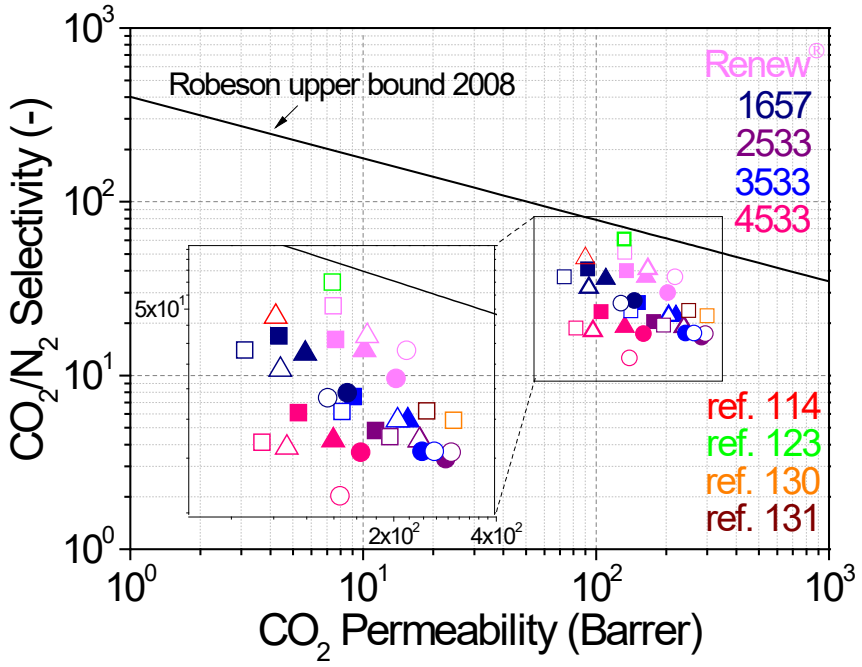

Figure 4.1. Robeson type graphic comparing the gas permeation results of the membranes prepared in this chapter with other data found in the literature at different temperatures: 25 °C (squares), 35 °C (triangles) and 50 °C (circles). Empty scatters correspond to the data obtained by time lag and filled scatters to mixed gas permeation.

4.2.4 Comparison between single and mixture gas permeation

Figure 4.8 plots CO_2 and N_2 permeabilities and CO_2/N_2 selectivities obtained under gas mixture conditions as a function of their respective single gas permeability values, for all the Pebax codes and temperatures. Figure 4.8a depicts a relatively good lineal correlation for CO_2 permeabilities. However, at about 150 Barrer of CO_2 single gas permeability the CO_2 mixture permeability tends to be smaller than the expected value (the equal). This can be due to the fact that a large CO_2 permeability (e.g. obtained by increasing the temperature) runs parallel to a low CO_2/N_2 separation selectivity, what means more N_2 in the membrane hindering the CO_2 permeability in the mixture. In case of N_2 permeability, most of the dots tend to be closer to the diagonal. This, together with the fact that the relative error must be larger for this molecule (due to the lower permeability values as compared to those of CO_2), allows to infer that both single and mixture permeability differences can be considered within the experimental error. The question for the CO_2/N_2 selectivity is not that clear. The expected trend would be larger

separation selectivities than ideal selectivities due to the fact that the more soluble CO_2 hinders the N_2 diffusion when operating at mixture conditions. A trend can be envisaged in this sense with most of the dots in Figure 4.8c placed above the diagonal. Nevertheless, Pebax® Renew® shows ideal selectivities clearly larger than the corresponding separation selectivities obtained from the mixture studies. This can be related to the large CO_2/N_2 solubility selectivity that this polymer exhibits compared to the other codes (see Figure 4.5b). Moreover, it should be noted for this polymer code that in the experiments with single gases the CO_2 pressure is 3 bar, while in the mixture the CO_2 partial pressure is 0.45 bar. This means that in polymers such as Pebax® Renew®, which bases its separation on the selectivity by solubility in a prominent way with respect to the other polymers (Figure 4.5b), the selectivity is greater with the pressure due to the greater solubility of CO_2. On the other hand, polymers such as Pebax® 1657 with a notable separation component in terms of diffusion selectivity with respect to the other polymers (Figure 4.5a) or the Pebax® 4533 polymer with the lowest CO_2 solubility (Table S4.3) are clearly found above the diagonal.

These plots demonstrate that, at least in case of the Pebax® codes studied there is a relatively good correlation between single gas permeability results and mixture separation results, the former providing, with the exception of the Renew® code, a conservative estimation of the membrane separation selectivity. It should be noted that although greater differences between single gas and mixed gas separations could be expected depending on the working conditions (e.g. CO_2 partial pressure),[133] the good correlation found in this study is probably due to the relatively low concentration of CO_2 (15 %) in the feed stream during the mixed gas separation tests. In any event, every gas permeation technique has its typical operation conditions (e.g. use of pure gases in case of time lag, while 10-15 % mixture CO_2 concentration when emulating post-combustion separation conditions). Our results suggest that the application of a simple and cheaper measurement technique (i.e. single gas permeation testing) as characterization of the membrane separation performance can be appropriate in most of the cases. However, for either non-very studied polymers or new membrane polymers it can be prudent the permeation study under more realistic conditions feeding a gas mixture to the membrane.

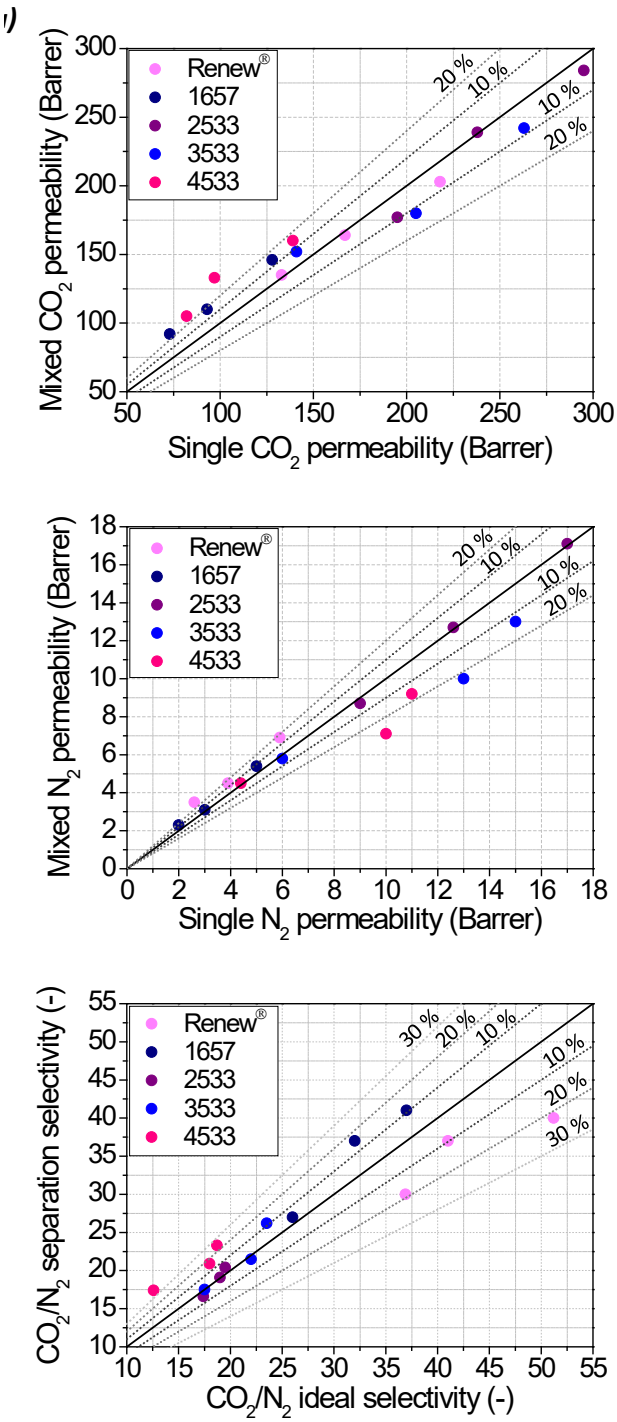

Figure 4.2. CO_2 and N_2 permeabilities (a, b) and CO_2/N_2 selectivities (c) obtained under gas mixture conditions as a function of their respective single gas permeability values, for all the Pebax® codes and temperatures. Values taken from Tables S4.4 and S4.5. Variation lines are also plotted.

4.3 Conclusions

Pebax® type copolymers are composed of polyamide (PA) and polyether (PE) segments. In the market, there is a great variety of codes that differ in the nature and proportion of each segment within the copolymer. The gas separation performance of

five different Pebax® type membranes was analyzed by single and mixed gas permeation. Single gas permeation, using the constant volume/pressure method (time lag), leads to the estimation of ideal selectivities, whereas mixed gas separation is closer to a real situation and allows the calculation of separation selectivities. In dense polymeric membranes, gases follow the solution-diffusion mechanism. Once the gas is in contact with one side of the membrane, it is solubilized and diffuses through the membrane until it reaches the other side and is desorbed. Therefore, the permeability of dense membranes directly depends on the solubility and diffusivity of the gas. These parameters can only be estimated by the time lag method (single gas). Moreover, the composition, thermal stability and crystallinity of the membranes, investigated by elemental, TGA and XRD analyses, can be correlated to their gas separation performance. Although all membranes have similar thermal stability, the greater proportion of soft phase (PE) leads to a slight decrease in the degradation temperature. Moreover, the membranes with greater PE/PA ratio are also those with higher CO_2 permeability (Pebax® 2533, 3533 and Renew®). The nature of the hard segment (PA) was also found to have an effect on the performance of the membrane. Polyamides are named based on their chain length, and this parameter has an effect on the packing efficiency. Usually, the higher the chain length, the worse the packing efficiency, which leads to higher free volumes and gas permeabilities. Besides, the lower CO_2/N_2 selectivity values of the codes made of PA12 (2533, 3533 and 3533) can also be related to the worst packing efficiency of these polymers. Conversely, the renewable source code (Pebax® Renew®), in spite of being composed of PA11, which has a similar chain length than PA12, holds the best CO_2/N_2 selectivity value (37 and 41, for mixed and single gas, respectively). This can be related to the nature of the PE segment. While Pebax® Renew® is composed of PEO, the others (2533, 3533 and 4533) are composed of PTMO and the interactions between these segments and the CO_2 are different. The solubility of CO_2 is higher in the case of the Renew® code favoring its CO_2/N_2 selectivity.

Additional characterization was carried out by measuring the single and mixed gas permeation performance at different temperatures. These allowed the calculation of the apparent activation energy of permeation for CO_2 and N_2. As expected, the apparent activation energy was higher for N_2, the gas with lower solubility. Besides, the CO_2

activation energy calculated by single gas separation was slightly higher than that obtained by mixed gas separation, which can be related to the presence of N_2 in the mixture. Moreover, the values obtained in this study were in agreement with those found in the literature for this type of polymers.

Finally, comparing the gas separation results obtained with both, single and mixture gas permeation, where the CO_2 partial pressure is different affecting the permeation, it was found that there is a relatively good correlation between single gas permeability and mixture separation results for the Pebax® codes. Being acceptable, the correlation between the ideal selectivity and the mixture selectivity is tuned by the solubility and diffusion properties of the polymers. This suggests that the application of a simple and cheaper measurement technique (i.e. single gas permeation testing) as characterization of the membrane separation performance can be appropriate in most of the cases.

4.4 Supplementary Information

Mixed and single gas separation results measured at 3 bar feed pressure and 35 °C are collected in Table S4.1 and Table S4.2, respectively. The solubility and diffusivity values for CO_2 and N_2 at 3 bar and 35 °C are collected in Table S4.3. The values of permeability, solubility and diffusivity measured at different temperatures, corresponding to the single and mixed gas separation experiments are collected in Tables S4.4 and S4.5, respectively.

Table S4.1. Mixed gas separation results were measured at 3 bar feed pressure and 35 °C.

Pebax® code	CO_2 Permeability (Barrer)	N_2 Permeability (Barrer)	CO_2/N_2 Separation selectivity (-)
Renew®	164 ± 2	4.5 ± 0.1	37 ± 1
1657	110 ± 4	3.1 ± 0.5	36 ± 4
2533	239 ± 11	12.7 ± 0.7	19 ± 1
3533	220 ± 10	10.0 ± 0.9	22 ± 1
4533	133 ± 1	7.1 ± 0.8	19 ± 2

Table S4.2. Single gas (time lag) separation results measured at 3 bar feed pressure and 35 °C.

Pebax® code	CO_2 Permeability (Barrer)	N_2 Permeability (Barrer)	CO_2/N_2 Ideal selectivity (-)
Renew®	167 ± 7	3.9 ± 0.1	41 ± 3
1657	93 ± 1	2.9 ± 0.1	32 ± 1
2533	238 ± 8	12.4 ± 0.3	19 ± 1
3533	205 ± 13	13.0 ± 9.5	22 ± 1
4533	97 ± 10	10.0 ± 5.7	18 ± 3

Table S4.3. Solubility and diffusivity values obtained by the time lag method at 3 bar feed pressure and 35 °C.

Pebax® code	CO_2 Solubility	N_2 Solubility	CO_2 Diffusivity	N_2 Diffusivity	S_{CO2}/S_{N2}	D_{CO2}/D_{N2}
	(10^{-4} cm^3(STP) cm^{-3} $cmHg^{-1}$)		(10^{-7} cm^2 s^{-1})		(-)	
Renew®	131 ± 16	4.3 ± 0.3	12.9 ± 1.2	9.2 ± 0.6	30.5 ± 5.6	1.4 ± 0.2
1657	127 ± 4	7.3 ± 0.3	7.3 ± 0.3	3.2 ± 0.5	17.5 ± 0.1	2.3 ± 0.3
2533	118 ± 23	8.0 ± 1.0	21.1 ± 4.7	15.8 ± 1.6	14.7 ± 1.1	1.3 ± 0.2
3533	111 ± 34	5.6 ± 0.4	12.5 ± 0.8	11.0 ± 3.2	19.4 ± 4.6	1.2 ± 0.3
4533	92 ± 25	5.2 ± 0.9	11.0 ± 2.0	10.9 ± 2.2	17.4 ± 2.5	1.1 ± 0.3

Table S4.4. Permeability and CO_2/N_2 ideal selectivity values measured by single gas separation at 3 bar feed pressure and different temperatures.

Pebax® code	T (°C)	P CO_2 (Barrer)	P N_2 (Barrer)	$\alpha CO_2/N_2$ (-)
Renew®	25	133	2.6	51.2
	35	167	4.1	41.0
	50	218	5.9	36.9
1657	25	73.0	2.0	37.0
	35	93.0	2.9	32.0
	50	128	5.0	26.0
2533	25	195	9.0	19.5
	35	238	12.4	19.0
	50	295	17.0	17.4
3533	25	141	6.0	23.5
	35	205	13.0	22.0
	50	263	15.0	17.5
4533	25	82.0	4.4	18.7
	35	97.0	10.0	18.0
	50	139	11.0	12.6

Table S4.5. Gas separation performance (permeabilities and CO_2/N_2 selectivities) of membranes measured by mixed gas separation at 3 bar feed pressure and different temperatures.

Pebax® code	T	P CO_2	P N_2	$\alpha CO_2/N_2$
	(°C)	(Barrer)		(-)
Renew®	25	135	3.5	40.0
	35	164	4.5	37.0
	50	203	6.9	30.0
1657	25	92.0	2.3	41.0
	35	110	3.0	37.0
	50	146	5.4	27.0
2533	25	177	8.7	20.4
	35	239	12.6	19.1
	50	284	17.1	16.6
3533	25	152	5.8	26.2
	35	180	8.3	21.5
	50	242	13.0	17.5
4533	25	105	4.5	23.3
	35	133	6.4	20.9
	50	160	9.2	17.4

Capítulo 5: "Poly(ether-block-amide) copolymer membrane for CO_2/N_2 separation: The Influence of the casting solution concentration on its morphology, thermal properties and gas separation performance"

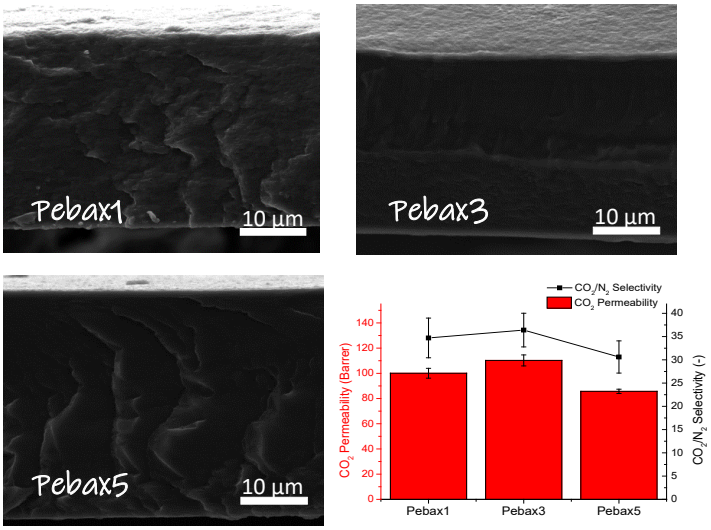

Adapted from "L. Martínez-Izquierdo, M. Malankowska, J. Sánchez-Laínez, C. Téllez, J. Coronas. Poly(ether-block-amide) copolymer membrane for CO_2/N_2 separation: The Influence of the casting solution concentration on its morphology, thermal properties and gas separation performance. Royal Society Open Science 6 (2019) 190866. DOI: 10.1098/rsos.190866", with permission from The Royal Society.

5. Poly(ether-block-amide) copolymer membrane for CO_2/N_2 separation: The Influence of the casting solution concentration on its morphology, thermal properties and gas separation performance

5.1 Introduction

Carbon dioxide is a final combustion product of carbon-containing fuels. It is generated in big quantities and emitted in the gaseous form in case of industrial and energy production sites, transportation, building heating etc. Such emission causes an increase in the CO_2 concentration in the atmosphere and contributes to the so called Climate Change. CO_2 is a primary greenhouse gas (GHG) and it is estimated that stationary CO_2 emissions are responsible for more than 60% of the overall CO_2 global emissions. To mitigate the effect of CO_2 in the atmosphere, its emission needs to be reduced by a substantial amount.[134,135]

Membrane technology is, since the 1970s, one of the most studied techniques for the separation and sequestration of CO_2 from non-polar gases (such as CO_2/N_2, H_2/CO_2 and CO_2/CH_4 gas mixtures) due to its well-known advantages over the conventional methods i.e. mechanical simplicity, easy to scale up, lower energy consumption and smaller footprints.[18] Li and Freeman reviewed the design strategies of membrane materials selection for the separation of CO_2 from gas mixtures.[41] Introduction of polar groups with affinity to CO_2 is a promising method to raise CO_2/nonpolar gases selectivity. Poly(ether-*block*-amide) (PEBA) copolymers are especially interesting due to the permeation selectivity of polar to non-polar gases. PEBA block copolymers, are synthesized from polyoxyalkylene glycols (PEG or PTMG) and dicarboxylic acid terminated aliphatic polyamides (such as nylon-6 or nylon-12).[18] Such block copolymers consist of soft (rubbery) and hard (glassy) segments that provide high gas permeability without loss of selectivity and mechanical stability.[42,108] Nevertheless, in spite of its good

properties, many efforts are still being made to improve even more its CO_2 separation performance, although the majority of them concern the incorporation of nanoparticles into the polymeric matrix or the synthesis of a composite membrane.[20,136–138]

In the open literature there are still few studies concerning the raw material, which should be taken more into account to choose the best conditions for further applications. The way in which membranes are prepared i.e. solvent selection, solvent evaporation temperature, etc. is proved to have an effect on its morphology and hence, on its gas separation performance.[43,139] Shao et al.[44] studied the influence of solvents on the morphology of 6FDA/PMDA–TMMDA copolyimide membranes. They found that those prepared with solvents possessing solubility parameters closer to that of the polymer had a better affinity to it and thus, polymer chains mobility was higher, resulting in more crystalline structures and therefore, in less permeable membranes. Karamouz et al.[43] studied the effect that the solvent evaporation temperature had on the membrane performance in gas separation. They found that the evaporation rate (higher when increasing the temperature) resulted in a more disordered phase at the top of the membrane, which led to more permeable and selective membranes.

As far as we are concerned, while these aforementioned parameters have already been studied for PEBA,[139] there is no study about how the concentration in the casting solution affects the crystallinity and thermal properties of the polymer Pebax® 1657, although already studied by Ren et al.[108] for the gas separation performance. This is of great importance to find correlation between the casting conditions and the whole membrane performance, i.e. not only what limits the separation performance but what relates other issues such as morphology, preparation reproducibility, long period stability, etc. The changes in the concentration of polymer in the casting solution directly affects the viscosity, which will lead to differences in the behavior of membranes. As well as the solvent type, the viscosity will affect the evaporation time and this will result in differences in crystallinity and hence in permeability and selectivity, as occurred in the studies of Shao et al.[44] and Karamouz et al.[43] Therefore, with the aim of further optimize the PEBA, in this work, we have carried out a study of the influence of the concentration of Pebax® 1657 in the casting solution on the corresponding gas separation membranes. In particular, the morphology, thermal properties and CO_2

separation performance of the PEBA membranes have been studied. With this aim, three different casting solutions of PEBA (1, 3 and 5 wt%) have been prepared and the resulting membranes have been tested for gas separation using the CO_2/N_2 gas mixture.

5.2 Results

5.2.1 Membrane characterization

Dense membranes with no defects usually follow the solution-diffusion model. This model assumes that no pores exist in the membrane, and thus species are separated based on their solubility and diffusivity through the membrane, instead of molecular sieving.[115] Figure 5.1 shows the cross-sectional images of the three different membranes prepared in this work. For the three casting solution concentrations, the SEM images confirm the defect-free morphology of the PEBA membranes, without the existence of porosity or pinholes, which suggests that gases are transported following the solution-diffusion mechanism.

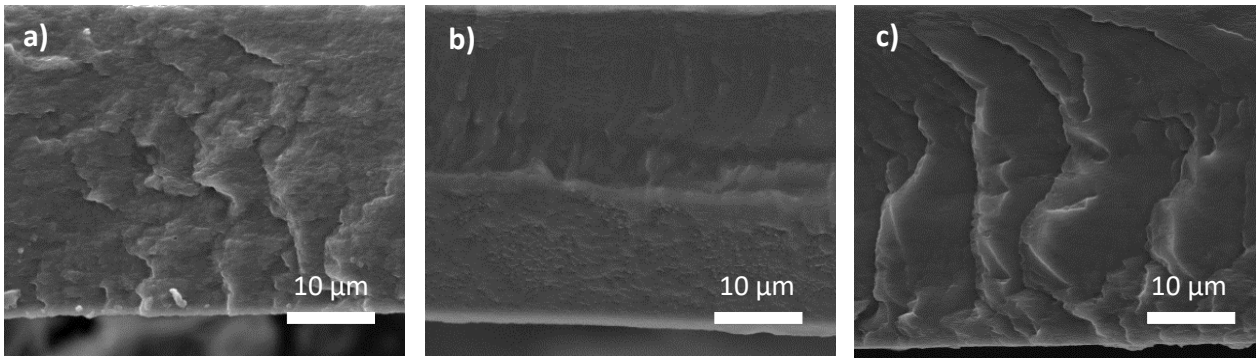

Figure 5.1. Scanning electron microscopy (SEM) images of dense PEBA membranes: PEBA1 (a), PEBA3 (b) and PEBA5 (c).

Figure 5.2 shows the XRD spectra of the PEBA membranes. Poly(ether-*block*-amide) copolymers are semi-crystalline polymers which consist of both amorphous and crystalline PEO and PA phases. In particular, Pebax® MH 1657 possesses two crystalline characteristic peaks. The first peak appears at a 2θ value of 20.0°, attributed to the α crystalline phase of PA6, the most probable and stable phase presented in this polymer,[140] corresponding to a *d*-spacing of 0.44 nm, and the other one at a 2θ value of 23.8°, mainly associated with the less bulkier PEO segments,[141] and to a molecular distance of 0.37 nm (see equation S5.1 in Supplementary Information section). The amorphous region in these membranes comprises the incidence angle interval from

12.0° to 27.0°. Differences or displacements of crystalline peaks associated to the different concentration of PEBA used for the preparation of each membrane were not appreciated, so it can be stated that the three samples tested possessed similar molecular distances between their polymeric chains, in principle not being a crucial factor for gas permeabilities.

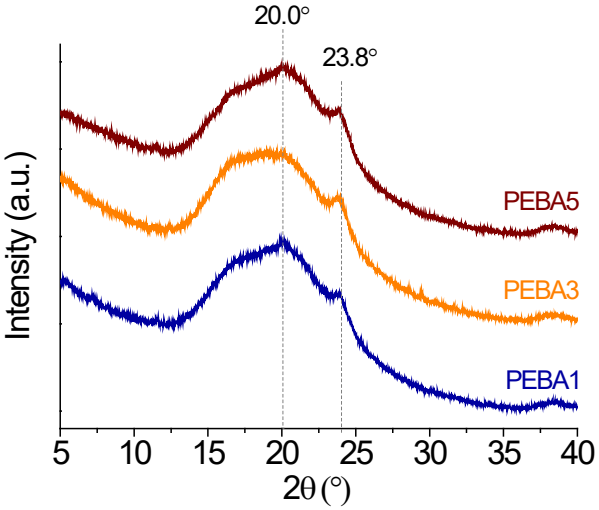

Figure 5.2. X-Ray diffraction (XRD) patterns of PEBA dense membranes

XRD analyses have been also carried out for the membranes subjected to thermal annealing, in order to analyze how crystallinity is affected by post-treatment at high temperature. Figure S5.1 shows a comparison of the XRD diffraction peaks of the membranes with and without thermal treatment. As expected, the peak at 23.8° becomes more intense as days of treatment increase, suggesting a higher crystallinity. Despite this fact, the membranes acquired a toasted color after each thermal treatment (Figure S5.2), revealing that a partial degradation has taken place during the heating. This fact was corroborated by TGA analyses (see apparent activation energy section).

From the results obtained by DSC, it was possible to evaluate the crystallinity of the membranes without post-treatment (Table 5.1). Figure 5.3 shows the thermograms of PEBA at the three tested concentrations. In this figure, two different melting peaks can be observed corresponding to the soft (PEO) and the hard (PA6) segments. The melting temperature of both segments was around 14 °C for the PEO and 204 °C for the PA, being in coherence with those reported previously in the literature.[142] The slight

decrease in the melting temperature of both segments suggests that the crystallinity of samples becomes lower as the PEBA concentration in the casting solution increases. This fact means that the crystalline regions in the membrane decreased when the amount of solvent in the PEBA solution was lower, as previously reported with analogous polymers.[143] Crystallinity data collected in Table 5.1 verify this phenomenon. The higher crystallinity of PEBA when decreasing its concentration could be explained taking into account the time required to completely evaporate the solvent. In fact, for the same amount of polymer the higher the quantity of solvent, the longer the evaporation time becomes and hence, the polymeric chains have more time to rearrange and form more organized crystalline structures.[144]

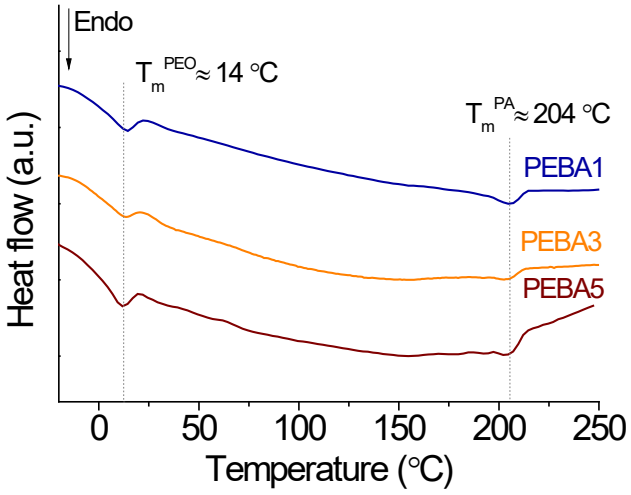

Figure 5.3. DSC thermograms of PEBA dense membranes.

Table 5.1. Melting temperatures, crystallinity, maximum degradation temperatures and apparent activation energies for degradation of the PEBA membranes extracted from DSC and TGA analyses.

	T_m PEO (°C)	T_m PA (°C)	X_c PEO (%)	X_c PA (%)	T_{max}(1) (°C)	T_{max}(2) (°C)	E_a(a) (kJ mol^{-1})	E_a(b) (kJ mol^{-1})
PEBA1	14	206	15	6	414	521	277	274
PEBA3	14	204	9	3	420	515	263	261
PEBA5	12	203	8	3	418	511	218	218

(1) Thermal decomposition at a heating rate of 10 °C min^{-1}, (2) oxidation step at a heating rate of 10 °C min^{-1}, (a) calculated with Kissinger equation and (b) with Ozawa method

Viscosity tests were conducted in order to corroborate the influence of the PEBA concentration on the viscosity of the casting solutions and its possible correlation with the evaporation time and crystallinity. Figure 5.4 compares, at different rotational speeds, the viscosity of the three casting solutions with that of the solvent. For all the solutions tested, the viscosity decreased with the increment of the rotational speed, which means that these solutions behave as non-Newtonian pseudoplastic fluids. As expected, an increase in viscosity with the increment of PEBA concentration can be clearly observed. Besides, while for the casting solutions prepared with 1 and 3 wt% of the polymer the viscosity seems to follow the same tendency, a major increment can be observed in the case of the one with 5 wt% of PEBA. This fact suggests that the gas separation performance of the membrane prepared with 5 wt% casting solution may differ from the others. This statement will be confirmed in the gas separation section (see Figures 5.6 and 5.7).

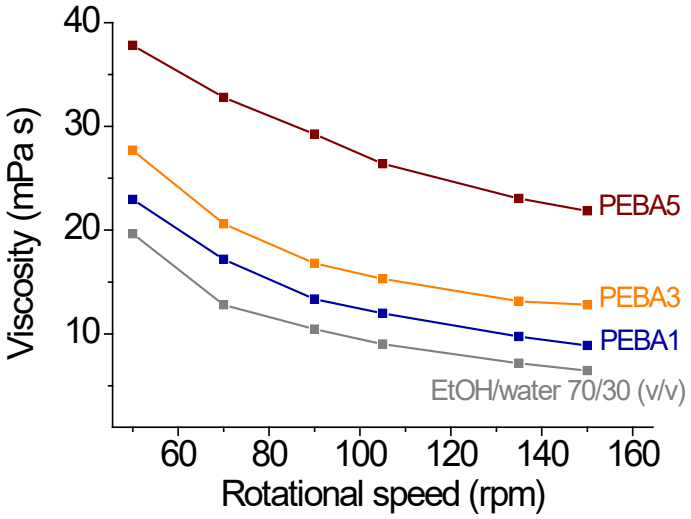

Figure 5.4. Viscosity of the three casting solutions (1, 3 and 5 wt%) and the EtOH/water (70/30 v/v) solvent at different rotational speeds.

5.2.2 Apparent activation energy

The thermal stability of the prepared membranes was studied by TGA and DTG analyses. Figure 5.5 shows the thermograms obtained for the membranes tested in this work (with and without thermal post-treatment). As observed in Figure 5.5a and collected in Table 5.1, the Pebax® 1657 is thermally stable up to 360 °C (the temperature at which samples start to lose weight), and they reach their maximum degradation at

417 °C. A second degradation step can also be observed related to the oxidation mechanism, in which the combustion of aromatic compounds and residues of the thermal degradation occurs.[145] This oxidative stage begins at 464 °C, reaching its maximum peak at 516 °C. Changes in the maximum degradation temperature associated to the different concentration of PEBA in the casting solution cannot be appreciated. With the data collected from the experiments carried out at different heating rates (Figures S5.3a, S5.3b, and S5.3c of the Supplementary Information section) it was possible to calculate the apparent activation energy (Table 5.1) with the Kissinger and Ozawa integral methods (Equations S5.4 and S5.5).

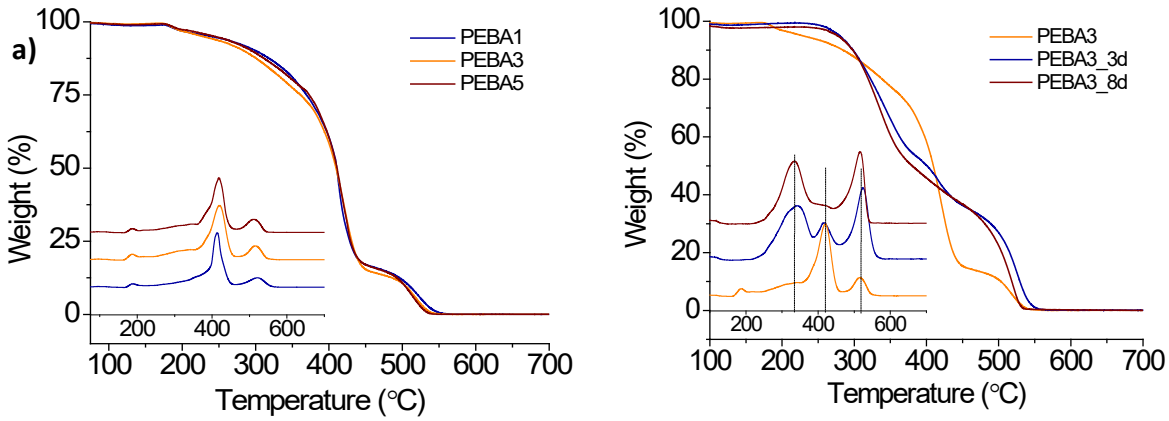

Figure 5.5. TGA and DTG curves of Pebax® MH 1657 at different concentrations (1, 3 and 5 wt%) (a) and with thermal annealing at 150 °C for different periods of time (0, 3 and 8 days) (b), oxidized in air atmosphere at 10 °C min^{-1}

A drop in the apparent activation energy was noticed when the concentration of PEBA in the casting solution increased. Such fall could be related to the reduction of the membrane crystallinity, which means more labile polymer chains (since chain mobility is higher). This way, the energy required to degrade the polymer decreases. The weaker polymeric chain interaction (inter- and intra-bonding between chains) renders to a reduction of the thermal stability of membranes.[146] This result suggests that the reduction in the polymer concentration, and thus in the viscosity of the polymer solution, may facilitate to some extension the interaction between the polymer chains, helping them to reach a more favorable orientation to maximize the polymer-polymer interactions. On the contrary, an increase in the viscosity of the polymer solution would hinder the polymer chain interactions decreasing the crystallinity of the final solid

polymer. It will be shown in the next section that the differences in crystallinity affect the permeation performance.

As mentioned before, thermogravimetric analyses were also carried out with the post-treated membranes in order to verify their partial degradation. As depicted in figure 5.5b and collected in Table S5.1, the membranes subjected to thermal treatment began to lose weight at lower temperatures (240 °C). Furthermore, the final weight loss associated to the aromatic compounds (the peak at ~520 °C) becomes higher, which indicates that the samples have lost part of its lineal compounds during the treatment. To aid in the corroboration of this statement of partial degradation, values of apparent activation energy have been calculated for these membranes (Figure S5.4a and S5.4b and Table S5.1). Results indicate that the membranes subjected to thermal annealing have lower apparent activation energies than the ones without post-treatment, meaning that the samples have lost part of their thermal stability.

5.2.3 Gas permeation measurements

Gas permeation measurements were conducted for the post-combustion gaseous mixture (CO_2/N_2, (15/85)) under a feed pressure of 3 bar and different temperatures (25, 35 and 50 °C), in order to study the dependence of CO_2 permeability with the operating temperature. Figure 5.6 shows the effect of the operating temperature on PEBA membranes. It can be observed that for the three casting solution concentrations tested, the CO_2 permeability increased when the temperature raised, due to the thermal activation process.

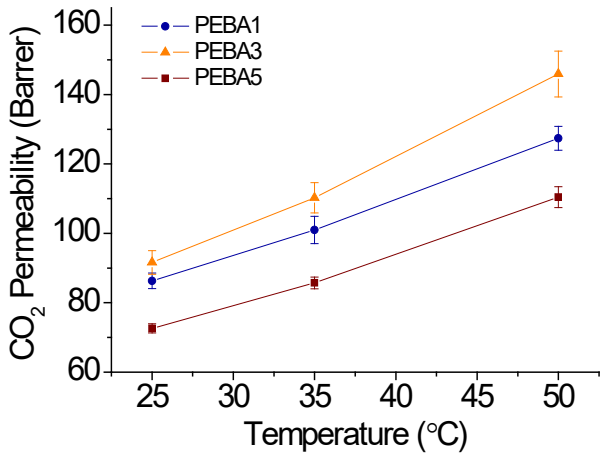

Figure 5.6. Comparison of CO_2 permeability at different temperatures (25, 35, and 50 °C) and 3 bar feed pressure for the three concentrations of Pebax® MH1657 tested in this work. Error bars come from the testing of at least 3 different membrane samples

To study this behavior more in depth, an Arrhenius modified model was applied to the permeability data as explained in section 2.4.1.3 (equation 2.11).[53] Based on this equation, the activation energy will be higher for less permeable gases.[147]

In this study, the E_p for CO_2 (the most permeable gas of the mixture) was lower than that for the N_2 (listed in Table 5.2), corroborating the previous statement. Furthermore, values of activation energy for permeation were very similar to those found in the literature for this polymer (13.3 kJ·mol^{-1} for CO_2 and 30.4 kJ·mol^{-1} for N_2).[114] Besides, the highest activation energies for both CO_2 and N_2 permeations were those of PEBA3 (14.9 kJ·mol^{-1} and 28.0 kJ·mol^{-1} for CO_2 and N_2, respectively), being this sample which provided the highest permeability and selectivity (146 Barrer of CO_2 with a CO_2/N_2 selectivity of 27 at 50 °C), although the three membranes tested possessed comparable values at the same temperature. A comparison of the permeability of CO_2 for the three membranes prepared is depicted in Figure 5.6. As shown in this figure, the highest CO_2 permeabilities were those of PEBA3 (92, 110 and 146 Barrer at 25, 35 and 50 °C, respectively) whereas PEBA5 provided the lowest flow values (73, 86, and 110 Barrer of CO_2 at 25, 35 and 50 °C, respectively). Usually, crystalline polymers tend to be less permeable than the amorphous ones, since hard segments in semi-crystalline polymers block the movement of gas molecules through the membrane, due to the inflexibility of the chains.[148] Based on this statement, PEBA5 was expected to be the sample with the

highest gas permeability in this study because it was the membrane with the lowest crystallinity, according to DSC analyses (see Table 5.1 and Figure 5.3), followed by PEBA3 and PEBA1. Conversely, PEBA5 did not followed this behavior. The explanation for such decrease in permeability may be linked to the solvent evaporation time. As aforementioned, for the same amount of polymer, PEBA5 required less time to

Table 5.2. Gas permeation properties of PEBA dense membranes tested at different operating temperatures (25, 35 and 50 °C) and under a feed pressure of 3 bar

	Temperature (°C)	CO_2 Permeability (Barrer)	CO_2/N_2 Selectivity	E_p CO_2 (kJ mol^{-1})	E_p N_2 (kJ mol^{-1})
PEBA1	25	86 ± 2	39 ± 6	12.5	27.0
	35	100 ± 4	35 ± 4		
	50	127 ± 3	26 ± 3		
PEBA3	25	92 ± 4	41 ± 4	14.9	28.0
	35	110 ± 4	36 ± 4		
	50	146 ± 7	27 ± 4		
PEBA5	25	73 ± 1	34 ± 5	13.5	25.1
	35	86 ± 2	31 ± 4		
	50	110 ± 3	24 ± 1		

evaporate the solvent, leading to a more entangled structure because the polymer chains do not have enough time to reorder. Furthermore, the interactions between macromolecules increase when the polymer solution is more concentrated due to the rise of viscosity, which also leads to chain entanglement and network formation.[149] Such entanglement could be acting as a barrier for the carbon dioxide to diffuse through the membrane, reducing the gas permeability. This effect of entanglement has been previously reported by Isanejad et al.[139] In their case, differences of crystallinity were related to the volatility of the solvent used to dissolve the PEBA. Such volatility implied that the time required to completely evaporate the solvent was distinct and so was the separation performance of membranes. In fact, they found that the most crystalline membranes were those with the highest selectivity and lowest permeability, in agreement with our findings.

Figure 5.7 depicts the effect that the operating temperature has on the CO_2/N_2 selectivity and compares the three membranes studied. While as shown above, the gas permeability increased when raising the working temperature (see Figure 5.6), the CO_2/N_2 selectivity became lower, hence following the Robeson trade-off relationship between permeability and selectivity.[4] In any event, activation energy values are always higher for the slowest permeating compound in the mixture (N_2), what is consistent with the decrease in selectivity observed as a function of temperature. Selectivity and permeability data obtained from gas chromatography tests are collected in Table 5.2. When comparing the selectivities achieved for each sample, PEBA3 can be considered the membrane with the highest separation capacity, independently on the operating temperature (with 41 as the highest selectivity at 25 °C). This fact means that this membrane was able to differentiate in a better way between both gas molecules, thus reaching a slightly higher separation capacity. Again, PEBA5 was found to be the sample with the lowest values (with a CO_2/N_2 selectivity of 34 at 25 °C), whereas PEBA1 selectivity performance was similar to that of PEBA3 (39 at 25 °C). Comparing the permeability and selectivity values presented in Table 5.2, it can be observed that both gas selectivity and permeability are similarly influenced by the changes in the PEBA concentration in the casting solution. On the other hand, these two parameters (selectivity and permeability) are also influenced by the operating temperature. Taking PEBA1 as an example, permeability increased 48%, whereas the CO_2/N_2 selectivity decreased 52%, when increasing the temperature from 25 to 50 °C.

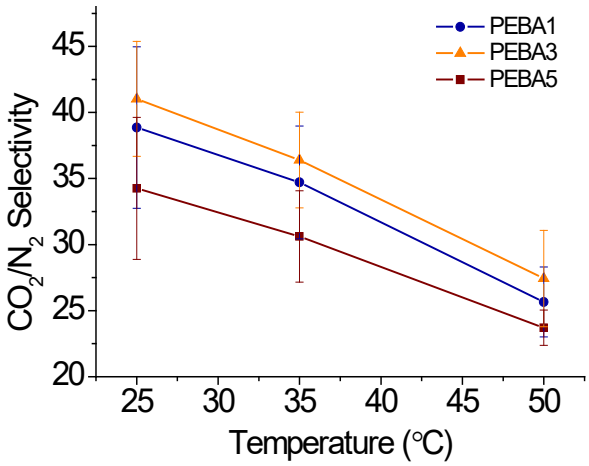

Figure 5.7. Comparison of CO_2/N_2 Selectivity at different temperatures (25, 35, and 50 °C) and 3 bar of feed pressure for the three concentrations tested.

5.3 Conclusions

Dense Pebax® 1657 membranes, with a thickness of 40 µm, were successfully prepared varying the polymer concentration in the 70/30 (v/v) ethanol/water solvent mixture. As predicted, membranes showed different behaviors depending on the PEBA concentration used to prepare the casting solution. The sample with the lowest concentration (1 wt%) and thus, the highest percentage of solvent, resulted in the most crystalline film. This characteristic was principally attributed to the polymer chain interactions established in the solvent solution (due to the changes in the solution viscosity) and the evaporation time, which seemed to be an important factor in the fabrication of organized structures. Crystallinity, besides, played a key role in the thermal degradation, being the most stable membranes those with the highest crystalline domain, indicative of the rigidity of the polymer chains. Apparent activation energies aided in confirming this behavior. The PEBA membrane obtained from the most diluted polymer solution (1 wt%) was found to be the most crystalline film (15% and 6% related to the crystalline PEO and PA segments respectively) and therefore, its apparent activation energy (calculated applying two different integral methods) was also the highest (ca. 275 $kJ \cdot mol^{-1}$). Thermal annealing has been demonstrated by treating the PEBA3 at 150 °C and different periods of time (3 and 8 days). In contrast to the samples not treated, although the crystallinity increases after the thermal treatment,

membranes are partially degraded and hence, they start to lose weight at lower temperatures.

The polymer crystallinity decreased with the polymer concentration (tested at 1, 3 and 5 wt%) in the casting solution. However, from the point of view of the CO_2 permeability and CO_2/N_2 separation selectivity, a trade-off was reached between crystallinity and separation properties, being 3 wt% the most suitable polymer concentration studied. The operating temperature (25, 35 and 50 °C) exerted an important influence in the permeability and selectivity of the membranes. The activation energy values of permeation obtained after applying the Arrhenius equation to the collected data were similar to those found in the literature (ca. 13 $kJmol^{-1}$ and 26 $kJmol^{-1}$ for CO_2 and N_2, respectively) and higher for the less permeable gas (N_2 in this study). Consistent as expected with the decrease of CO_2/N_2 selectivity as a function of temperature. In summary, the membranes prepared from a 3 wt% PEBA solution, were found to be the most permeable and selective membranes, independently on the operating temperature.

5.4 Supplementary Information

Theoretical background

d-spacing and crystallinity (X_c) calculations

In order to study the morphology of the membranes, the molecular distances between polymer chains (d-spacing) and the crystallinity can be estimated using different techniques such as X-ray diffraction (XRD) or differential scanning calorimetry (DSC). In this study, the d-spacing was calculated applying Bragg's law to the data collected from XRD, (eq. S5.1):

$$n \cdot \lambda = 2 \cdot d_{sp} \cdot \sin\theta \qquad \text{(eq. S5.1)}$$

where n is a positive integer, λ is the wavelength (λ=0.154 nm), d_{sp} is the d-spacing (nm) and θ is the angle of incidence. The polymer crystallinity was estimated with the data obtained by DSC, applying the following equation, (eq. S5.2):

$$X_c\ (\%) = \frac{\Delta H_m}{\Delta H_m^0} \cdot 100 \qquad \text{(eq. S5.2)}$$

where Xc is the crystallinity in %, ΔH_m is the melting enthalpy ($J \cdot g^{-1}$), calculated integrating the area under the melting peak, and ΔH_m^0 ($J \cdot g^{-1}$) is the melting enthalpy of the polymer 100 % crystalline. In the case of PEBA, the crystallinity of both segments has been determined using 147 $J \cdot g^{-1}$ and 230 $J \cdot g^{-1}$ as the enthalpy of the 100 % crystalline polyethylene oxide (PEO) and polyamide (PA), respectively.[150]

Apparent activation energy (Ea)

In chemistry, the minimum amount of energy required by a chemical reaction to occur is called activation energy. Changes in temperature or pressure also imply changes in other molecular properties such as chemical velocity, gas permeability, gas diffusivity and solubility, relative crystallinity, etc.[151,152] usually following an Arrhenius equation, (eq. S5.3):

$$k(T) = k_0 \cdot \exp\left(-\frac{E_a}{R \cdot T}\right) \qquad \text{(eq. S5.3)}$$

where k(T) is a rate constant, k_0 is the pre-exponential factor, Ea is the apparent activation energy in J·mol^{-1}, R the ideal gas constant 8.314 J mol^{-1}·K^{-1} and T is the temperature in K.

Very often, the knowledge of the kinetic model becomes a problem in a kinetic study. For this reason, integral methods, which do not assume any kinetic model, are widely employed for the estimation of the apparent activation energy.[153–155] In the present study, two different integral methods have been used to calculate the apparent activation energy of the membranes thermal degradation. These are the Kissinger and Ozawa Integral methods.

Kissinger,[156] developed a procedure to calculate the activation energy collecting data of thermal degradation (differential thermal analysis) at different heating rates, demonstrating that the increment of the heating rate led to a displacement of the maximum degradation peak to higher temperatures, (eq. S5.4):

$$\ln \frac{\beta}{T_m^2} = \ln \frac{k_0 \cdot R}{E_a} - \frac{E_a}{R \cdot T_m} \qquad \text{(eq. S5.4)}$$

Ozawa,[157] suggested a method to study the process of nucleation and growth in non-isothermal cold crystallization. Such technique was based on the estimation of the modified activation energy with data obtained from tests conducted by cooling poly(ethylene-terephthalate) at constant heating rates, using DSC, (eq. S5.5):[158]

$$\ln \beta = \ln \frac{0.00484 \cdot k_0 \cdot E_a}{G(\alpha) \cdot R} - 1.0516 \cdot \frac{E_a}{R \cdot T_m} \qquad \text{(eq. S5.5)}$$

In both equations (S5.4) and (S5.5), β is the heating rate (K·min^{-1}), Tm is the temperature of the maximum weight loss (K), Ea is the degradation apparent activation energy (J·mol^{-1}), k_0 is the pre-exponential factor in s^{-1} and R is the ideal gas constant in J·mol^{-1}·K^{-1}. In Ozawa's equation, G(α) is a constant value.

Results

Experimental X-ray diffraction (XRD) of PEBA3 membranes with and without thermal treatment at 150 °C for different periods of time (3 and 8 days) (Figure S5.1) suggests that the crystallinity is affected by the time that the membrane is at this conditions. In fact, the crystallinity is higher when the time that the sample is under this conditions increase. Despite the higher crystallinity, the sample changed its color when subjected

to thermal treatment, indicating that a partial degradation has taken place during the heating (Figure S5.2).

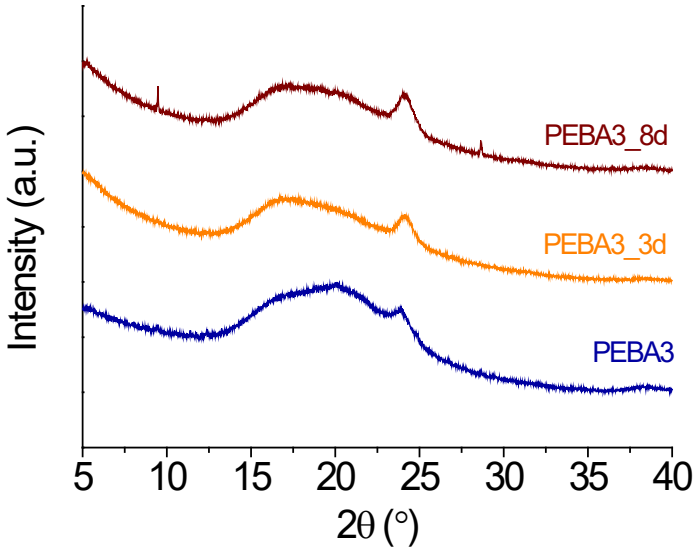

Figure S5.1. XRD patterns of PEBA membranes with and without thermal treatment (3 and 8 days at 150 °C).

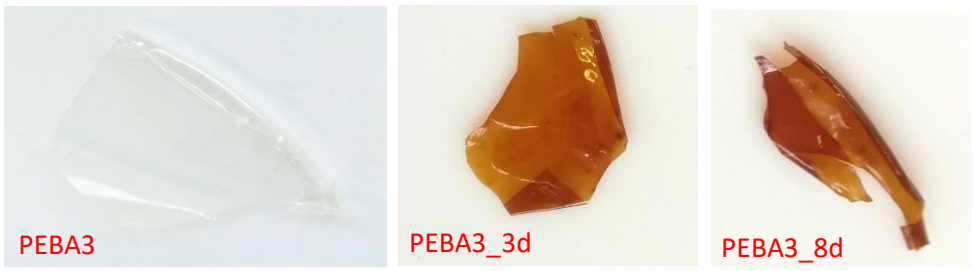

Figure S5.2. Pictures of the membranes without (PEBA3) and with thermal treatment after 3 (PEBA3_3d) and 8 (PEBA3_8d) days at 150 °C.

With the data obtained by TGA, the apparent activation energy of these treated membranes was calculated and compared with that of the PEBA3 without post-treatment. The values obtained show an important decrease in the activation energy, which corroborates the partial degradation of the samples. This fact also implies that the membranes have lost thermal stability.

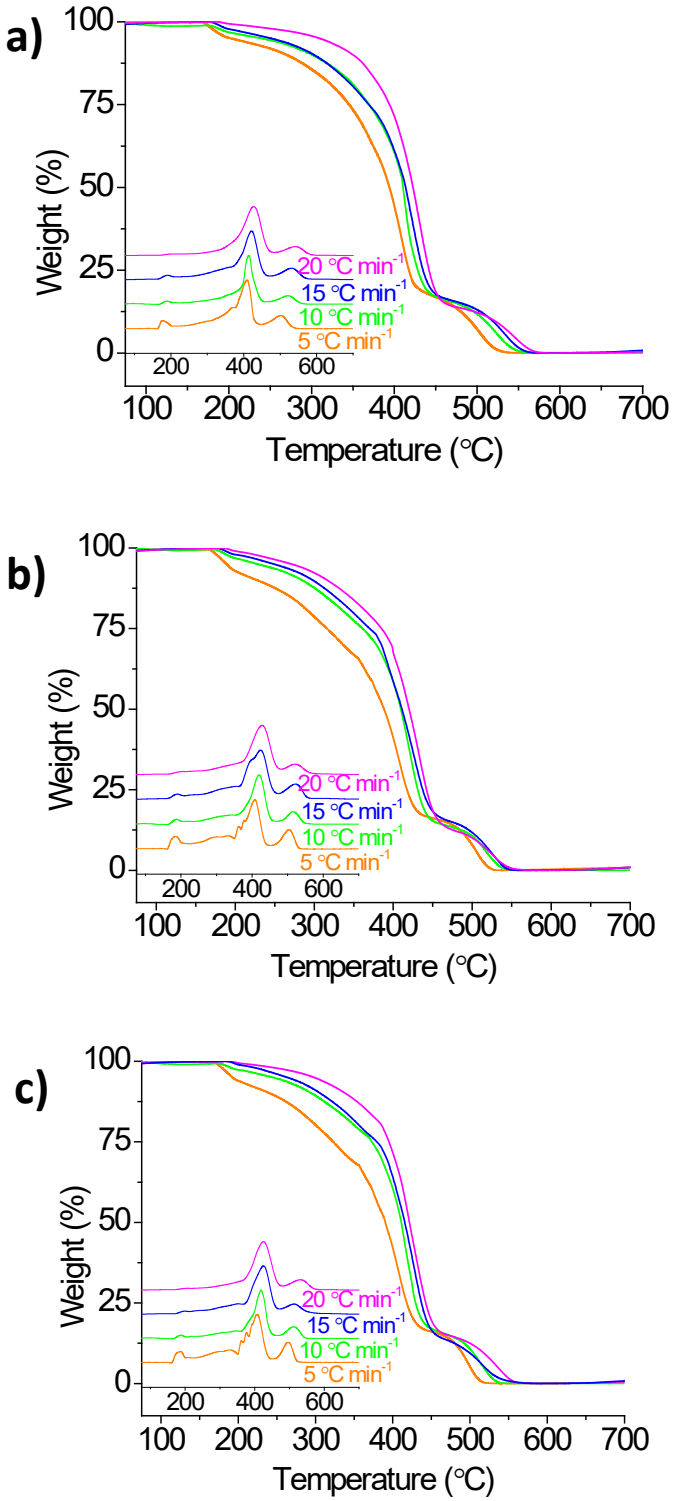

Figure S5.3. TGA and DTG curves of PEBA1 (a), PEBA3 (b) and PEBA5 (c) at different heating rates (5, 10, 15 and 20 °C min^{-1}), in air atmosphere.

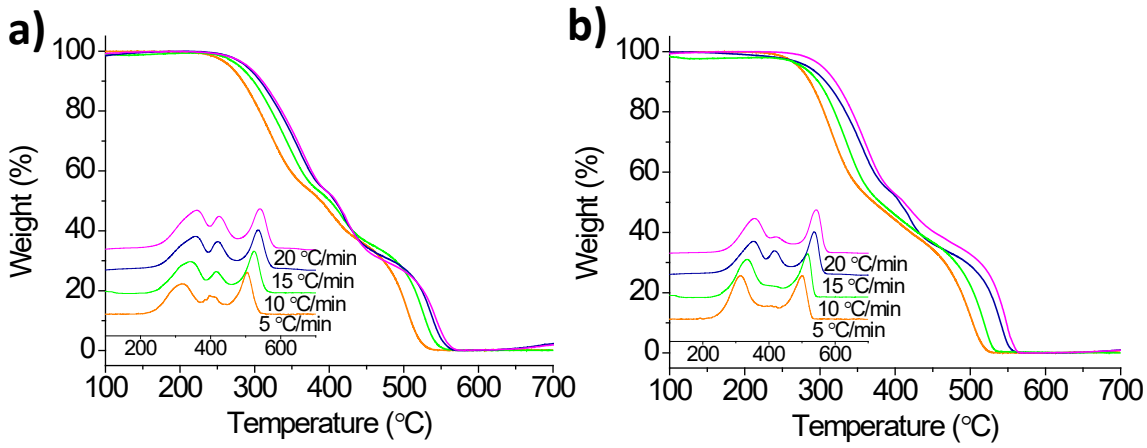

Figure S5.4. TGA and DTG curves of PEBA3 treated at 150 °C during 3 days (a) and 8 days (b), at different heating rates (5, 10, 15 and 20 °C min^{-1}) in air atmosphere.

Table S5.1. Apparent activation energies calculated with the Kissinger and Ozawa methods for the membranes treated at 150 °C.

	Tmax(1) (°C)	Tmax(2) (°C)	Ea(a) (kJ mol^{-1})	Ea(b) (kJ mol^{-1})
PEBA3	420	515	263	261
PEBA3_3d	342 - 417	523	180	184
PEBA3_8d	335 - 417	518	148	153
(1) Thermal decomposition at a heating rate of 10 °C min^{-1} (for PEBA3_3d and PEBA3_8d, the two values of temperature correspond to the two peaks that appear in this decomposition step), (2) oxidation step at a heating rate of 10 °C min^{-1}, (a) calculated with Kissinger equation and (b) with Ozawa method.				

Capítulo 6: "Phase inversion method for the preparation of Pebax® 3533 thin film membranes for CO_2/N_2 separation"

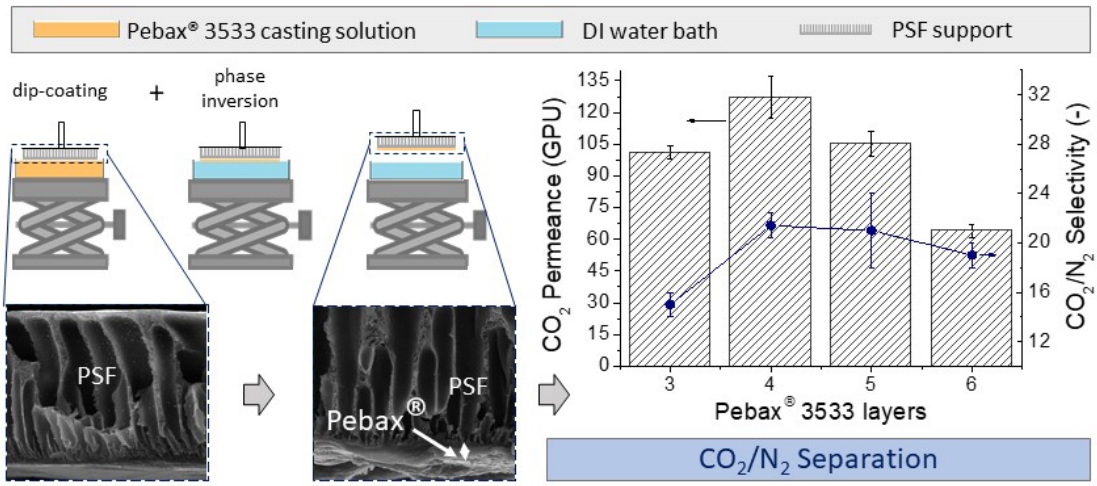

Adapted from "L. Martínez-Izquierdo, M. Malankowska, C. Téllez, J. Coronas. Phase inversion method for the preparation of Pebax® 3533 thin film membranes for CO_2/N_2 separation. Journal of Environmental Chemical Engineering 9 (2021) 105624", with permission from Elsevier.

6. Phase inversion method for the preparation of Pebax® 3533 thin film membranes for CO_2/N_2 separation

6.1 Introduction

Among the most common greenhouse gases, carbon dioxide (CO_2) is considered to be the main cause of the global temperature rise. To alleviate this negative effect, there is a demand for CO_2 capture and sequestration technologies.[159] Such technologies must be able to remove CO_2 from fuels and exhaust gases to achieve a clean stream to be used in other industrial processes.[160] Within these processes, post-combustion CO_2 capture is the simplest approach to be implemented due to its ease to be adapted to the already existing industrial facilities. In this field, technologies like physical or chemical absorption with amines, cryogenic distillation, and adsorption[161] have been the most commonly used for CO_2 capture, although some drawbacks such as their potential toxicity or the difficulties derived from the regeneration of the solvent (in the case of chemical absorption with amines) resulted in many studies focusing on greener approaches.[94] With this aim, gas separation via polymeric membranes is now gaining more attention over the traditional techniques due to its well-known advantages, i.e. mechanical simplicity, easy to scale up, lower energy consumption and cost, and smaller footprint.

CO_2 capture from post-combustion streams is based on the separation of CO_2 from a CO_2/N_2 mixture, where CO_2 concentration can go from ca. 15% in case of typical combustion processes to ca. 30% in case of stainless steel and cement industries, important producers of this gas. In this sense, working with polymers with excellent properties and facilitated transport parameters for this mixture is mandatory to obtain effective membranes. Poly(ether-block-amide) copolymers (PEBA, usually commercialized as Pebax®) are composed of two different polymer segments (polyamide (PA) and polyether (PE)). Each segment provides different material characteristics and combined make Pebax® a very promising candidate.[18,61,105–108] In this work, Pebax® 3533 code was used due to its solubility in an alcohol (1-propanol/1-

butanol) mixture, which suggests higher chemical stability of the obtained membranes when exposed to moisture since the most common Pebax® 1657 membranes are obtained from water/ethanol polymer solutions. A good stability of membranes to water vapor is needed since in real post-combustion processes coal-derived flue gases not only contain CO_2 and N_2 but also oxygen, SO_x and NO_x compounds and other minor contaminants like water vapor.[13]

To achieve an efficient separation, which exceeds the Robeson trade-off relationship between permeability and selectivity, [4] an ideal membrane for gas separation should be as thin as possible, to maximize the flux through it (high CO_2 permeance), highly selective and mechanically robust.[35] To accomplish this target, composite membranes must be prepared with a very thin selective layer.

In the open literature, the methods for preparing composite membranes are diverse. The most typical approaches include dip-coating,[95,162] spin-coating[163,164] and interfacial polymerization,[165] being the dip-coating the most commonly used for gas separation membranes due to its easy implementation. According to this method, Ren et al. prepared a multilayer polyetherimide (PEI)/polydimethylsiloxane (PDMS)/Pebax® 1657/PDMS composite membrane.[108] With this composite membrane the authors achieved, at 5 bar and 25 °C, a CO_2 permeance of 157 GPU and a CO_2/N_2 selectivity of 64. Zhao et al. developed a similar multilayer structure based on a polysulfone (PSF) support covered by a PDMS gutter layer modified with plasma and a Pebax® 1657 selective layer.[166] In this case, the authors obtained a CO_2 permeance of 170 GPU and an ideal CO_2/N_2 selectivity of 49, measured at 7 bar and 30 °C.

In this work, we report the preparation for the first time of Pebax® 3533 thin film composite membranes via a phase inversion method (immersion-precipitation with a non-solvent). Following this approach, different membranes were prepared varying the concentration of Pebax® 3533 in the casting solution (0.25, 0.5, 1.0 and 1.5 wt%) as well as the number of layers deposited (1 to 6). The best condition found was chosen to prepare supported membranes by dip-coating, tested for the separation of CO_2/N_2 mixtures. Finally, Pebax® 3533 has only rarely been studied, and in a few publications: as dense membrane for CO_2 separation,[123] to improve impact strength[167] and in drug release.[168]

6.2 Results

6.2.1 Membranes preparation and characterization

Figures 6.1a and b show the cross-sections of the PSF support and the Pebax® 3533 dense membrane, respectively, prepared by the conventional casting solution method. These images were taken for comparison with the supported membranes. As can be seen in Figure 6.1a, the PSF support prepared in this work has a thickness of around 150 µm and is constituted by two different porous layers, finger-like macropores at the top of the film and thick sponge-like micropores at the bottom. Moreover, Figure 6.1b confirms the Pebax® 3533 dense morphology without the existence of apparent porosity, as expected for this kind of polymers when prepared by the casting-solution technique. Membranes prepared in this way had a thickness of approximately 55 µm.

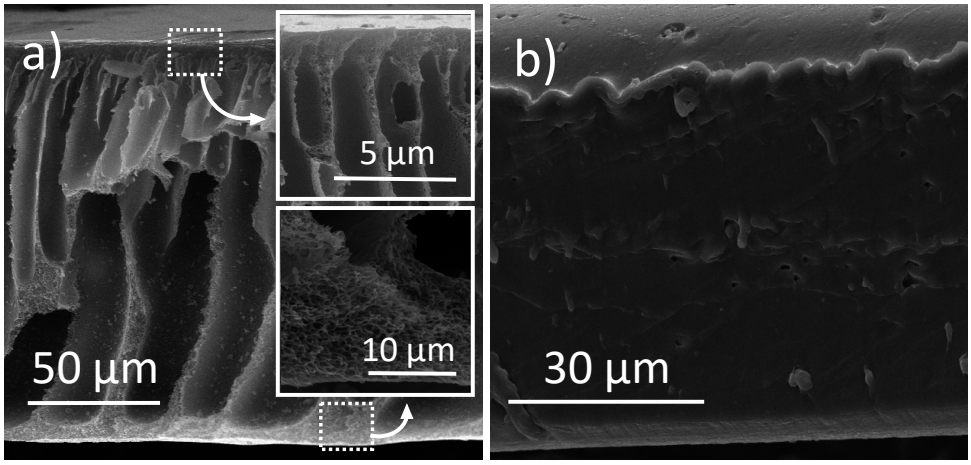

Figure 6.1. Cross-section images of the PFS support (a) and the Pebax® 3533 dense membrane prepared by the conventional casting-solution method (b). Insets correspond to the top and bottom sides of the PSF support.

Pebax® 3533 thin film composite membranes (TFC) were prepared by phase inversion method on top of asymmetric PSF supports. Although this approach has been widely used for the preparation of asymmetric supports,[68] to the best of our knowledge, only a recent article published in our research group considers this route for Pebax®-type polymers (Pebax® 1041).[94] In contrast to this previous work, in which a polymer emulsion was drop-cast on a porous support, here we focus on the preparation of thin film composites of Pebax® 3533/PSF via layer-by-layer method. An ideal membrane for gas separation must be as thin as possible to reach a high flow through it without losing selectivity. To this aim, different conditions were tested in this work varying the

concentration of Pebax® in the casting solution as well as the number of layers applied on top of the supports. Figures 6.2a, b, c and d show the supported membranes prepared with the 0.5 wt% casting solution after the application of 3, 4, 5 and 6 polymer layers, respectively. TFC membranes prepared with the casting solutions of 0.25, 1.0 and 1.5 wt% are shown in Figures S6.1, S6.2 and S6.3 of the Supplementary Information section, respectively. It can be seen that in all cases a very thin layer of Pebax® was deposited on top of the PSF supports (ranging from 400 nm to 1.3 µm, see Table 6.1) and that the number of layers cannot be differentiated. Furthermore, dense morphology obtained in all cases differs from the high-porosity expected in membranes prepared via phase inversion. Since Pebax®-type polymers behave as an elastomer-thermoplastic, such differences in morphology could be related to the collapse of the porous structure during the drying state. This behavior was also found by Sánchez-Laínez et al. in Pebax® 1041 membranes when prepared through the phase inversion method.[94]

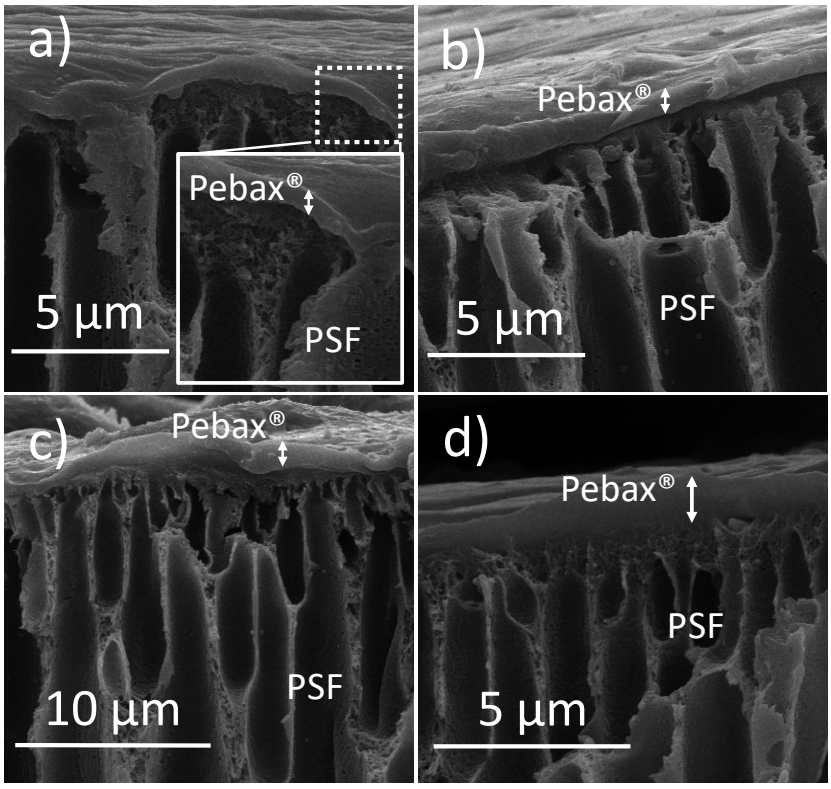

Figure 6.2. Cross-section images of the supported membranes prepared with the 0.5 wt% casting solution via phase inversion after the deposition of 3 (a), 4 (b), 5 (c) and 6 (d) Pebax® layers. Inset in (a) corresponds to the top layer of the membrane.

The thickness of each supported membrane obtained by SEM is collected in Table 6.1. As expected, for the same number of layers, the selective layer total thickness decreased when the casting solution concentration was lower. Besides, for the same casting solution concentration, the total thickness increased with the number of layers.

Table 6.1. Thickness of supported membranes prepared in this work via phase inversion.

Membrane	Pebax® 3533 (wt%)	Layers	Thickness (μm)	Thickness increase (μm)
1.5wt%_1	1.5	1	1.0 ± 0.2	1.0
1.5wt%_2	1.5	2	1.8 ± 0.1	0.8
1.0wt%_1	1.0	1	0.5 ± 0.1	0.5
1.0wt%_2	1.0	2	1.5 ± 0.1	1.0
0.5wt%_3	0.5	3	0.4 ± 0.1	0.4
0.5wt%_4	0.5	4	0.7 ± 0.2	0.3
0.5wt%_5	0.5	5	1.0 ± 0.2	0.3
0.5wt%_6	0.5	6	1.3 ± 0.3	0.3
0.25wt%_4	0.25	4	0.2 ± 0.0	0.2
0.25wt%_5	0.25	5	0.5 ± 0.0	0.3
0.25wt%_6	0.25	6	0.8 ± 0.0	0.3

Table 6.1 also shows the contribution of each layer to the thickness increase. In the case of the membranes prepared with the 0.5 wt% casting solution, for example, each additional layer made the total thickness to increase by ca. 300 nm. With this in mind, a total thickness of 900 nm would be expected for the 3-layered membrane instead of 400 nm. This difference could be due to the slight pore filling with the casting solution and the compatibility of the Pebax® polymer with the support. Once the support is covered with a layer of Pebax®, regardless of the thickness, compatibility increases and so does the homogeneity of the deposited Pebax® layers. The penetration of the casting solution into the support porosity is favored with less concentrated and less viscous polymer solutions.

From these results, we can conclude that from casting solution concentrations of 1.0 wt%, the more diluted the casting solution is, the more pore filling takes place and more

defects must be repaired by the subsequent coatings. Therefore, a greater number of Pebax® layers will be required to obtain a homogeneous supported membrane. This statement can be justified if we take into account the casting solution viscosities. Figure 6.3 shows the intrinsic viscosity of each casting solution concentration tested in this work at different rotational speeds compared with that of the pure mixture of solvents. As expected, the most concentrated casting solutions resulted in the most viscous ones as well. Such differences in viscosity seem to have an impact on the final characteristics of the Pebax® skin layer, as reduced solution viscosity is usually translated into faster exchange rate between casting solution solvent and water during the phase inversion. This phenomenon may lead to the formation of macro-voids (defects).[169] Furthermore, for all cases, the viscosity decreased with the rotational speed, which means that all solutions behave as non-Newtonian pseudo-plastic fluids.

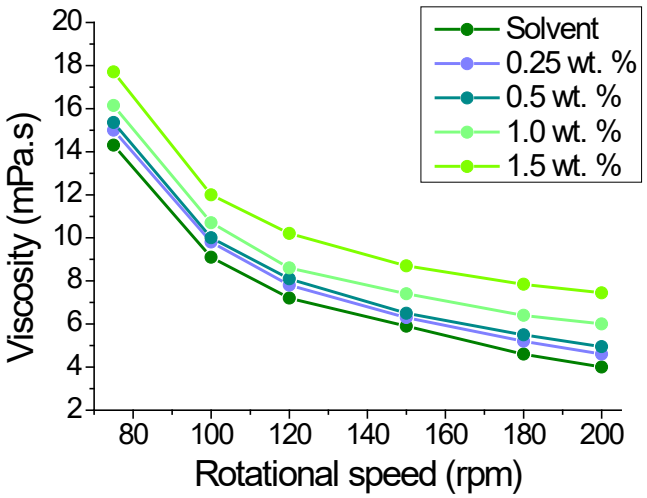

Figure 6.3. Viscosity tests conducted at 24 °C and different rotational speeds for all the casting solution concentrations tested (0.25, 0.5, 1.0 and 1.5 wt%).

The chemical structures of the TFC membranes were also studied using an FTIR-ATR spectrometer. Figure 6.4 shows the FTIR spectra of the supported membranes prepared with the 0.5 wt% casting solution, compared to that of the bare PSF support and the self-supported Pebax® 3533 dense membrane. The same comparison can be found in Figure S6.4 of the Supplementary Information section, corresponding to the membranes prepared with the rest of the casting solutions tested (0.25, 1.0 and 1.5 wt%). As seen in these figures, several bands can be differentiated in the PSF spectrum. Bands at 1583 and 1486 cm^{-1} are associated to the aromatic C=C stretching vibration.[170] The strong

band that appears at 1236 cm^{-1} is related to the asymmetric C-O-C stretching of the aryl ether. Symmetric and asymmetric O=S=O stretching of the sulfone group is visible in the bands at 1148 and 1102 cm^{-1}. Finally, the two bands in the range of 900-800 cm^{-1} correspond to the vibrations of the aliphatic C-H bonds.[171] In the case of the Pebax® 3533 spectrum, three main bands can be differentiated at 2925, 1640 and 1100 cm^{-1} associated to both, the polyamide and the PTMO segments. Regarding the hard segment (PA-12), the band at 1640 cm^{-1} corresponds to the vibrations of the H-N-C=O group.[125] Vibrations corresponding to the soft segment (PTMO) are visible in the bands at 2925 and 1100 cm^{-1}, assigned to the stretching and bending vibrations of the aliphatic C-H group and the stretching vibration of the C-O-C ether group, respectively, which are in accordance with the literature.[94,126]

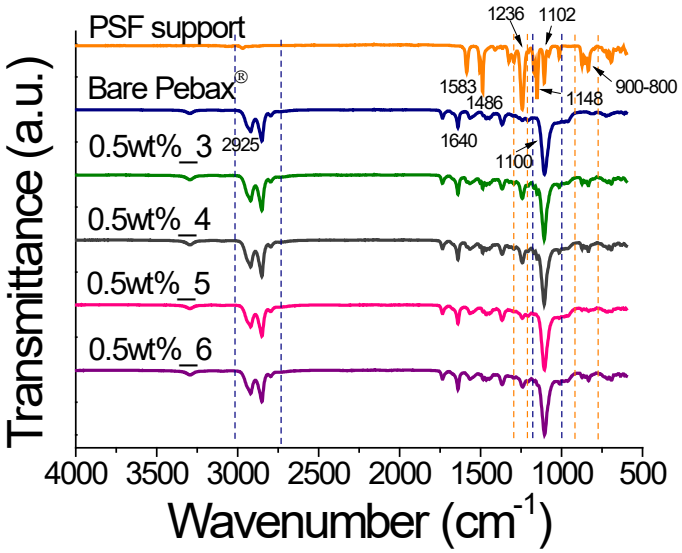

Figure 6.4. FTIR-ATR spectra of membranes prepared by phase inversion with the 0.5 wt% casting solution concentration and a different number of layers (from 3 to 6) compared to that of the bare PSF support and the Pebax® 3533 dense membrane.

Some of these main bands can be appreciated in the TFC spectrum. Figure S6.4a shows the spectra of the TFC membranes prepared with the 1.5 wt% casting solution, which confirms that just with a single layer of Pebax® the surface of the porous support was covered uniformly since no band associated to the PSF can be appreciated. In contrast, when decreasing the casting solution concentration, for the TFC membranes prepared with the 1.0 wt% casting solution (Figure S6.4b), the bands at 1236 cm^{-1} and 900-800 cm^{-1}, associated to the C-O-C stretching and C-H bonds of the PSF, are visible.

In spite of that, the bands related to the Pebax® selective layer are stronger, indicating that bands of PSF observed can be due to the Pebax® thickness, which is thinner than that obtained with the more concentrated solution. These bands disappear when applying a second polymer layer. The same behavior is observed for the membranes prepared with the 0.5 wt% casting solution (Figure 6.4). However, the strong bands at 1236 and 900-800 cm^{-1} are present in all cases, no matter the number of layers applied. In the case of membranes prepared with more diluted casting solution (Figure S6.4c), the spectra obtained with all samples are more similar to that of the PSF support, despite the fact that the thicknesses of membranes prepared with 0.25 wt% casting solution after 5 and 6 layers are analogous to those of the membranes prepared with the 0.5 wt% solution after 4 and 5 layers, respectively. Such differences could be due to some defects possibly related to the concentration of the casting solution, which alters the viscosity and hence the behavior of the polymer in the phase inversion process.[172–174] This statement was confirmed when testing the membranes for the CO_2/N_2 gas separation (see gas permeation section).

Furthermore, an additional comparison illustrating the differences between each casting solution concentration is shown in Figure S6.5 of the Supplementary Information section. In this figure, the FTIR spectra of the supported membranes prepared with each casting solution concentration after the deposition of 1 layer are compared with that of the bare PSF and the Pebax® 3533 dense membrane. As can be seen, this figure also demonstrates the previous statement. As the casting solution concentration decreases, the bands associated to the PSF support are stronger whereas that associated to the Pebax® becomes weaker. This fact confirms the need to apply more layers to the PSF when a very diluted solution is used.

The thermal stability of the membranes was studied by thermogravimetric analysis. The TGA and DTG results of the supported membranes prepared with the 0.5 wt% casting solution, compared with that of the bare PSF and Pebax® 3533 can be visualized in Figure 6.5. As expected, due to the ultrathin layers deposited on top of the PSF supports, the thermal stability of membranes remains almost the same. In fact, Pebax® maximum degradation peak at 422 °C cannot be appreciated in TFC thermograms. Otherwise, only the peaks related to the thermal degradation of PSF at 515 and 635 °C

are visible in the supported membranes, despite containing two different polymers. The greater proportion of PSF is responsible for this behavior.[33] Apart from that, TGA curves of the membranes prepared with 4-6 layers of Pebax® show a greater weight loss in the first degradation step, which suggest that the thermal degradation of the Pebax® selective layer is taking place at the same time as the PSF support. Furthermore, while degradation peaks of the membrane prepared with the lowest number of layers (0.5wt%_3) remained unaltered, it can be seen that the maximum PSF degradation that takes place at 515 °C was delayed in membranes with 4, 5 and 6 layers. Such delay can be related to a diffusion limitation, as PSF pores are covered by the more restrictive to the gas passage Pebax® 3533 selective layer. The same behavior was found for the rest of the casting solution concentrations tested in this work, whose thermograms can be found in Figures S6.6-S6.8 of the Supplementary Information section.

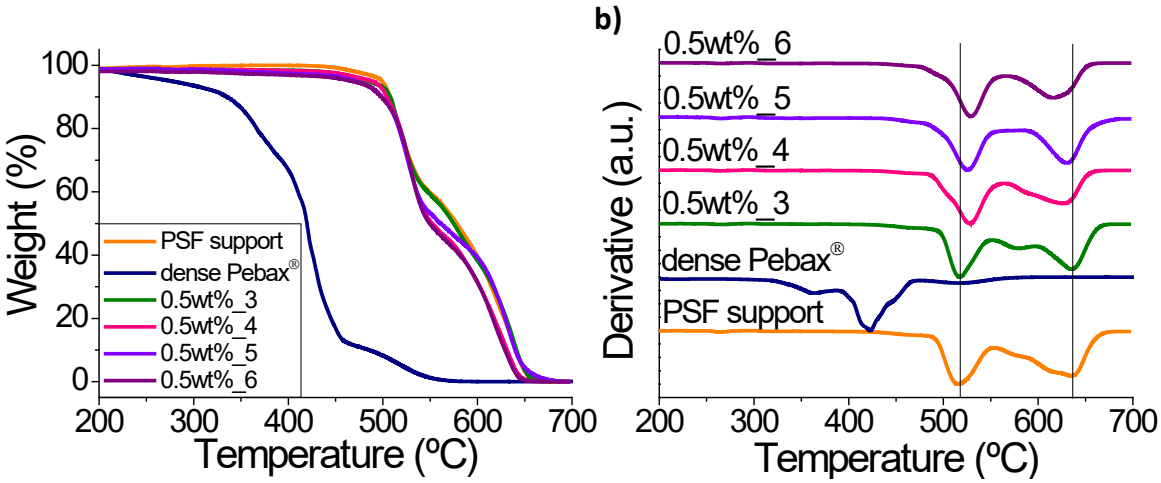

Figure 6.5. TGA and DTG analyses of TFC membranes prepared by the phase inversion method with the 0.5 wt% casting solution compared to that of the PSF support and the bare Pebax® 3533.

6.2.2 Gas permeation tests

The gas separation performance of the supported membranes was tested for the CO_2/N_2 mixture under a feed pressure of 3 bar and 35 °C and can be seen in Figure 6.6. In this figure, error bars correspond to the testing of at least three different membrane samples at the same conditions. Data shown in this figure are also collected in Table S6.1 of the Supplementary Information section. As expected, CO_2 permeance increased with the dilution of the Pebax® solution and decreased with the application of additional layers. However, some deviations were found for the membranes prepared with the

most diluted solutions. In the case of those prepared with the 0.5 wt% casting solution, far from expected, the CO_2 permeance of the membrane with three polymer layers was lower than that with four and even five layers, these permeances being 101 ± 3 GPU, 127 ± 10 GPU and 105 ± 6 GPU, respectively.

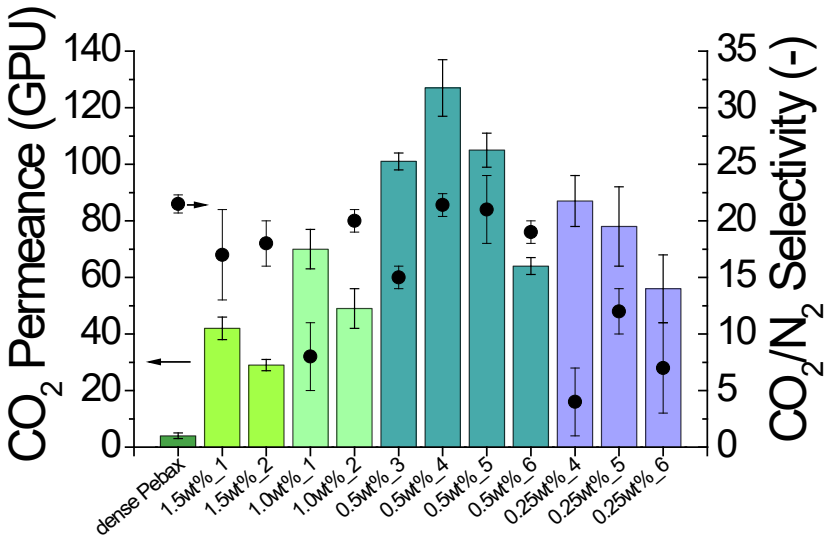

Figure 6.6. Comparison of the CO_2 permeance and CO_2/N_2 selectivity of membranes prepared via phase inversion obtained at 35 °C and 3 bar. Bars stand for permeance and scatters for selectivity.

As shown in Figure 6.7, such deviation could be related to the higher N_2 permeance of membranes prepared with three layers. In fact, N_2 permeance decrease with the application of additional layers. This phenomenon suggests the presence of micro-defects at the top layer of the 0.5wt%_3 membranes, which hinder the selective diffusion of CO_2 molecules with the consequential decrease of selectivity. These defects were repaired after the application of an additional layer, which acts as healing and increased not only the CO_2 permeance but also the membrane selectivity. After the application of four Pebax® 3533 layers, the supported membranes followed the typical behavior described before. Otherwise, the lower CO_2 permeances of the membranes prepared with the 0.25 wt% casting solution compared to that of the 0.5 wt%, could be due to the decrease in the solution viscosity.

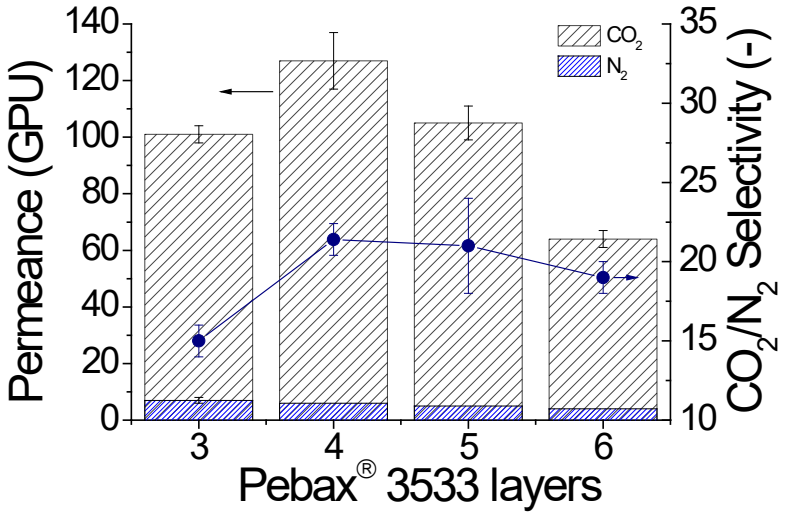

Figure 6.7. Comparison of the gas separation results obtained for the supported membranes prepared with the 0.5 wt. % casting solution tested at 35 °C and a feed pressure of 3 bar. Bars stand for permeance and scatters for selectivity.

As mentioned before, the reduction in viscosity can favor the pore penetration hindering the diffusion of gas molecules. Apart from that, defects obtained with this casting solution were more visible, since it was not possible to obtain a membrane with a CO_2/N_2 selectivity similar to that of the dense Pebax® 3533, ca. 21.5. In addition, larger error bars demonstrate a worse reproducibility. With this data, the optimal casting solution corresponds to that prepared with the 0.5 wt% of Pebax® and the best results were achieved with the application of four and five layers on top of the PSF supports. For these membranes, the CO_2/N_2 selectivity was the same as that of the dense Pebax® 3533.

To further validate this procedure, supported membranes were also prepared by the conventional dip-coating method. Gas separation results (Figure S6.9), indicated that the CO_2 permeance of the membranes prepared by dip-coating was lower (61 ± 15 GPU) than that of those prepared by phase inversion (127 ± 10 GPU), whereas the selectivity was almost unaltered. These results suggest that a greater pore filling takes place when using the conventional dip-coating method, since the time needed to evaporate the solvent allows the casting solution to penetrate into the support pores. In the case of membranes prepared by phase inversion this phenomenon is reduced due to the very fast precipitation of the polymer.

Therefore, it can be concluded that the membrane preparation method developed in this work can be used in the same way as the conventional methods to achieve perm-selective membranes, with the advantages of being an easier and faster procedure, requiring each layer just 4-5 min to be completely formed, and being able to enhance the performance of membranes increasing the CO_2 permeance. It Is worth mentioning that a certain number of Pebax® coatings is needed to conform supported membranes with desirable separation properties. This is because the first coatings act as a gutter layer for the subsequent polymer layers. However, a clear trade-off is established as a high number of layers punish the CO_2 permeance without improving the CO_2/N_2 separation selectivity.

An additional comparison with other Pebax® based supported membranes can also be found in Figure 6.8 and Table S6.2. Figure 6.8 shows a CO_2/N_2 log-log plot similar to that used by Robeson to compare the performance of different membranes.[4] In this case, the best supported membranes prepared in this work (0.5wt%_4 and 0.5wt%_5) are plotted together with other Pebax® based membranes reported in bibliography.[94,108,125,166,175,176]

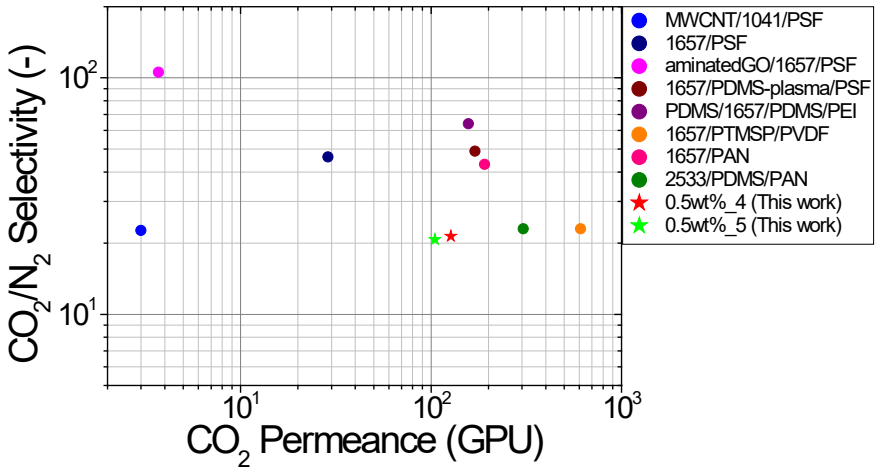

Figure 6.8. Comparison of the separation performance of Pebax® based supported membranes. Conditions used for each membrane are specified in Table S6.2.

As seen in Figure 6.8, both the 0.5wt%_4 and 0.5wt%_5 supported membranes demonstrate exceptional gas separation performances, being also close to those previously reported for this kind of polymers. It is worth mentioning that this Pebax® code has not been as widely studied as other codes such as Pebax® 1657, and never as

a thin composite membrane. In consequence, this work demonstrates the feasibility of the new preparation approach to obtain membranes which may be advantageous due to the fact that the studied Pebax® code is only soluble in an alcohol (1-propanol/1-butanol) mixture. This suggests higher chemical stability of the obtained membranes when exposed to moisture since typical Pebax® 1657 membranes are obtained from water/ethanol polymer solutions.

Moreover, to study the CO_2 and N_2 permeance, as well as the CO_2/N_2 selectivity dependence of temperature, gas permeation tests were also carried out at 25 and 50 °C and the same pressure conditions (3 bar) with the membrane which offered the best separation properties, 0.5wt%_4 as demonstrated in Figure 6.8. As observed in Figure S6.10 of the Supplementary Information section, whereas the CO_2 and N_2 permeance increased almost linearly with temperature, the CO_2/N_2 selectivity decreased, due to the thermal activation process which favored N_2 over CO_2 transport. This behavior was studied more in depth applying an Arrhenius modified model to the data of CO_2 and N_2 permeance and temperature (see equation S6.1 and Figure S6.11).[53] Based on this model, the activation energy (E_p) of the Pebax® 3533 supported membranes associated to the CO_2 and N_2 permeations were 14.2 kJ mol^{-1} and 29.6 kJ mol^{-1}, respectively, close to the values found in the literature for other Pebax®-type membranes (in the ranges of 13.3 to 18.2 kJ mol^{-1} for CO_2 and 27.2 to 32.0 kJ mol^{-1} for N_2) (see Table 6.2).

Table 6.2. Apparent activation energies of Pebax®-type films reported in the literature.

Polymer	E_p CO_2 (kJ mol^{-1})	E_p N_2 (kJ mol^{-1})	Reference
Pebax® 1657	13.3	30.4	[114]
Pebax® 1657	14.9	28.0	Chapter 5
Pebax® 1657	18.6	32.0	[130]
Pebax® 2533	16.7	27.2	[130]
Pebax® 2533	18.2	31.0	[131]
Pebax® 1074	13.4	30.3	[53]
Pebax® 3533	14.2	29.6	This chapter

It must be noted that the activation energies of both composite and self-supported membranes are comparable. This suggests that the Pebax selective layer is the main responsible of the final separation properties in a composite membrane. Additionally, the higher activation energy of N_2 with respect to that of CO_2 justifies the reduction of the CO_2/N_2 selectivity as a function of temperature, as shown in Figure S6.10b of the Supplementary Information section.[177]

6.2.3 Membrane calculations. Resistance in series Model

The flow rate of a gas through a membrane can be expressed as a function of a resistance to flow.[52] According to this statement, gas transport trough a layered membrane can be described as an analogy to the electric flow in the serial connection of conductors. In this sense, each layer provides a resistance to the flow proportional to the thickness and inversely proportional to its permeability and surface area (see equation 2.9). Based on this model, the total resistance and permeance of a composite membrane can be estimated by equations 2.10 and S6.3, respectively, using permeability values of 96,800 and 220 Barrer for the PSF porous support and the Pebax® 3533 polymer, respectively. The theoretical performance of the membranes fabricated with the 0.5 wt% casting solution was estimated using the equations above mentioned and the results can be found in Table 6.3 and Figure S6.13. As seen in this figure, greater permeance values should be obtained as calculated by the resistance-in-series model (i.e. 162 GPU vs. 127 GPU and 111 GPU vs. 105 GPU for the membranes composed of 4 and 5 Pebax® layers, respectively). As mentioned in previous sections, filling of large support pores could be the cause of such reduction since theoretical calculations assume that the Pebax® solution did not penetrate into the support porosity. Furthermore, the deviation found with the membrane composed of 3 Pebax® layers could be due to the presence of defects in the selective layer, which hinder the selective diffusion of CO_2 molecules. For this reason, additional layers are needed to obtain a better performance, as experimentally determined. Additionally, the contribution of Pebax® layers to the overall resistance of the composite membrane has been calculated. As seen in Table 6.3, the experimental Pebax® layer resistance of membranes composed of 4 and 5 layers were the closest to those estimated with the resistance-in-series model. Finally, the contribution of Pebax® to the total resistance increases from 31% to 59%

when the number of Pebax® went from 3 to 6, respectively, (see Table 6.3), in line with the achievement of the optimum separation conditions of the composite membranes.

Table 6.3. Comparison of experimental and RSM (resistance in series model) calculated values for permeance and resistance of TFC membranes prepared with the 0.5 wt.% casting solution.

Membrane	Permeance (GPU)		Total resistance ($GPU^{-1}m^{-2}$)		Pebax® resistance ($GPU^{-1}m^{-2}$)	
	Experimental	RSM	Experimental	RSM	RSM	Contribution to total resistance (%)
0.5wt.%_3	101 ± 3	168	46.7	28.1	8.6	31
0.5wt.%_4	127 ± 10	137	37.1	34.5	15.0	44
0.5wt.%_5	105 ± 6	115	44.9	40.9	21.4	52
0.5wt.%_6	64 ± 3	100	73.7	47.4	27.9	59

6.3 Conclusions

A phase inversion method has been developed in this work for the preparation of Pebax® 3533 supported membranes. The method consisting of the deposition of various thin layers of Pebax® on top of polysulfone porous supports was optimized and the influence of the casting solution concentration, as well as the number of polymer layers was studied. The polymer concentration in the casting solution altered its viscosity with the consequent impact on the gas separation performance. Moreover, the application of additional polymer layers allowed to repair the micro-defects improving the membrane selectivity. The characterization of the chemical structure of the membranes by FTIR showed the correct deposition of the Pebax® layers on top of the PSF supports for the membranes prepared with the 1.5, 1.0 and 0.5 wt% casting solution concentration. The thermal stability of the membranes was confirmed by TGA. Regarding the CO_2/N_2 separation performance, the dilution of the casting solution concentration together with the appropriate number of Pebax® layers allowed to increase the CO_2 permeance. The best performance was obtained with the membranes prepared with the 0.5 wt% casting solution after the deposition of 4 layers, reaching a CO_2 permeance of 127 ± 10 GPU and a CO_2/N_2 selectivity of 21.4. The implementation

of the phase inversion method for the coating of dense selective layers was also validated by testing the gas separation performance of supported membranes prepared by dip-coating. Additionally, the activation energy values for permeance (14.2 kJ mol^{-1} for CO_2 and 29.6 kJ mol^{-1} for N_2) revealed the analogy of these supported membranes with dense membranes prepared with other codes of Pebax®.

6.4 Supplementary Information

Membrane characterization

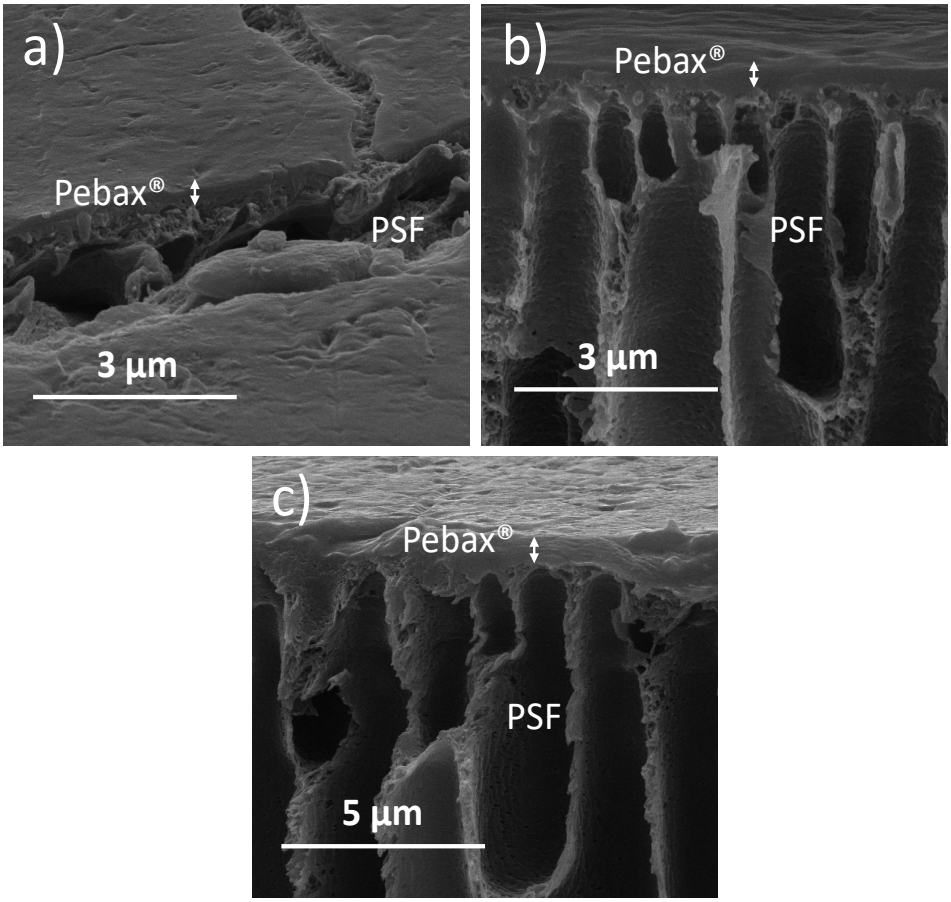

Figure S6.1. Cross-section images of the supported membranes prepared by phase inversion with the 0.25 wt% casting solution after the application of 4 (a), 5 (b) and 6 (c) layers.

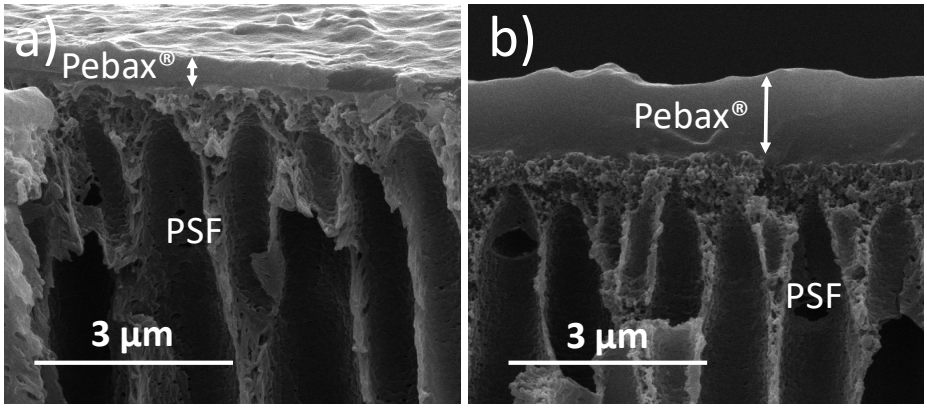

Figure S6.2. Cross-section images of the supported membranes prepared by phase inversion with the 1.0 wt% casting solution after the application of 1 (a) and 2 (b) layers.

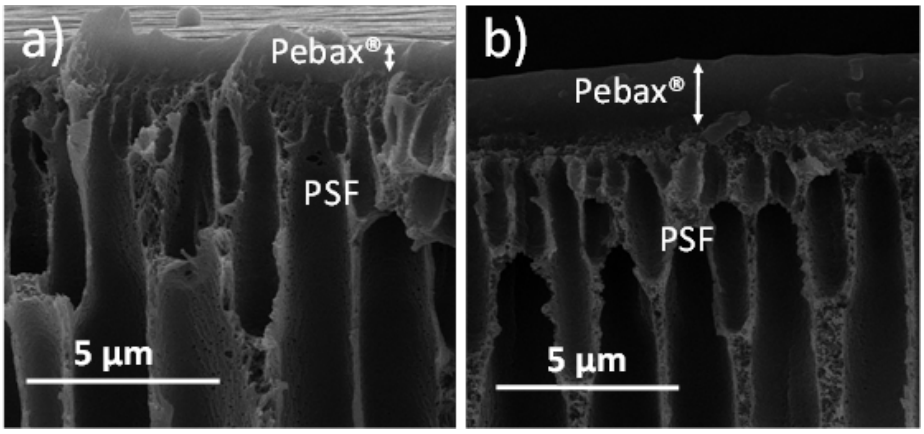

Figure S6.3. Cross-section images of the supported membranes prepared by phase inversion with the 1.5 wt% casting solution after the application of 1 (a) and 2 (b) layers.

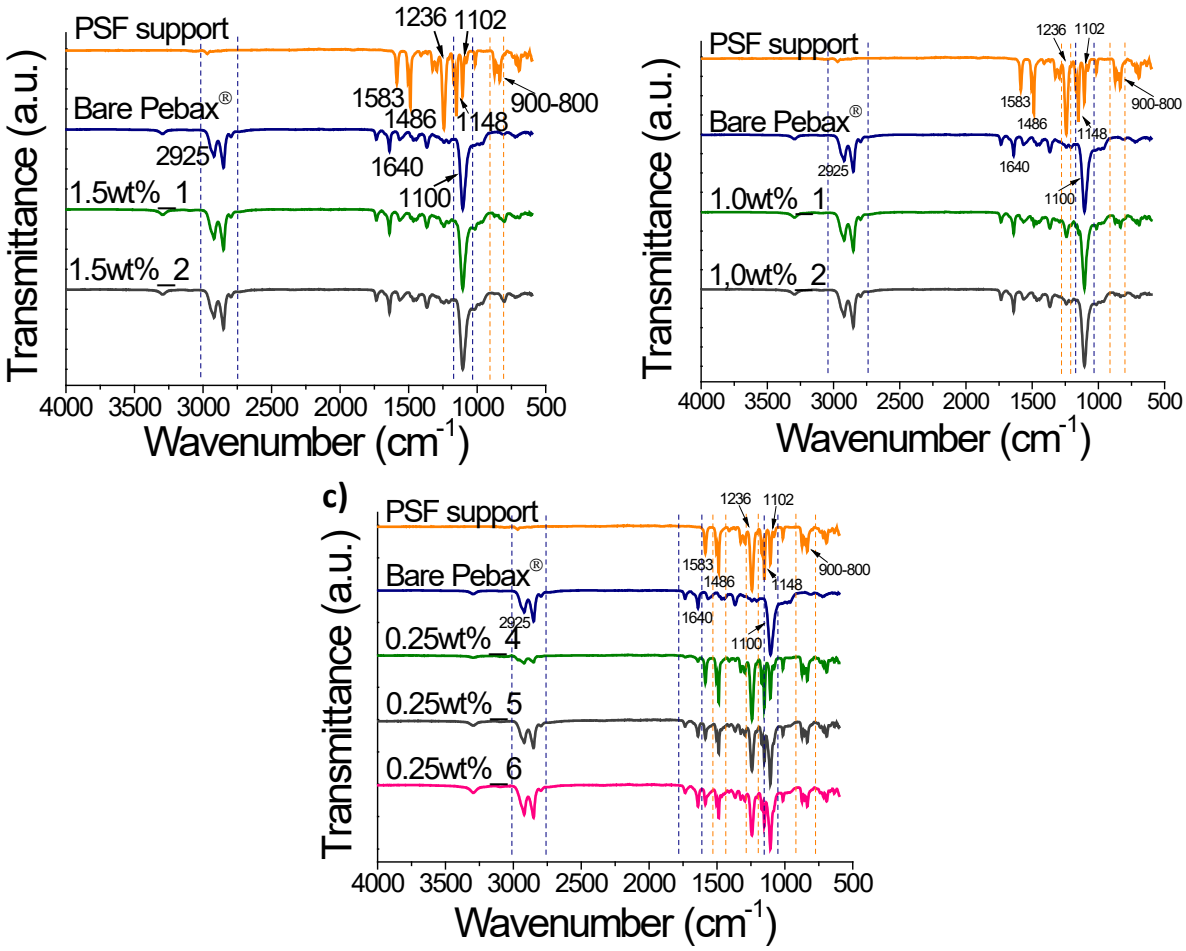

Figure S6.4. FTIR-ATR spectra of membranes prepared by phase inversion with the1.5 wt% (a), 1.0 wt% (b) and 0.25 wt% (c) casting solution concentrations and different number of layers (from 1 to 6) compared to that of the bare PSF support and the Pebax® 3533 dense membrane.

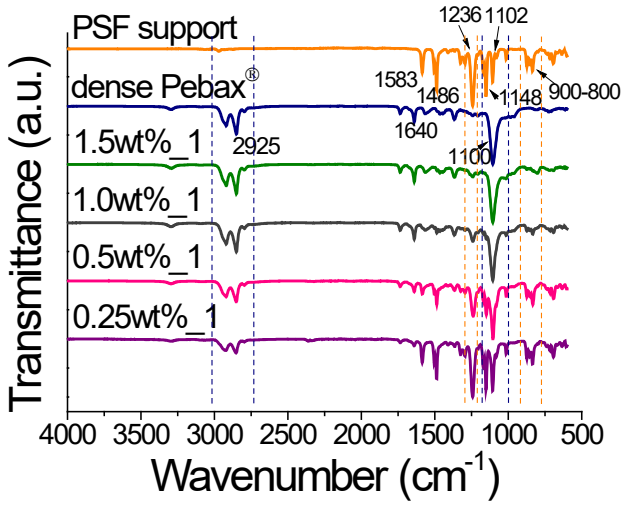

Figure S6.5. Comparison of the FTIR-ATR spectra of membranes prepared with each casting solution concentration tested in this work (0.25, 0.5, 1.0 and 1.5 wt%) after the deposition of 1 polymer layer on top of PSF supports.

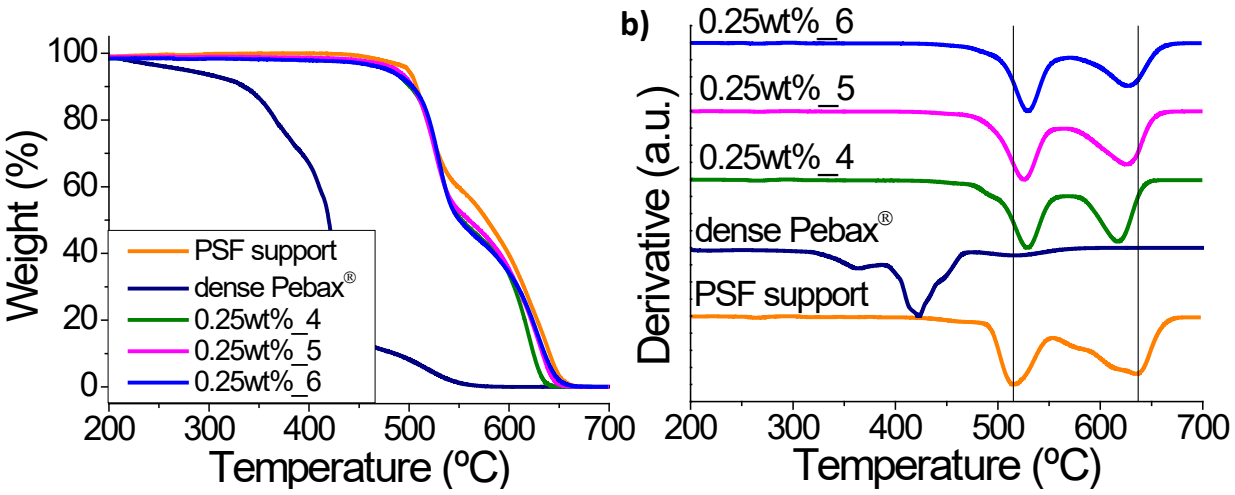

Figure S6.6. TGA (a) and DTG (b) curves of the supported membranes prepared with the 0.25 wt% casting solution by phase inversion.

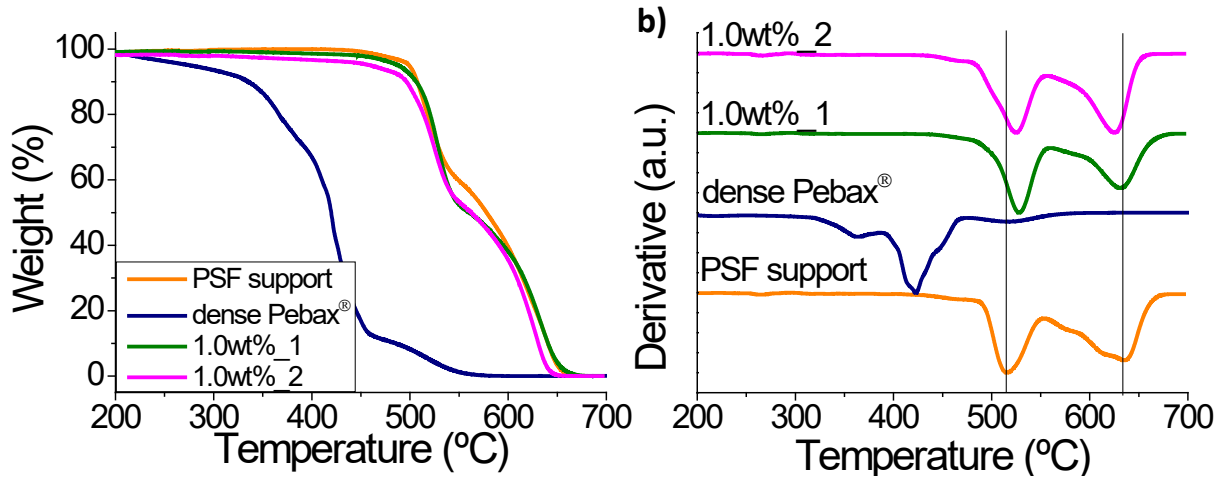

Figure S6.7. TGA (a) and DTG (b) curves of the supported membranes prepared with the 1.0 wt% casting solution by phase inversion.

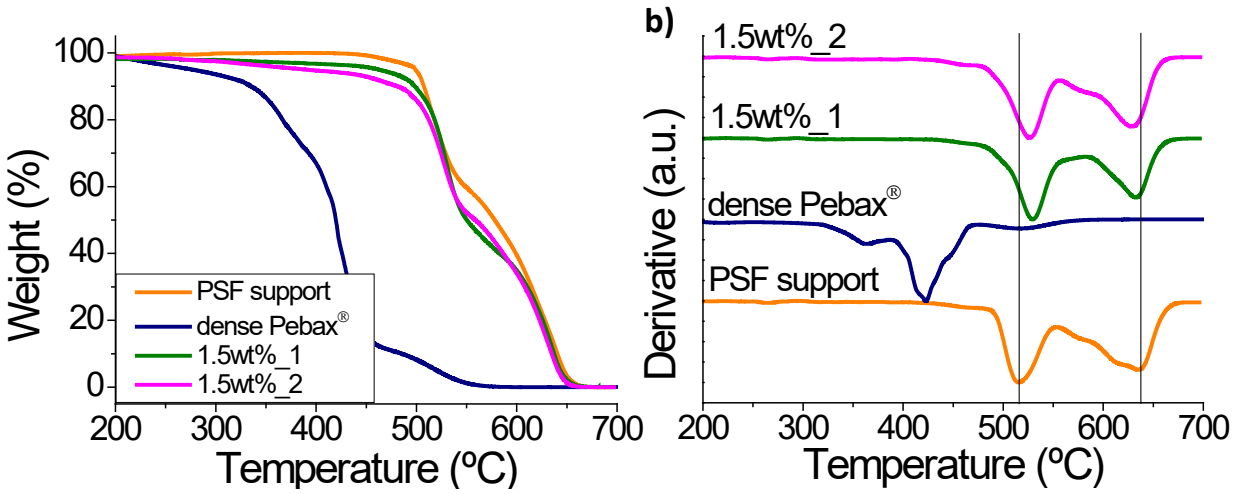

Figure S6.8. TGA (a) and DTG (b) curves of the supported membranes prepared with the 1.5 wt% casting solution by phase inversion

Gas separation performance

The gas separation performance of the supported membranes was studied for the CO_2/N_2 gas mixture at an operating temperature of 35 °C and feed pressure of 3 bar. Results are shown in Table S6.1.

Table S6.1. Gas permeation results obtained for the CO_2/N_2 gaseous mixture operating at 35 °C and feed pressure of 3 bar.

Membrane	wt% Pebax® 3533	Layers	CO_2 Permeance (GPU)	N_2 Permeance (GPU)	CO_2/N_2 Selectivity
dense Pebax®	3.0	-	4 ± 1	0.2 ± 0.0	21.5 ± 0.8
1.5wt%_1	1.5	1	42 ± 4	3 ± 1	16.9 ± 3.7
1.5wt%_2	1.5	2	29 ± 2	2 ± 0	18.3 ± 2.3
1.0wt%_1	1.0	1	70 ± 7	9 ± 2	8.4 ± 2.5
1.0wt%_2	1.0	2	49 ± 7	2 ± 0	20.4 ± 0.9
0.5wt%_3	0.5	3	101 ± 3	7 ± 1	15.4 ± 1.1
0.5wt%_4	0.5	4	127 ± 10	6 ± 0	21.4 ± 1.0
0.5wt%_5	0.5	5	105 ± 6	5 ± 0	20.7 ± 2.6
0.5wt%_6	0.5	6	64 ± 3	4 ± 0	19.1 ± 1.4
0.25wt%_4	0.25	4	87 ± 9	48 ± 27	3.5 ± 3.0
0.25wt%_5	0.25	5	78 ± 14	7 ± 2	12.0 ± 2.0
0.25wt%_6	0.25	6	56 ± 12	10 ± 4	6.9 ± 3.7

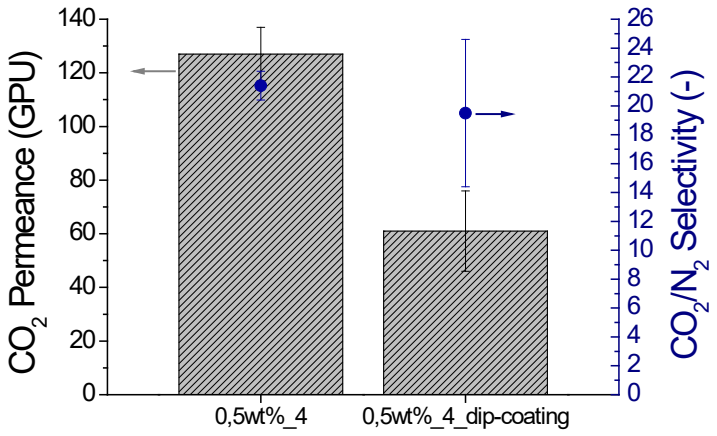

Figure S6.9. Gas separation performance of membranes prepared with 4 coatings of Pebax® 3533 in a concentration of 0.5 wt% in the mixture of 1-propanol/1-butanol. Comparison between supported membranes prepared by phase inversion and dip-coating.

Table S6.2. CO_2/N_2 separation performance of Pebax® based thin film composite membranes reported in the literature

Membrane	Operating temperature (°C)	Feed pressure (bar)	selective layer thickness (µm)	CO_2 Permeance (GPU)	CO_2/N_2 Selectivity (-)	Ref.
PSF/Pebax® 1041/MWCNT[a,d]	35	3	8.2	3.0	22.6	94
PSF/Pebax® 1657/aminatedGO[b,f]	25	4	12.8	3.7	105.6	175
PSF/Pebax® 1657[b,f]	25	7	2.0	28.8	46.3	125
PEI/PDMS/Pebax® 1657/PDMS[b,f]	25	5	0.5	157	64	108
PSF/PDMS plasma/Pebax® 1657[b,f]	30	7	0.5	170	49	166
PAN/PDMS/Pebax® 2533[c,g]	35	3	0.6	305	23	176
0.5wt%_4[a,e] **(PSF/Pebax® 3533)**	35	3	0.7	127	21.4	This chapter
0.5wt%_5[a,e] **(PSF/Pebax® 3533)**	35	3	1.0	105	20.7	This chapter
a: mixed gases, b: time-lag, c: single gases, d: phase inversion and drop-casting, e: dip-coating and phase inversion, f: dip-coating, g: spin-coating						

Apparent activation energy

An Arrhenius model was applied to the permeance data as explained in section 2.4.1.3 (equation 2.11).

Data obtained at different temperatures with the 0.5wt%_4 supported membrane are represented in Figure S6.10 and the fittings to calculate the activation energy of permeance (in GPU) are shown in Figure S6.11. In this Figure, the opposite of the slope in the lnP vs. R^{-1} T^{-1} (J^{-1} mol) plot is the apparent activation energy of permeation in J mol^{-1}.

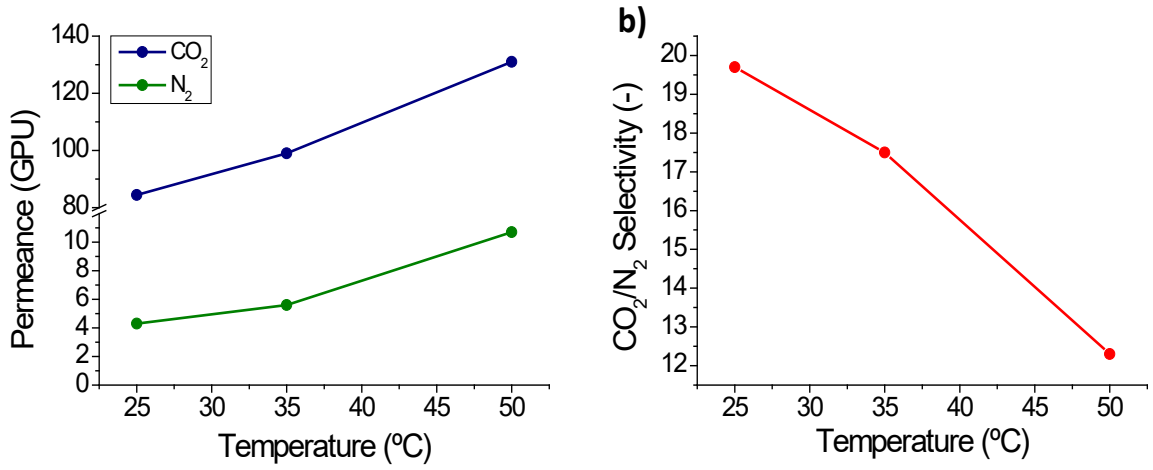

Figure S6.10. CO_2 and N_2 permeance (a) and CO_2/N_2 Selectivity (b) dependence of temperature measured at a feed pressure of 3 bar with the 0.5wt%_4 supported membrane.

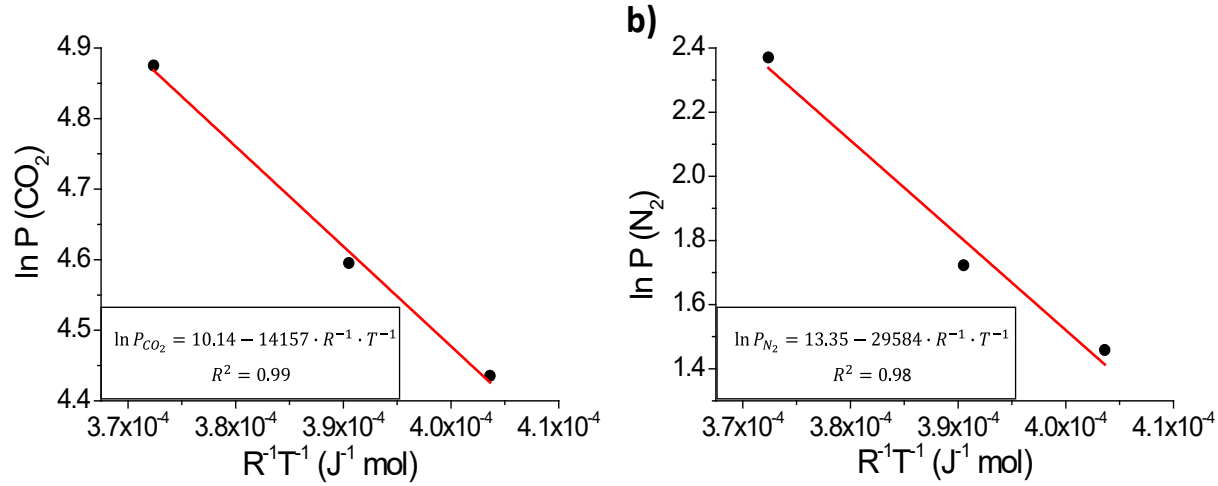

Figure S6.11. Arrhenius model linear fitting for the calculation of the apparent activation energy of permeation of CO_2 (a) and N_2 (b) estimated with the 0.5wt%_4 supported membrane.

Membrane calculations. Resistance-in-series Model (RSM)

As proposed by Henis and Tripodi,[52] the resistance to the gas flow is analogous in a mathematical sense to the electrical resistance of a material to current flow. According to this model, in a multilayer composite membrane each layer provides a resistance to the gas flow such that the multicomponent membrane can be compared to the analogous electrical circuit (Figure S6.12). Therefore, the overall resistance of a composite membrane R_m is given by the sum of those resistances. This model is explained more in depth in **chapter 2**, section 2.4.1.2.

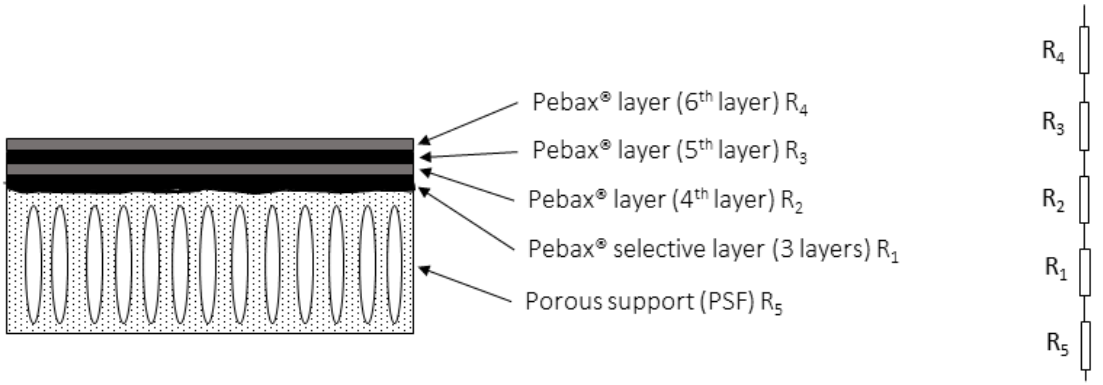

Figure S6.5. Resistance-in-series model for the Pebax®/PSF TFC membrane prepared with the 0.5 wt% casting solution by phase inversion.

Based on this model, the gas permeance J_m of a composite membrane can also be estimated by:

$$J_m = \frac{1}{R_m A} \quad \text{(eq. S6.1)}$$

$$\frac{1}{J_m} = \frac{1}{J_1} + \frac{1}{J_2} + \cdots + \frac{1}{J_i} \quad \text{(eq. S6.2)}$$

$$J_m = \frac{1}{\frac{l_1}{P_1} + \frac{l_2}{P_2} + \cdots + \frac{l_i}{P_i}} \quad \text{(eq. S6.3)}$$

where J_i is the gas permeance of each layer. Thus, we can calculate both, the resistance and permeance of every composite membrane using the measured thickness of each layer (l_i) and the porous support and Pebax® 3533 permeability values (96,800 and 220 Barrer, respectively). Results are collected in Table 6.3 and Figure S6.13.

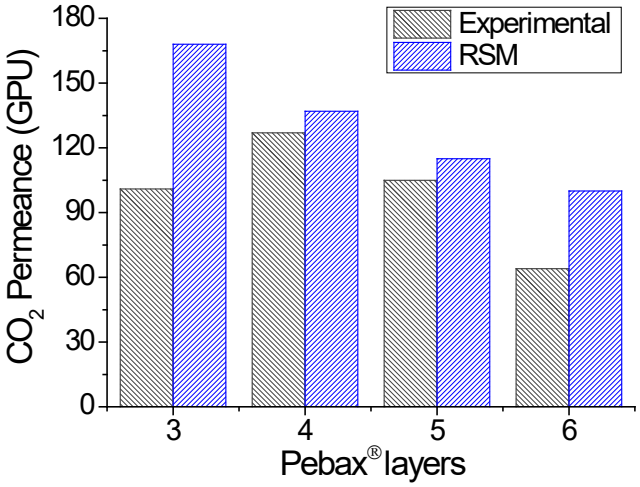

Figure S6.6. Comparison of experimental and RSM calculated values for permeance and resistance of TFC membranes prepared with the 0.5 wt% casting solution.

Capítulo 7: "Ultra-small functionalized MOF UiO-66/polymer Pebax® 1657 thin film nanocomposite membranes for CO2 separation"

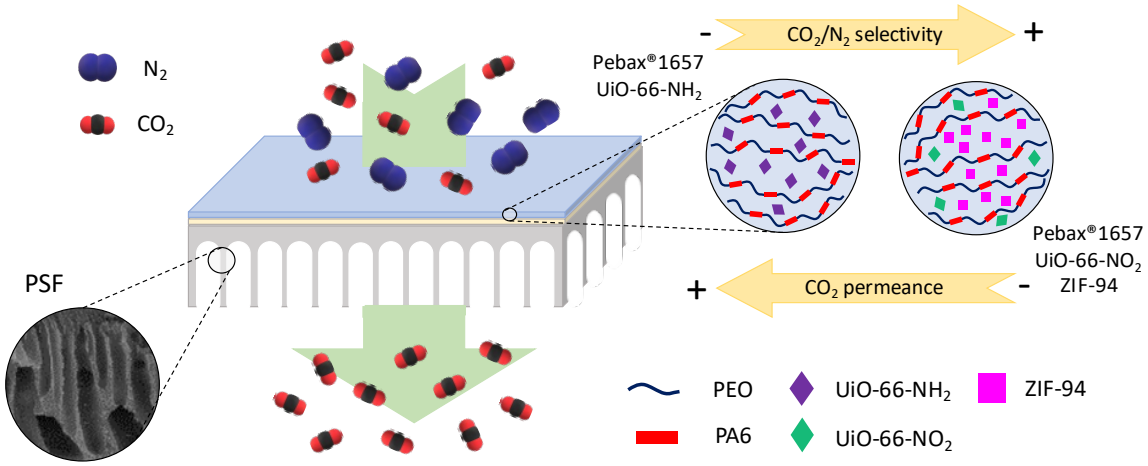

Adapted from "L. Martínez-Izquierdo, C. García-Comas, M. Navarro, S. Dai, A. Tissot, C. Serre, C. Téllez, J. Coronas. Ultra-small functionalized MOF UiO-66/polymer Pebax® 1657 thin film nanocomposite membranes for CO_2 separation". Publishing pending.

7. Ultra-small functionalized MOF UiO-66/polymer Pebax® 1657 thin film nanocomposite membranes for CO_2 separation

7.1 Introduction

To achieve the Paris Agreement (reinforced in the Glasgow COP26 in 2021) target of below 1.5 °C in the global average temperature rising, harmful greenhouse gas emissions must be considerably reduced in the coming decades. In order to accomplish this target, energy-efficient and low-carbon footprint technologies, as well as CO_2 capture and storage approaches, must be developed. Membrane-based processes have emerged as attractive candidates for energy-efficient gas separations.[178] However, current dense membranes are not competitive for large-scale applications because of their very low CO_2 permeance (flux through it).[34] Recently, the development of composite membranes with a very thin selective layer has attracted much attention due to their potential to achieve efficient separations, which exceed the permeance-selectivity inherent upper bound for a given separation, visualized for dense membranes as the so-called Robeson trade-off relationship between permeability and selectivity.[4] The formation of defect-free thin film composite (TFC) membranes with a selective layer thickness lower than 1 µm may exhibit high CO_2 permeances while maintaining selectivity. Such improvements over current dense films make TFC membranes economically viable for implementation in the processing of power station flue gases.[163]

However, not only the membrane structure is important, the polymer matrices used for CO_2 separation also play a critical role.[179] Block copolymers made of glassy and rubbery segments in different ratios are promising materials showing good performance in gas separation.[180] Among them, poly(ether-*block*-amide) copolymers known under the trademark Pebax® are being widely studied.[111,114] These copolymers, comprising aliphatic polyamides and polyether segments provide high gas permeability and mechanical stability without a high level selectivity to CO_2. Such is possible due to the introduction of polar groups with affinity to CO_2 that improve CO_2/non-polar gases selectivity.[41] Furthermore the polymers can be enhanced with fillers to give the so-called

Mixed Matrix Membranes. Metal-organic frameworks (MOFs) with molecular sieving properties are regarded as promising filler materials to improve the separation performance of Pebax® based membranes.[181] In addition to the nanostructured and adsorption properties of inorganic additives (e.g. zeolites), MOFs offer enhanced matrix compatibility and tunability due to the presence of organic linkers.[182] Besides, functionalization of MOFs with amino (-NH_2), alkoxy (RO-) or nitro (-NO_2) functional groups may improve their compatibility and adsorption properties.[62,88,183] Anjum et al.[184] reported a MMM made of Matrimid and UiO-66 as filler. They found that the modulation of MOF with amine-functionalized linkers enhanced the intrinsic separation performance of the MOF and improved the MOF-polymer compatibility. By contrast to the unfilled Matrimid membrane, they achieved a 50% more selective and 540% more permeable membrane when UiO-66-NH_2 particles were used at 30 wt% of loading for CO_2/CH_4 separations. Qian et al.[102] combined a high-molecular-weight polyimide of identical chemical structure to that of amine functionalized UiO-66 nanoparticles to improve their interfacial compatibility. This strategy enabled them to create defect-free MMM 48% more permeable and 18% more selective than the bare membrane in CO_2/N_2 separations.

In TFCs, as in MMMs, polymer enhancement can be done with the introduction of fillers to give what have been called thin film nanocomposite (TFN) membranes. TFN membranes have been widely applied in nanofiltration and osmosis processes,[185–187] but their application to gas separation is scarce.[188,189] In this sense, MOF nanoparticles of UiO-66 have been widely used in TFN membranes for separations in liquid phase[68,190,191] and only some attempt has been made in gas phase.[192–194] In gases, the development of TFN membranes requires the smallest possible fillers given the nanometric thickness of the selective layers and to avoid defects that are critical in gas separation, in this sense particle agglomerations must be avoided and the interaction filler-polymer must be improved. Recently, UiO-66 based MOFs have been synthesized as ultra-small nanoparticles (e.g. 8-15 nm in case of UiO-66-NH_2),[195] which represents a new opportunity of membrane improvement, particularly in the form of thin film nanocomposite (TFN) membranes. Likewise, combining two fillers in the same membrane has been tested in MMMs and in TFN membranes for liquid separation.[196,197]

In this work, we incorporate amino (–NH_2) and nitro (–NO_2) functionalized UiO-66 ultra-small nanoparticles with an average particle size ranging from 4 to 10 nm into Pebax® 1657 polymer for the fabrication of TFN membranes for the separation of CO_2/N_2 and CO_2/CH_4 mixtures. Moreover, the possibility of combining the separation properties of these MOFs with that of ZIF-94 has been explored. To the best of our knowledge, this is the first time that such small UiO-66 nanoparticles have been introduced into a membrane for gas separation. Furthermore, the simultaneous formulation of functionalized UiO-66 and ZIF-94 nanoparticles in the same TFN membrane has never been explored in gas separation.

7.2 Results

7.2.1 MOFs characterization

The UiO-66-NH_2 and UiO-66-NO_2 were prepared through a new stepwise room temperature strategy, where the pre-synthesized Zr_6 oxoclusters were required. The prerequisite Zr_6 oxoclusters were prepared successfully according to the identical powder X-ray diffraction (PXRD) pattern compared to the literature.[198] The PXRD pattern of the synthesized UiO-66-NH_2 and UiO-66-NO_2 showed very broadened Bragg peaks (Figure 7.1a), suggesting the absence of long-range order. This is often related to the formation of either the amorphous phase or the ultra-small crystals. The N_2 isotherms in Figure 7.1b revealed the high porosity of the synthesized materials, with BET specific surface areas of 586 (±3) m^2/g for UiO-66-NO_2 and 842 (±4) m^2/g for UiO-66-NH_2. These values indicate the high-quality of the ultra-small MOFs despite the amorphous-like diffraction patterns. Subsequently, high-resolution transmission electron microscopy (HRTEM) was performed to confirm the size and the crystallization of MOFs. As shown in Figure 7.1c and d, the HRTEM images evidenced the formation of very well crystallized (crystal lattices) and ultra-small MOF nanoparticles. The prepared UiO-66-NH_2 and UiO-66-NO_2 were single crystals with average sizes of 4 nm and 6 nm, respectively, in line with the broad PXRD peaks mentioned above.

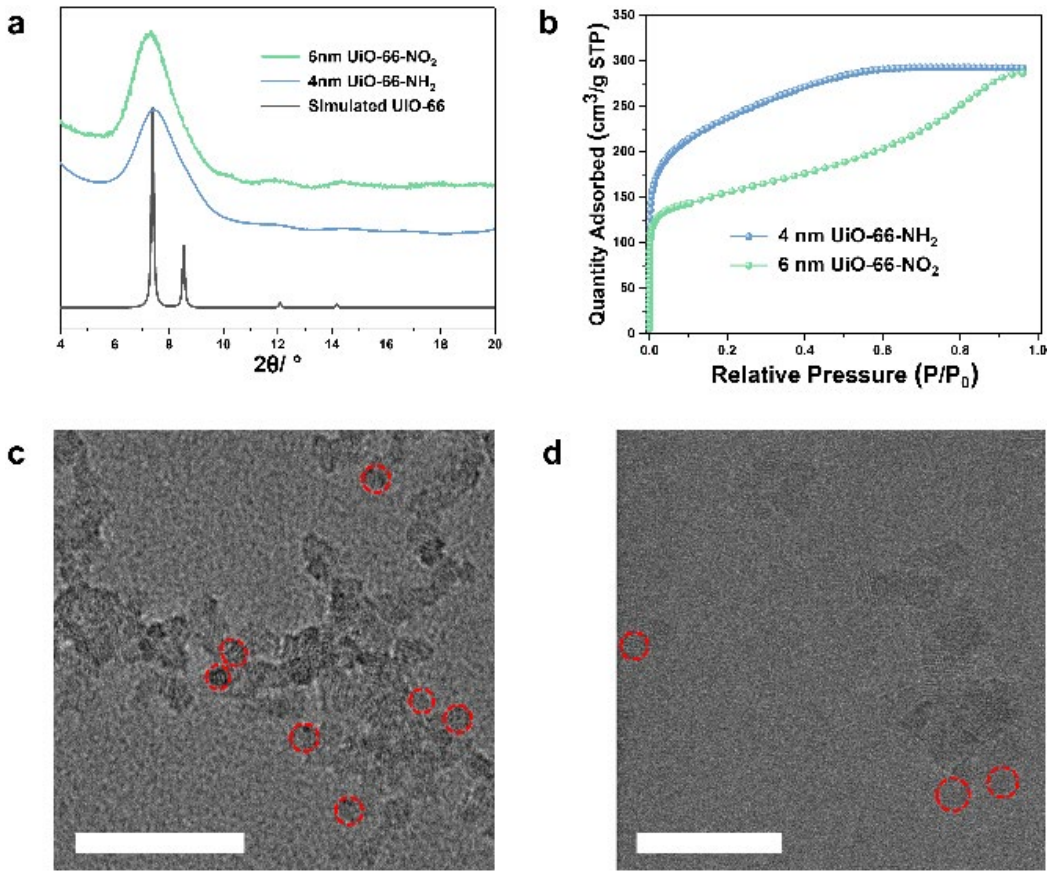

Figure 7.1. PXRD (λCu = 1.5406 Å) patterns of the synthesized UiO-66-NH_2 and UiO-66-NO_2 and the corresponding simulated PXRD pattern (a), -196 °C N_2 sorption isotherms of the ultra-small UiO-66-NH_2 and UiO-66-NO_2 (b); HRTEM images of 4 nm UiO-66-NH_2 (c), and 6 nm UiO-66-NO_2 (d). Scale bar= 50 nm.

ZIF-94 particles were synthesized from ZIF-8 crystals via a SALE reaction. As observed in Figure S1a, the average particle size of synthesized ZIF-94 was 45 nm. This image further emphasizes the homogeneity of the size distribution. By using this method, ZIF-94 is produced with the regulated particle size of ZIF-8 and the strong CO_2-philicity of ZIF-94, while avoiding the use of other harmful solvents like tetrahydrofuran (THF) or dimethylformamide (DMF).[84] The crystallinity and purity of the ZIF particles were confirmed by PXRD. The patterns of the simulated ZIF and the synthesized ZIF-94 are plotted together for comparison in Figure S1b. As seen in this figure, the peak positions match well with those of the simulated ZIF-94 (SOD structure).

7.2.2 Membranes characterization

The TFC and TFN membranes prepared in this work were abbreviated depending on the type of MOF and the percentage of it (in wt%) in the polymer matrix and the names are collected in Table 7.1.

Table 7.1. TFC and TFN preparation conditions.

Membrane	UiO-66	wt% UiO-66	wt% ZIF-94
TFC_P1657	-	0	0
TFN_U(5)	UiO-66	5	0
TFN_U(7.5)	UiO-66	7.5	0
TFN_U(10)	UiO-66	10	0
TFN_UNH2(5)	UiO-66-NH_2	5	0
TFN_UNH2(7.5)	UiO-66-NH_2	7.5	0
TFN_UNH2(10)	UiO-66-NH_2	10	0
TFN_UNO2(5)	UiO-66-NO_2	5	0
TFN_UNO2(5)_Z94(5)	UiO-66-NO_2	5	5
TFN_UNO2(5)_Z94(10)	UiO-66-NO_2	5	10
TFN_UNO2(5)_Z94(15)	UiO-66-NO_2	5	15

Cross-sections of the TFC (only polymer) and TFN (including nanoparticles in the skin layer) membranes were explored by SEM and are depicted in Figure 7.2a-d. Membranes show three different layers, corresponding to the PSF support, the PTMSP gutter layer and the selective skin layer (Pebax® or Pebax®/MOF). The thickness of both the gutter layer and the selective layer were also estimated by SEM, being approximately 1 µm and 600 nm, respectively. A TEM image of a cross section of the TFN membrane prepared with 5wt% of UiO-66-NO_2 and 10 wt% of ZIF-94 prepared by ultramicrotomy is shown in the zoom of Figure 7.1d and it allows to distinguish the two polymer layers on top of the PSF support. This detailed characterization was only carried out on the best performing membranes (shown below) and the image further highlights that the MOF nanoparticles are located exclusively in the Pebax® layer and that are evenly distributed through it. The presence of MOF nanoparticles in the membrane was also confirmed by high-angle annular dark field-scanning transmission electron microscopy (HAADF-STEM) and energy dispersive X-ray spectroscopy (EDX). The corresponding Zn- and Zr- scans are depicted in Figure 7.2e and f, respectively. As expected, Zn and Zr contributions from ZIF-94 and UiO-66-NO_2, respectively, were detected although their weight composition is below 1 wt%. This is mainly explained by the fact that the percentage of metal in the MOF is low compared to that of the rest of the elements present in the membrane and

in the sample prepared for observation (Cl in the resin, C in the MOF, polymers and in the TEM grid itself). This is the reason why the element percentages are shown with or without the carbon signal to emphasize the metal signal. It must be noted that Si signal observed in Figures 2e and f come from the detector itself. In any event, the HAADF-STEM characterization shows that the ultra-small functionalized UiO-66 is individually present, non-agglomerated in the polymer.

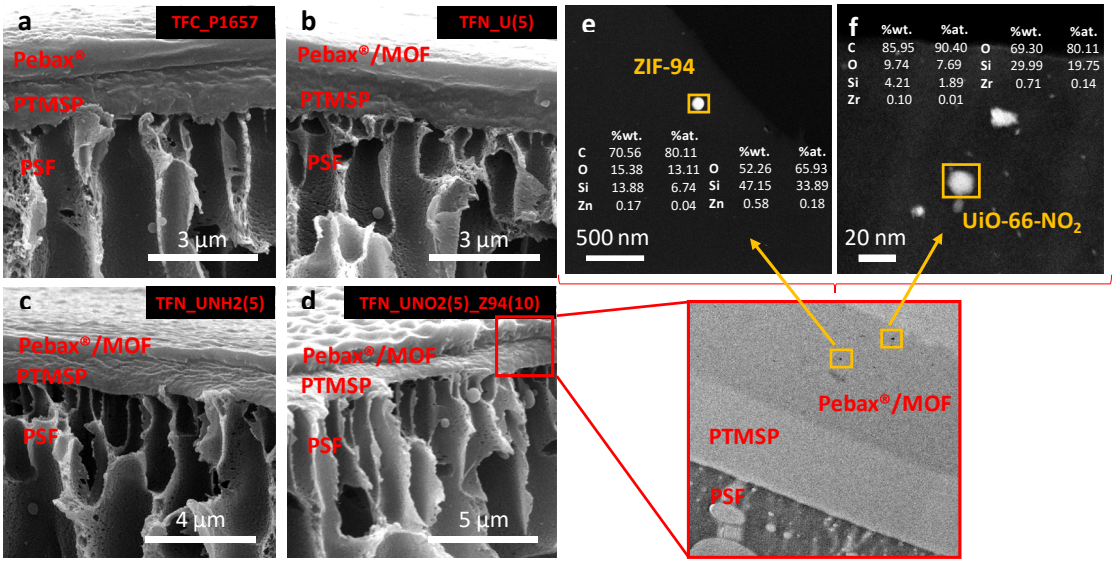

Figure 7.2. SEM cross-section images of the Pebax® TFC membrane (a) and the TFN membranes prepared with 5 wt% of UiO-66 (b), 5 wt% of UiO-66-NH_2 (c) and 5wt% of UiO-66-NO_2 and 10 wt% of ZIF-94 (d). Inset corresponds to a TEM cross-section image of the Pebax® TFN membranes prepared with 5wt% of UiO-66-NO_2 and 10 wt% of ZIF-94. High-angle annular dark field-scanning transmission electron microscopy (HAADF-STEM) and energy dispersive X-ray spectroscopy (EDX) of the corresponding Zn- (e) and Zr- (f) scans.

The thermal stability and crystallinity of the membranes were studied by TGA and XRD analyses. Due to the huge dilution effect that the membrane support produces, the TFC or TFN membranes were not directly examined by these two techniques but only the materials constituting their thin skin layers. With this aim, dense membranes were prepared by casting the remaining Pebax®/MOF solution onto a glass Petri dish and treated under the same conditions (40 °C overnight). Results of TGA and XRD analyses are depicted in Figures 3a1-3 and b1-3, respectively. As seen in Figure 7.3a1 and a2, the membranes fabricated with UiO-66 and UiO-66-NH_2 are stable up to 350 °C, with no significant weight loss before that temperature, which indicates the successful

activation of membranes (i.e. no loss of solvents is appreciated). From this point onwards membranes undergo a sharp degradation until 450 °C. Next, membranes experience a second degradation step, related to the combustion of aromatic compounds, which continues until 560 °C. At this temperature, the residue of the bare membrane is below 1% of its initial weight. This residue increases with the concentration of MOF in the polymer matrix due to the ZrO_2 and ZnO generated during the thermal oxidation step.[199,200] In the particular case of the membranes fabricated with UiO-66-NO_2 (Figure 3a3), their thermal degradation starts at a lower temperature (220 °C), which suggests that the thermal stability of these membranes is highly affected by the incorporation of the -NO_2 functionalized UiO-66 particles, which show significant weight losses at 400 °C due to ligand decomposition.[201] The XRD patterns depicted in Figure 3b1-3 reveal the increase of crystallinity with the amount of MOF, which is evidenced by the intensification of the peak at a 2θ value of 7.3°, related to both, UiO-66 (with and without functionalization) and ZIF-94.[202] In contrast, the peak at 2θ=24.4° corresponding to the Pebax® polymer[20] decrease at high loadings (10 wt%), suggesting that the MOF particles hinder the entanglement of the polymer chains, which in turn decreases the membrane crystallinity.

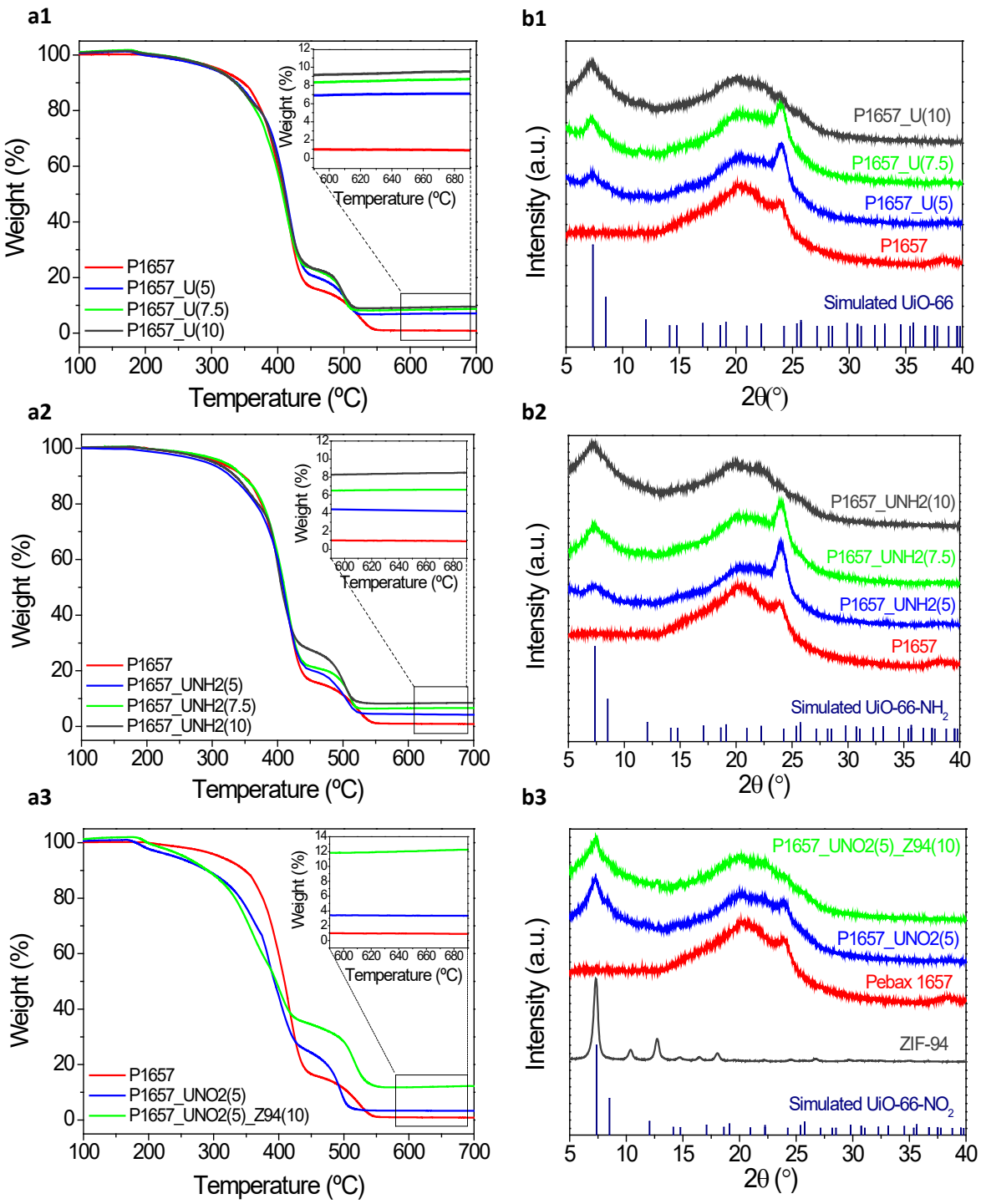

Figure 7.3. TGA curves (a1-a3) and XRD (b1-b3) diffractograms of the dense membranes prepared with the remaining casting solution.

7.2.3 Gas separation tests

The CO_2/N_2 and CO_2/CH_4 gas separation performance of the TFC and TFN membranes was studied at 35 °C and 3 bar feed pressure. Figure 7.4 depicts the gas separation properties of the TFN membranes fabricated with UiO-66 (a), UiO-66-NH_2 (b)

and UiO-66-NO_2 + ZIF-94 (c) compared to that of the bare Pebax® 1657 TFC membrane. Moreover, the best conditions found for the CO_2/N_2 separation have been compared and tested for the CO_2/CH_4 separation (Figure 4d). The results plotted in Figure 7.4 are collected as well in Tables S1-4 of the SI. As seen in Figure7.4a and Table S7.1, the addition of 5 wt% of UiO-66 increases the CO_2 permeance from 181 to 202 GPU, although the CO_2/N_2 selectivity decreases from 43.5 to 30.5. At higher loadings, the CO_2 permeance is below the value obtained with the bare TFC membrane. These results suggest a limitation in the compatibility between this MOF and the Pebax® 1657 polymer. As expected, the introduction of functional groups within the MOF structure enhances the MOF-polymer compatibility due to the hydrogen bonds created between the polymer chains (with N and O electronegative atoms bonded to hydrogens) and the functional group.[203] As observed in Figures 4b and c and Tables S7.2 and 7.3, this allows obtaining the highest CO_2 permeance with a 7.5 wt% of UiO-66-NH_2 (277 GPU), without affecting the CO_2/N_2 separation selectivity (44.6). Furthermore, the increase in the CO_2–philicity due to the introduction of amino groups in the MOF structure may also be responsible of such enhancement.[183] Increasing the amount of UiO-66-NH_2 in the polymer matrix above 7.5 wt% is translated into a decrease of both, the CO_2 permeance and CO_2/N_2 selectivity, probably due to the agglomeration of the particles inside the membrane.[204] Particularly, with the UiO-66-NO_2 the maximum loading is 5 wt%. Unlike UiO-66 and UiO-66-NH_2, which were dispersed in the mixture EtOH/water, this MOF was suspended only in water, making it difficult to dissolve the polymer in the rest of the solvent. Taking into account the amount of water added with the MOF suspension, the ratio between EtOH and water was recalculated in order to dissolve the Pebax® and obtain the final MOF-Pebax® solution in the mixture EtOH/water 70/30. With 5 wt% of UiO-66-NO_2 the CO_2 permeance decreases from 181 to 155 GPU, however, the CO_2/N_2 selectivity increases by 17%, from 43.5 to 51.0, being the highest separation selectivity obtained in this work.

In view of this result, 45 nm ZIF-94 particles were added to the UiO-66-NO_2/Pebax® solution with the aim of increasing the CO_2 permeance (due to the increase of the total MOF loading in the TFN membrane), while maintaining or increasing the CO_2/N_2 selectivity (due to the fact that ZIF-94 is also a suitable material for CO_2 separation[85]). In

addition, it has been shown in previous works that the combination of two MOFs with different characteristics (one more hydrophilic and the other more hydrophobic) in a membrane can have a synergistic effect on the separation of mixtures with CO2 due to the fact that dispersion is improved by avoiding the agglomeration.[205] As observed in Figure 4c, the CO_2 permeance of the membranes with both UiO-66-NO_2 and ZIF-94 reaches a maximum of 192 GPU at 10 wt% of ZIF-94 at a maintained CO_2/N_2 separation selectivity of ca. 51, the best values in this work. This is related to the properties of MOFs and the synergistic effect that would improve their dispersion as seen by microscopy. As for the UiO-66-NH_2 TFN membranes, from this loading both the CO_2 permeance and CO_2/N_2 selectivity decrease due to the particle agglomeration, even though the combination of the two different fillers allowed a highest total effective MOF loading of 15 wt%).

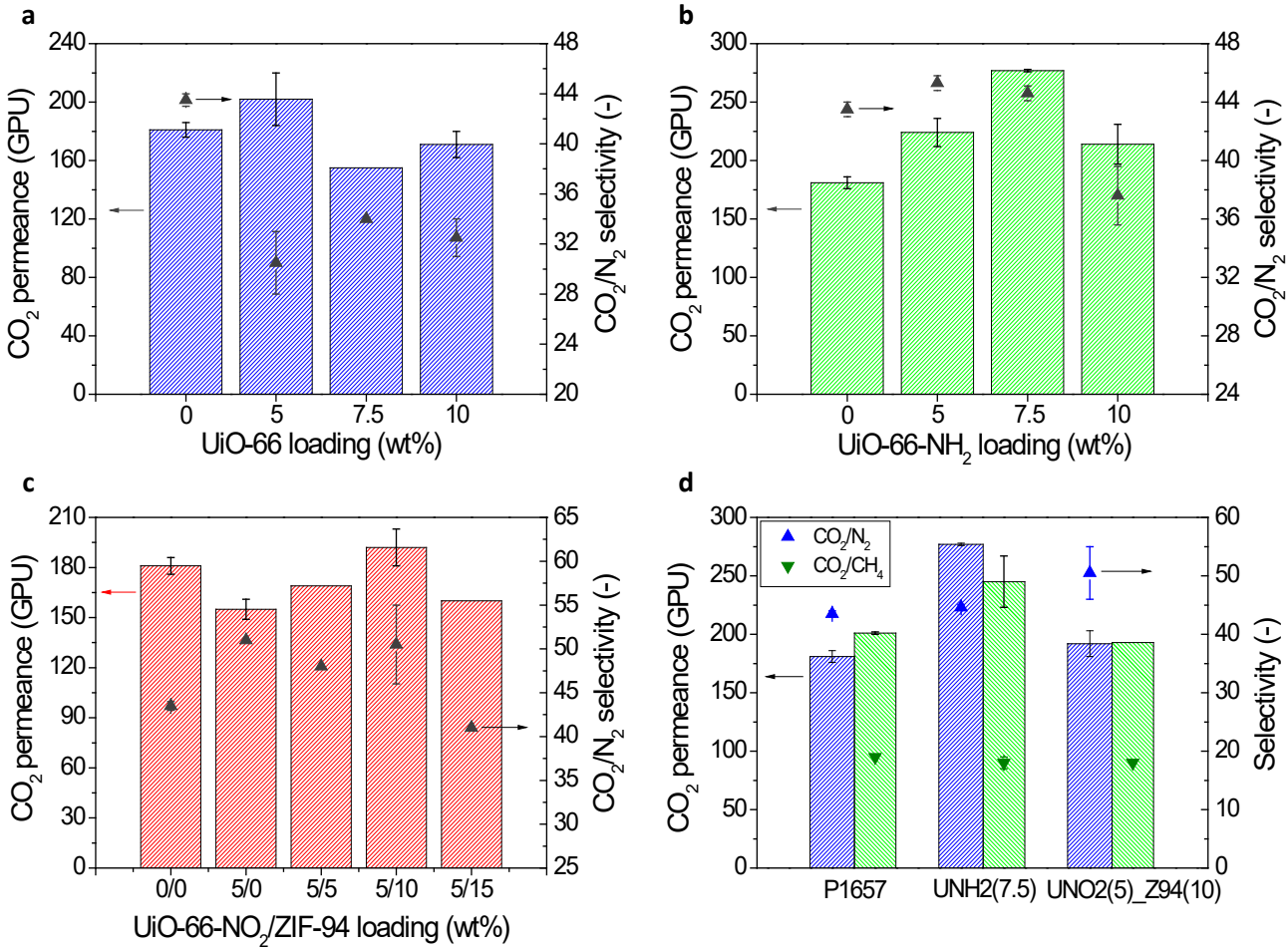

Figure 7.4. CO_2/N_2 separation performance of the TFC and TFN membranes fabricated with UiO-66 (A), UiO-66-NH_2 (B) and UiO-66-NO_2 and ZIF-94 (C), and a comparison of both, CO_2/N_2 and CO_2/CH_4 separation performance of the membranes prepared with the best conditions.

At this point, the best separation conditions were found with the TFN_UNH2(7.5) (highest CO_2 permeance) and TFN_UNO2(5)_Z94(10) (highest CO_2/N_2 selectivity) membranes. Figure 4d depicts a comparison of the results obtained with these membranes, in which the CO_2/CH_4 separation performance is also included. Although the CO_2/N_2 selectivity of the TFN_UNO2(5)_Z94(10) membrane is higher than that of the TFC_P1657 and TFN_UNH2(7.5) membranes, the CO_2/CH_4 selectivity does not experience such enhancement, and neither the CO_2 permeance. In this sense, the only membrane which clearly improves the CO_2 permeance in CO_2/CH_4 separations is the one fabricated with 7.5 wt% of UiO-66-NH_2.

It is worth mentioning that the ultra-small MOF, in addition to being the suitable material to prepare very thin selective membranes, allows an optimum effect on the gas separation properties at lower filler concentration than larger UiO-66 based fillers (typically working in the 10-50 wt% range composing in turn thicker membranes).[206,207] This would allow to reduce the membrane cost in an eventual large scale production. Therefore, to investigate the effect of the particle size on the gas separation performance, TFN membranes were also fabricated with a 7.5 wt% of UiO-66-NH_2 with an average particle size of 150 nm. Figure S2 shows that the improvement of the gas separation performance of the membranes prepared with larger UiO-66-NH_2 particles is not as significant as that obtained with the smaller particles, suggesting that higher loadings of large UiO-66-NH_2 particles are required to achieve comparable gas separation properties. This can be due to the fact that large particles have a lower external surface area, which is translated into a weakened interaction between the filler and the polymer matrix.[208] Small particles tend to agglomerate but the design of their morphology is crucial to prevent it.[209] This seems to have been accomplished in the functionalized UiO-66 nanoparticles prepared here. In consequence, the CO_2 permeance of the TFN_UNH2(7.5)_large membrane (205 GPU) is quite similar to that of the bare TFC_P1657 membrane (181 GPU). Moreover, the CO_2/N_2 selectivity value decreases from 44 to 38 when large UiO-66-NH_2 particles are used while it is relatively improved when smaller particles are incorporated into the polymer matrix, achieving a CO_2/N_2 selectivity of 45. As reported elsewhere,[210,211] a high specific surface area contributes to increase the CO_2/N_2 selectivity due to the increase in the CO_2 capture active sites and

the larger N_2 mass transfer resistance. Additionally, it is worth mentioning that ultra-small particles allow achieving both, high CO_2 permeance and CO_2/N_2 selectivity with the advantage of requiring a lower MOF mass density (0.036 g m^{-2}) than larger particles, since higher loadings of large UiO-66-NH_2 particles should be added to the membrane in order to obtain comparable gas separation results, as mentioned before.

7.3 Conclusions

Pebax® 1657 TFN membranes have been successfully fabricated by spin-coating obtaining robust and selective skin layer thicknesses of around 700 nm. The functionalization of MOF with amino (-NH_2) and nitro (-NO_2) groups significantly enhances the gas separation performance of membranes due to the increase in MOF/polymer compatibility derived from the hydrogen bonds created between the polymer chains and the MOF functional groups. TEM observation proved that both UiO-66 and ZIF-94 nanoparticles (with particle sizes of as low as 4-6 nm and 45 nm, respectively) are located in the selective top layer of the TFN membrane and that they are uniformly distributed through it. The highest CO_2 permeance was obtained with the TFN membrane containing 7.5 wt% of UiO-66-NH_2, which improved by 47% the CO_2 permeance of the TFC membrane in the case of CO_2/N_2 separations and by 22% in CO_2/CH_4 mixtures. Above 7.5wt%, UiO-66-NH_2 nanoparticles create aggregates that hinder the diffusion of CO_2 through the membrane which, in turn, decreases the CO_2 permeance. Furthermore, such aggregates generate micro-defects that entail a reduction of separation selectivity. TFN membranes containing 5 wt% of UiO-66-NO_2 reached the highest value of CO_2/N_2 selectivity (51), although the CO_2 permeance decreases by 14% in comparison to the TFC membrane. To maintain the CO_2/N_2 selectivity of 51 and increase the CO_2 permeance, UiO-66-NO_2 and ZIF-94 nanoparticles were combined in the same TFN membrane to achieve a synergic effect that improves dispersion. This allowed to achieve a CO_2 permeance of 192 GPU, close to that obtained with the pristine TFC membrane (181 GPU. Finally, to corroborate the effect of particle size in the gas separation performance, TFN membranes were fabricated with larger UiO-66-NH_2 particles. As expected, the improvement in the gas separation performance was not as significant as that obtained with the ultra-small nanocrystals due to the reduction of the MOF specific surface area.

7.4 Supplementary Information

ZIF-94 characterization

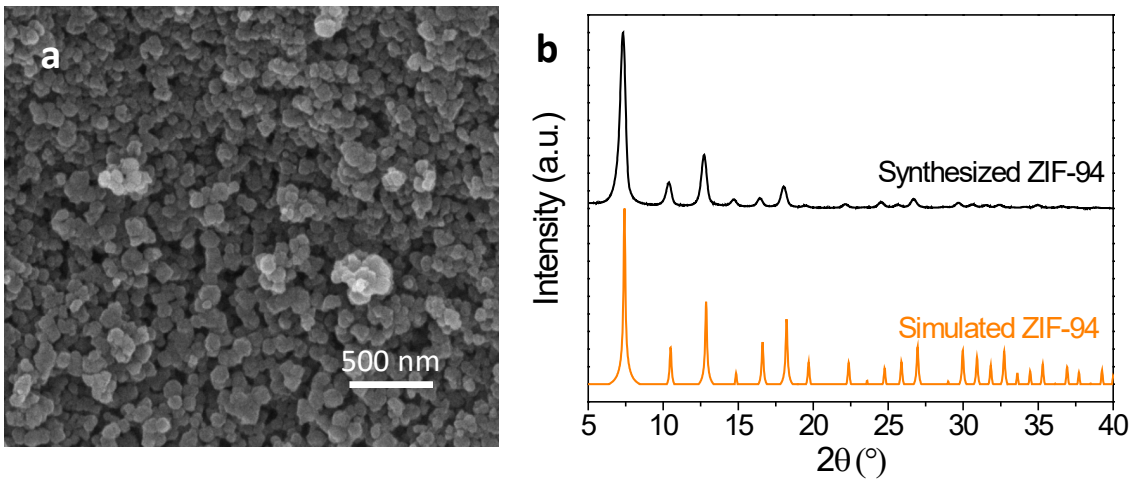

Figure S7.1. SEM image of ZIF-94 crystals (average particle size = 45 nm) (a), XRD patterns of the simulated and synthesized ZIF-94 (b).

Gas separation performance

Table S7.1. CO_2/N_2 separation results of the TFN membranes prepared with Pebax® 1657 and UiO-66 (4-6 nm) at 35 °C and 3 bar.

Membrane	CO_2 permeance GPU	CO_2/N_2 selectivity (-)
TFC_P1657	181 ± 5	43.5 ± 0.5
TFN_U(5)	202 ± 18	30.5 ± 2.5
TFN_U(7.5)	155 ± 0	34.0 ± 0.0
TFN_U(10)	171 ± 9	32.5 ± 1.5

Table S7.2. CO_2/N_2 separation results of the TFN membranes prepared with Pebax® 1657 and UiO-66-NH_2 (4-6 nm) at 35 °C and 3 bar.

Membrane	CO_2 permeance GPU	CO_2/N_2 selectivity (-)
TFC_P1657	181 ± 5	43.5 ± 0.5
TFN_UNH2(5)	224 ± 12	45.3 ± 0.5
TFN_UNH2(7.5)	277 ± 1	44.6 ± 0.5
TFN_UNH2(10)	214 ± 17	37.6 ± 2.0

Table S7.3. CO_2/N_2 separation results of the TFN membranes prepared with Pebax® 1657, UiO-66-NO_2 (4-6 nm) and ZIF-94 at 35 °C and 3 bar.

Membrane	CO_2 permeance GPU	CO_2/N_2 selectivity (-)
TFC_P1657	181 ± 5	43.5 ± 0.5
TFN_UNO2(5)	155 ± 6	51.0 ± 0.0
TFN_UNO2(5)_Z94(5)	169 ± 0	48 ± 0.0
TFN_UNO2(5)_Z94(10)	192 ± 11	50.5 ± 4.5
TFN_UNO2(5)_Z94(15)	160 ± 0	41.0 ± 0.0

Table S7.4. CO_2/N_2 and CO_2/CH_4 separation results of the best TFN membranes prepared in this work. Measured at 35 °C and 3 bar.

Membrane	CO_2/N_2		CO_2/CH_4	
	CO_2 permeance GPU	selectivity (-)	CO_2 permeance GPU	selectivity (-)
TFC_P1657	181 ± 5	43.5 ± 0.5	201 ± 1	19.0 ± 0.0
TFN_UNH2(7.5)	277 ± 1	44.6 ± 0.5	245 ± 22	18.0 ± 1.0
TFN_UNO2(5)_Z94(10)	192 ± 11	50.5 ± 4.5	193 ± 0.0	18.0 ± 0.0

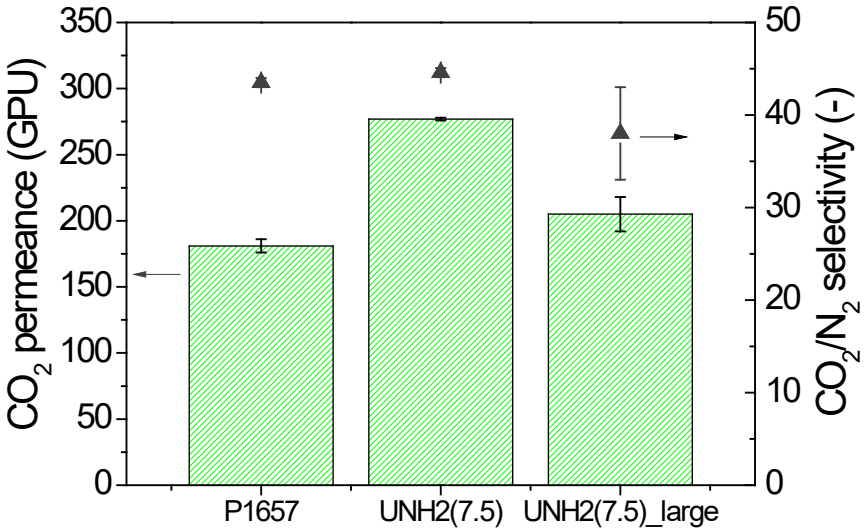

Figure S7.2. CO_2/N_2 separation performance of the TFC and TFN membranes fabricated with 7.5 wt% of UiO-66-NH_2. Influence of the particle size. Ultra-small UiO-66-NH_2 = 4-6 nm and large UiO-66-NH_2 = 150 nm.

Table S7.5. Comparison of the CO_2/N_2 separation results obtained with the TFN membranes prepared with Pebax® 1657 and UiO-66-NH_2 at 35 °C and 3 bar. Influence of particle size. Ultra-small UiO-66-NH_2 = 4-6 nm and large UiO-66-NH_2 = 150 nm.

Membrane	CO_2 permeance GPU	CO_2/N_2 selectivity (-)
TFC_P1657	181 ± 5	43.5 ± 0.5
TFN_UNH2(7.5)	277 ± 1	44.6 ± 0.5
TFN_UNH2(7.5)_large	205 ± 13	38.0 ± 5.0

Capítulo 8: "Highly stable Pebax® Renew® thin-film nanocomposite membranes with metal organic framework ZIF-94 and ionic liquid [Bmim][BF_4] for CO_2 capture"

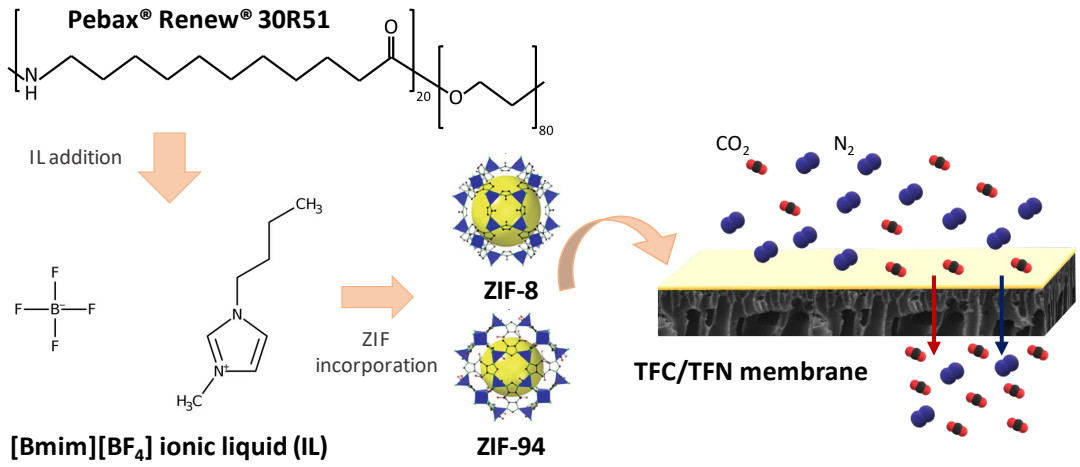

Adapted from "L. Martínez-Izquierdo, C. Téllez, J. Coronas. Highly stable Pebax® Renew® thin-film nanocomposite membranes with ZIF-94 and ionic liquid [Bmim][BF4] for CO_2 capture. J. Mater. Chem. A **2022**, 10, 18822-18833", with permission from The Royal Society of Chemistry.

8. Highly stable Pebax® Renew® thin-film nanocomposite membranes with metal organic framework ZIF-94 and ionic liquid [Bmim][BF_4] for CO_2 capture

8.1 Introduction

To reach the international target of net-zero CO_2 emissions by 2050, the use of green and renewable energy has drawn remarkable attention. Moreover, the development of technologies capable of separating and capturing CO_2 is also the scope of many studies.[212–214] Among the existing methods of CO_2 separation (e.g. amine absorption, cryogenic distillation and adsorption), membrane technology has many advantages such as simple processing equipment, operating flexibility, high reliability, small footprint, low energy requirement and environment friendliness.[215–218] However, current dense membranes suffer from very low CO_2 permeance, which makes them non-competitive for industrial applications.[34] To achieve efficient separations, exceeding the Robeson trade-off relationship between permeability and selectivity,[4] thin film composite membranes (TFC) must be prepared with a very thin selective layer (with a thickness lower than 1 μm).

In addition, the introduction of nanoparticles with molecular sieving properties within the polymer matrix is also regarded to improve the gas separation performance.[219,220] A variety of nano-fillers have been proved to enhance the separation performance of membranes, e.g. carbon derivatives,[64,65,221] zeolites[60,61] and metal-organic frameworks (MOFs).[180,181,222,223] Among them, MOFs and in particular zeolitic imidazolate frameworks (ZIFs), a sub-class of MOF, are being widely studied due to their improved affinity to the polymer matrix.[224] Such increased compatibility in MOF-type fillers is possible due to the presence of organic linkers within their structure.[182] Besides solid nano-fillers, the incorporation of liquids (e.g. ionic liquids, ILs) with increased mass transport in comparison to the polymer matrix is also the subject of many studies.[225,226] Such increment in the mass transport velocity allows higher permeances of CO_2 through

the membrane and more efficient separations.[227] Interestingly, this approach has been followed to prepare a mix of both solid particles and ILs, which is now gaining special attention due to the possibility of boosting the gas separation performance of membranes by combining their properties. Lu et al.[228] prepared PIM-1 mixed matrix membranes (MMMs) with an IL-modified UiO-66-NH_2 filler. They found that the IL improved not only the hydrophobicity of UiO-66-NH_2, thus facilitating the dispersion of the particles into the polymer, but also the affinity between the MOF and polymer. By using this strategy, they were able to reduce the non-selective interfacial defects with the corresponding enhancement of the gas separation behavior. Attempts to combine the advantages of solid and liquid additives have also been made with carbonaceous based particles. Huang et al.[37] prepared a Pebax®/ionic liquid modified graphene oxide (GO-IL) MMM with enhanced CO_2 separation performance. They found that the IL improved both the CO_2 solubility and the CO_2/gas selectivity of the MMMs. This allowed them to increase the CO_2/N_2 selectivity and the CO_2 permeability over 90% and 50%, respectively, compared to the pristine membrane. Jomekian et al.[229] prepared surface IL-modified Pebax® 1657 membranes filled with ZIF-8 particles. These MMMs with a 13 µm thick Pebax® layer on a polyethersulfone (PES) support had an insignificant content of IL, whose mission was to functionalize the Pebax® surface. This caused an increase in the CO_2 selectivity in the membranes with ZIF-8 due to the better interaction between the components of the MMM. Such improvement in the interaction of the filler with the polymer due to the presence of an ionic liquid has also been reported in other works.[230,231]

ZIF-94, also named as SIM-1, is a zeolitic imidazolate framework synthesized from Zn atoms and 4-methyl-5-imidazolate-carboxaldehyde linkers sharing the same SOD type topology than ZIF-8.[85,232] In the present work, ZIF-94 nanoparticles were combined with the anionic liquid1-butyl-3-methylimidazolium tetrafluoroborate [Bmim][BF_4] and incorporated into a Pebax® Renew® polymer to prepare thin film nanocomposite (TFN) membranes, which, unlike a typical dense MMM, are supported membranes whose selective layer incorporates nanoparticles. Pebax® is a commercial brand of block copolymer elastomers buildup of rigid polyamide blocks and soft polyether blocks (PEBA). Pebax® Renew® code was chosen for this project due to its renewable nature (it

contains 41% of renewable carbon, as measured by ASTM D6866), similar composition to Pebax® 1657, and anticipated similar separation properties. As previously noted by Neves et al.[233] and Jiang et al.[234] the IL [Bmim][BF_4] was selected over other imidazolium-based ionic liquids due to its improved performance in gas separation. To the best of our knowledge this is a non-studied system,[235,236] the closest situation includes Pebax® 1657/graphene oxide-IL TFN membranes, whose operation stability was studied for only up to 28 h.[37,237] Besides, it is worth mentioning that the ZIF-94 crystals used for this research were prepared via a solvent assisted ligand exchange (SALE) reaction using 1–butanol as reaction medium and nano-ZIF-8 as precursor material. With this strategy, the obtained ZIF has the controlled particle size of ZIF-8 and the high CO_2-philicity of ZIF-94 due to the aldehyde group in its ligand. This SALE method avoids the use of other toxic solvents such as tetrahydrofuran (THF) or dimethylformamide (DMF),[84] while taking advance of the easy control of ZIF-8 synthesis in terms of particle size and geometry. ILs and MOFs have been previously incorporated together into PEBA membranes for gas separation.[135,225,238] However, the vast majority of reports available concerning this topic are related to self-supported MMMs. The intent of this research is to prepare a new generation of TFN membranes for CO_2/N_2 and CO_2/CH_4 separation with improved gas separation performance over time.

8.2 Results

8.2.1 Characterization of ZIF-8 and ZIF-94

ZIF-8 and ZIF-94 were synthesized in order to be used as loadings for Pebax® Renew® thin film nanocomposite (TFN) membranes. As seen in Figure 8.1a and b, the average particle sizes of synthesized ZIF-8 and ZIF-94 (SALE) were 30 ± 5 nm and 48 ± 6 nm, respectively. Furthermore, the ZIF-94 particles have a less round shape and a larger particle size which may be related to an Ostwald ripening effect during the SALE.[239] To confirm the ligand exchange, TGA analyses were carried out from 35 to 700 °C under air atmosphere. Results (Figure 8.1c) revealed that the particles synthesized from ZIF-8 (ZIF-94 (SALE)) had the same degradation behavior that the ones synthesized by the original route (ZIF-94 (OR)), which besides differs from the degradation behavior of ZIF-8. While the maximum degradation of ZIF-94 nanoparticles takes place between 375 °C and 400

°C, the one of ZIF-8 happens at a higher temperature, ca. 450 °C. It is also worth mentioning that the ZIF-8 weight loss is more abrupt than those of ZIF-94 OR and SALE. Furthermore, the weight loss between 100-200 °C in the ZIF-94 (OR) thermogram suggests that there is still some remaining solvent from the ZIF synthesis. Conversely, the ZIF-94 (SALE) particles do not present such weight loss, indicating that the powder was successfully activated, probably due to the washing produced during the SALE process. The crystallinity and purity of the ZIF particles were confirmed by XRD. The patterns of the simulated ZIFs and the synthesized ones are plotted together for comparison in Figure 8.1d. As seen in this figure, the peak positions match well with those of the simulated ZIF-8. In fact, as both ZIFs share the same SOD type structure, the simulated patterns of ZIF-8 and ZIF-94 can be considered the same.[85,240] The FTIR-ATR spectra of ZIFs are depicted in Figure 8.1e, revealing a similar spectrum for ZIF-94 (SALE) than for ZIF-94 (OR), with the main bands of ZIF-94 at 1660 cm^{-1}, which corresponds to the aldehyde group (-CHO),[202] and 1496 cm^{-1}, related to the C=C bond. Besides the similar FTIR spectra of ZIF-94 (SALE) and (OR), the absence of the main bands of ZIF-8 at 1147 cm^{-1} and 993 cm^{-1} (both corresponding to the C-N bond)[69] agree with the successful ligand exchange. The N_2 adsorption isotherms and BET SSA values also confirm the ligand exchange (Figure 8.1f). In this case, the BET SSA decreases from 1350 $cm^2\ g^{-1}$ for the ZIF-8 to 464 $cm^2\ g^{-1}$ for the ZIF-94 (OR) and to 645 $cm^2\ g^{-1}$ for the ZIF-94 (SALE), which is in accordance with the literature for synthesized ZIF-94 particles.[202,241] However, these values suggest that the conversion of ZIF-8 into ZIF-94 was high but not complete with a remain of the ZIF-8 composition responsible for the larger value of BET SSA for ZIF-94 (SALE) as compared to that of the as-made ZIF-94. Furthermore, Figure 8.1f reveals the type I IUPAC classification of adsorption isotherms for both products, thus indicating dominant microporosity of these materials.[242]

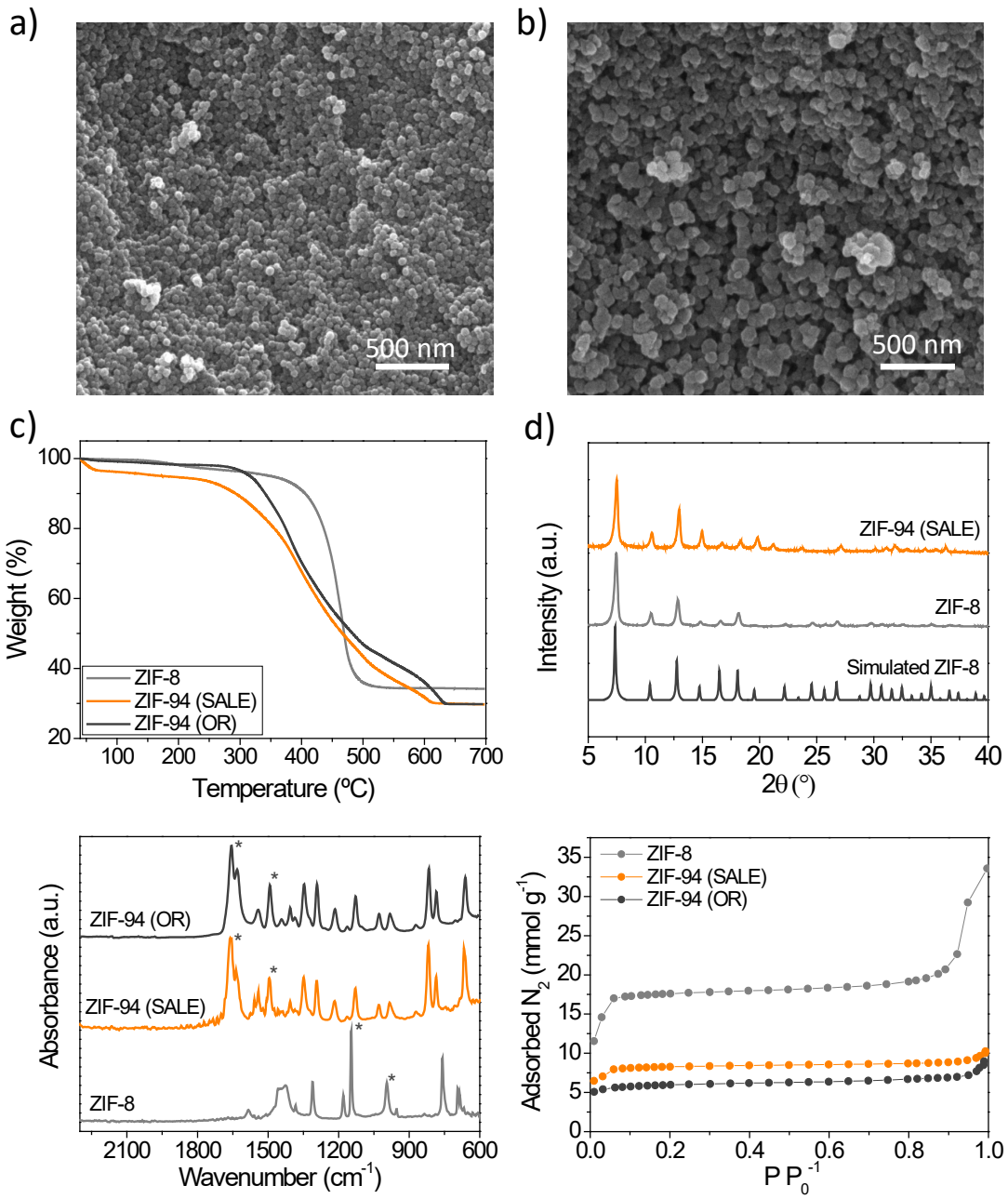

Figure 8.1. Characterization of ZIF particles. SEM images of ZIF-8 (a) and ZIF-94 (SALE) (b), thermal properties of ZIF-8, ZIF-94 (OR) and ZIF-94 (SALE) powders (c), XRD patterns of ZIF-94 (SALE), ZIF-8 and the simulated ZIF-8 (d), ATR-FTIR spectra of ZIFs and N_2 adsorption isotherms at -196 ºC of ZIF-8, ZIF-94 (OR) and ZIF-94 (SALE) particles (f).

8.2.2 Characterization of membranes

The thicknesses of the PTMSP and Pebax® layers were measured by SEM. Cross-sections of the membranes are depicted in Figure 8.2a-d. As observed in all images, a very thin layer of Pebax® Renew® (300 nm) was coated on top of a 1 µm thick PTMSP

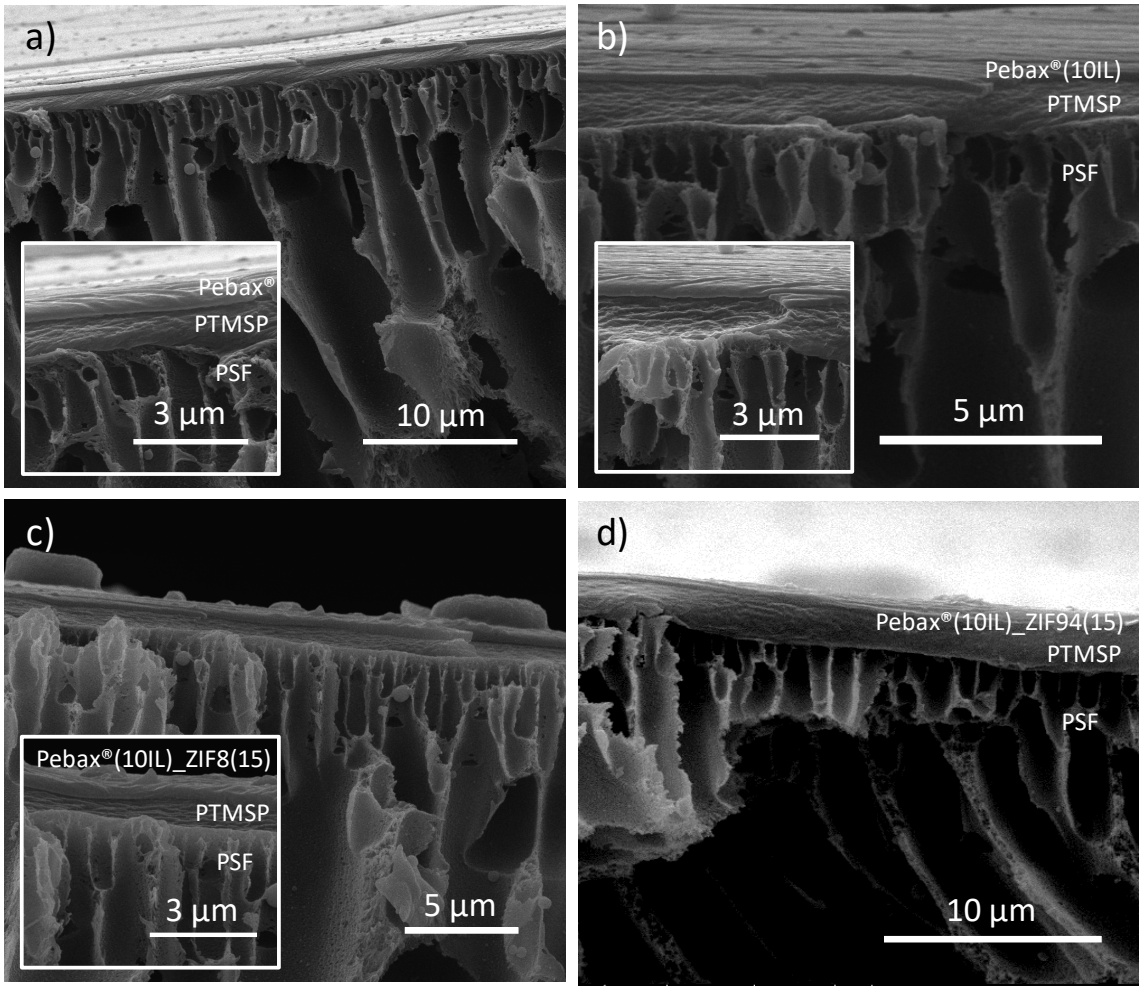

Figure 8.2. Cross-section SEM images of some of the Pebax® Renew® TFC membranes prepared in this work. (a) TFC_PEBA, (b) TFC_PEBA(10IL), (c) TFN_PEBA(10IL)_ZIF8(15) and (d) TFN_PEBA(10IL)_ZIF94(15).

gutter layer. The PTMSP gutter layer is placed between the support and the selective layer to avoid the polymer penetration of the latest into the support,[40] which would be detrimental for the final gas separation performance unnecessarily increasing the transport resistance. Indeed, PTMSP constitutes a poorly selective and highly permeable glassy polymeric material and it is expected that its contribution to the final resistance to the gas permeation is negligible.[243] Further characterization was carried out to study the stability and crystallinity of the membranes by TGA, DTG and XRD analyses. With this purpose, a dense Pebax® Renew® membrane was prepared via casting-solution and the results are depicted in Figure S8.1a and b, respectively. As seen in Figure S8.1a, the Pebax® Renew® polymer is stable up to 300 °C and it is degraded completely at 540 °C. In this figure, two degradation steps are appreciable. The first one (from 300 °C to 460 °C) is related to the major thermal degradation of the polymer, whereas the second

(from 460 °C to 540 °C) corresponds to the carbonization of the degraded polymer chains.[94] The XRD pattern shown in Figure S8.1b depicts the semicrystalline nature of Pebax® type copolymers.[111,112,222] In the case of this renewable code, three main crystalline peaks are noticeable in the diffractogram at 7.6°, 20.4° and 24.3° 2θ values, the first and second corresponding to the PEO and the third to the PA11 segments.[124]

8.2.3 Gas separation performance

8.2.3.1 Incorporation of ionic liquid [Bmim][BF_4]

Before attacking the effect of MOFs, the optimal concentration of ionic liquid [Bmim][BF_4] in the Pebax® Renew® composite membrane was studied by incorporating different weight percentages (from 5 to 20 wt%, respect to the polymer) into the polymer solution. The results in Figure 8.3a and Table S8.1 indicate that the best separation performance was obtained for the membranes with a 10 wt% of IL loading, achieving a CO_2 permeance of 629 ± 74 GPU and a CO_2/N_2 selectivity of 29 ± 1. The increase in CO_2 permeance can be due to the fact that the IL, which is in liquid state, is placed in low quantity between the polymer chains increasing mobility and free volume.[147] Furthermore, the increment of CO_2 permeance can be also attributed to the increase of CO_2 solubility, induced by the presence of the IL which has a strong affinity with CO_2. From 10 wt% of IL, the CO_2 permeance decreased progressively to values below that of the bare TFC membrane (438 ± 66 vs. 497 ± 71 GPU of CO_2 and a CO_2/N_2 selectivity of 25 ± 1 vs. 27 ± 3 for the membranes with a 20 wt% and 0 wt% of IL, respectively). The decrease of CO_2 permeance with the increment of IL up to 20 wt% can be due to the fact that ionic liquids have a relatively high viscosity, which may result in slow mass transfer rates.[244] In addition, as the amount of the liquid phase increases, there may be regions in the membrane in which the transport happens through a liquid medium with worse interfacial contact with the polymer (responsible of the decrease of CO_2/N_2 selectivity) and less diffusivity than the bare polymer (responsible of the decrease of CO_2 permeance). Analogous effects have been reported for the CO_2/N_2 mixture at much higher IL concentrations when operating with dense membranes.[245] Therefore, a maximum IL loading of 10 wt% was chosen to prepare the membranes with ZIFs.

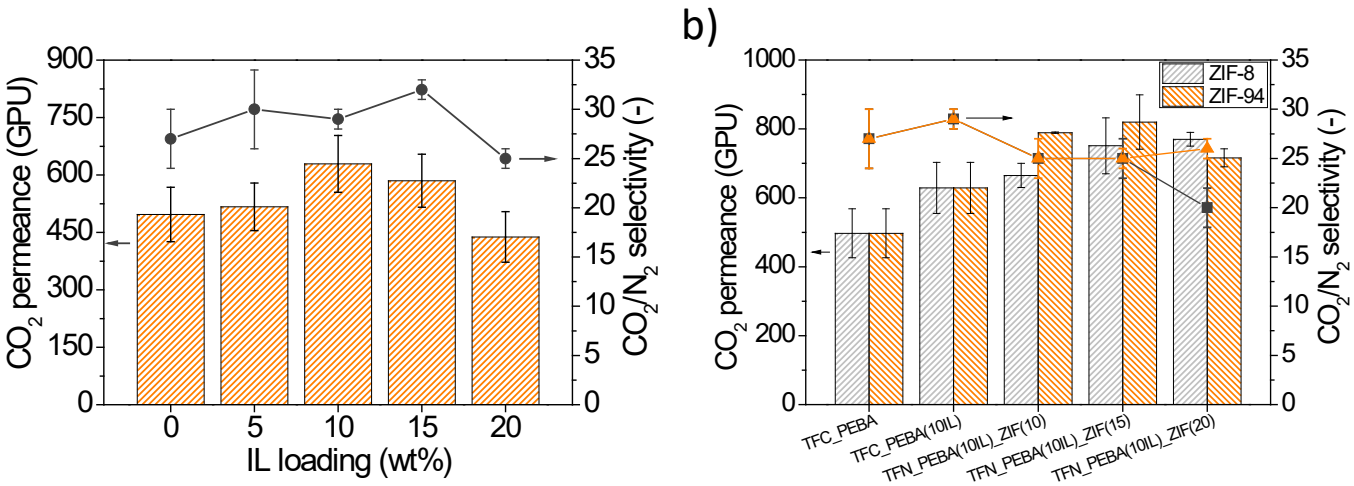

Figure 8.3. Gas separation performance of the TFC membranes prepared with different IL content dispersed on Pebax® Renew® (a) and CO_2/N_2 separation performance of the membranes with 10 wt% of IL and ZIFs (ZIF-8 and ZIF-94 (SALE)) (b). Measured at 35 ^oC and 3 bar.

8.2.3.2 Incorporation of ZIF-8 and ZIF-94 (SALE)

As explained before in the experimental section, two different ZIF nanoparticles (ZIF-8 and ZIF-94) were incorporated into the Pebax® Renew® nanocomposite membranes. First, ZIF-8 nano-crystals with an average size of ca. 30 nm were loaded at different concentrations (10, 15 and 20 wt%, respect to the polymer) into the TFC_PEBA(10IL) membranes with 10 wt% IL. As expected, the CO_2 separation performance of the membranes after the incorporation of ZIF-8 increased synergistically, reaching the highest CO_2 permeance at 20 wt% of ZIF-8 loading (770 ± 20 GPU) together with the lowest CO_2/N_2 selectivity (20 ± 2) (Figure 8.3b and Table S8.2).

The chemical similarity between the ZIFs and the IL, having both imidazole groups, suggests good interaction between them justifying the mentioned synergistic behavior. This will also contribute to the enhance of the IL stability assessed in the long term CO_2/N_2 separation experiments (see below). In addition, the incorporation of the IL into the Pebax®/ZIF-8 matrix also contributes to improve the MOF-polymer interface, thus enhancing the CO_2/N_2 separation performance of the MMM, as expected.[229] The decrease of selectivity at high loadings can be attributed to the aggregation of particles inside the Pebax® matrix, which may create a non-ideal interface between the polymer and the ZIF crystals.[246] It is also worth mentioning that ZIF-8 particles are hydrophobic whereas Pebax® polymer is hydrophilic. This fact can also be detrimental to the gas

separation performance of the membranes, since the lack of compatibility between the polymer and the filler may create voids in the polymer matrix which results in the loss of separation efficiency. Therefore, it is expected that the replacement of these hydrophobic particles with hydrophilic ones (i.e. ZIF-94) would be beneficial to achieving a significant increase in the gas separation performance.

ZIF-94, as ZIF-8, is a Zn^{2+} based MOF but with 4-methyl-5-imidazolate-carboxyaldehyde as organic linker, which makes it hydrophilic as compared to ZIF-8[27,69] and also more inclined to adsorb CO_2 (the CO_2 uptake of ZIF-8 at 298 K and 1 bar being 0.7 mmol g^{-1} [86,247] and that of ZIF-94, 2.4-2.9 mmol g^{-1} [202]). The same amounts of ZIF-94 have been tested in membranes with a 10 wt% of IL and the results can be also observed in Figure 8.3b and Table S8.3. As expected, the membranes prepared with ZIF-94 reached higher permeation values up to 15 wt% of loading, this being the highest CO_2 permeance value obtained in this work (820 ± 79 GPU) and with a CO_2/N_2 selectivity of 25 ± 1. Such CO_2/N_2 selectivity value is only slightly lower than that obtained with the less permeable (497 ± 71 GPU) bare TFC_PEBA membrane (27 ± 3) and with the membrane with a 10 wt% of IL but without ZIF (TFC_PEBA(10IL), 29 ± 1 with 629 ± 74 GPU CO_2 permeance. As for ZIF-8 particles, at high loadings of ZIF-94, the CO_2 permeance decreases due to particle agglomeration reaching a value of 716 ± 26 GPU at 20 wt% of ZIF-94. Nevertheless, the CO_2/N_2 selectivity is maintained (26 ± 1).

8.2.3.3 Gas separation as a function of temperature

To study the behavior of the Pebax® Renew® TFC and TFN membranes with temperature, gas separation experiments were carried out at 25, 35 and 50 °C with the membranes chosen as optimal in this work: TFC_PEBA, TFC_PEBA(10IL) and TFN_PEBA(10IL)_ZIF94(15) (Figure 8.4). This study is important since the temperature usually improves the membrane permeance with the limitation of the loss of separation selectivity and the membrane stability. Only ZIF-94 was tested for these experiments due to its better performance as compared to ZIF-8. With the obtained data, the apparent activation energies of permeation were calculated using the Arrhenius equation as reported elsewhere (equation 2.11, section 2.4.1.3).

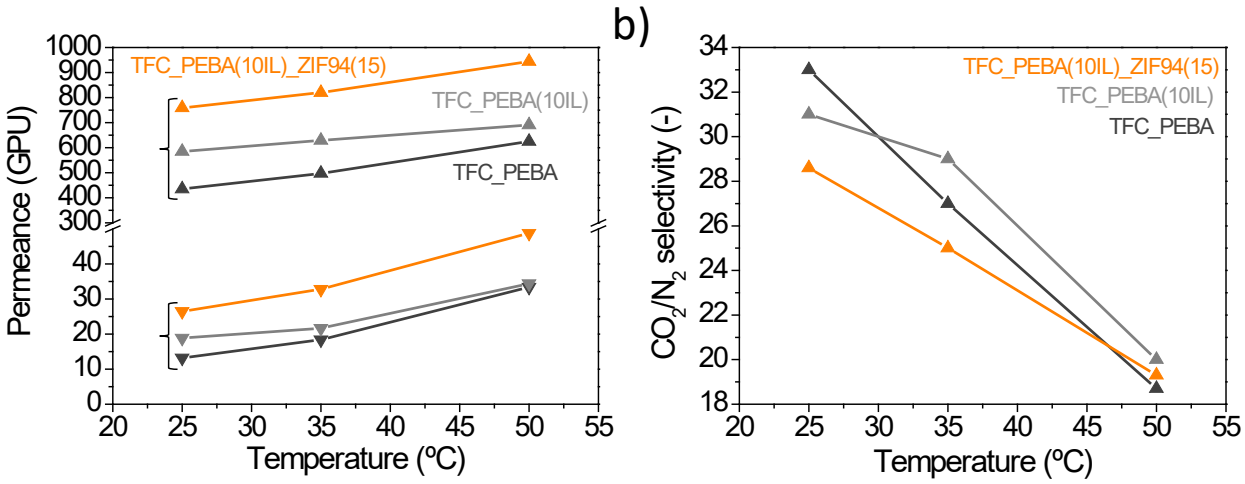

Figure 8.4. Gas separation performance as a function of temperature. Measured at 25, 35 and 50 ºC and 3 bar. (a) CO_2 and N_2 permeances and (b) CO_2/N_2 selectivity.

It is expected that the sensitivity of permeance coefficients of penetrants to temperature (expressed through the E_p) increases for those with lower permeability.[248] In this sense, the E_p of permeation would be higher for N_2 than for CO_2. Therefore, the CO_2/N_2 separation selectivity decreases with increasing temperature, as observed in Figure 8.4a and b. In addition, it must be taken into account that permeance is the product of solubility and diffusivity and that diffusivity increases with temperature for all gases, which is translated into an increase of permeance for all the membranes. Such diffusion variation is relatively similar for CO_2 and N_2 whose molecular size is very close; however, the solubility of CO_2 in all the actors (PEBA polymer, IL and ZIF-94) decreases with temperature, which undoubtedly produces the decrease of the CO_2/N_2 selectivity with temperature.

The permeation E_p values calculated for the optimal membranes are collected in Table 8.1 and compared with analogous data found in the literature for dense membranes (since, as far as we know, Pebax® TFC/TFN membranes have not been studied as a function of temperature). As observed in this table, the values of the CO_2 and N_2 activation energies of the TFC_PEBA membrane are in accordance with those reported in the literature for several Pebax® codes. Moreover, as expected, the E_p of N_2 (30.1 kJ mol^{-1}) is much higher than that of CO_2 (11.7 kJ mol^{-1}). It is worth mentioning that the CO_2 E_p for the TFC_PEBA(10IL) membrane is ca. two times lower (5.3 kJ mol^{-1}) than that for the TFC_PEBA membrane (11.7 kJ mol^{-1}). This behavior was already observed by

Rabiee *et al.,*[147] who evaluated the effect of feed temperature on gas permeability and selectivity of PEBA/[Emim][BF_4] gel membranes and estimated the E_p for permeation of CO_2 and N_2 as a function of the IL content. They found that the E_p decreased with the increase of IL content for all penetrants. This observation is consistent with the fact that the permeations of CO_2 and N_2 increase with the addition of IL.

Table 8.1. Apparent activation energies for permeation of CO_2 and N_2.

Membrane	E_p CO_2	E_p N_2	Ref.
	kJ mol^{-1}		
Pebax® 1657	13.3	30.4	[114]
Pebax® 1657	14.9	28.0	Chapter 5
Pebax® 1657	14.6	33.6	[123]
Pebax® 2533	16.7	27.2	[130]
Pebax® 2533	18.2	31.0	[131]
Pebax® 3533	14.2	29.6	[53]
Pebax® 1074	13.4	30.3	[53]
TFC_PEBA	11.7	30.1	This chapter
TFC_PEBA(10IL)	5.3	19.6	This chapter
TFC_PEBA(10IL)_ZIF94(15)	7.0	19.7	This chapter

Interestingly, the membrane with 15 wt% of ZIF-94 (SALE) provided and intermediate CO_2 E_p (7.0 kJ mol^{-1}) with similar N_2 E_p than the TFC_PEBA(10IL) membrane, in agreement with the less abrupt loss of CO_2/N_2 separation selectivity as a function of temperature for the membrane with the IL and the ZIF (Figure 8.4b) related to the lower N_2 E_p - CO_2 E_p difference of 12.7 kJ mol^{-1}. All these results suggest that the temperature increase of permeation is affected by both the addition of IL and incorporation of ZIF nanoparticles. Specially, the decrease in selectivity with temperature is different depending on the membrane, which undoubtedly indicates that the introduction of IL and/or ZIF-94 changes the transport properties of the membranes. It is worth mentioning that measurement error may be the cause of the lower selectivity of TFC PEBA(10IL) than TFC PEBA at 25 °C, which would be expected to be higher as found at 35 °C. In fact, the variation in selectivity is around 3–10%, as seen in Figure 8.3a.

8.2.3.4 Long-term stability studies

PTMSP is a highly permeable glassy polymer that possesses an unrelaxed free fractional volume (FFV) and due to that undergoes physical aging because of the chain rearrangement, resulting in the reduction of the membrane permeance.[249] Therefore, one major concern when using this polymer as gutter layer is its aging. Chen *et al.*[250] demonstrated that a thin coating of PTMSP can lose up to 80% of the CO_2 permeance within 14 days. In this work, the long-term stability of the optimal membranes was tested for 18 days at 35 °C and 3 bar feed pressure. It must be noted that during the long-term stability tests, the membranes were periodically exposed to the gas mixture and stored at RT between each measurement.

In the open literature, other authors attempted to study the long-term stability of Pebax® membranes. Sungjin Lee et al.[92] studied the stability of Pebax® 2333 TFC membranes for 36 days, without changes in the separation performance. Jae Eun Shin et al.[251] tested the long-term stability of a dense Pebax®1657/PEG/GO MMM for 100 days. They observed that after such period of time, membranes did not have any problems associated with aging. Although these papers evaluate the stability of the membranes for longer periods of time, these configurations do not incorporate an ionic liquid, which highly affects the aging of the membrane, as found in this work. F. Pardo et al.[252] evaluated the long-term stability of a Pebax® 1657/IL dense membrane for 25 days, however, their aim was to separate a refrigerant blend instead of a gas mixture.

In this work, to evaluate the stability of the membranes for longer periods of time, a linear regression was conducted with the data of CO_2 permeance and operation time, as explained in the Supplementary Information section. The results showed good fitting in all configurations, as depicted in Figure S8.2. Figure 8.5 indicates that the membranes gradually lose their permeance along the 18 days of testing. The maximum loss of permeance was experienced by the TFC_PEBA(10IL) membrane, which decreased its CO_2 permeance by 28%, from 629 GPU to 460 GPU followed by the membrane with ZIF-94 (membrane TFC_PEBA(10IL)_ZIF94(15)), whose CO_2 permeance decreased by 25% (from 820 GPU to 611 GPU). The pristine TFC membrane lost a 20 % of its CO_2 permeance (from 497 GPU to 395 GPU).

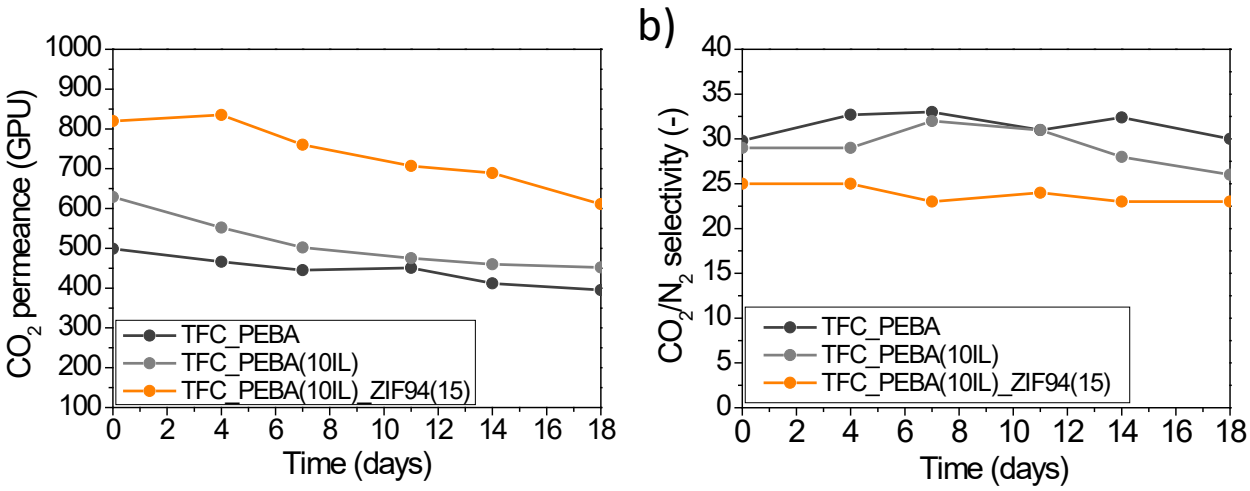

Figure 8.5. Long-term stability of the TFC and TFN membranes prepared in this chapter. Measured at 35 ^{o}C and 3 bar feed pressure.

Considering these results, it is noticeable that the IL worsens the stability of the membranes, which can be associated with the increment in the mass transport velocity as well as the exudation followed by the displacement of the IL through the membrane.[253] Nevertheless, such deterioration was mitigated with the incorporation of ZIF-94, which partially avoids the exudation of the IL. Due to their chemical affinity based on their common imidazole species, IL [Bmim][BF_4] should interact more strongly with ZIF-94 than with the polymer. In consequence, the ZIF-94 is trapped in the polymer matrix as an anchor point for the IL enhancing its stability in the TFN membrane.

This was also demonstrated after the evaluation of the half-life time of each configuration. As collected in Table S8.4, the time at which the CO_2 permeance of the membrane with a 10 wt% of IL is reduced by half is 23 days, whereas that of the membrane that incorporates ZIF-94 is prolonged to 39 days, which is closer to the time achieved with the pristine membrane (44 days). In agreement with this, despite the loss of performance after 18 days of tests, it is worth mentioning that the CO_2 permeance decrease is far from the values previously reported by Chen *et al.*[250] for thin film coatings of PTMSP without selective layer where the reduction in permeance was 80% in 14 days compared to the 20-28% reduction represented here in a similar period of time. The improvement in the long-term stability of the membranes can be also due to the partial penetration of the Pebax® chains into the PTMSP gutter layer, meaning that polymeric chains for both polymers could be intertwined, stabilizing the non-equilibrium PTMSP

structure.[254] In any event, after 18 days of separation activity membrane TFC_PEBA(10IL)_ZIF94(15) is 55% and 35% more permeable than the bare polymer and the membrane with only IL maintaining a CO_2/N_2 separation selectivity of 25.

8.2.3.5 Comparison with other TFC and TFN membranes that contain Pebax® and IL

The CO_2/N_2 separation performance of the membranes prepared in this work has been compared with those of other TFC and TFN membranes found in the literature containing IL.[37,237,255–257] As seen in Table 8.2, Fam et al.[237] obtained a similar CO_2/N_2 separation performance that the one obtained in this work with the TFC_PEBA(10IL) membrane by incorporating GO and [Emim][BF_4] IL into Pebax® 1657. Nevertheless, it is worth mentioning that they fabricated hollow fibers (HF) instead of flat sheet membranes, as reported in this work. Additionally, to obtain similar results, they needed from the addition of graphene oxide (GO) to the solution, since the CO_2 permeance of the Pebax®/IL HF itself only reached up to 300 GPU, as reported previously.[256] Yeon et al.[255] also prepared TFC membranes with [Bmim][BF_4] but using Pebax® 2533 instead of Pebax® Renew® 30R51. With this membrane, they obtained a CO_2 permeance of 101 GPU and a CO_2/N_2 selectivity of 42. Finally, Dai et al.[257] prepared a TFC membrane with a Pebax®/task-specific ionic liquid (TSIL) blend selective layer coated on top of a PSF ultrafiltration support and studied its CO_2 separation performance as a function of the relative humidity (RH). At 0% RH (which is the condition used in this research), they reached up to 250 GPU of CO_2 and a CO_2/N_2 selectivity of 30. In any event, the closest situation to our TFN membranes includes Pebax® 1657/graphene oxide-IL TFN membranes,[37,237] whose stability was studied for only up to 28 h.[237]

Table 8.2. Comparison with other TFC and TFN membranes containing Pebax® and IL.

Membrane	CO_2 Permeance (GPU)	CO_2/N_2 Selectivity	Ref.
Pebax®2533/[Bmim][BF_4]	101	42	[255]
Pebax®1657/GO-IL	905	45	[37]
Pebax®1657/[Emim][BF_4]/GO*	642	34	[237]
Pebax1657/[Emim][BF_4]*	300	36	[256]
Pebax®2533/TSIL	250	30	[257]
TFC_PEBA	497	27	This chapter
TFC_PEBA(10IL)	629	29	This chapter
TFC_PEBA(10IL)_ZIF8(15)	751	25	This chapter
TFC_PEBA(10IL)_ZIF94(15)	819	25	This chapter
* Hollow fibers			

8.2.3.6 CO_2/CH_4 separation performance

To further complete this work, the CO_2/CH_4 separation performance of the optimal membranes prepared in terms of CO_2/N_2 (TFC_PEBA, TFC_PEBA(10IL) and TFC_PEBA(10IL)_ZIF94(15)) was studied and the results obtained are depicted in Figure S8.3. As observed in this figure, the membranes followed a similar trend for the separation of CO_2 from CH_4 than from N_2, enhancing the CO_2 permeance with the incorporation of IL and ZIF-94 without affecting the separation selectivity. In fact, the CO_2 permeance increased from 581 GPU to 689 GPU after the addition of 10 wt% of IL, and to 838 GPU after the incorporation of both, 10 wt% of IL and 15 wt% of ZIF-94 (SALE), which means improvements of 19% and 48%, respectively. As mentioned, the CO_2/CH_4 selectivity was maintained at a value of 10, considerably lower than the CO_2/N_2 selectivity in line with the general behavior of PEBA type polymers.[111]

8.3 Conclusions

Pebax® Renew® 30R51 TFC membranes and ZIF-8 or ZIF-94/IL/Pebax® Renew® TFN membranes were prepared and characterized for the CO_2/N_2 separation. ZIF-94 was prepared via a solvent assisted ligand exchange (SALE) reaction using ZIF-8 as precursor

material suspended in 1-butanol. The high extension of the ligand exchange was confirmed by TGA, DTG, XRD, FTIR and BET analyses. The addition of [Bmim][BF_4] into the Pebax® Renew® composite membranes enhanced the CO_2 separation performance of the membranes up to 10 wt% of loading, reaching a CO_2 permeance of 629 GPU and a CO_2/N_2 selectivity of 29, which means increases of 27% and 11% compared with the CO_2 permeance and the CO_2/N_2 separation selectivity of the pristine membrane, respectively. The incorporation of ZIF-8 or ZIF-94 particles into the IL/Pebax® matrix also improved the CO_2 permeance of the membranes over the ones which only had IL, which was attributed to the improved compatibility between ZIFs and the polymer matrix due to the presence of the IL. For both ZIFs, the best gas separation results were obtained at 15 wt% of ZIF loading and 10 wt% of IL, reaching CO_2 permeances of 751 GPU and 819 GPU for ZIF-8 and ZIF-94, respectively, together with a CO_2/N_2 selectivity of 25 in both cases. It is worth mentioning that it was up to 15 wt% of ZIF loading that the membranes with ZIF-94 were more permeable than those with ZIF-8. This behavior was attributed to the CO_2-philic nature of ZIF-94, due to its aldehyde group which in turn increases its hydrophilicity and compatibility with the polymer and the IL. In addition, the apparent activation energies of permeation were also calculated for the optimal membranes, obtaining similar results to those reported in the literature for Pebax® type copolymer with the pristine TFC membrane, but lower values with the membranes with IL and IL/ZIF-94. These results were related to the increment of CO_2 and N_2 permeation, clearly supporting the positive influence of IL and ZIF on the diffusion and solubility properties of the membranes with respect to the pure polymer.

The long-term stability of the membranes was studied for 18 days. Results indicated that the IL affected the stability of the membrane increasing the CO_2 permeance loss from 20% to 28%. However, the incorporation of ZIF-94 partially mitigated such deterioration reaching a CO_2 permeance loss of 25 % after 18 days of testing. In spite of the fact that the long-term stability of the membranes was affected by the use of PTMSP as a gutter layer, the CO_2 permeance loss was far from previous results found in the literature. In any event, after the 18 days of continuous performance, the membrane with IL and ZIF-94 was 55% and 35% more CO_2 permeable than the bare polymer and the membrane with only IL, respectively, maintaining a CO_2/N_2 selectivity of 25.

8.4 Supplementary Information

Membrane characterization

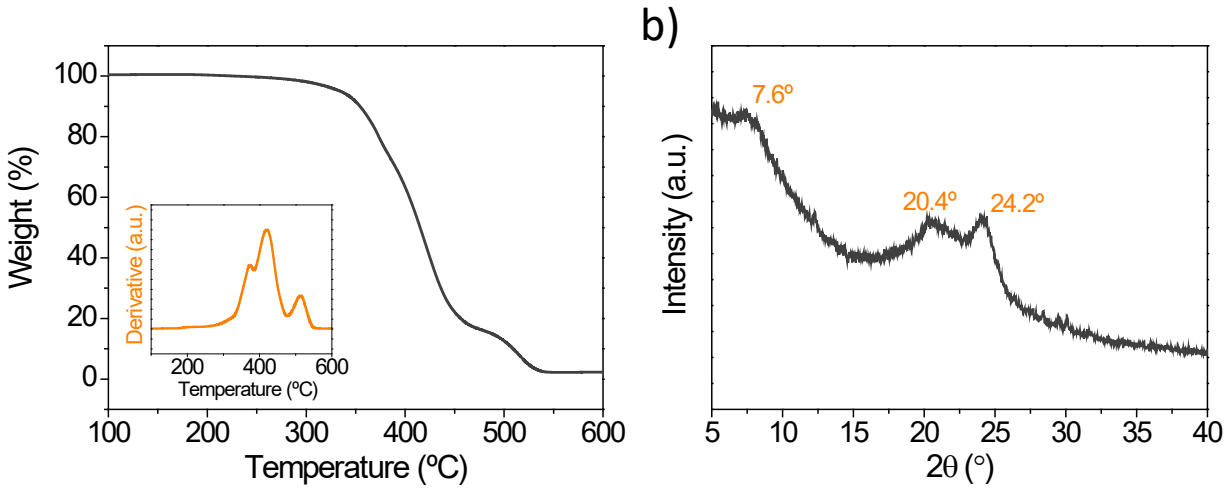

Figure S8.1. Pebax® Renew® dense membrane: thermal stability in terms of TGA and DTG (a), and XRD pattern (b).

Gas separation results

CO_2/N_2 separation

Table S8.1. CO_2/N_2 separation performance of the TFC membranes prepared with different ionic liquid [Bmim][BF_4] content dispersed in Pebax® Renew®. Measured at 35 °C and 3 bar feed pressure.

Membrane	wt% IL	CO_2 permeance (GPU)	N_2 permeance (GPU)	CO_2/N_2 selectivity
TFC_PEBA	0	497 ± 71	21 ± 4	27 ± 3
TFC_PEBA(5IL)	5	517 ± 62	18 ± 5	30 ± 4
TFC_PEBA(10IL)	10	629 ± 74	22 ± 4	29 ± 1
TFC_PEBA(15IL)	15	585 ± 69	18 ± 3	32 ± 1
TFC_PEBA(20IL)	20	438 ± 66	18 ± 3	25 ± 1

Table S8.2. CO_2/N_2 separation performance of the TFN membranes prepared with 10 wt% of ionic liquid [Bmim][BF_4] and different ZIF-8 content. Measured at 35 °C and 3 bar.

Membrane	wt% ZIF-8	CO_2 permeance (GPU)	N_2 permeance (GPU)	CO_2/N_2 selectivity
TFC_PEBA	0	497 ± 71	21 ± 4	27 ± 3
TFC_PEBA(10IL)	0	629 ± 74	22 ± 4	29 ± 1
TFN_PEBA(10IL)_ZIF8(10)	10	665 ± 35	27 ± 2	25 ± 0
TFN_PEBA(10IL)_ZIF8(15)	15	751 ± 81	33 ± 8	25 ± 2
TFN_PEBA(10IL)_ZIF8(20)	20	770 ± 20	39 ± 2	20 ± 2

Table S8.3. CO_2/N_2 separation performance of the TFN membranes prepared with 10 wt% of ionic liquid [Bmim][BF_4] and different ZIF-94 (SALE) content. Measured at 35 °C and 3 bar.

Membrane	wt% ZIF-94	CO_2 permeance (GPU)	N_2 permeance (GPU)	CO_2/N_2 selectivity
TFC_PEBA	0	497 ± 71	21 ± 4	27 ± 3
TFC_PEBA(10IL)	0	629 ± 74	22 ± 4	29 ± 1
TFC_PEBA(10IL)_ZIF94(10)	10	789 ± 2	32 ± 2	25 ± 2
TFC_PEBA(10IL)_ZIF94(15)	15	819 ± 79	34 ± 4	25 ± 1
TFC_PEBA(10IL)_ZIF94(20)	20	716 ± 26	37 ± 13	26 ± 1

Figure S8.2 illustrates the fitting of a linear regression of the long-term stability studies. The intercept for each regression has been determined to equal the fresh membrane's CO_2 permeance. The figure shows R^2 regression and equations. The time at which the CO_2 permeance is lowered by two has been determined as the half-life of each configuration and values are presented in Table S8.4.

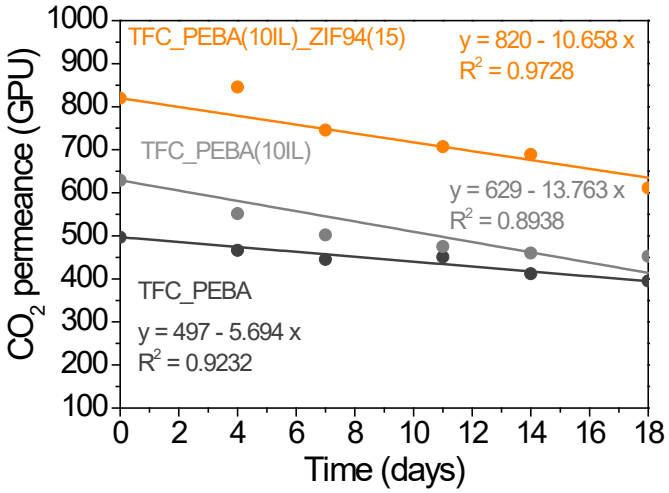

Figure S8.2. Linear fitting of the long-term stability studies of the TFC_PEBA, TFN_PEBA(10IL) and TFN_PEBA(10IL)_ZIF94(15) membranes with equations and R^2 regression.

Table S8.4. Half-time in days calculated with the linear equations depicted in Figure S8.2.

Membrane	$PCO_{2,1/2}$ (GPU)	$t_{1/2}$ (days)
TFC_PEBA	248.5	44
TFC_PEBA(10IL)	314.5	23
TFC_PEBA(10IL)_ZIF94(15)	410.0	39

CO_2/CH_4 separation

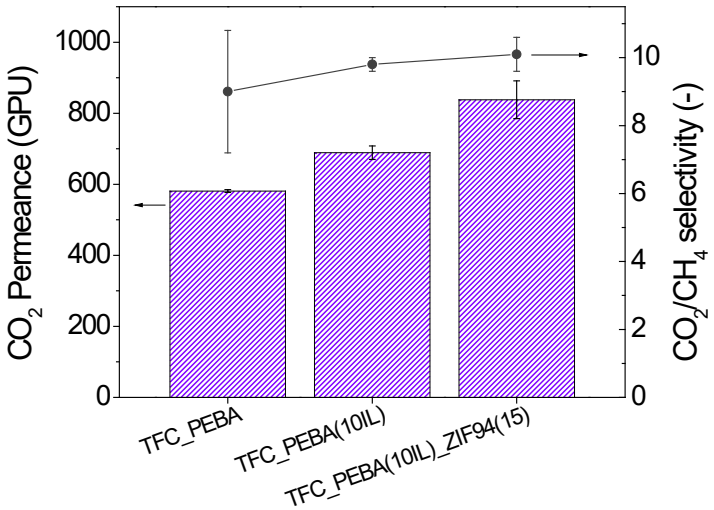

Figure S8.3. CO_2/CH_4 separation performance of the TFC and TFN membranes prepared with the optimal conditions. Measured at 3 bar and 35 °C.

Capítulo 9: Resumen y conclusiones

9. Resumen y conclusiones

En esta tesis doctoral se ha progresado en el ámbito de las membranas de capa fina para separación de mezclas gaseosas con CO_2, obteniéndose membranas con mayor rendimiento que han permitido mejorar los valores de separación (entendiéndose estos como el permeación de gas a través de la membrana y su selectividad) obtenidos hasta la fecha.

En el primer capítulo de resultados (**capítulo 4**) se estudia el rendimiento de separación de gases de cinco copolímeros de tipo poliéter-bloque-amida (códigos Pebax® 1657, Renew®, 2533, 3533 y 4533) que se preparan en forma de membranas densas por el método de casting. Los códigos están compuestos por diferentes segmentos rígidos y flexibles, por lo que se investiga cómo la naturaleza de estos segmentos y su proporción (PEO/PA) afecta a los parámetros de solubilidad, difusividad y permeabilidad y, por lo tanto, al rendimiento de separación de gases de las membranas. Además, la intención de este primer estudio es comparar dos métodos bien establecidos para la estimación del rendimiento de la separación de gases a partir de experimentos de permeación de gases individuales y mezclas. Las medidas de permeación de un solo gas (el conocido método de *time-lag*) permiten estimar los parámetros de solubilidad y difusión, mientras que la permeación de gases mixtos constituye un enfoque más realista para la evaluación de la capacidad de separación de la membrana. Asimismo, se ha llevado a cabo una investigación adicional midiendo el rendimiento de separación de gases a diferentes temperaturas de operación para calcular la energía de activación aparente de la permeación. Las membranas también se han caracterizado en términos de estabilidad térmica y cristalinidad mediante análisis termogravimétricos y de difracción de rayos X, respectivamente. Otros trabajos ya han informado sobre los métodos de preparación y el rendimiento de separación de CO_2 de los copolímeros tipo Pebax®; sin embargo, hasta la fecha, nunca antes se había realizado un estudio tan completo. Por otro lado, los resultados recopilados aquí permitirán obtener información sobre el uso de mediciones de permeabilidad de un solo gas como un medio para predecir el rendimiento de separación de gases de un determinado material de membrana.

Con la intención de profundizar en el comportamiento de los copolímeros tipo Pebax® como membranas para separación de gases, el **capítulo 5** se centra en estudiar el efecto que tiene la concentración de polímero en la disolución de *casting* sobre la morfología y el rendimiento de separación de gases de membranas densas de Pebax® 1657. Aunque estos parámetros ya han sido estudiados previamente para copolímeros de tipo polieter-bloque-amida, hasta la fecha no se ha publicado ningún estudio relacionado con cómo la concentración de polímero afecta a la cristalinidad y a las propiedades térmicas de la membrana. Con este objetivo, se han probado diferentes concentraciones de Pebax® 1657 (1, 3 y 5% en peso) en la disolución de *casting*, obteniéndose membranas densas de 40 µm de espesor. La morfología y estabilidad térmica de todas las membranas se ha estudiado mediante SEM, XRD, DSC, viscosímetro rotacional y TGA. Mediante XRD se ha apreciado un aumento de la cristalinidad con la concentración de polímero, relacionado principalmente con la reorganización de las cadenas poliméricas y el tiempo de evaporación del disolvente. Esta característica parece ser un factor clave en la degradación de las membranas, confirmando que los materiales más cristalinos tienden a ser térmicamente más estables. Para estudiar la influencia tanto de la morfología como de la temperatura de operación en la separación de CO_2, se han realizado ensayos de separación de gases con la mezcla CO_2/N_2. Los resultados obtenidos indican que, para alcanzar un buen rendimiento de separación de gases, se debe llegar a un compromiso entre la cantidad de disolvente empleado para preparar la membrana y la cristalinidad de la misma. A lo largo de este estudio, ha sido la membrana preparada con un 3% en peso de polímero la que mejores resultados de separación de gases ha arrojado, alcanzando (a 35 °C y 3 bar) una permeabilidad de CO_2 de 110 Barrer y una selectividad CO_2/N_2 de 36.

Una vez conocidos los parámetros que afectan al rendimiento de separación de gases, así como a su estabilidad térmica, y establecidos los códigos idóneos para llevar a cabo la sepración de mezclas gaseosas de CO_2/N_2 y CO_2/CH_4, en los **capítulos 6, 7 y 8**, se han preparado membranas de capa fina mediante distintos métodos: inversión de fases, "*spin-coating*" y "*dip-coating*". Además, se ha estudiado como la incoporación de distintos materiales de relleno de tipo MOF y de un líquido iónico pueden mejorar el rendimiento de separación de gases de estas membranas.

En primer lugar, en el **capítulo 6** se han preparado por primera vez membranas compuestas de película delgada de copolímero poli(éter-bloque-amida) Pebax® 3533 sobre soportes asimétricos de polisulfona mediante el método de inversión de fases. Con el fin de optimizar este método de preparación de membranas, se ha variado la concentración de la disolución de *casting* y el número de capas para estudiar su influencia en el espesor de la capa selectiva y el rendimiento de separación de gases. Las concentraciones de polímero en la disolución de *casting* han sido 0,25, 0,5, 1,0 y 1,5% en peso. Con estas condiciones, se han obtenido membranas con capas selectivas con espesores entre 0,2 y 1,8 µm. Todas las membranas se han caracterizado por SEM, TGA y FTIR-ATR. Además, se ha medido la viscosidad intrínseca de todas las disoluciones de *casting* para comprender el efecto de la concentración de polímero en la homogeneidad y las propiedades de separación de gases de las membranas obtenidas. En general, una menor viscosidad genera un mayor número de defectos en las capas superficiales, lo que implica que se requiera un mayor número de capas para obtener membranas selectivas. El rendimiento de separación de gases se ha estudiado para la mezcla CO_2/N_2 en una relación 15/85 %v/v a 25-50 °C y bajo una presión de alimentación de 3 bar. El mejor rendimiento de separación se ha logrado con las membranas preparadas con la disolución de *casting* al 0,5% en peso tras la aplicación de cuatro capas de polímero, obteniendo una permeación de CO_2 de 127 GPU y una selectividad de CO_2/N_2 de 21,4 a 35 °C, la misma selectividad que otorga la membrana densa correspondiente, pero con una permeación mucho mayor.

En el cuarto capítulo de resultados (**capítulo 7**), se han preparado membranas nanocompuestas de capa fina de Pebax® 1657 mediante *spin-coating*. Para ello, se han empleado como relleno nanoparticulas de UiO-66 funcionalizadas con grupos amina (-NH_2) y nitro (-NO_2) con un tamaño de partícula promedio de 4-6 nm. Estas membranas se han aplicado a la separación de mezclas gaseosas CO_2/N_2 (en una relación 15/85 %v/v) y CO_2/CH_4 (en una relación 50/50 %v/v). Se ha demostrado que la funcionalización de UiO-66 mejora significativamente el rendimiento de separación de gases de las membranas. En las separaciones de CO_2/N_2, el valor más alto de permeabilidad de CO_2 (277 GPU) se ha logrado con la membrana con un 7,5% en peso de nanopartículas de UiO-66 funcionalizadas con el grupo amino (TFN_UNH2(7.5)), lo que representa un

aumento del 47% con respecto a la membrana sin MOF. En cuanto a la selectividad CO_2/N_2, las membranas preparadas con una carga del 5% en peso de partículas de UiO-66-NO_2 (TFN_UNO2(5)) han supuesto un incremento del 17% sobre la membrana sin MOF (51,0 frente a 43,5). A pesar del aumento de la selectividad, la permeabilidad de CO_2 de la membrana TFN_UNO2(5) disminuye de 181 a 155 GPU. La adición de un 10% en peso de partículas ZIF-94 con un tamaño de partícula promedio de 45 nm en la membrana TFN_UNO2(5) ha permitido aumentar la permeación de CO_2 a 192 GPU mientras se mantiene la selectividad de CO_2/N_2 en 51. En mezclas CO_2/CH_4, la membrana TFN_UNH2(7.5) ha aportado el mejor rendimiento con un aumento de la permeación de CO_2 de 201 GPU a 245 GPU. Finalmente, la membrana TFN_UNH2(7.5) se ha fabricado con partículas más grandes (150 nm) demostrándose que las partículas de menor tamaño proporcionan un mejor rendimiento de separación debido a su mayor área superficial específica. Es importante mencionar que esta es la primera vez que se emplean nanopartículas de UiO-66 tan pequeñas como relleno en una membrana para separación de gases y que la aplicación simultanea de partículas de UiO-66 y ZIF-94 no se había estudiado con anterioridad.

Por último, en el **capítulo 8** se han incorporado un líquido iónico (IL) [Bmim][BF_4] y nanopartículas de ZIF-8 y ZIF-94 en el polímero Pebax® Renew® 30R51 para obtener membranas nanocompuestas de película delgada altamente eficientes de 300 nm de espesor mediante *spin-coating*. Las partículas de ZIF-94 se han sintetizado a través de una reacción de intercambio de ligando asistido por disolvente a partir de ZIF-8. Para fabricar las membranas, en primer lugar, se ha variado el porcentaje en peso de [Bmim][BF_4] del 5 al 20% en peso para establecer el contenido óptimo del mismo (10% en peso). Las nanopartículas de ZIF-8 y ZIF-94 se han incorporado por separado (del 10 al 20% en peso) en la matriz de Pebax®/IL con el fin de mejorar el rendimiento de separación de CO_2. En comparación con la membrana de Pebax® sin relleno, el líquido iónico (10% en peso) aumenta la permeación de CO_2 en un 27% hasta llegar a 629 GPU y la selectividad de separación de CO_2/N_2 en un 7% hasta 29, debido al incremento de la transferencia de materia de CO_2. Tras la incorporación de ZIF, la permeación de CO_2 aumenta en un 51% hasta 751 GPU y en un 65% hasta 819 GPU, con cargas del 15% en peso de ZIF-8 y ZIF-94, respectivamente, aunque la selectividad de separación de CO_2/N_2

disminuye en un 7% hasta 25 en ambos casos. De manera adicional, se ha realizado el cálculo de las energías de activación aparentes de permeación de CO_2 y N_2, así como un estudio de estabilidad a largo plazo, esto ha demostrado que la incorporación de MOF mejora la estabilidad del líquido iónico en la membrana, siendo un 55% y un 35% más permeable (611 GPU) que el polímero sin relleno y que la membrana con líquido iónico, respectivamente, manteniendo la selectividad CO_2/N_2 en 25.

A continuación, se detallan las conclusiones extraídas en la investigación de esta tesis y que muestran como se han alcanzado los objetivos parciales:

9.1 Estudio comparativo entre la permeación de gas individual y de mezcla en membranas de copolímero de tipo poliéter-bloque-amida

- **El aumento de la relación PE/PA** en copolímeros de bloque tipo Pebax® **conlleva un aumento de la permeabilidad** de la membrana.
- Por lo general, el **aumento** de la longitud de cadena de PA se traduce en un **peor empaquetamiento** de las cadenas poliméricas, dando como resultado un **aumento del volumen libre**. Esto da lugar a una **mayor difusión y permeabilidad**, y una **menor selectividad**, como ocurre, por ejemplo, con los códigos de Pebax® 2533, 3533 y 4533, compuestos de PA12 y PTMO.
- En el caso particular del **Pebax® Renew® 30R51**, a pesar de estar constituido por PA11 y, por tanto, tener también una longitud de cadena larga, el estar **compuesto de PEO** en lugar de PTMO hace que las **interacciones** entre este segmento y el **CO_2** sean **mayores**. Con esto se consiguen los **mejores valores de selectividad CO_2/N_2** (41 y 37, medidos mediante time-lag y mezcla de gases, respectivamente), debido al **aumento de la solubilidad del CO_2**.
- **El aumento de la proporción PE/PA reduce ligeramente la temperatura de degradación del polímero**.

- Los **valores de energía de activación** de la permeación de **CO_2** calculados **a partir** de los datos de **permeación individual** son ligeramente **superiores** a los obtenidos mediante los ensayos con **mezcla de gases**. Esto podría estar relacionado con la presencia de N_2 en la mezcla.

- Las selectividades ideal y de mezcla vienen ajustadas por los parámetros de solubilidad y difusión. Esto sugiere que **la aplicación del método de "*time-lag*"**, además de ser más barato, puede resultar **apropiado para el cálculo del rendimiento de las membranas en separación de gases**.

9.2 Membrana de copolímero de poli(éter-bloque-amida) para la separación de CO_2/N_2: Influencia de la concentración en la disolución de casting en su morfología, propiedades térmicas y rendimiento de separación de gases

- El **aumento** de la cantidad de **disolvente respecto del polímero** en la disolución de *casting* provoca un **aumento de la cristalinidad** del material. Esto es debido, en gran medida, al **mayor empaquetamiento** de las cadenas poliméricas como resultado del aumento del tiempo necesario para la evaporación total del disolvente.

- El **aumento de la cristalinidad** juega un papel **importante** tanto en la **degradación** de las membranas (ya que al aumentar la cristalinidad aumenta la temperatura de degradación) como en las **propiedades de separación de gases**.

- En cuanto al rendimiento en separación de gases, se debe llegar a un **compromiso entre la cantidad de disolvente** empleado para preparar las membranas **y la cristalinidad** de estas, a fin de **obtener membranas lo más eficientes posible**.

- De las tres **membranas densas de Pebax® 1657** estudiadas, preparadas a partir de disoluciones de polímero con un 1, 3 y 5% en peso, fue la preparada con una **composición intermedia** (3% en peso) la que arrojó los **mejores resultados de separación de gases**. Esto permitió obtener una permeabilidad de CO_2 de 110 Barrer correspondiente a una selectividad CO_2/N_2 de 36, medidas a 35 °C y 3 bar.

- Los valores de **energía de activación** de la permeación obtenidos después de aplicar la ecuación de Arrhenius a los datos recogidos fueron **similares** a los encontrados en la **literatura** (aprox. **13 kJ mol^{-1} y 26 kJ mol^{-1} para CO_2 y N_2**, respectivamente) y mayores para el gas menos permeable. (N_2 en este estudio). Consistente con esto hay una **disminución de la selectividad** de CO_2/N_2 en función de la **temperatura**.

9.3 Método de inversión de fase para la preparación de membranas de capa fina de Pebax® 3533 para la separación de CO_2/N_2

- Por **primera vez** se ha aplicado el método de **inversión de fases** a la **preparación de capas finas** de polímero.

- En la optimización **del método variando** la **concentración de polímero** en la disolución y el **número de capas** de éste depositadas sobre un soporte poroso de polisulfona (PSF) se ha obtenido membranas con **espesores** de capa selectiva oscilando **entre 0,2 y 1,8 µm**.

- Al **disminuir la concentración** de polímero en la disolución, **disminuye la viscosidad** de la misma, lo que genera una **mayor** cantidad de **defectos** en las capas de polímero, requiriéndose de un mayor número de éstas para obtener membranas selectivas.

- De todas las condiciones estudiadas, las membranas preparadas con **4 capas de Pebax® 3533 al 0,5% en peso** fueron las que produjeron los **mejores resultados de separación de gases**. Así se consiguió llegar hasta 127 GPU de

permeación de CO_2 manteniendo la selectividad CO_2/N_2 intrínseca del polímero de 21,4 (a 35 °C y 3 bar).

- El **modelo de resistencias en serie estima de manera satisfactoria la permeación de CO_2 y la resistencia aportada por las capas de Pebax® 3533**.
- Este **procedimiento** se ha **validado** tras la preparación de membranas TFC mediante el método de ***dip-coating***. El empleo de este último método ha dado como resultado membranas con menor permeación de CO_2 (61 GPU vs. 127 GPU). Esto sugiere que la disolución de "casting" penetra en mayor medida en los poros del soporte debido al aumento del tiempo necesario para conformar cada capa.
- Los valores de **energía de activación** de la permeación (14.2 kJ mol^{-1} para CO_2 y 29.6 kJ mol^{-1} para N_2) han revelado la **analogía** que existe entre las membranas soportadas preparadas mediante el método de inversión de fases y las **membranas densas** preparadas con otros códigos de Pebax®.

9.4 Membranas nanocompuestas de capa fina de MOF UiO-66 funcionalizado ultrapequeño/ polímero Pebax® 1657 para la separación de CO_2

- El método de ***spin-coating*** se ha mostrado adecuado para preparar membranas **TFN con Pebax® 1657, distintos UiO-66 funcionalizados (5-10 nm) y ZIF-94 (20 nm).** Este método ha permitido depositar capas de polímero muy finas, en torno a 700 nm, y de manera rápida (20 s).
- La **funcionalización del MOF** con **grupos amina (-NH_2) y nitro (-NO_2) mejora** de manera significativa el **rendimiento de separación** de gases de las membranas TFN. Esto es debido al **aumento de la compatibilidad** del polímero con el MOF.
- El **valor más alto de permeación de CO_2** se ha obtenido con las membranas preparadas con un **7.5% en peso de UiO-66-NH_2** (277 GPU en mezclas CO_2/N_2 y 245 GPU para CO_2/CH_4). El aumento de la permeación de CO_2 se debe a la

mejora de la compatibilidad entre el MOF y el polímero por los enlaces de hidrógeno que se forman entre las cadenas de polímero y el grupo funcional amina.

- El valor de **selectividad CO_2/N_2 más alto (51)** se obtuvo con las membranas preparadas **con UiO-66-NO_2**, lo que supuso una **mejora del 17%** con respecto a la selectividad de la TFC. A pesar de ello, la **permeación de CO_2** se vio **reducida** de 181 GPU (TFC) a 155 GPU (TFN). La **incorporación de ZIF-94** en un **10% en peso** a estas membranas con UiO-66-NO_2 permitió **aumentar la permeación de CO_2** hasta 192 GPU, sin afectar a la selectividad obtenida con el UiO-66-NO_2. Esto se debe a un efecto sinérgico entre ambos tipos de relleno que mejora la dispersión de estos.

- El **uso de un menor tamaño de partícula** al preparar membranas TFN con partículas de UiO-66-NH_2 **permite obtener un mejor rendimiento** en separación de gases, puesto que las partículas de MOF de 5-10 nm poseen un **área específica mayor**, así como membranas que incorporan apenas 0,036 g de MOF por m^2 de área de membrana.

9.5 Membranas nanocompuestas de capa fina de Pebax® Renew® altamente estables con ZIF-94 y líquido iónico [Bmim][BF_4] para la captura de CO_2

- En las **membranas TFN de Pebax® Renew® 30R51**, la incorporación de **líquido iónico [Bmim][BF_4]** ha supuesto un **incremento** en la **permeación** de **CO_2** y en la **selectividad CO_2/N_2** del 27% y el 11%, respectivamente, en referencia a la membrana TFC.

- Los **valores de separación** de gases se han visto a su vez **mejorados** con la **incorporación de ZIF-8 y ZIF-94**. Esta mejora se atribuye a la **mayor compatibilidad** de los ZIF con la matriz polimérica **debido** a la presencia del **líquido iónico**.

- Las **membranas** preparadas **con ZIF-94** arrojan **mejores valores** de permeación de CO_2 que las que incorporan ZIF-8. Esto se debe principalmente a la presencia del **grupo aldehído** en la estructura del ZIF-94, el cual **aumenta la hidrofilia** del ZIF, aumentando así su **compatibilidad** con el polímero. Además, la **mayor capacidad de adsorción de CO_2** del ZIF-94 respecto al ZIF-8, siendo hasta 3 veces mayor, contribuiría también a la mejora mencionada.

- La **membrana** preparada **con líquido iónico y ZIF-94 mejoró la permeación de CO_2 en un 65% respecto a la TFC**, llegando hasta 820 GPU y manteniendo la selectividad CO_2/N_2 en 25. De igual forma, **para mezclas CO_2/CH_4**, la membrana con liquido iónico y ZIF-94 presentó una elevada permeación de CO_2 (838 GPU) suponiendo un **incremento del 48%** respecto a la TFC.

- Las **energías aparentes de activación** de permeación para las membranas óptimas dan **resultados similares a los reportados en la literatura** para el copolímero tipo Pebax® con la membrana TFC, pero **valores menores** con las membranas **con IL e IL/ZIF-94**. Esto se relaciona con el incremento de la permeación de CO_2 y N_2, apoyando claramente la influencia positiva del IL y ZIF en las propiedades de difusión y solubilidad de las membranas con respecto al polímero puro.

- Los estudios de estabilidad llevados a cabo con las membranas de Pebax® Renew®, líquido iónico y ZIF-94 evidenciaron la **menor estabilidad** de las **membranas con líquido iónico**, pero sin ZIF. Así mismo, se comprobó que **el MOF mitiga** en cierta medida **la pérdida de permeación** de estas membranas.

Fnalmente, la Figura 9.1 muestra una gráfica a modo de resumen con los resultados obtenidos al aplicar las membranas preparadas en esta tesis en la separación de mezclas de CO_2/N_2 y CO_2/CH_4. Las membranas TFN han conseguido mejorar las propiedades de separación de manera sustancial respecto a las TFC, debido a la incorporación de los distintos materiales de relleno (MOF y líquido iónico, en su caso). En cuanto a selectividad, los mejores resultados se han obtenido con las membranas con MOF tipo

UiO-66, siendo superior la de la membrana con la presencia simultánea de UiO-66-NO_2 y ZIF-94 (51). Sin embargo, atendiendo a la permeación de CO_2 a través de la membrana, son las TFN con líquido iónico y ZIF-94 las que mejores resultados arrojan, llegando a superar los 800 GPU cuando se combinan los dos materiales. Por tanto, se ha conseguido la finalidad de esta tésis de desarrollar métodos de preparación de membranas de capa ultrafina que contengan MOF que permitan la separación del CO_2 en mezclas gaseosas con resultados destacados en la literatura.

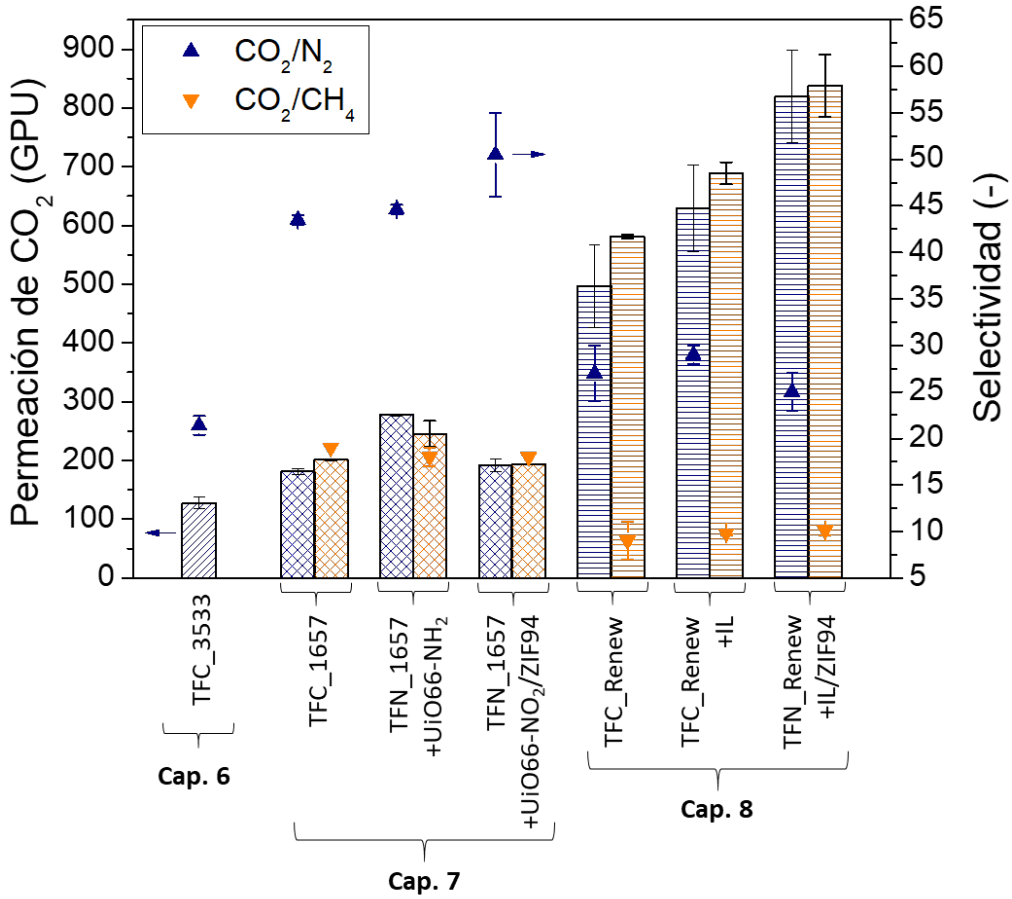

Figura 9.1. Gráfica resumen con los resultados de separación de gases de las membranas TFC y TCN preparadas a lo largo de la tesis. Medidas a 35 °C y 3 bar de presión de alimentación. Los errores vienen de la medida de al menos 2-3 membranas.

Capítulo 10: Bibliografía

10. Bibliografía

1. Climate Change 2021: The Physical Science Basis. at <https://www.ipcc.ch/report/ar6/wg1/> Date accessed: 2022-09-04.

2. Vitillo, J. G., Eisaman, M. D., Aradóttir, E. S. P., Passarini, F., Wang, T. & Sheehan, S. W. The role of carbon capture, utilization, and storage for economic pathways that limit global warming to below 1.5 °C. *iScience* **25,** 104237 (2022).

3. Hou, R., Fong, C., Freeman, B. D., Hill, M. R. & Xie, Z. Current status and advances in membrane technology for carbon capture. *Sep. Purif. Technol.* **300,** 121863 (2022).

4. Robeson, L. M. The upper bound revisited. *J. Membr. Sci.* **320,** 390–400 (2008).

5. Chung, T. S., Jiang, L. Y., Li, Y. & Kulprathipanja, S. Mixed matrix membranes (MMMs) comprising organic polymers with dispersed inorganic fillers for gas separation. *Prog. Polym. Sci.* **32,** 483–507 (2007).

6. Hoskins, B. F. & Robson, R. Infinite polymeric frameworks consisting of three dimensionally linked rod-like segments. *J. Am. Chem. Soc.* **111,** 5962–5964 (1989).

7. Yaghi, O. M., Li, G. & Li, H. Selective binding and removal of guests in a microporous metal–organic framework. *Nature* **378,** 703–706 (1995).

8. Kitagawa, S., Okubo, T., Kawata, S., Kondo, M., Katada, M. & Kobayashi, H. An oxalate-linked Copper(II) coordination polymer, $[Cu_2(oxalate)_2(pyrazine)_3]_n$, constructed with two different copper units: X-ray crystallographic and electronic structures. *Inorg. Chem.* **34,** 4790–4796 (1995).

9. Fasihi, M., Efimova, O. & Breyer, C. Techno-economic assessment of CO_2 direct air capture plants. *J. Clean. Prod.* **224,** 957–980 (2019).

10. Luo, J.-P., Zhang, J., Yin, N., Wang, T.-P., Tan, Z.-C., Han, W. & Shi, Q. An experimental strategy for evaluating the energy performance of metal–organic framework-based carbon dioxide adsorbents. *Chem. Eng. J.* **442,** 136210 (2022).

11. COP26 | Naciones Unidas. at <https://www.un.org/es/climatechange/cop26> Date accessed: 2022-09-30.

12. Sánchez-Laínez, J., Zornoza, B., Friebe, S., Caro, J., Cao, S., Sabetghadam, A., Seoane, B., Gascon, J., Kapteijn, F., Guillouzer, C. Le, Clet, G., Daturi, M., Téllez, C., Coronas, J., Le Guillouzer, C., Clet, G., Daturi, M., Téllez, C. & Coronas, J. Influence of ZIF-8 particle size in the performance of polybenzimidazole mixed matrix membranes for pre-combustion CO_2 capture and its validation through interlaboratory test. *J. Membr. Sci.* **515,** 45–53 (2016).

13. Merkel, T. C., Lin, H., Wei, X. & Baker, R. Power plant post-combustion carbon dioxide capture: An opportunity for membranes. *J. Membr. Sci.* **359,** 126–139 (2010).

14. Danaei Kenarsari, S., Yang, D., Jiang, G., Suojiang Zhang, A., Wang, J., Russell, A. G., Wei, Q. & Fan, M. Review of recent advances in carbon dioxide separation and capture. *RSC Adv.* **3,** 22739–22773 (2013).

15. Budzianowski, W. M. Explorative analysis of advanced solvent processes for energy efficient carbon dioxide capture by gas–liquid absorption. *Int. J. Greenh. Gas Control* **49,** 108–120 (2016).

16. Zhao, B., Sun, Y., Yuan, Y., Gao, J., Wang, S., Zhuo, Y. & Chen, C. Study on corrosion in CO_2 chemical absorption process using amine solution. *Energy Procedia* **4,** 93–100 (2011).

17. Akeeb, O., Wang, L., Xie, W., Davis, R., Alkasrawi, M. & Toan, S. Post-combustion CO_2 capture via a variety of temperature ranges and material adsorption process: A review. *J. Environ. Manage.* **313,** 115026 (2022).

18. Reijerkerk, S. R., Knoef, M. H., Nijmeijer, K. & Wessling, M. Poly(ethylene glycol) and poly(dimethyl siloxane): Combining their advantages into efficient CO_2 gas separation membranes. *J. Membr. Sci.* **352,** 126–135 (2010).

19. Singh, P., Shah, S. & Kumar Rai, S. Post-combustion carbon capture by polymeric membrane: A review. *Mater. Today Proc.* **62,** 318–324 (2022).

20. Sánchez-Laínez, J., Gracia-Guillén, I., Zornoza, B., Téllez, C. & Coronas, J. Thin supported MOF based mixed matrix membranes of Pebax® 1657 for biogas upgrade. *New J. Chem.* **43,** 312–319 (2018).

21. Paseta, L., Echaide-Górriz, C., Téllez, C. & Coronas, J. Vapor phase interfacial polymerization: a method to synthesize thin film composite membranes without using organic solvents. *Green Chem.* **23,** 2449–2456 (2021).

22. Navarro, M., Benito, J., Paseta, L., Gascón, I., Coronas, J. & Téllez, C. Thin-film nanocomposite membrane with the minimum amount of MOF by the Langmuir-Schaefer technique for nanofiltration. *ACS Appl. Mater. Interfaces* **10,** 1278–1287 (2018).

23. Echaide-Górriz, C., Clément, C., Cacho-Bailo, F., Téllez, C. & Coronas, J. New strategies based on microfluidics for the synthesis of metal–organic frameworks and their membranes. *J. Mater. Chem. A* **6,** 5485–5506 (2018).

24. Paseta, L., Luque-Alled, J. M., Malankowska, M., Navarro, M., Gorgojo, P., Coronas, J. & Téllez, C. Functionalized graphene-based polyamide thin film nanocomposite membranes for organic solvent nanofiltration. *Sep. Purif. Technol.* **247,** 116995 (2020).

25. Arena, J. T., McCloskey, B., Freeman, B. D. & McCutcheon, J. R. Surface modification of thin film composite membrane support layers with polydopamine: Enabling use of reverse osmosis membranes in pressure retarded osmosis. *J. Membr. Sci.* **375,** 55–62 (2011).

26. Yang, T., Wan, C. F., Zhang, J., Gudipati, C. & Chung, T. S. Optimization of interfacial polymerization to fabricate thin-film composite hollow fiber membranes in modules for brackish water reverse osmosis. *J. Membr. Sci.* **626,** 119187 (2021).

27. Gupta, K. M., Qiao, Z., Zhang, K. & Jiang, J. Seawater pervaporation through zeolitic imidazolate framework membranes: atomistic simulation study. *Appl. Mater. Interfaces* **8,** 13392–13399 (2016).

28. Castro-Muñoz, R., Galiano, F., de la Iglesia, Ó., Fíla, V., Téllez, C., Coronas, J. & Figoli, A. Graphene oxide – filled polyimide membranes in pervaporative separation of azeotropic methanol–MTBE mixtures. *Sep. Purif. Technol.* **224,** 265–272 (2019).

29. Castro-Muñoz, R., Buera-González, J., Iglesia, Ó. de la, Galiano, F., Fíla, V., Malankowska, M., Rubio, C., Figoli, A., Téllez, C. & Coronas, J. Towards the dehydration of ethanol using pervaporation cross-linked poly(vinyl alcohol)/graphene oxide membranes. *J. Membr. Sci.* **582,** 423–434 (2019).

30. Esteras-Saz, J., de la Iglesia, Ó., Peña, C., Escudero, A., Téllez, C. & Coronas, J. Theoretical and practical approach to the dealcoholization of water-ethanol mixtures and red wine by osmotic distillation. *Sep. Purif. Technol.* **270,** 118793 (2021).

31. Gao, C., Zhang, Q., Yang, Y., Li, Y. & Lin, W. Recent trends in therapeutic application of engineered blood purification materials for kidney disease. *Biomater. Res.* **26,** 5 (2022).

32. Choi, J., Kim, W.-S., Kim, H. K., Yang, S. C., Han, J.-H., Jeung, Y. C. & Jeong, N. J. Fouling behavior of wavy-patterned pore-filling membranes in reverse electrodialysis under natural seawater and sewage effluents. *Clean Water* **5,** 6 (2022).

33. Sánchez-Laínez, J., Zornoza, B., Téllez, C. & Coronas, J. Asymmetric polybenzimidazole membranes with thin selective skin layer containing ZIF-8 for H_2/CO_2 separation at pre-combustion capture conditions. *J. Membr. Sci.* **563,** 427–434 (2018).

34. Yave, W., Car, A., Wind, J. & Peinemann, K.-V. Nanometric thin film membranes manufactured on square meter scale: ultra-thin films for CO_2 capture. *Nanotechnology* **21,** 7 (2010).

35. Benito, J., Sánchez-Laínez, J., Zornoza, B., Martín, S., Carta, M., Malpass-Evans, R., Téllez, C., Mckeown, N. B., Joaquínc,], Gascón, I., Coronas,]oaquín & Gascón, I. Ultrathin composite polymeric membranes for CO_2/N_2 separation with minimum thickness and high CO_2 permeance. *ChemSusChem* **10,** 4014–4017 (2017).

36. Fu, Q., Halim, A., Kim, J., Scofield, J. M. P., Gurr, P. A., Kentish, S. E. & Qiao, G. G. Highly permeable membrane materials for CO_2 capture. *J.Mater.Chem. A* **1,** 13769–13778 (2013).

37. Huang, G., Isfahani, A. P., Muchtar, A., Sakurai, K., Shrestha, B. B., Qin, D., Yamaguchi, D., Sivaniah, E. & Ghalei, B. Pebax/ionic liquid modified graphene oxide mixed matrix membranes for enhanced CO_2 capture. *J. Membr. Sci.* **565,** 370–379 (2018).

38. Selyanchyn, R., Ariyoshi, M. & Fujikawa, S. Thickness effect on CO_2/N_2 separation in double layer Pebax-1657®/PDMS membranes. *Membranes (Basel).* **8,** 121 (2018).

39. Bernardo, P., Drioli, E. & Golemme, G. Membrane gas separation: A review/state of the art. *Ind. Eng. Chem. Res.* **48,** 4638–4663 (2009).

40. Kattula, M., Ponnuru, K., Zhu, L., Jia, W., Lin, H. & Furlani, E. P. Designing ultrathin film composite membranes: the impact of a gutter layer. *Sci. Reports 2015 51* **5,** 1–9 (2015).

41. Lin, H. & Freeman, B. D. Materials selection guidelines for membranes that remove CO_2 from gas mixtures. *J. Mol. Struct.* **739,** 57–74 (2005).

42. Armstrong, S., Freeman, B., Hiltner, A. & Baer, E. Gas permeability of melt-processed poly(ether block amide) copolymers and the effects of orientation. *Polymer.* **53,** 1383–1392 (2012).

43. Karamouz, F., Maghsoudi, H. & Yegani, R. Synthesis and characterization of high permeable PEBA membranes for CO_2/CH_4 separation. *J. Nat. Gas Sci. Eng.* **35,** 980–985 (2016).

44. Shao, L., Chung, T. S., Wensley, G., Goh, S. H. & Pramoda, K. P. Casting solvent effects on morphologies, gas transport properties of a novel 6FDA/PMDA–TMMDA copolyimide membrane and its derived carbon membranes. *J. Membr. Sci.* **244,** 77–87 (2004).

45. Lin, H., Van Wagner, E., Raharjo, R., Freeman, B. D. & Roman, I. High-performance polymer membranes for natural-gas sweetening. *Adv. Mater.* **18,** 39–44 (2006).

46. Abdullah, N., Rahman, M. A., Othman, M. H. D., Jaafar, J. & Ismail, A. F. Membranes and membrane processes: fundamentals. *Curr. Trends Futur. Dev. Membr. Photocatalytic Membr. Photocatalytic Membr. React.* 45–70 (2018).

47. Vermaak, L., Neomagus, H. W. J. P. & Bessarabov, D. G. Recent advances in membrane-based electrochemical hydrogen separation: A review. *Membranes.* **11,** 127 (2021).

48. Karimi, M. B., Hassanajili, S. & Khanbabaei, G. Capillary condensation mechanism for gas transport in fiber reinforced poly (ether-b-amide) membranes. *Chem. Eng. Res. Des.* **148,** 180–190 (2019).

49. Lonsdale, H. K., Merten, U. & Riley, R. L. Transport properties of cellulose acetate osmotic membranes. *J. Appl. Polym. Sci.* **9,** 1341–1362 (1965).

50. Paul, D. R. Reformulation of the solution-diffusion theory of reverse osmosis. *J. Membr. Sci.* **241,** 371–386 (2004).

51. Wijmans, J. G. & Baker, R. W. The solution-diffusion model: a review. *J. Membr. Sci.* **107,** 1–21 (1995).

52. Henis, J. M. S. & Tripodi, M. K. *United States Patent (19) Henis et al. 54 MULTICOMPONENT MEMBRANES FOR GAS SEPARATIONS 75) Inventors*.

53. Feng, S., Ren, J., Zhao, D., Li, H., Hua, K., Li, X. & Deng, M. Effect of poly(ethylene glycol) molecular

weight on CO_2/N_2 separation performance of poly(amide-12-b-ethylene oxide)/poly(ethylene glycol) blend membranes. *J. Energy Chem.* **28,** 39–45 (2019).

54. Ahmad, M. Z., Peters, T. A., Konnertz, N. M., Visser, T., Téllez, C., Coronas, J., Fila, V., de Vos, W. M. & Benes, N. E. High-pressure CO_2/CH_4 separation of Zr-MOFs based mixed matrix membranes. *Sep. Purif. Technol.* **230,** 115858 (2020).

55. Bos, A., Pünt, I. G. M., Wessling, M. & Strathmann, H. CO_2-induced plasticization phenomena in glassy polymers. *J. Membr. Sci.* **155,** 67–78 (1999).

56. Sidhikku Kandath Valappil, R., Ghasem, N. & Al-Marzouqi, M. Current and future trends in polymer membrane-based gas separation technology: A comprehensive review. *J. Ind. Eng. Chem.* **98,** 103–129 (2021).

57. Robeson, L. M. Correlation of separation factor versus permeability for polymeric membranes. *J. Membr. Sci.* **62,** 165–185 (1991).

58. Comesaña-Gándara, B., Chen, J., Bezzu, C. G., Carta, M., Rose, I., Ferrari, M. C., Esposito, E., Fuoco, A., Jansen, J. C. & McKeown, N. B. Redefining the Robeson upper bounds for CO_2/CH_4 and CO_2/N_2 separations using a series of ultrapermeable benzotriptycene-based polymers of intrinsic microporosity. *Energy Environ. Sci.* **12,** 2733–2740 (2019).

59. Lau, C. H., Nguyen, P. T., Hill, M. R., Thornton, A. W., Konstas, K., Doherty, C. M., Mulder, R. J., Bourgeois, L., Liu, A. C. Y., Sprouster, D. J., Sullivan, J. P., Bastow, T. J., Hill, A. J., Gin, D. L. & Noble, R. D. Ending aging in super glassy polymer membranes. *Angew. Chemie Int. Ed.* **53,** 5322–5326 (2014).

60. Zhang, S., Zheng, Y., Wu, Y. & Zhang, B. Fabrication of Pebax/SAPO mixed matrix membranes for CO_2/N_2 separation. *J. Appl. Polym. Sci.* **138,** 51336 (2021).

61. Zheng, Y., Wu, Y., Zhang, B. & Wang, Z. Preparation and characterization of CO_2-selective Pebax/NaY mixed matrix membranes. *J. Appl. Polym. Sci.* **137,** 48398 (2020).

62. Hu, L., Clark, K., Alebrahim, T. & Lin, H. Mixed matrix membranes for post-combustion carbon capture: From materials design to membrane engineering. *J. Membr. Sci.* **644,** 120140 (2022).

63. Zhang, Y., Ma, L., Lv, Y. & Tan, T. Facile manufacture of COF-based mixed matrix membranes for efficient CO2 separation. *Chem. Eng. J.* **430,** 133001 (2022).

64. Amirkhani, F., Mosadegh, M., Asgharia, M. & Parnian, M. J. The beneficial impacts of functional groups of CNT on structure and gas separation properties of PEBA mixed matrix membranes. *Polym. Test.* **82,** 106285 (2020).

65. Peng, D., Wang, S., Tian, Z., Wu, X., Wu, Y., Wu, H., Xin, Q., Chen, J., Cao, X. & Jiang, Z. Facilitated transport membranes by incorporating graphene nanosheets with high zinc ion loading for enhanced CO_2 separation. *J. Membr. Sci.* **522,** 351–362 (2017).

66. Ding, M., Liu, X., Ma, P. & Yao, J. Porous materials for capture and catalytic conversion of CO_2 at low concentration. *Coord. Chem. Rev.* **465,** 214576 (2022).

67. Lu, W., Wei, Z., Gu, Z.-Y., Liu, T.-F., Park, J., Park, J., Tian, J., Zhang, M., Zhang, Q., Iii, T. G., Bosch, M. & Zhou, H.-C. Tuning the structure and function of metal-organic frameworks via linker design. *Chem. Soc. Rev* **43,** 5561 (2014).

68. Paseta, L., Navarro, M., Coronas, J. & Téllez, C. Greener processes in the preparation of thin film nanocomposite membranes with diverse metal-organic frameworks for organic solvent nanofiltration. *J. Ind. Eng. Chem.* **77,** 344–354 (2019).

69. Berned-Samatán, V., Rubio, C., Galán-González, A., Muñoz, E., Benito, A. M., Maser, W. K., Coronas, J. & Téllez, C. Single-walled carbon nanotube buckypaper as support for highly permeable double layer polyamide/zeolitic imidazolate framework in nanofiltration processes. *J. Membr. Sci.* **652,** 120490 (2022).

70. Xu, W., Zhang, Y., Wang, J., Xu, Y., Bian, L., Ju, Q., Wang, Y. & Fang, Z. Defects engineering simultaneously enhances activity and recyclability of MOFs in selective hydrogenation of biomass. *Nat. Commun. 2022 131* **13,** 1–9 (2022).

71. Alivand, M. S., Mazaheri, O., Wu, Y., Zavabeti, A., Christofferson, A. J., Meftahi, N., Russo, S. P., Stevens, G. W., Scholes, C. A. & Mumford, K. A. Engineered assembly of water-dispersible nanocatalysts enables low-cost and green CO_2 capture. *Nat. Commun. 2022 131* **13,** 1–11 (2022).

72. Sharifi-Rad, M., Kaykhaii, M., Khajeh, M. & Oveisi, A. Synthesis, characterization and application of a zirconium-based MOF-808 functionalized with isonicotinic acid for fast and efficient solid phase extraction of uranium(VI) from wastewater prior to its spectrophotometric determination. *BMC Chem. 161* **16,** 1–13 (2022).

73. Ahmad Isiyaka, H., Jumbri, K., Soraya Sambudi, N., Uba Zango, Z., Ain Fathihah Binti Abdullah, N. & Saad, B. Effective adsorption of metolachlor herbicide by MIL-53(Al) metal-organic framework: Optimization, validation and molecular docking simulation studies. *Environ. Nanotechnology, Monit. Manag.* **18,** 100663 (2022).

74. Zornoza, B., Rubio, C., Piera, E., Caballero, M. A., Julve, D., Pérez, J., Téllez, C. & Coronas, J. Caffeine encapsulation in metal organic framework MIL-53(Al) at pilot plant scale for preparation of polyamide textile fibers with cosmetic properties. *ACS Appl. Mater. Interfaces* **14,** 22476–22488 (2022).

75. Liédana, N., Galve, A., Rubio, C., Téllez, C. & Coronas, J. CAF@ZIF-8: One-step encapsulation of caffeine in MOF. *ACS Appl. Mater. Interfaces* **4,** 5016–5021 (2012).

76. Zhou, H.-C., Long, J. R. & Yaghi, O. M. Introduction to metal − organic frameworks. *Chem. Rev.* **112,** 673–674 (2012).

77. Marti, A. M., Van, M. & Balkus, K. J. Tuning the crystal size and morphology of the substituted imidazole material, SIM-1. *J. Porous Mater.* **21,** 889–902 (2014).

78. Chui, S. S. Y., Lo, S. M. F., Charmant, J. P. H., Orpen, A. G. & Williams, I. D. A chemically functionalizable nanoporous material. *Science* **283,** 1148–1150 (1999).

79. Serre, C., Millange, F., Thouvenot, C., Noguès, M., Marsolier, G., Louër, D. & Férey, G. Very large breathing effect in the first nanoporous chromium(III)-based solids: MIL-53 or CrIII(OH)·{O_2C-C_6H_4-CO_2}·{HO_2C-C_6H_4 -CO_2H}$_x$·H_2O_y. *J. Am. Chem. Soc.* **124,** 13519–13526 (2002).

80. Cavka, J. H., Jakobsen, S., Olsbye, U., Guillou, N., Lamberti, C., Bordiga, S. & Lillerud, K. P. A new zirconium inorganic building brick forming metal organic frameworks with exceptional stability. *J. Am. Chem. Soc.* **130,** 13850–13851 (2008).

81. Kouser, S., Hezam, A., Khadri, M. J. N. & Khanum, S. A. A review on zeolite imidazole frameworks: synthesis, properties, and applications. *J. Porous Mater.* **29,** 663–681 (2022).

82. Deacon, A., Briquet, L., Malankowska, M., Massingberd-Mundy, F., Rudić, S., Hyde, T. L., Cavaye, H., Coronas, J., Poulston, S. & Johnson, T. Understanding the ZIF-L to ZIF-8 transformation from fundamentals to fully costed kilogram-scale production. *Commun. Chem.* **5,** 1–10 (2022).

83. Park, K. S., Ni, Z., Cô, A. P., Choi, J. Y., Huang, R., Uribe-Romo, F. J., Chae, H. K., O'keeffe, M. & Yaghi, O. M. Exceptional chemical and thermal stability of zeolitic imidazolate frameworks. *PNAS* **103,** 10186–10191 (2006).

84. Johnson, T., Łozińska, M. M., Orsi, A. F., Wright, P. A., Hindocha, S. & Poulston, S. Improvements to the production of ZIF-94; a case study in MOF scale-up. *Green Chem.* **21,** 5665–5670 (2019).

85. Morris, W., He, N., Ray, K. G., Klonowski, P., Furukawa, H., Daniels, I. N., Houndonougbo, Y. A., Asta, M., Yaghi, O. M. & Laird, B. B. A combined experimental-computational study on the effect of topology on carbon dioxide adsorption in zeolitic imidazolate frameworks. *J. Phys. Chem. C* **116,** 24084–24090 (2012).

86. Gadipelli, S., Travis, W., Zhou, W. & Guo, Z. A thermally derived and optimized structure from ZIF-8 with giant enhancement in CO_2 uptake. *Energy Environ. Sci.* **7,** 2232–2238 (2014).

87. Yuan, S., Feng, L., Wang, K., Pang, J., Bosch, M., Lollar, C., Sun, Y., Qin, J., Yang, X., Zhang, P., Wang, Q., Zou, L., Zhang, Y., Zhang, L., Fang, Y., Li, J., Zhou, H.-C., Yuan, S., Feng, L., Wang, K., Pang, J., Bosch, M., Lollar, C., Sun, Y., Qin, J., Yang, X., Zhang, P., Wang, Q., Zou, L., Zhang, Y., Zhang, L., Fang, Y., Li, J. & Zhou, H. Stable metal–organic frameworks: Design, synthesis, and applications. *Adv. Mater.* **30,** 1704303 (2018).

88. Tanvidkar, P., Appari, S. & Kuncharam, B. V. R. A review of techniques to improve performance of metal organic framework (MOF) based mixed matrix membranes for CO_2/CH_4 separation. *Rev. Environ. Sci. Bio/Technology 212* **21,** 539–569 (2022).

89. Yuan, X., Yu, H., Xu, S., Huo, G., Cornelius, C. J., Fan, Y. & Li, N. Performance optimization of imidazole containing copolyimide/functionalized ZIF-8 mixed matrix membrane for gas separations. *J. Membr. Sci.* **644,** 120071 (2022).

90. Madhav, D., Malankowska, M. & Coronas, J. Synthesis of nanoparticles of zeolitic imidazolate framework ZIF-94 using inorganic deprotonators. *New J. Chem.* **44,** 20449–20457 (2020).

91. Dai, S., Nouar, F., Zhang, S., Tissot, A. & Serre, C. One-step room-temperature synthesis of metal(IV) carboxylate metal—organic frameworks. *Angew. Chemie Int. Ed.* **60,** 4282–4288 (2021).

92. Lee, S., Park, S. C., Kim, T. Y., Kang, S. W. & Kang, Y. S. Direct molecular interaction of CO_2 with KTFSI dissolved in Pebax 2533 and their use in facilitated CO_2 transport membranes. *J. Membr. Sci.* **548,** 358–362 (2018).

93. Deng, J., Dai, Z. & Deng, L. Effects of the morphology of the ZIF on the CO_2 separation performance of MMMs. *Ind. Eng. Chem. Res.* **59,** 14458–14466 (2020).

94. Sánchez-Laínez, J., Ballester-Catalán, M., Javierre-Ortín, E., Téllez, C. & Coronas, J. Pebax® 1041 supported membranes with carbon nanotubes prepared via phase inversion for CO_2/N_2 separation. *Dalt. Trans.* **49,** 2905–2913 (2020).

95. Wu, Y., Zhao, D., Ren, J., Qiu, Y. & Deng, M. A novel Pebax-$C_{60}(OH)_{24}$/PAN thin film composite membrane for carbon dioxide capture. *Sep. Purif. Technol.* **215,** 480–489 (2019).

96. Rutherford, S. W., Limmer, D. T., Smith, M. G. & Honnell, K. G. Gas transport in ethyleneepropyleneediene (EPDM) elastomer: Molecular simulation and experimental study. *Polymer.* **48,** 6719–6727 (2007).

97. Monteleone, M., Fuoco, A., Esposito, E., Rose, I., Chen, J., Comesaña-Gándara, B., Bezzu, C. G., Carta, M., McKeown, N. B., Shalygin, M. G., Teplyakov, V. V. & Jansen, J. C. Advanced methods for analysis of mixed gas diffusion in polymeric membranes. *J. Membr. Sci.* **648,** 120356 (2022).

98. Wu, H., Thibault, J. & Kruczek, B. The validity of the time-lag method for the characterization of mixed-matrix membranes. *J. Membr. Sci.* **618,** 118715 (2021).

99. Fuoco, A., Monteleone, M., Esposito, E., Bruno, R., Ferrando-Soria, J., Pardo, E., Armentano, D. & Carolus Jansen, J. Gas transport in mixed matrix membranes: Two methods for time lag determination. *Computation* **28** (2020).

100. Dhingra, S. S. & Marand, E. Mixed gas transport study through polymeric membranes. *J. Membr. Sci.* **141,** 45–63 (1998).

101. Giordano, L., Roizard, D. & Favre, E. Life cycle assessment of post-combustion CO_2 capture: A comparison between membrane separation and chemical absorption processes. *Int. J. Greenh. Gas Control* **68,** 146–163 (2018).

102. Qian, Q., Asinger, P. A., Lee, M. J., Han, G., Mizrahi Rodriguez, K., Lin, S., Benedetti, F. M., Wu, A. X., Chi, W. S. & Smith, Z. P. MOF-based membranes for gas separations. *Chem. Rev.* **120,** 8161–8266 (2020).

103. Stuart Haszeldine, R. Carbon capture and storage: How green can black be? *Science* **325,** 1647–1652 (2009).

104. Baker, R. W. Future directions of membrane gas separation technology. *Ind. Eng. Chem. Res.* **41,** 1393–1411 (2002).

105. Pazani, F. & Aroujalian, A. Enhanced CO_2-selective behavior of Pebax-1657: A comparative study between the influence of graphene-based fillers. *Polym. Test.* **81,** 106264 (2020).

106. Wang, J., Fang, W., Luo, J., Gao, M., Wan, Y., Zhang, S., Zhang, X. & Alissa Park, A.-H. Selective separation of CO_2 using novel mixed matrix membranes based on Pebax and liquid-like nanoparticle organic hybrid materials. *J. Membr. Sci.* **584,** 79–88 (2019).

107. Bernardo, P. & Clarizia, G. Enhancing gas permeation properties of Pebax® 1657 membranes via polysorbate nonionic surfactants doping. *Polymers.* **12,** 253 (2020).

108. Ren, X., Ren, J., Li, H., Feng, S. & Deng, M. Poly (amide-6-b-ethylene oxide) multilayer composite membrane for carbon dioxide separation. *Int. J. Greenh. Gas Control* **8,** 111–120 (2012).

109. Dai, Y., Ruan, X., Yan, Z., Yang, K., Yu, M., Li, H., Zhao, W. & He, G. Imidazole functionalized graphene oxide/PEBAX mixed matrix membranes for efficient CO_2 capture. *Sep. Purif. Technol.* **C,** 171–180 (2016).

110. Freeman, B. D. & Pinnau, I. Polymeric materials for gas separations. *Am. Chem. Soc.* **733,** 1–27 (1999).

111. Selomon, A., Martínez-Izquierdo, L., Malankowska, M., Téllez, C. & Coronas, J. Poly(ether-block-amide) copolymer membranes in CO_2 separation applications. *Energy & Fuels* **35,** 17085–17102 (2021).

112. Sheth, J. P., Xu, J. & Wilkes, G. L. Solid state structure–property behavior of semicrystalline poly(ether-block-amide) PEBAX® thermoplastic elastomers. *Polymer (Guildf).* **44,** 743–756 (2003).

113. Wang, Y., Li, H., Dong, G., Scholes, C. & Chen, V. Effect of fabrication and operation conditions on CO2 separation performance of PEO-PA block copolymer membranes. *Ind. Eng. Chem. Res.* **54,** 7273–7283 (2015).

114. Tena, A., Shishatskiy, S. & Filiz, V. Poly(ether-amide) vs. poly(ether-imide) copolymers for post-combustion membrane separation processes. *RSC Adv.* **5,** 22310 (2015).

115. Galizia, M., Chi, W. S., Smith, Z. P., Merkel, T. C., Baker, R. W. & Freeman, B. D. 50th anniversary perspective: polymers and mixed matrix membranes for gas and vapor separation: A review and prospective opportunities. *Macromolecules* **50,** 7809–7843 (2017).

116. Taheri, P., Raisi, A. & Maleh, M. S. CO_2-selective poly(ether-block-amide)/polyethylene glycol composite blend membrane for CO_2 separation from gas mixtures. *Environ. Sci. Pollut. Res.* **28,** 38274–38291 (2021).

117. Selyanchyn, O., Selyanchyn, R. & Fujikawa, S. Critical role of the molecular interface in double-layered Pebax-1657/PDMS nanomembranes for highly efficient CO_2/N_2 gas separation. *ACS Appl. Mater. Interfaces* **12,** 33196–33209 (2020).

118. Casadei, R., Baschetti, M. G., Yoo, M. J., Park, H. B. & Giorgini, L. Pebax® 2533/graphene oxide nanocomposite membranes for carbon capture. *Membr. 2020, Vol. 10, Page 188* **10,** 188 (2020).

119. Ansari, A., Navarchian, A. H. & Rajati, H. Permselectivity improvement of PEBAX® 2533 membrane by addition of glassy polymers (Matrimid® and polystyrene) for CO_2/N_2 separation. *J. Appl. Polym. Sci.* **139,** 51556 (2022).

120. Kim, J. H. & Lee, Y. M. Gas permeation properties of poly(amide-6-b-ethylene oxide)–silica hybrid membranes. *J. Membr. Sci.* **193,** 209–225 (2001).

121. Wu, Y., Zhao, D., Ren, J., Qiu, Y., Feng, Y. & Deng, M. Effect of triglyceride on the microstructure

and gas permeation performance of Pebax-based blend membranes. *Sep. Purif. Technol.* **256,** 117824 (2021).

122. Song, C., Li, R., Fan, Z., Liu, Q., Zhang, B. & Kitamura, Y. CO_2/N_2 separation performance of Pebax/MIL-101 and Pebax /NH2-MIL-101 mixed matrix membranes and intensification via sub-ambient operation. *Sep. Purif. Technol.* **238,** 116500 (2020).

123. Kim, J. H., Ha, S. Y., Lee, Y. M., Ha, Y. & Lee, Y. M. Gas permeation of poly(amide-6-b-ethylene oxide) copolymer. *J. Membr. Sci.* **190,** 179–193 (2001).

124. Yoshida, T., Nakane, T., Uchida, M. & Kaneko, Y. Mechanical modeling and testing of different polyamides considering molecular chain structure, crystallinity, and large strains. *Int. J. Solids Struct.* **239–240,** 111419 (2022).

125. Elyasi Kojabad, M., Momeni, M., Babaluo, A. A. & Vaezi, M. J. PEBA/PSf multilayer composite membranes for CO_2 separation: Influence of dip coating parameters. *Chem. Eng. Technol.* **43,** 1451–1460 (2020).

126. Sanaeepur, H., Mashhadikhan, S., Mardassi, G., Ebadi Amooghin, A., Van der Bruggen, B. & Moghadassi, A. Aminosilane cross-linked poly ether-block-amide PEBAX 2533: Characterization and CO_2 separation properties. *Korean J. Chem. Eng.* **36,** 1339–1349 (2019).

127. Zhao, D., Ren, J., Li, H., Li, X. & Deng, M. Gas separation properties of poly(amide-6-b-ethylene oxide)/amino modified multi-walled carbon nanotubes mixed matrix membranes. *J. Membr. Sci.* **467,** 41–47 (2014).

128. Wang, S., Liu, Y., Huang, S., Wu, H., Li, Y., Tian, Z. & Jiang, Z. Pebax–PEG–MWCNT hybrid membranes with enhanced CO_2 capture properties. *J. Membr. Sci.* **460,** 62–70 (2014).

129. Konyukhova, E. V., Buzin, A. I. & Godovsky, Y. U. K. Melting of polyether block amide (Pebax): the effect of stretching. *Thermochim. Acta* **391,** 271–277 (2002).

130. Rahman, M. M., Filiz, V., Shishatskiy, S., Abetz, C., Neumann, S., Bolmer, S., Khan, M. M. & Abetz, V. PEBAX® with PEG functionalized POSS as nanocomposite membranes for CO_2 separation. *J. Membr. Sci.* **437,** 286–297 (2013).

131. Tocci, E., Gugliuzza, A., De Lorenzo, L., Macchione, M., De Luca, G. & Drioli, E. Transport properties of a co-poly(amide-12-b-ethylene oxide) membrane: A comparative study between experimental and molecular modelling results. *J. Membr. Sci.* **323,** 316–327 (2008).

132. Clarizia, G., Bernardo, P., Gorrasi, G., Zampino, D. & Carroccio, S. C. Influence of the preparation method and photo-oxidation treatment on the thermal and gas transport properties of dense films based on a poly(ether-block-amide) copolymer. *Materials.* **11,** 1326 (2018).

133. Noroozi, Z. & Bakhtiari, O. Preparation of amino functionalized titanium oxide nanotubes and their incorporation within Pebax/PEG blended matrix for CO_2/CH_4 separation. *Chem. Eng. Res. Des.* **152,** 149–164 (2019).

134. Albo, J., Luis, P. & Irabien, A. Carbon dioxide capture from flue gases using a cross-flow membrane contactor and the ionic liquid 1-ethyl-3-methylimidazolium ethylsulfate. *Ind. Eng. Chem. Res.* **49,** 11045–11051 (2010).

135. Li, H., Tuo, L., Yang, K., Jeong, H. K., Dai, Y., He, G. & Zhao, W. Simultaneous enhancement of mechanical properties and CO2 selectivity of ZIF-8 mixed matrix membranes: Interfacial toughening effect of ionic liquid. *J. Membr. Sci.* **511,** 130–142 (2016).

136. Zhang, J., Xin, Q., Li, X., Yun, M., Xu, R., Wang, S., Li, Y., Lin, L., Ding, X., Ye, H. & Zhang, Y. Mixed matrix membranes comprising aminosilane-functionalized graphene oxide for enhanced CO_2 separation. *J. Membr. Sci.* **570–571,** 343–354 (2019).

137. Meshkat, S., Kaliaguine, S. & Rodrigue, D. Mixed matrix membranes based on amine and non-amine MIL-53(Al) in Pebax® MH-1657 for CO_2 separation. *Sep. Purif. Technol.* **200,** 177–190 (2018).

138. Wang, L., Li, Y., Li, S., Ji, P. & Jiang, C. Preparation of composite poly(ether block amide) membrane for CO_2 capture. *J. Energy Chem.* **23,** 717–725 (2014).

139. Isanejad, M., Azizi, N. & Mohammadi, T. Pebax membrane for CO_2/CH_4 separation: Effects of various solvents on morphology and performance. *J. Appl. Polym. Sci.* **134,** 44531 (2017).

140. Joshi, M. K., Tiwari, A. P., Maharjan, B., Won, K. S., Kim, H. J., Park, C. H. & Kim, C. S. Cellulose reinforced nylon-6 nanofibrous membrane: Fabrication strategies, physicochemical characterizations, wicking properties and biomimetic mineralization. *Carbohydr. Polym.* **147,** 104–113 (2016).

141. Abdollahi, S., Ehsani, M., Morshedian, J., Khonakdar, H. A. & Reuter, U. Structural and electrochemical properties of PEO/PAN nanofibrous blends: Prediction of graphene localization. *Polym. Compos.* **39,** 3626–3635 (2018).

142. Sole, B. B., Lohkna, S., Chhabra, P. K., Prakash, V., Seshadri, G. & Tyagi, A. K. Preparation of mechanically strong poly (ether block amide)/mercaptoethanol breathable membranes for biomedical applications. *J. Polym. Res.* **25,** 1–12 (2018).

143. Qiu, Y., Ren, J., Zhao, D., Li, H. & Deng, M. Poly(amide-6-b-ethylene oxide)/[Bmim][Tf_2N] blend membranes for carbon dioxide separation. *J. Energy Chem.* **25,** 122–130 (2016).

144. Khulbe, K. C., Matsuura, T., Lamarche, G. & Kim, H. J. The morphology characterisation and performance of dense PPO membranes for gas separation. *J. Membr. Sci.* **135,** 211–223 (1997).

145. Cacho-Bailo, F., Téllez, C. & Coronas, J. Interactive thermal effects on metal–organic framework polymer composite membranes. *Chem. – A Eur. J.* **22,** 9533–9536 (2016).

146. Lam, B., Wei, M., Zhu, L., Luo, S., Guo, R., Morisato, A., Alexandridis, P. & Lin, H. Cellulose triacetate doped with ionic liquids for membrane gas separation. *Polymer.* **89,** 1–11 (2016).

147. Rabiee, H., Ghadimi, A. & Mohammadi, T. Gas transport properties of reverse-selective poly(ether-b-amide)/[Emim][BF_4] gel membranes for CO_2/light gases separation. *J. Membr. Sci.* **476,** 286–302 (2015).

148. Guan, P., Luo, J., Li, W. & Si, Z. Enhancement of gas permeability for CH_4/N_2 separation membranes by blending SBS to Pebax polymers. *Macromol. Res. 2017 2510* **25,** 1007–1014 (2017).

149. Polotskaya, C. A., Acranova, S. A., Cazdina, N. V, Kuznetsov, Y. P. & Nesterov, V. V. Effect of molecular weight parameters on gas transport properties of poly(2,6-dimethyl-1,4-phenylene oxide). *J. Appl. Polym. Sci.* **62,** 2215–2218 (1996).

150. Kim, S. J., Jeon, H., Kim, D. J. & Kim, J. H. High-performance polymer membranes with multi-functional amphiphilic micelles for CO_2 capture. *ChemSusChem* **8,** 3783–3792 (2015).

151. Guo, A., Ban, Y., Yang, K. & Yang, W. Metal-organic framework-based mixed matrix membranes: Synergetic effect of adsorption and diffusion for CO_2/CH_4 separation. *J. Membr. Sci.* **562,** 76–84 (2018).

152. Wellen, R. M. R. & Canedo, E. L. On the Kissinger equation and the estimate of activation energies for non-isothermal cold crystallization of PET. *Polym. Test.* **40,** 33–38 (2014).

153. Rajeshwari, P. Kinetic analysis of the non-isothermal degradation of high-density polyethylene filled with multi-wall carbon nanotubes. *J. Therm. Anal. Calorim.* **123,** 1523–1544 (2016).

154. Snegirev, A. Y., Talalov, V. A., Stepanov, V. V. & Harris, J. N. Formal kinetics of polystyrene pyrolysis in non-oxidizing atmosphere. *Thermochim. Acta* **548,** 17–26 (2012).

155. Zuo, X., Shao, H., Zhang, D., Hao, Z. & Guo, J. Effects of thermal-oxidative aging on the flammability and thermal-oxidative degradation kinetics of tris(tribromophenyl) cyanurate flame retardant PA6/LGF composites. *Polym. Degrad. Stab.* **98,** 2774–2783 (2013).

156. Kissinger, H. E. Variation of peak temperature with heating rate in differential thermal analysis. *J.*

Res. Natl. Bur. Stand. (1934). **57,** 217 (1956).

157. Coburn, N., Douglas, P., Kaya, D., Gupta, J. & McNally, T. Isothermal and non-isothermal crystallization kinetics of composites of poly(propylene) and MWCNTs. *Adv. Ind. Eng. Polym. Res.* **1,** 99–110 (2018).

158. Cheng, H., Liu, Q., Xu, P. & Hao, R. A comparison of molecular structure and de-intercalation kinetics of kaolinite/quaternary ammonium salt and alkylamine intercalation compounds. *J. Solid State Chem.* **268,** 36–44 (2018).

159. Kárászová, M., Zach, B., Petrusová, Z., Červenka, V., Bobák, M., Šyc, M. & Izák, P. Post-combustion carbon capture by membrane separation, review. *Sep. Purif. Technol.* **238,** 116448 (2020).

160. Sánchez-Laínez, J., Pardillos-Ruiz, A., Carta, M., Malpass-Evans, R., McKeown, N. B., Téllez, C. & Coronas, J. Polymer engineering by blending PIM-1 and 6FDA-DAM for ZIF-8 containing mixed matrix membranes applied to CO_2 separations. *Sep. Purif. Technol.* **224,** 456–462 (2019).

161. Chao, C., Deng, Y., Dewil, R., Baeyens, J. & Fan, X. Post-combustion carbon capture. *Renew. Sustain. Energy Rev.* **138,** 110490 (2021).

162. Rahman, M. M., Abetz, C., Shishatskiy, S., Martin, J., Mü Ller, A. J. & Abetz, V. CO_2 selective PolyActive membrane: Thermal transitions and gas permeance as a function of thickness. *Appl. Mater. Interfaces* **10,** 26733–26744 (2018).

163. Scofield, J. M. P., Gurr, P. A., Kim, J., Fu, Q., Halim, A., Kentish, S. E. & Qiao, G. G. High-performance thin film composite membranes with well-defined poly(dimethylsiloxane)-b-poly(ethylene glycol) copolymer additives for CO_2 separation. *J. Polym. Sci. Part A Polym. Chem.* **53,** 1500–1511 (2015).

164. Scofield, J. M. P., Gurr, P. A., Kim, J., Fu, Q., Kentish, S. E. & Qiao, G. G. Blends of fluorinated additives with highly selective thin-film composite membranes to increase CO_2 permeability for CO_2/N_2 gas separation applications. *Ind. Eng. Chem. Res.* **55,** 8364–8372 (2016).

165. Sánchez-Laínez, J., Paseta, L., Navarro, M., Zornoza, B., Téllez, C. & Coronas, J. Ultrapermeable thin film ZIF-8/polyamide membrane for H_2/CO_2 separation at high temperature without using sweep gas. *Adv. Mater. Interfaces* **5,** 1800647 (2018).

166. Zhao, D., Wu, Y., Ren, J., Li, H., Qiu, Y. & Deng, M. Improved CO_2 separation performance of composite membrane with the aids of low-temperature plasma treatment. *J. Membr. Sci.* **570–571,** 184–193 (2019).

167. Jauzein, T., Huneault, M. A. & Heuzey, M. C. Crystallinity and mechanical properties of polylactide/ether-amide copolymer blends. *J. Appl. Polym. Sci.* **134,** 44677 (2017).

168. Devine, D. M., Geever, L. M. & Higginbotham, C. L. Drug release from a N-vinylpyrrolidinone/acrylic acid lubricious hydrophilic coating. *J. Mater. Sci.* **40,** 3429–3436 (2005).

169. Tavangar, T., Zokaee Ashtiani, F., Karimi, M., Farzin, &, Ashtiani, Z. & Karimi, M. Morphological and performance evaluation of highly sulfonated polyethersulfone/polyethersulfone membrane for oil/water separation. *J. Polym. Res.* **27,** 252 (2020).

170. Swain, S. S., Unnikrishnan, L., Mohanty, S. & Nayak, S. K. Gas permeation and selectivity characteristics of PSF based nanocomposite membranes. *Polymer (Guildf).* **180,** 121692 (2019).

171. Ullah Khan, I., Hafiz, M., Othman, D., Jilani, A., Ismail, A. F., Hashim, H., Jaafar, J., Zulhairun, A. K., Rahman, M. A. & Rehman, G. U. ZIF-8 based polysulfone hollow fiber membranes for natural gas purification. *Polym. Test.* **84,** 106415 (2020).

172. Eykens, L., De Sitter, K., Stoops, L., Dotremont, C., Pinoy, L. & Van Der Bruggen, B. Development of polyethersulfone phase-inversion membranes for membrane distillation using oleophobic coatings. *J. Appl. Polym. Sci* **134,** 45516 (2017).

173. Sugu, L. & Jawad, Z. A. Formation of low acetyl content cellulose acetate membrane for CO_2/N_2 separation. *J. Phys. Sci.* **30,** 111–125 (2019).

174. Roslan, R. A., Lau, W. J., Zulhairun, A. K., Goh, P. S. & Ismail, A. F. Improving CO_2/CH_4 and O_2/N_2 separation by using surface-modified polysulfone hollow fiber membranes. *J. Polym. Res.* **27,** 1–14 (2020).

175. Mohammed, S. A., Nasir, A. M., Aziz, F., Kumar, G., Sallehhudin, W., Jaafar, J., Lau, W. J., Yusof, N., Salleh, W. N. W. & Ismail, A. F. CO_2/N_2 selectivity enhancement of PEBAX MH 1657/Aminated partially reduced graphene oxide mixed matrix composite membrane. *Sep. Purif. Technol.* **223,** 142–153 (2019).

176. Fu, Q., Halim, A., Kim, J., Scofield, J. M. P., Gurr, P. A., Kentish, S. E. & Qiao, G. G. Highly permeable membrane materials for CO_2 capture. *J. Mater. Chem. A* **1,** 13769–13778 (2013).

177. Zhu, T., Yang, X., Zheng, Y., He, X., Chen, F. & Luo, J. Preparation of poly(ether-block-amide)/poly(amide- co -poly(propylene glycol)) random copolymer blend membranes for CO_2/N_2 separation. *Polym. Eng. Sci.* **59,** E14–E23 (2019).

178. Dong, G., Li, H. & Chen, V. Challenges and opportunities for mixed-matrix membranes for gas separation. *J. Mater. Chem. A* **1,** 4610–4630 (2013).

179. Wang, H., Zheng, W., Yang, X., Ning, M., Li, X., Xi, Y., Yan, X., Zhang, X., Dai, Y., Liu, H. & He, G. Pebax-based mixed matrix membranes derived from microporous carbon nanospheres for permeable and selective CO_2 separation. *Sep. Purif. Technol.* **274,** 119015 (2021).

180. Tang, P.-H., So, P. B., Li, W.-H., Hui, Z.-Y., Hu, C.-C. & Lin, C.-H. Carbon dioxide enrichment PEBAX/MOF composite membrane for CO_2 separation. *Membranes.* **11,** 404 (2021).

181. Yapeng Shi, Wu, S., Wang, Z., Bi, X., Huang, M., Zhang, Y. & Jin, J. Mixed matrix membranes with highly dispersed MOF nanoparticles for improved gas separation. *Sep. Purif. Technol.* **277,** 119449 (2021).

182. Essen, M. van, Thür, R., Akker, L. van den, Houben, M., F.J.Vankelecom, I., Nijmeijer, K. & Borneman, Z. Tailoring the separation performance of ZIF-based mixed matrix membranes by MOF-matrix interfacial compatibilization. *J. Membr. Sci.* **637,** 119642 (2021).

183. Ahmad, M. Z., Navarro, M., Lhotka, M., Zornoza, B., Téllez, C., de Vos, W. M., Benes, N. E., Konnertz, N. M., Visser, T., Semino, R., Maurin, G., Fila, V. & Coronas, J. Enhanced gas separation performance of 6FDA-DAM based mixed matrix membranes by incorporating MOF UiO-66 and its derivatives. *J. Membr. Sci.* **558,** 64–77 (2018).

184. Anjum, M. W., Vermoortele, F., Khan, A. L., Bueken, B., De Vos, D. E. & Vankelecom, I. F. J. Modulated UiO-66-based mixed-matrix membranes for CO_2 separation. *ACS Appl. Mater. Interfaces* **7,** 25193–25201 (2015).

185. Lau, W. J., Gray, S., Matsuura, T., Emadzadeh, D., Paul Chen, J. & Ismail, A. F. A review on polyamide thin film nanocomposite (TFN) membranes: History, applications, challenges and approaches. *Water Res.* **80,** 306–324 (2015).

186. Zhao, D. L., Japip, S., Zhang, Y., Weber, M., Maletzko, C. & Chung, T. S. Emerging thin-film nanocomposite (TFN) membranes for reverse osmosis: A review. *Water Res.* **173,** 115557 (2020).

187. Yang, Z., Sun, P. F., Li, X., Gan, B., Wang, L., Song, X., Park, H. D. & Tang, C. Y. A critical review on thin-film nanocomposite membranes with interlayered structure: Mechanisms, recent developments, and environmental applications. *Environ. Sci. Technol.* **54,** 15563–15583 (2020).

188. Wong, K. C., Goh, P. S. & Ismail, A. F. Thin film nanocomposite: the next generation selective membrane for CO_2 removal. *J. Mater. Chem. A* **4,** 15726–15748 (2016).

189. Liao, Z., Zhu, J., Li, X. & Van der Bruggen, B. Regulating composition and structure of nanofillers in thin film nanocomposite (TFN) membranes for enhanced separation performance: A critical review. *Sep. Purif. Technol.* **266,** 118567 (2021).

190. Ma, D., Peh, S. B., Han, G. & Chen, S. B. Thin-film nanocomposite (TFN) membranes incorporated

with super-hydrophilic metal-organic framework (MOF) UiO-66: Toward enhancement of water flux and salt rejection. *ACS Appl. Mater. Interfaces* **9,** 7523–7534 (2017).

191. Zhao, D. L., Yeung, W. S., Zhao, Q. & Chung, T. S. Thin-film nanocomposite membranes incorporated with UiO-66-NH_2 nanoparticles for brackish water and seawater desalination. *J. Membr. Sci.* **604,** 118039 (2020).

192. Zhu, S., Bi, X., Shi, Y., Shi, Y., Zhang, Y., Jin, J. & Wang, Z. Thin films based on polyimide/metal-organic framework nanoparticle composite membranes with substantially improved stability for CO_2/CH_4 separation. *ACS Appl. Nano Mater.* **5,** 8997–9007 (2022).

193. Mozafari, M., Abedini, R. & Rahimpour, A. Zr-MOFs-incorporated thin film nanocomposite Pebax 1657 membranes dip-coated on polymethylpentyne layer for efficient separation of CO_2/CH_4. *J. Mater. Chem. A* **6,** 12380–12392 (2018).

194. Jiao, C., Song, X., Zhang, X., Sun, L. & Jiang, H. MOF-mediated interfacial polymerization to fabricate polyamide membranes with a homogeneous nanoscale striped turing structure for CO_2/CH_4 separation. *ACS Appl. Mater. Interfaces* **13,** 18380–18388 (2021).

195. Su, Z., Zhang, B., Cheng, X., Zhang, F., Wan, Q., Liu, L., Tan, X., Tan, D., Zheng, L. & Zhang, J. Ultra-small UiO-66-NH_2 nanoparticles immobilized on g-C3N4 nanosheets for enhanced catalytic activity. *Green Energy Environ.* **7,** 512–518 (2022).

196. Zornoza, B., Seoane, B., Zamaro, J. M., Téllez, C. & Coronas, J. Combination of MOFs and zeolites for mixed-matrix membranes. *Chemphyschem* **12,** 2781–2785 (2011).

197. Echaide-Górriz, C., Navarro, M., Téllez, C. & Coronas, J. Simultaneous use of MOFs MIL-101(Cr) and ZIF-11 in thin film nanocomposite membranes for organic solvent nanofiltration. *Dalt. Trans.* **46,** 6244–6252 (2017).

198. Dai, S., Simms, C., Dovgaliuk, I., Patriarche, G., Tissot, A., Parac-Vogt, T. N. & Serre, C. Monodispersed MOF-808 nanocrystals synthesized via a scalable room-temperature approach for efficient heterogeneous peptide bond hydrolysis. *Chem. Mater.* **33,** 7057–7066 (2021).

199. Shafiq, S., Al-Maythalony, B. A., Usman, M., Ba-Shammakh, M. S. & Al-Shammari, A. A. ZIF-95 as a filler for enhanced gas separation performance of polysulfone membrane. *RSC Adv.* **11,** 34319–34328 (2021).

200. Sun, J., Li, Q., Chen, G., Duan, J., Liu, G. & Jin, W. MOF-801 incorporated PEBA mixed-matrix composite membranes for CO2 capture. *Sep. Purif. Technol.* **217,** 229–239 (2019).

201. Garibay, S. J. & Cohen, S. M. Isoreticular synthesis and modification of frameworks with the UiO-66 topology. *Chem. Commun.* **46,** 7700–7702 (2010).

202. Cacho-Bailo, F., Etxeberría-Benavides, M., Karvan, O., Téllez, C. & Coronas, J. Sequential amine functionalization inducing structural transition in an aldehyde-containing zeolitic imidazolate framework: application to gas separation membranes. *CrystEngComm* **19,** 1545–1554 (2017).

203. Wang, R., Zhang, Y., Xie, X., Song, Q., Liu, P., Liu, Y. & Zhang, X. Hydrogen-bonded polyamide 6/Zr-MOF mixed matrix membranes for efficient natural gas dehydration. *Fuel* **285,** 119161 (2021).

204. Zamidi Ahmad, M., Navarro, M., Lhotka, M., Zornoza, B., Téllez, C., Fila, V. & Coronas, J. Enhancement of CO_2/CH_4 separation performances of 6FDA-based co-polyimides mixed matrix membranes embedded with UiO-66 nanoparticles. *Sep. Purif. Technol.* **192,** 465–474 (2018).

205. Tanh Jeazet, H. B., Sorribas, S., Román-Marín, J. M., Zornoza, B., Téllez, C., Coronas, J. & Janiak, C. Increased selectivity in CO_2/CH_4 separation with mixed-matrix membranes of polysulfone and mixed-MOFs MIL-101(Cr) and ZIF-8. *Eur. J. Inorg. Chem.* **2016,** 4363–4367 (2016).

206. Sutrisna, P. D., Hou, J., Zulkifli, M. Y., Li, H., Zhang, Y., Liang, W., D'Alessandro, D. M. & Chen, V. Surface functionalized UiO-66/Pebax-based ultrathin composite hollow fiber gas separation membranes. *J. Mater. Chem. A* **6,** 918–931 (2018).

207. Shen, J., Liu, G., Huang, K., Li, Q., Guan, K., Li, Y. & Jin, W. UiO-66-polyether block amide mixed matrix membranes for CO_2 separation. *J. Membr. Sci.* **513,** 155–165 (2016).

208. Tantekin-Ersolmaz, Ş. B., Atalay-Oral, Ç., Tatlier, M., Erdem-Şenatalar, A., Schoeman, B. & Sterte, J. Effect of zeolite particle size on the performance of polymer-zeolite mixed matrix membranes. *J. Membr. Sci.* **175,** 285–288 (2000).

209. Deng, J., Dai, Z., Hou, J. & Deng, L. Morphologically tunable MOF nanosheets in mixed matrix membranes for CO_2 separation. *Chem. Mater.* **32,** 4174–4184 (2020).

210. Song, Q., Nataraj, S. K., Roussenova, M. V., Tan, J. C., Hughes, D. J., Li, W., Bourgoin, P., Alam, M. A., Cheetham, A. K., Al-Muhtaseb, S. A. & Sivaniah, E. Zeolitic imidazolate framework (ZIF-8) based polymer nanocomposite membranes for gas separation. *Energy Environ. Sci.* **5,** 8359–8369 (2012).

211. Zheng, W., Ding, R., Yang, K., Dai, Y., Yan, X. & He, G. ZIF-8 nanoparticles with tunable size for enhanced CO_2 capture of Pebax based MMMs. *Sep. Purif. Technol.* **214,** 111–119 (2019).

212. Zhang, Y., Sunarso, J., Liu, S. & Wang, R. Current status and development of membranes for CO_2/CH_4 separation: A review. *Int. J. Greenh. Gas Control* **12,** 84–107 (2013).

213. Saini, N. & Awasthi, K. Insights into the progress of polymeric nano-composite membranes for hydrogen separation and purification in the direction of sustainable energy resources. *Sep. Purif. Technol.* **282,** 120029 (2022).

214. Solangi, N. H., Anjum, A., Tanjung, F. A., Mazari, S. A. & Mubarak, N. M. A review of recent trends and emerging perspectives of ionic liquid membranes for CO_2 separation. *J. Environ. Chem. Eng.* **9,** 105860 (2021).

215. Zhu, B., He, S., Wu, Y., Li, S. & Shao, L. One-step synthesis of structurally stable CO_2-philic membranes with ultra-high PEO loading for enhanced carbon capture. *Engineering* (2022).

216. He, S., Zhu, B., Jiang, X., Han, G., Li, S., Lau, C. H., Wu, Y., Zhang, Y. & Shao, L. Symbiosis-inspired de novo synthesis of ultrahigh MOF growth mixed matrix membranes for sustainable carbon capture. *Proc. Natl. Acad. Sci. U. S. A.* **119,** 1–9 (2022).

217. Ding, S., Li, X., Ding, S., Zhang, W., Guo, R. & Zhang, J. Ionic liquid-decorated nanocages for cooperative CO_2 transport in mixed matrix membranes. *Sep. Purif. Technol.* **239,** 116539 (2020).

218. Brunetti, A., Scura, F., Barbieri, G. & Drioli, E. Membrane technologies for CO_2 separation. *J. Membr. Sci.* **359,** 115–125 (2010).

219. Guo, A., Ban, Y., Yang, K., Zhou, Y., Cao, N., Zhao, M. & Yang, W. Molecular sieving mixed matrix membranes embodying nano-fillers with extremely narrow pore-openings. *J. Membr. Sci.* **601,** 117880 (2020).

220. Dechnik, J., Gascon, J., Doonan, C. J., Janiak, C. & Sumby, C. J. Mixed-matrix membranes. *Angew. Chemie Int. Ed.* **56,** 9292–9310 (2017).

221. Huang, T.-C., Liu, Y.-C., Lin, G.-S., Lin, C.-H., Liu, W.-R. & Tung, K.-L. Fabrication of pebax-1657-based mixed-matrix membranes incorporating N-doped few-layer graphene for carbon dioxide capture enhancement. *J. Membr. Sci.* **602,** 117946 (2020).

222. Sánchez-Laínez, J., Gracia-Guillé, I., Zornoza, B., Téllez, C. & Coronas, J. Thin supported MOF based mixed matrix membranes of Pebax 1657 for biogas upgrade. *New J. Chem* **43,** 312–319 (2019).

223. Benzaqui, M., Wahiduzzaman, M., Zhao, H., Hasan, M. R., Steenhaut, T., Saad, A., Marrot, J., Normand, E., Grenèche, J.-M., Heymans, N., De Weireld, G., Tissot, A., Shepard, W., Filinchuk, Y., Hermans, S., Carn, F., Manlankowska, M., Téllez, C., Coronas, J., Maurin, G., Steunou, N. & Serre, C. A robust eco-compatible microporous iron coordination polymer for CO_2 capture. *J. Mater. Chem. A* **10,** 8535–8545 (2022).

224. Benzaqui, M., Semino, R., Menguy, N., Carn, F., Kundu, T., Guigner, J.-M., Mckeown, N. B., Msayib, K. J., Carta, M., Malpass-Evans, R., Clément, ⊥, Le Guillouzer, C., Clet, G., Ramsahye, N. A., Serre,

C., Maurin, G. & Steunou, N. Toward an understanding of the microstructure and interfacial properties of PIMs/ZIF-8 mixed matrix membranes. *Appl. Mater. Interfaces* **8,** 27311–27321 (2016).

225. Guo, Z., Zheng, W., Yan, X., Dai, Y., Ruan, X., Yang, X., Li, X., Zhang, N. & He, G. Ionic liquid tuning nanocage size of MOFs through a two-step adsorption/infiltration strategy for enhanced gas screening of mixed-matrix membranes. *J. Membr. Sci.* **605,** 118101 (2020).

226. Galiano, F., Mancuso, R., Guazzelli, L., Mauri, M., Chiappe, C., Simonutti, R., Brunetti, A., Pomelli, C. S., Barbieri, G., Gabriele, B. & Figoli, A. Phosphonium ionic liquid-polyacrylate copolymer membranes for improved CO_2 separations. *J. Membr. Sci.* **635,** 119479 (2021).

227. Hermida-Merino, C., Pardo, F., Zarca, G., Araújo, J. M. M., Urtiaga, A., Piñeiro, M. M. & Pereiro, A. B. Integration of stable ionic liquid-based nanofluids into polymer membranes. Part I: Membrane synthesis and characterization. *Nanomater.* **11,** 607 (2021).

228. Lu, J., Zhang, X., Xu, L., Zhang, G., Zheng, J., Tong, Z., Shen, C. & Meng, Q. Preparation of amino-functional UiO-66/PIMs mixed matrix membranes with [bmim][Tf_2N] as regulator for enhanced gas separation. *Membr. 2021, Vol. 11, Page* **11,** 35 (2021).

229. Jomekian, A., Bazooyar, B., Behbahani, R. M., Mohammadi, T. & Kargari, A. Ionic liquid-modified Pebax® 1657 membrane filled by ZIF-8 particles for separation of CO_2 from CH_4, N_2 and H_2. *J. Membr. Sci.* **524,** 652–662 (2017).

230. Casado-Coterillo, C., Fernández-Barquín, A., Zornoza, B., Téllez, C., Coronas, J. & Irabien, Á. Synthesis and characterisation of MOF/ionic liquid/chitosan mixed matrix membranes for CO_2/N_2 separation. *RSC Adv.* **5,** 102350–102361 (2015).

231. Vu, M. T., Lin, R., Diao, H., Zhu, Z., Bhatia, S. K. & Smart, S. Effect of ionic liquids (ILs) on MOFs/polymer interfacial enhancement in mixed matrix membranes. *J. Membr. Sci.* **587,** 117157 (2019).

232. Aguado, S., Canivet, J. & Farrusseng, D. Facile shaping of an imidazolate-based MOF on ceramic beads for adsorption and catalytic applications. *Chem. Commun.* **46,** 7999–8001 (2010).

233. Neves, L. A., Nemestóthy, N., Alves, V. D., Cserjési, P., Bélafi-Bakó, K. & Coelhoso, I. M. Separation of biohydrogen by supported ionic liquid membranes. *Desalination* **240,** 311–315 (2009).

234. JIANG, Y., WU, Y., WANG, W., LI, L., ZHOU, Z. & ZHANG, Z. Permeability and selectivity of sulfur dioxide and carbon dioxide in supported ionic liquid membranes. *Chinese J. Chem. Eng.* **17,** 594–601 (2009).

235. Yan, X., Anguille, S., Bendahan, M. & Moulin, P. Ionic liquids combined with membrane separation processes: A review. *Sep. Purif. Technol.* **222,** 230–253 (2019).

236. Friess, K., Izák, P., Kárászová, M., Pasichnyk, M., Lanč, M., Nikolaeva, D., Luis, P. & Jansen, J. C. A review on ionic liquid gas separation membranes. *Membr.* **11,** 97 (2021).

237. Fam, W., Mansouri, J., Li, H., Hou, J. & Chen, V. Gelled graphene oxide-ionic liquid composite membranes with enriched ionic liquid surfaces for improved CO_2 separation. *ACS Appl. Mater. Interfaces* **10,** 7389–7400 (2018).

238. Yang, Z., Ying, Y., Pu, Y., Wang, D., Yang, H. & Zhao, D. Poly(ionic liquid)-functionalized UiO-66-$(OH)_2$: improved interfacial compatibility and separation ability in mixed matrix membranes for CO_2 separation. *Ind. Eng. Chem. Res.* **61,** 7626–7633 (2022).

239. Tsai, C. W., Niemantsverdriet, J. W. & Langner, E. H. G. Enhanced CO_2 adsorption in nano-ZIF-8 modified by solvent assisted ligand exchange. *Microporous Mesoporous Mater.* **262,** 98–105 (2018).

240. Etxeberria-Benavides, M., David, O., Johnson, T., Łozińska, M. M., Orsi, A., Wright, P. A., Mastel, S., Hillenbrand, R., Kapteijn, F. & Gascon, J. High performance mixed matrix membranes (MMMs)

composed of ZIF-94 filler and 6FDA-DAM polymer. *J. Membr. Sci.* **550,** 198–207 (2018).

241. Hasan, M. R., Paseta, L., Malankowska, M., Téllez, C. & Coronas, J. Synthesis of ZIF-94 from recycled mother liquors: Study of the influence of its loading on postcombustion CO_2 capture with Pebax based mixed matrix membranes. *Adv. Sustain. Syst.* **6,** 2100317 (2021).

242. Akbari Beni, F. & Niknam Shahrak, M. Alkali metals-promoted capacity of ZIF-8 and ZIF-90 for carbon capturing: A molecular simulation study. *Polyhedron* **178,** 114338 (2020).

243. Li, T., Pan, Y., Peinemann, K. V. & Lai, Z. Carbon dioxide selective mixed matrix composite membrane containing ZIF-7 nano-fillers. *J. Membr. Sci.* **425–426,** 235–242 (2013).

244. Luo, Q. & Pentzer, E. Encapsulation of ionic liquids for tailored applications. *ACS Appl. Mater. Interfaces* **12,** 5169–5176 (2020).

245. Friess, K., Jansen, J. C., Bazzarelli, F., Izák, P., Jarmarová, V., Kačírková, M., Schauer, J., Clarizia, G. & Bernardo, P. High ionic liquid content polymeric gel membranes: Correlation of membrane structure with gas and vapour transport properties. *J. Membr. Sci.* **415–416,** 801–809 (2012).

246. Husna, A., Hossain, I., Jeong, I. & Kim, T. H. Mixed matrix membranes for efficient CO_2 separation using an engineered UiO-66 MOF in a Pebax polymer. *Polymers (Basel).* **14,** 655 (2022).

247. Liu, D., Gu, J., Liu, Q., Tan, Y., Li, Z., Zhang, W., Su, Y., Li, W., Cui, A., Gu, C. & Zhang, D. Metal-organic frameworks reactivate deceased diatoms to be efficient CO_2 absorbents. *Adv. Mater.* **26,** 1229–1234 (2014).

248. Ghadimi, A., Amirilargani, M., Mohammadi, T., Kasiri, N. & Sadatnia, B. Preparation of alloyed poly(ether block amide)/poly(ethylene glycol diacrylate) membranes for separation of CO_2/H_2 (syngas application). *J. Membr. Sci.* **458,** 14–26 (2014).

249. Bakhtin, D., Bazhenov, S., Polevaya, V., Grushevenko, E., Makaev, S., Karpacheva, G., Volkov, V. & Volkov, A. Aging of thin-film composite membranes based on crosslinked PTMSP/PEI loaded with highly porous carbon nanoparticles of infrared pyrolyzed polyacrylonitrile. *Membr.* **10,** 419 (2020).

250. Chen, H. Z., Thong, Z., Li, P. & Chung, T. S. High performance composite hollow fiber membranes for CO_2/H_2 and CO_2/N_2 separation. *Int. J. Hydrogen Energy* **39,** 5043–5053 (2014).

251. Shin, J. E., Lee, S. K., Cho, Y. H. & Park, H. B. Effect of PEG-MEA and graphene oxide additives on the performance of Pebax®1657 mixed matrix membranes for CO_2 separation. *J. Membr. Sci.* **572,** 300–308 (2019).

252. Pardo, F., Zarca, G. & Urtiaga, A. Effect of feed pressure and long-term separation performance of Pebax-ionic liquid membranes for the recovery of difluoromethane (R32) from refrigerant mixture R410A. *J. Membr. Sci.* **618,** 118744 (2021).

253. Nabais, A. R., Neves, L. A. & Tomé, L. C. Mixed-matrix ion gel membranes for gas separation. *ACS Appl. Polym. Mater.* **4,** 3098–3119 (2021).

254. Sutrisna, P. D., Hou, J., Li, H., Zhang, Y. & Chen, V. Improved operational stability of Pebax-based gas separation membranes with ZIF-8: A comparative study of flat sheet and composite hollow fibre membranes. *J. Membr. Sci.* **524,** 266–279 (2017).

255. Rhyu, S. Y. & Kang, S. W. Accelerated CO_2 transport by synergy effect of ionic liquid and Zn particles. *J. Ind. Eng. Chem.* **103,** 216–221 (2021).

256. Fam, W., Mansouri, J., Li, H. & Chen, V. Improving CO_2 separation performance of thin film composite hollow fiber with Pebax®1657/ionic liquid gel membranes. *J. Membr. Sci.* **537,** 54–68 (2017).

257. Dai, Z. De, Bai, L., Hval, K. N., Zhang, X. P., Zhang, S. J. & Deng, L. Y. Pebax®/TSIL blend thin film composite membranes for CO_2 separation. *Sci. China Chem.* **59,** 538–546 (2016).

Capítulo 11: Glosario de términos

11. Glosario de términos

[Bmim][BF_4]	1-Butyl-3-methylimidazolium tetrafluoroborate
1-ButOH	1-Butanol
1-PrOH	1-Propanol
2-mIm	2-Methylimidazole
AEI	Agencia Estatal de Investigación
BDC	Benzenedicarboxylate (Tereftalato)
BET	Brunauer-Emmett-Teller
CCS	Carbon capture and storage
CFCs	Clorofluorocarbonos
COF	Covalent organic framework
COP26	26ª Conferencia de las Naciones Unidas sobre el Cambio Climático
CREG	Catálisis, Separaciones Moleculares e Ingeniería de Reactores
CSIC	Centro Superior de Investigaciones Científicas
DI	Deionized [water]
DMF	Dimethylformamide
DSC	Differential scanning calorimetry
DTG	Differential termogravimetry
EtOH	Ethanol
FFV	Free fractional volume
FTIR-ATR	Fourier transform infrared spectroscopy-attenuated total reflectance
GHG	Green house gas
GO	Graphene oxide
GPU	Gas permeation unit
HF	Hollow fiber
HKUST	Hong Kong University of Science and Technology
IL	Ionic liquid
INMA-CSIC	Instituto de Nanociencia y Materiales de Aragón-Centro Superior de Investigaciones Científicas

IPCC	Intergovernmental Panel on Climate Change – [Grupo Intergubernamental de Expertos sobre el Cambio Climático]
IQTMA	[Departamento de] Ingeniería Química y Tecnologías del Medio Ambiente
MCIN	Ministerio de Ciencia e Innovación
MEMBER	Advanced MEMBranes and membrane assisted processes for pre- and post- combustion CO_2 captuRe
MeOH	Methanol
MIL	Materials Institute Lavoisier
MMM	Mixed matrix membranes
MOF	Metal-organic framework
NMP	N-Methyl-2-pyrrolidone
OR	Original route
PA	Poliamida – [Polyamide]
PA11	Poliamida 11 – [Polyamide 11]
PA12	Poliamida 12 – [Polyamide 12]
PA6	Poliamida 6 – [Polyamide 6]
PCP	Porous coordination polymer
PDMS	Polydimethylsiloxane
PE	Polyether
PEBA	Poly(ether-block-amide)
PEBAX®	Poly(ether-block-amide) extreme
PEG	Polyethyleneglycol
PEI	Polyetherimide
PEO	Polyether oxide – [Óxido de polietileno]
PES	Polyethersulfone
PI	Polyimides
PS	Polystyrene
PSF	Polysulfone – [Polisulfona]
PTMG	Polytetramethyleneglycol
PTMO	Polytetramethyleneoxide

PTMSP	Poly[1-(trimethylsilyl)prop-1-yne]
RH	Relative humidity
RSM	Resistance in series model
RT	Room temperature
SALE	Solvent assisted ligand exchange
SEM	Scanning electron microscopy
SIM-1	Substituted Imidazolate Material-1
SSA	Specific surface area
STP	Standard temperature and pressure
TEM	Transmission electron microscopy
TFC	Thin film composite
TFN	Thin film nanocomposite
TGA	Thermogravimetric analysis
THF	Tetrahydrofuran
TSIL	Task-specific ionic liquid
UiO	University of Oslo
UNE	Una Norma Española
UZ	Universidad de Zaragoza
WGSR	Water-gas shift reaction
XRD	X-ray difraction
ZIF	Zeolitic imidazolate framework